THE UNIVERSITY
of EDINBURGH

This thesis has been submitted in fulfilment of the requirements for a postgraduate degree (e.g. PhD, MPhil, DClinPsychol) at the University of Edinburgh. Please note the following terms and conditions of use:

This work is protected by copyright and other intellectual property rights, which are retained by the thesis author, unless otherwise stated.
A copy can be downloaded for personal non-commercial research or study, without prior permission or charge.
This thesis cannot be reproduced or quoted extensively from without first obtaining permission in writing from the author.
The content must not be changed in any way or sold commercially in any format or medium without the formal permission of the author.
When referring to this work, full bibliographic details including the author, title, awarding institution and date of the thesis must be given.

Mixed-mode oscillations in singularly perturbed three-timescale systems

Panagiotis Kaklamanos

Doctor of Philosophy
University of Edinburgh

Declaration

I declare that this thesis was composed by myself and that the work contained therein is my own, except where explicitly stated otherwise in the text, and that this work has not been submitted for any other degree or professional qualification except as specified.

P. Kaklamanos,
July 2021

To my family

Lay summary

Many natural systems are characterised by the presence of multiple timescales. Considering the whole Universe itself, for instance, stellar phenomena are very slow compared to Earthly ones, for example compared to how long it takes for Earth to complete a rotation around the Sun or to how long it takes for Earth to complete a rotation around its axis. The timescale-separation is even more extreme when such macroscopic phenomena are compared to microscopic ones, like atomic and subatomic phenomena etc.

However, different timescales are apparent even in smaller, more contained and maybe closed systems, were the dynamics between different components are not as seemingly unrelated as in the example of Earth's orbit and atomic particles. Some examples of such systems include biological systems, were electrical phenomena happen faster than chemical ones and where even chemical reactions can occur at very different rates, or climate systems, where pressure, temperature, humidity and other quantities vary at different rates, leading to complicated meteorological phenomena, like the weather in Scotland.

The focus of this work is the study of a class of dynamical systems, i.e. of mathematical formulations that are used to model natural systems, that are characterised by the presence and interaction of three distinct timescales. The aim is to uncover the mechanisms that distinguish between qualitatively different oscillatory dynamics of the system, explaining, for instance, why for some particular choices of the parameters of the system only two timescales seem to manifest themselves, while for other choices of the parameters, all three timescales seem to manifest themselves in the behaviour of the system.

Abstract

In this work, we are concerned with the dynamics of three-dimensional, three-timescale systems of ordinary differential equations. Systems with two timescales have been extensively studied, while the theory of systems with three or more timescales is less developed, although in some cases they provide more realistic modelling of natural systems. Our focus is on mixed-mode oscillations (MMOs), i.e., on trajectories which consist of alternating small-amplitude oscillations (SAOs) and large excursions or large-amplitude oscillations (LAOs). We aim to understand the underlying mechanisms that are responsible for the qualitative properties of these trajectories, as well as to classify the various behaviours of these systems upon variation of their parameters, using geometric singular perturbation theory (GSPT).

In the first part, we present a new prototypical system that captures a geometric mechanism which distinguishes between MMOs that feature SAOs only in one region of the phase space from those which feature SAOs in two distinct regions of the phase space; we refer to the former as MMOs with single SAO-epochs and to the latter as MMOs with double SAO-epochs. In essence, this distinction is based on the relative position of points where normal hyperbolicity with respect to the fast flow is lost.

In the second part, we show that the Koper model, a well known system from chemical kinetics, is merely a particular realisation of the prototypical example that we introduced in the first part. This system has been extensively studied in the two-timescale context, but, to our knowledge, it has not been studied in the three-timescale context before. We hence classify its dynamics in dependence of its parameters in the three-timescale context, and we show that some phenomena that are delicate in the two-timescale setting, like MMOs with double SAO epochs, become robust in the three-timescale one.

In the third part, we show that the four-dimensional Hodgkin-Huxley equations from mathematical neuroscience can be reduced to a three-dimensional, three-timescale system. We then illustrate that, in particular parameter regimes, this system features similar properties to the prototypical example that we introduced in the first part, and we show how the theory that we introduced in the previous chapters can be used to explain its behaviour. From another point of view, we show that the system can be written in the non-standard form of GSPT, and we show that its oscillatory dynamics can be explained by extending the notions that we introduced in the previous chapters.

In the fourth part, we study a three-dimensional system that describes the El-Niño Southern Oscillation (ENSO) phenomenon. This system has too been extensively studied in the two-timescale context but not in the three-timescale one. However, this system is more complicated in terms of its invariant manifold structure compared to the other two systems mentioned above. Extending some notions from the previous parts and based again on the relative position of sets where normal hyperbolicity with respect to the fast flow is lost, we

distinguish between oscillations with different qualitative properties. Moreover, we perform a desingularisation analysis of the sets where normal hyperbolicity is lost and we give estimates on bifurcation-delay phenomena, which are points that had not been addressed in previous works.

In summary, this work is concerned with local and global phenomena in three-timescale systems. The focus is (a) on systems that have previously been analysed only in the two-timescale context, like the Koper and ENSO models, thus exploring the dynamics in the three-timescale setting, and (b) on systems that have been studied in the multi-timescale context (more than two) in the past, but not in the GSPT framework, and where the mechanisms that encode transitions between qualitatively different behaviours were elusive, like the Hodgkin-Huxley equations. The various qualitative behaviours depend on the underlying geometry of these systems, and the extended prototypical example that we propose does not only provide a geometric mechanism that is directly applicable to other systems, like the Koper model and the Hodgkin-Huxley equations, but also, by simple extension of some notions, provides insight on the dynamics and possible behaviours in three-timescale systems with more complicated geometry, like the ENSO model. Finally, we remark on some phenomena that are not robust in the two-timescale setting, but become robust in the three timescale one.

Acknowledgements

I would first and foremost like to thank my supervisors, Dr. Nikola Popovic, University of Edinburgh (UoE), and Dr. Kristian Uldall Kristiansen, Technical University of Denmark (DTU), who have both provided ample support and guidance all these years. Nikola set the main questions of the PhD project, provided feedback on a regular basis and insightful suggestions when things were stuck, and always gave me the freedom to explore alternative directions and implement my ideas. He has also been very supportive and encouraging of my other activities, like gaining exposure and being more involved in the Dynamical Systems community through various presentations, participations in conferences, organising events, etc. Kristian has also been providing ample and constructive feedback, and his attention to detail and mathematical rigour have been exemplary. He has too been very supportive throughout my trajectory, from supervising my MSc Thesis at DTU, then supporting me during my search for a PhD, and now co-supervising this one, and his input has been valuable. I have learned a lot from both of them, and they have both been a source of inspiration.

Another source of inspiration has been Prof. Martin Krupa, Université Côte d'Azur, whom I would like to thank for being my host and supervisor during my Erasmus-plus Research Traineeship at his department, and also for the many insightful discussions that we had prior to that and for his valuable feedback on this project, which has also led to other open questions that are included in plans for future work.

I would next like to thank the Maxwell Institute for Mathematical Sciences, as well as the International Centre for Mathematical Sciences at University of Edinburgh & Heriot-Watt University; they built an incredible feeling of community at the Bayes Centre, and it always felt more than "people just doing their job" there. Of great value have been the opportunities to be involved with the Industrial Stream as part of my PhD training, as well as to be part of the Edinburgh SIAM-IMA Student Chapter Committee, both of which have been a pleasure; I would therefore like to thank everyone who was involved.

I would also particularly like to thank Dr. Mariya Ptashnyk for her support at many levels and for all the insightful discussions that we had, as well as the fellow PhD students and friends: Spyros Dimoudis, George Farmakis, Tatiana Filatova, Christina Lazaridou and Thomas Zacharis, for all the nice times that we had at the Bayes Centre, the University Library or the JCMB (and sometimes outside), either discussing maths, or just hanging out.

I will close with thanking my parents, Ioannis and Thessalia, and my brothers, Georgios and Charalambis, for always being there for me. Finally, I would like to thank Nina-Lydia Kazakou for accompanying me through a big part of this journey, providing me with BioRender figures, supporting me and bearing with me when times were hectic, and generally for making this journey more beautiful.

Contents

Abstract **x**

Introduction **1**

1 Geometric singular perturbation theory: basic notions and background **7**
1.1 The standard form of GSPT 7
1.2 The non-standard form of GSPT 8
1.3 Hierarchy of timescales and iterative reductions 9
1.4 Non-hyperbolic sets and geometric desingularisation 12
1.5 Relaxation oscillations in $\mathbb{R}^3$ 15
1.6 Folded singularities and canards in $\mathbb{R}^3$ 17

2 Three-timescale systems: an extended prototypical example **22**
2.1 Introduction 22
2.2 The double singular limit: geometry and singular cycles 25
2.2.1 The critical manifold $\mathcal{M}_1$ 25
2.2.2 The supercritical manifold $\mathcal{M}_2$ 28
2.2.3 Relative geometry 30
2.2.4 Singular cycles 32
2.3 Global dynamics and MMOs 34
2.3.1 Aligned or connected singularities 36
2.3.2 Remote singularities 38
2.4 Local dynamics and SAOs 45
2.4.1 Bifurcation delay 49
2.4.2 Sector-type dynamics 51
2.5 Summary 54
2.6 Blow-up of folded singularities 55
2.6.1 The entry chart $\kappa_1 : \{\bar{y} = 1\}$ 56
2.6.2 The rescaling chart $\kappa_2 : \{\bar{y} = 1\}$ 58
2.7 The "double fold" case 59
2.7.1 The entry chart $\kappa_1 : \{\bar{y} = 1\}$ 60
2.7.2 The rescaling chart $\kappa_2 : \{\bar{\varepsilon} = 1\}$ 62

3 The Koper model from chemical kinetics **66**
3.1 Singular geometry 67
3.2 Classification of three-timescale dynamics 68

3.2.1 The passage from two to three timescales . . . 70
3.3 Numerical verification . . . 70

4 The Hodgkin-Huxley equations from mathematical neuroscience 77
4.1 Introduction . . . 77
4.2 Global multi-timescale reduction . . . 84
4.3 The h-slow regime . . . 88
4.3.1 Singular geometry . . . 89
4.3.2 Perturbed dynamics and and MMOs . . . 92
4.3.3 Onset and cessation of oscillatory dynamics . . . 93
4.3.4 From double to single SAO-epochs . . . 94
4.3.5 Transitive, "exotic" MMOs . . . 95
4.3.6 From MMOs to relaxation . . . 97
4.4 The n-slow case . . . 99
4.4.1 Singular geometry . . . 100
4.4.2 Perturbed dynamics and MMOs . . . 102
4.4.3 Onset and cessation of oscillatory dynamics . . . 103
4.4.4 From double to single SAO-epochs . . . 104
4.5 Local dynamics and SAOs . . . 107
4.6 Summary . . . 109
4.7 Reduced flow on $\mathcal{M}_1$ in the non-standard form of GSPT . . . 110
4.7.1 The h-slow case . . . 110
4.7.2 The n-slow case . . . 112

5 The El-Niño Southern Oscillation model from climate science 117
5.1 Introduction . . . 117
5.2 Singular limit . . . 119
5.2.1 The slow manifold $\mathcal{M}_1 = \mathcal{M}_{\mathcal{P}} \cup \mathcal{M}_{\mathcal{S}}$ . . . 119
5.2.2 The reduced flow on $\mathcal{M}_{\mathcal{P}}$ . . . 121
5.2.3 The reduced flow on $\mathcal{M}_{\mathcal{S}}$ . . . 123
5.3 Outline of dynamics . . . 130
5.3.1 Perturbed dynamics and delayed loss of stability . . . 131
5.3.2 Oscillatory trajectories . . . 132
5.4 Summary . . . 139
5.5 Blow-up analysis of $\mathcal{F}_P$ . . . 140
5.5.1 The entry chart $\kappa_1 : \{\bar{z} = 1\}$ . . . 142
5.5.2 The rescaling chart $\kappa_2 : \{\bar{\delta} = 1\}$ . . . 144
5.5.3 The exit chart $\kappa_3 : \{\bar{z} = -1\}$ . . . 144
5.5.4 Summary . . . 146

6 Conclusions 150

Introduction

Mixed-mode oscillations (MMOs) are trajectories that are characterised by the alternation of small-amplitude oscillations (SAOs) and large-amplitude excursions (LAOs) in the corresponding time series, and are frequently observed in dynamical systems that feature multiple timescales. Representative MMO trajectories can be seen in Figure 1; each such trajectory can be associated with a sequence of the form $\{F_0F_1\ldots\}$, called the *Farey sequence*, that describes the succession of large excursions and small oscillations, where the segments F_j are of the form

$$F_j = \begin{cases} L^s \text{ if the segment consists of } L \text{ LAOs, followed by } s \text{ SAOs "above";} \\ L_s \text{ if the segment consists of } L \text{ LAOs, followed by } s \text{ SAOs "below".} \end{cases}$$

If a Farey sequence consists of L^s-type or L_s-type segments only, we say that the corresponding MMO trajectory contains *single epochs* of SAOs, as seen in panels (a) and (b) of Figure 1, respectively; Farey sequences that consist of both L^s-type and L_s-type segments correspond to MMO trajectories that contain *double epochs* of SAOs, as shown in Figure 1(c). Finally, relaxation oscillation refers to oscillatory trajectories that contain large excursions and no SAO segments, i.e., trajectories with associated Farey sequence $\{L^0\}$; cf. Figure 1(d).

MMO dynamics has been widely studied in systems with two distinct timescales. Consider a system of the form

$$x' = f(x, y, z), \tag{1a}$$
$$y' = \varepsilon g(x, y, z), \tag{1b}$$
$$z' = \varepsilon h(x, y, z), \tag{1c}$$

with $(x, y, z) \in \mathbb{R}^3$, $\varepsilon \in \mathbb{R}^+$, and $f, g, h : \mathbb{R}^3 \to \mathbb{R}$ smooth, and where the prime denotes differentiation with respect to time. If the parameter ε is sufficiently small, then the rates of change of the variables y and z are slower than the rate of change of the variable x, as can be seen from the RHS of (1). Correspondingly, y and z are then referred to as the *slow* variables, x is referred to as the *fast* variable, and system (1) is said to be a *slow-fast* system.

Systems of the form of Equations (1) have been extensively studied using Fenichel's geometric singular perturbation theory (GSPT) [Fenichel, 1979]. In essence, this approach is based on finding locally invariant slow manifolds in the phase space of (1), that is, manifolds on which the dynamics evolves in the timescale of y and z, i.e. the slow timescale. Crudely speaking, trajectories that evolve along the fast direction are attracted exponentially close to these manifolds, and then they evolve in the slow timescale until they reach vicinities where stability changes from attracting to repelling, where we say that *normal hyperbolicity* is lost; we make this idea precise in Chapter 1. It is exactly at these regions of the phase

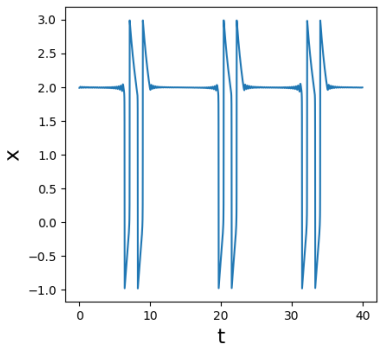

(a) SAOs "above"

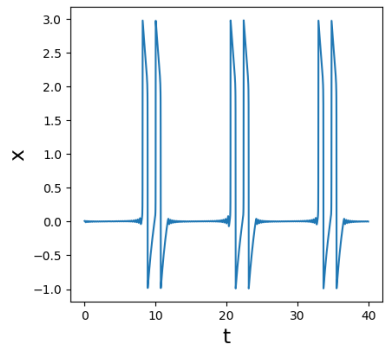

(b) SAOs "below"

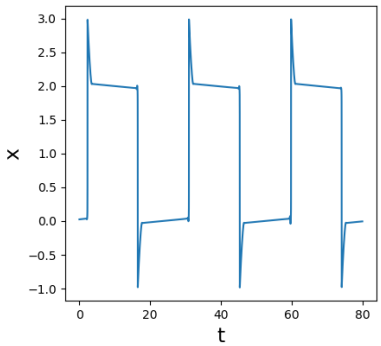

(c) Double epochs of SAOs

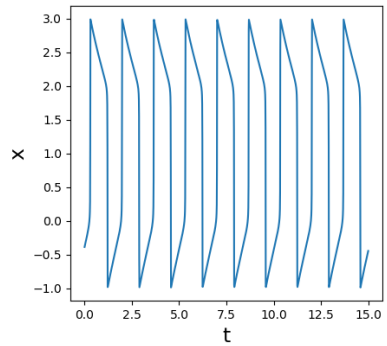

(d) Relaxation oscillation

Figure 1: (a) MMO trajectory with single epochs of SAOs and Farey sequence $2^{s_1}2^{s_2}2^{s_3}\cdots$; (b) MMO trajectory with single epochs of SAOs and Farey sequence $2_{s_1}2_{s_2}2_{s_3}\cdots$; (c) MMO trajectory with double epochs of SAOs and Farey sequence $1^{s_1}1_{s_2}1^{s_3}1_{s_4}\cdots$; (d) relaxation oscillation.

space where SAOs can occur, followed by large excursions to other attracting portions of the slow manifold, which give the LAOs.

The geometric theory of MMO dynamics in slow-fast systems with more than two timescales is less well-developed. Consider a system of the form

$$x' = f(x, y, z), \tag{2a}$$
$$y' = \varepsilon g(x, y, z), \tag{2b}$$
$$z' = \varepsilon\delta h(x, y, z), \tag{2c}$$

with $\varepsilon, \delta > 0$ small, and f, g, h smooth. In this case, x is the *fast* variable, y is the *intermediate* variable, and z is the *slow* variable.

In [Krupa et al., 2008], a *prototypical example* is considered, namely

$$x' = -y + f_2x^2 + f_3x^3, \tag{3a}$$
$$y' = \varepsilon\,(x - z)\,, \tag{3b}$$
$$z' = \varepsilon^2\,(\mu + \phi(x, y, z))\,, \tag{3c}$$

which is a special case of (2), where in particular $\delta = \varepsilon$. Asymptotic formulae for the return map induced by the flow of (3) are derived; in particular, an underlying near-integrable structure allows for a both qualitative and quantitative description of the corresponding MMO dynamics which includes predictions on the associated Farey sequences and estimates for the relevant parameter regimes, see Chapter 2 for more details. In a follow-up article [De Maesschalck et al., 2016], a two-parameter modification of Equation (3c) is considered, with ε replaced by an independent parameter δ in (3c); crucially, it is shown that the interplay between ε and δ can affect the local qualitative properties of MMOs, see Section 2.4 for details. However, this system is quite restrictive, because, as will become apparent, the absence of y-terms in (3b) makes it impossible for (3) to fully capture the dynamics of relevant three-timescale systems from applications, such as the Koper model from chemical kinetics and the Hodgkin-Huxley equations from mathematical neuroscience described below.

In [Letson et al., 2017], the local *canonical form*

$$x' = y + x^2, \tag{4a}$$
$$y' = \varepsilon \left(-\alpha^2 x + \beta y + z\right), \tag{4b}$$
$$z' = \varepsilon\delta, \tag{4c}$$

was considered. This system has richer local dynamics due to the additional y-terms in the intermediate equation, cf. (4a) and (3b). However, MMOs are not possible in (4), since the system lacks a return mechanism, due to the absence of cubic x-terms in the fast equation, cf. (4a) and (3a); and trajectories that escape the vicinity of the non-hyperbolic region cannot return, as will become apparent in Chapter 2.

In this work, we introduce an *extended prototypical example*

$$x' = -y + f_2 x^2 + f_3 x^3, \tag{5a}$$
$$y' = \varepsilon \left(\alpha x + \beta y - z\right), \tag{5b}$$
$$z' = \varepsilon\delta \left(\mu + \phi(x, y, z)\right), \tag{5c}$$

which combines features from both the prototypical system (3) and the canonical form (4), namely:

1. Due to the presence of cubic x-terms in the fast equation (5a), it features a return mechanism which allows for MMO dynamics, in contrast to the canonical form (4);

2. Due to the presence of y-terms in the intermediate equation (5a), it features richer SAO dynamics, and also geometric mechanisms that allow for additional global scenarios compared to the prototypical system (3), in which, for instance, MMOs with double epochs are not possible, cf. Figure 1 (c);

3. The timescale-separation parameters ε and δ in (5c) are independent.

In Chapter 2, we study the various possible qualitative scenarios of MMO dynamics of system (5) in dependence of its parameters. One of the main results of this work is the uncovering of the mechanisms responsible for the transition between MMO scenarios with different qualitative properties in dependence of the parameters of the system, cf. Figure 1.

A particular realisation of the extended prototypical example is the Koper model from chemical kinetics [Koper, 1995]

$$x' = ky + 3x - x^3 - \lambda, \tag{6a}$$
$$y' = \varepsilon\,(x - 2y + z)\,, \tag{6b}$$
$$z' = \varepsilon\delta\,(y - z)\,, \tag{6c}$$

which, after affine transformation, can be written in the form of (5). In Chapter 3, we therefore show that the results presented in Chapter 2 extend directly to this system. In particular, we demonstrate that MMOs with double SAO epochs are robust in the three-timescale context, in contrast to the two-timescale one, where they are very delicate as the parameter regimes in which they are observed are very narrow [Desroches et al., 2012].

Further, in Chapter 4 we consider the four-dimensional, four-timescale Hodgkin-Huxley equations from mathematical neuroscience [Hodgkin and Huxley, 1952]. We propose a novel, three-dimensional reduction of these equations of the form

$$v' = U(v, h, n) + \mathcal{O}(\varepsilon), \tag{7a}$$
$$h' = \varepsilon\delta_h H(v, h), \tag{7b}$$
$$n' = \varepsilon\delta_n N(v, h), \tag{7c}$$

with $\varepsilon > 0$ small, which is based on GSPT. We study the two different cases where either h or n is taken to be the slowest variable (by setting $\delta_n = 1$ and considering $0 < \delta_h \ll 1$, or $\delta_h = 1$ and $0 < \delta_n \ll 1$, respectively), and we show that system (7) exhibits the same underlying mechanisms that produce different MMO behaviours and encode the transitions between them as the extended prototypical example (5) studied in Chapter 2. These two different limits have been considered in previous works [Doi et al., 2001] and various scenarios have been documented, and here we aim to explain them in the framework of GSPT. We emphasize that an alternative three-dimensional reduction of the Hodgkin-Huxley equations has been derived in [Rubin and Wechselberger, 2007], and it is equivalent in predicting the transitions between qualitatively different behaviours of the systems in dependence of its parameters when treated as a three-timescale system; however, in [Rubin and Wechselberger, 2007, Rubin and Wechselberger, 2008], the corresponding three-dimensional system was treated solely as a two-timescale system, i.e. $\varepsilon > 0$ small and $\delta_h, \delta_n = \mathcal{O}(1)$ in (7).

The final three-timescale system that we are considering in this work is a model that describes the El-Niño Southern Oscillation (ENSO) phenomenon [Roberts et al., 2016]

$$x' = x\,(x + y + c(1 - \tanh\,(x + z))) + \rho\delta(x^2 - ax), \tag{8a}$$
$$y' = -\rho\delta(ay + x^2), \tag{8b}$$
$$z' = \delta(k - z - \frac{x}{2}), \tag{8c}$$

whith $\rho, \delta > 0$ small and $c, k, a > 0$. To our knowledge, this system has not been previously studied in the three-timescale context. In this setting, it features richer geometric scenarios in terms of its slow manifolds compared to the Koper model (6) and the Hodgkin-Huxley equations (7). Our approach with this system goes in the opposite direction than the one

with the Hodgkin-Huxley equations (7); that is, we study its geometry in order to gain insight about possible qualitative properties of MMO trajectories and we then classify those in dependence of the parameters of the system, instead of attempting to geometrically explain behaviours that have been documented in previous works. This way, we uncover qualitative behaviours that have not been observed in previous works.

Chapter 1

Geometric singular perturbation theory: basic notions and background

1.1 The standard form of GSPT

Consider the following ODE-system

$$x' = f(x, y, \varepsilon), \tag{1.1a}$$
$$y' = \varepsilon g(x, y, \varepsilon), \tag{1.1b}$$

where $x \in \mathbb{R}^m$, $y \in \mathbb{R}^n$, $f, g : \mathbb{R}^{m+n+1} \to \mathbb{R}$ smooth, $\varepsilon \in \mathbb{R}^+$, and where the prime denotes differentiation with respect to time t. If ε is considered "small", then the dynamics of (1.1b) is "slow" compared to the dynamics of (1.1a). Rescaling time as $\tau = t/\varepsilon$ in (1.1) gives

$$\varepsilon \dot{x} = f(x, y, \varepsilon), \tag{1.2a}$$
$$\dot{y} = g(x, y, \varepsilon). \tag{1.2b}$$

We then refer to systems (1.1) and (1.2) as the *fast* and *slow* formulations, respectively, and the two systems are equivalent in terms of their phase space.

The main idea behind GSPT, is to view the fast and slow systems (1.1) and (1.2) as perturbations of two *limit* or *singular* systems, namely of the *layer problem*

$$x' = f(x, y, 0), \tag{1.3a}$$
$$y' = 0 \tag{1.3b}$$

obtained by setting $\varepsilon = 0$ in (1.1), and of the *reduced problem*

$$0 = f(x, y, 0), \tag{1.4a}$$
$$\dot{y} = g(x, y, 0). \tag{1.4b}$$

obtained by setting $\varepsilon = 0$ in (1.2).

System (1.3) corresponds to a family of m one-dimensional ODE problems where t is the independent variable, x are the dependent variables and y are parameters

The set of equilibria of the m-dimensional layer problem defines the *critical manifold*

$$\mathcal{M} = \{(x, y) \in \mathbb{R}^m \times \mathbb{R}^n \mid f(x, y, 0) = 0\}. \tag{1.5}$$

The normally hyperbolic subset $\mathcal{S}$ of $\mathcal{M}$ is defined as the set where the eigenvalues $\lambda(x, y)$ of the $m \times m$ Jacobian matrix $D_x f(x, y, 0)$ satisfy $\Re(\lambda(x, y)) \neq 0$. This implies that $\mathcal{S}$ has stable and unstable manifolds $\mathcal{W}_s(\mathcal{M}_\varepsilon)$ and $\mathcal{W}_u(\mathcal{M}_\varepsilon)$, respectively, with respect to the fast flow x given by (1.3).

Definition 1 ([Fenichel, 1979]; reformulation from [Kuehn, 2015])**.** *A normally hyperbolic subset $\mathcal{S} \subset \mathcal{M}$ is called attracting if all eigenvalues of $D_x f(x, y, 0)$ have negative real part for $(x, y) \in \mathcal{S}$; similarly, $\mathcal{S}$ is called repelling if all eigenvalues have positive real part. If $\mathcal{S}$ is normally hyperbolic and neither attracting nor repelling, it is of saddle type.*

Throughout this work, we will denote the normally hyperbolic and attracting subsets of $\mathcal{M}$ by $\mathcal{S}^a$, and the normally hyperbolic and repelling subsets of $\mathcal{M}$ by $\mathcal{S}^r$.

On the other hand, equations (1.4) comprise a differential-algebraic system. Equation (1.4b) defines the reduced flow on the manifold characterised by the algebraic constraint (1.4a), i.e. $\mathcal{M}$. A particular example with $n = 1 = m$ is shown in Section 1.4 below.

We emphasize that, although systems (1.1) and (1.2) are topologically equivalent, the limit systems (1.3) and (1.4) are two distinct problems. That is, at the singular limit $\varepsilon = 0$, $\mathcal{M}$ consists of *equilibria* of (1.3a), which means that solutions of (1.3a) do not actually reach $\mathcal{M}$ in finite forward or backward time, while (1.4) describes the flow *on* $\mathcal{M}$. The main idea behind GSPT is, rather, that information obtained by the two limiting systems can be combined to give insight about the "perturbed" system (1.1) with $\varepsilon > 0$ small, as follows.

Theorem 1 ([Fenichel, 1979]; reformulation from [Hek, 2010])**.** *Suppose $\mathcal{M}_0 \subset \mathcal{M}$ is compact, possibly with boundary, and normally hyperbolic. Then for $\varepsilon > 0$ and sufficiently small, there exists a manifold $\mathcal{M}_\varepsilon$, $\mathcal{O}(\varepsilon)$ close and diffeomorphic to $\mathcal{M}_0$, that is locally invariant under the flow of the full problem (1.1).*

Theorem 2 ([Fenichel, 1979]; reformulation from [Hek, 2010])**.** *Suppose $\mathcal{M}_0 \subset \mathcal{M}$ is compact, possibly with boundary, and normally hyperbolic. Then for $\varepsilon > 0$ and sufficiently small, there exist manifolds $\mathcal{W}_s(\mathcal{M}_\varepsilon)$ and $\mathcal{W}_u(\mathcal{M}_\varepsilon)$, that are $\mathcal{O}(\varepsilon)$ close and diffeomorphic to $\mathcal{W}_s(\mathcal{M}_0)$ and $\mathcal{W}_s(\mathcal{M}_0)$, respectively, and that are locally invariant under the flow of (1.1).*

Therefore, near normally hyperbolic sets of $\mathcal{M}$, the dynamics of the full system (1.1) is $\mathcal{O}(\varepsilon)$ close to the dynamics of the limiting problems (1.3) and (1.4). We will address the regions where normal hyperbolicity is lost in a following subsection. However, a quite particular feature of fast-slow systems written in the standard form (1.1) is that, at the singular limit $\varepsilon = 0$ (1.3), one can identify linear subspaces where the fast dynamics evolve, by $y = const.$ In the following section, we introduce systems in the "non-standard form", where there is no global distinct separation between linear slow and fast subspaces.

1.2 The non-standard form of GSPT

Consider a system of the form

$$w' = B(w)H(w) + \varepsilon P(w, \varepsilon), \tag{1.6}$$

where $w \in \mathbb{R}^k$, $B(w)$ is a $k \times (k-l)$-matrix with column vectors $B^i(w) = (B^i_1(w), \ldots, B^i_k(w))$ with sufficiently smooth functions $B^i : \mathbb{R}^k \to \mathbb{R}, i = 1, ..., k-l$, $H(w) = (H^1(w), \ldots, H^{k-l}(w))$ is a column vector of sufficiently smooth functions $H^i : \mathbb{R}^k \to \mathbb{R}$, $i = 1, \ldots, k-l$, $P(w, \varepsilon) = (P^1(w, \varepsilon), \ldots, P^{k-l}(w, \varepsilon))$ is a column vector of sufficiently smooth functions $P^i : \mathbb{R}^{k+1} \to \mathbb{R}$, $i = 1, \ldots, k-l$, $\varepsilon > 0$ small, and where the prime denotes differentiation with respect to time t. We will further assume that the set given by $\{H(w) = 0\}$ is an l-dimensional differentiable manifold, where $1 \leq l < k$; in this case, (1.6) is a *singular perturbation problem*, see [Wechselberger, 2020, Definition 3.2].

In particular, we will say that system (1.6) is a slow-fast system written in the *non-standard form* of GSPT. Setting $\varepsilon = 0$ in (1.6) gives the k-dimensional layer problem

$$w' = B(w)H(w) \tag{1.7}$$

Equilibria of (1.7) define the critical manifold

$$\mathcal{M} = \left\{ w \in \mathbb{R}^k \mid B(w)H(w) = \mathbb{O}_k \right\}, \tag{1.8}$$

where $\mathbb{O}_k$ denotes the k-dimensional zero vector. The $(k-l) \times (k-l)$ Jacobian matrix of the linearisation of the layer problem (1.7) about $\mathcal{M}$ has l trivial eigenvalues $\lambda_i = 0$, $i = 1, \ldots, l$ and a $k-l$ nontrivial ones, corresponding to the eigenvalues of the $k-l$ square matrix

$$A = \langle \nabla H, B \rangle . \tag{1.9}$$

Non-stationary solutions of (1.7) will be called the *fast fibres*; these solutions are $k-l$ dimensional geometric objects related to their corresponding base points on $\mathcal{M}$. To see the inherent difference between the layer problem (1.3) and the layer problem (1.7), set $n = 1 = m$ in the former and $k = 2$ in the latter; the layer problem (1.3) then becomes one-dimensional and its solutions are horizontal lines in the xy-plane, while the layer problem (1.7) is two dimensional and its solutions are in general curves in the plane; therefore, there are typically no directions in the plane along which solutions of (1.6) are characterised exclusively as fast or slow.

Definition 2 ([Fenichel, 1979]; reformulation from [Wechselberger, 2020])**.** *An l-dimensional (sub)manifold $\mathcal{S} \subset \mathcal{M}$ is called normally hyperbolic if all nontrivial eigenvalues (1.9) have nonzero real part. Such a manifold $\mathcal{S}$ is called attracting if all nontrivial eigenvalues have negative real parts, repelling, if all nontrivial eigenvalues have positive real parts or saddle-type otherwise.*

We emphasise that Theorem 1 and Theorem 2 apply to both the cases of slow-fast systems written in the standard and in the non-standard form of GSPT, see [Fenichel, 1979, Wechselberger, 2020] for more details.

1.3 Hierarchy of timescales and iterative reductions

In this section, we study iterative reductions to critical manifolds due to a hierarchy of timescales. For simplicitly, we will consider three-dimensional systems with three timescales

written in the standard form:

$$x' = f(x, y, z), \tag{1.10a}$$
$$y' = \varepsilon g(x, y, z), \tag{1.10b}$$
$$z' = \varepsilon\delta h(x, y, z), \tag{1.10c}$$

with $\varepsilon, \delta > 0$ sufficiently small. We will say that x is the *fast* variable, y is the *intermediate* variable, and z is the *slow* variable.

At the singular limit $\varepsilon = 0$, the layer problem of (1.10) is

$$x' = f(x, y, z), \tag{1.11a}$$
$$y' = 0, \tag{1.11b}$$
$$z' = 0, \tag{1.11c}$$

The critical manifold $\mathcal{M}_1$ is defined by $f(x, y, z) = 0$. Rescaling time by a factor of ε in (1.10) we obtain the slow formulation

$$\varepsilon\dot{x} = f(x, y, z), \tag{1.12a}$$
$$\dot{y} = g(x, y, z), \tag{1.12b}$$
$$\dot{z} = \delta h(x, y, z), \tag{1.12c}$$

and the reduced flow on $\mathcal{M}_1$ is obtained by setting $\varepsilon = 0$ in (1.12)

$$0 = f(x, y, z), \tag{1.13a}$$
$$\dot{y} = g(x, y, z), \tag{1.13b}$$
$$\dot{z} = \delta h(x, y, z). \tag{1.13c}$$

We will now show that, maybe in contrast to what one would a priori expect, the reduced flow on $\mathcal{M}_1$ can potentially be a slow-fast system written either in the standard or in the non-standard form of GSPT, depending on the properties of the function $f(x, y, z)$ in (1.10a). We will distinguish between two different cases, namely between the case where $\mathcal{M}_1$ can be globally written as a graph of the intermediate variable y over the other two variables x, z, and the case where $\mathcal{M}_1$ can be globally written as a graph of the slow variable z over the other two variables x, y.

Assume that $\mathcal{M}_1$ can be globally written as a graph $y = Y(x, z)$, i.e., without loss of generality, that $f(x, y, z) = -y + Y(x, z)$. Assume further that there exists a set

$$\mathcal{F}_{\mathcal{M}_1} = \{(x, y, z) \in \mathcal{M}_1 \mid \partial_x [Y(x, z)] = 0\}, \tag{1.14}$$

and that $\partial_x^2 [Y(x, z)] \neq 0$ for $(x, y, z) \in \mathcal{F}_{\mathcal{M}_1}$; then, $\mathcal{F}_{\mathcal{M}_1}$ is a *fold* set that separates the normally hyperbolic set

$$\mathcal{S} = \{\partial_x [Y(x, z)] \neq 0\}$$

into the attracting and repelling portions

$$\mathcal{S}^a = \{(x, y, z) \in \mathcal{S} \mid \partial_x [Y(x, z)] < 0\}, \qquad \mathcal{S}^r = \{(x, y, z) \in \mathcal{S} \mid \partial_x [Y(x, z)] > 0\}.$$

Differentiating the algebraic constraint (1.13a) yields

$$-\partial_x \left[f(x,y,z)\right] \dot{x} = \partial_y \left[f(x,y,z)\right] \dot{y} + \partial_z \left[f(x,y,z)\right] \dot{z}$$

Making use of (1.12) and of the fact that $\partial_x \left[f(x,y,z)\right] = \partial_x \left[Y(x,z)\right]$, $\partial_y \left[f(x,y,z)\right] = -1$, $\partial_z \left[f(x,y,z)\right] = \partial_z \left[Y(x,z)\right]$, we obtain the reduced flow on $\mathcal{S}$ as

$$-\partial_x \left[Y(x,z)\right] \dot{x} = -g(x,Y(x,z),z) + \delta \partial_z \left[Y(x,z)\right] h\left(x,Y(x,z),z\right), \tag{1.15a}$$

$$\dot{z} = \delta h\left(x,Y(x,z),z\right). \tag{1.15b}$$

Rescaling time by a factor of $-\left(\partial_x \left[Y(x,z)\right]\right)^{-1}$ in (1.15) gives

$$\dot{x} = -g(x,Y(x,z),z) + \delta \partial_z \left[Y(x,z)\right] h\left(x,Y(x,z),z\right), \tag{1.16a}$$

$$\dot{z} = -\delta \partial_x \left[Y(x,z)\right] h\left(x,Y(x,z),z\right); \tag{1.16b}$$

this transformation reverses the direction of time on $\mathcal{S}^r$ and maintains it on $\mathcal{S}^a$. Away from $\mathcal{F}_{\mathcal{M}_1}$, we have the following observation:

Lemma 1. *Assume that $f(x,y,z) = -y + Y(x,z)$ in (1.10) and consider $\varepsilon, \delta > 0$ sufficiently small. Then, the reduced flow on $\mathcal{S}$, equations (1.16), is a slow-fast system written in the standard form of GSPT.*

Assume now that $\mathcal{M}_1$ can be globally written as a graph $z = Z(x,y)$, i.e., without loss of generality, that $f(x,y,z) = -z + Z(x,y)$. Assume further that there exists a set

$$\mathcal{F}_{\mathcal{M}_1} = \left\{(x,y,z) \in \mathcal{M}_1 \mid \partial_x \left[Z(x,y)\right] = 0\right\}, \tag{1.17}$$

and that $\partial_x^2 \left[Z(x,y)\right] \neq 0$ for $(x,y,z) \in \mathcal{F}_{\mathcal{M}_1}$; then, $\mathcal{F}_{\mathcal{M}_1}$ is a *fold* set that separates the normally hyperbolic set

$$\mathcal{S} = \left\{\partial_x \left[Z(x,y)\right] \neq 0\right\}$$

into the attracting and repelling portions

$$\mathcal{S}^a = \left\{(x,y,z) \in \mathcal{S} \mid \partial_x \left[Z(x,y)\right] < 0\right\}, \qquad \mathcal{S}^r = \left\{(x,y,z) \in \mathcal{S} \mid \partial_x \left[Z(x,y)\right] > 0\right\}.$$

Differentiating the algebraic constraint (1.13a) yields

$$-\partial_x \left[f(x,y,z)\right] \dot{x} = \partial_y \left[f(x,y,z)\right] \dot{y} + \partial_z \left[f(x,y,z)\right] \dot{z}.$$

Making use of (1.12) and of the fact that now $\partial_x \left[f(x,y,z)\right] = \partial_x \left[Z(x,y)\right]$, $\partial_y \left[f(x,y,z)\right] = \partial_y \left[Z(x,y)\right]$, $\partial_z \left[f(x,y,z)\right] = -1$, we obtain the reduced flow on $\mathcal{S}$ as

$$-\partial_x \left[Z(x,y)\right] \dot{x} = \partial_y \left[Z(x,y)\right] g(x,y,Z(x,y)) - \delta h\left(x,y,Z(x,y)\right), \tag{1.18a}$$

$$\dot{y} = g\left(x,y,Z(x,y)\right). \tag{1.18b}$$

Rescaling time by a factor of $-\left(\partial_x \left[Z(x,y)\right]\right)^{-1}$ in (1.18) gives

$$\dot{x} = \partial_y \left[Z(x,y)\right] g(x,y,Z(x,y)) - \delta h\left(x,y,Z(x,y)\right), \tag{1.19a}$$
$$\dot{y} = -\partial_x \left[Z(x,y)\right] g\left(x,y,Z(x,y)\right). \tag{1.19b}$$

this transformation reverses the direction of time on $\mathcal{S}^r$ and maintains it on $\mathcal{S}^a$. Using the the formulation of (1.6), we can write

$$w' = B(w)H(w) + \delta P(w,\delta),$$

where

$$w = \begin{pmatrix} x \\ y \end{pmatrix}, \quad B(w) = \begin{pmatrix} \partial_y \left[Z(x,y)\right] \\ -\partial_z \left[Z(x,y)\right] \end{pmatrix}, \quad P(w,\delta) = \begin{pmatrix} h\left(x,y,Z(x,y)\right) \\ 0 \end{pmatrix},$$
$$H(w) = g(x,y,Z(x,y)).$$

Away from $\mathcal{F}_{\mathcal{M}_1}$, we therefore have the following observation:

Lemma 2. *Assume that $f(x,y,z) = -z + Z(x,y)$ in (1.10) and consider $\varepsilon, \delta > 0$ sufficiently small. Then, the reduced flow on $\mathcal{S}$, equations (1.19), is a slow-fast system written in the non-standard form of GSPT.*

Therefore, although the full system (1.10) is written in the standard form of GSPT, it is possible that the reduced flow on the slow manifold $\mathcal{M}_1$ is a slow-fast system in the non-standard form of GSPT.

In following Chapters we will see that the above observations are relevant in applications from the natural sciences where, either the intermediate and slow variables are swapped based on the choice of the parameters of the system, see Hodgkin-Huxley equations in Chapter 4, or the critical manifold $\mathcal{M}_1$ is simply the union of disjoint surfaces, and each expressed as the graph of a different variable over the others, see a model for the El-Niño Southern Oscillation phenomenon in Chapter 5

The analysis presented here is focused on the reduced flow on normally hyperbolic regions of $\mathcal{M}_1$, which is a slow-fast system itself for $\delta > 0$ sufficiently small. The existence of additional, one-dimensional critical manifolds at the double singular limit $\varepsilon = 0 = \delta$, as well as the existence of corresponding slow manifolds for $\varepsilon, \delta > 0$ is studied in [Cardin and Teixeira, 2017]. In Chapter 2 we outline an alternative approach to showing the existence and investigating the stability of these manifolds.

In Section 1.4 below, we outline how the the sets $\mathcal{F}_{\mathcal{M}_1}$ where normal hyperbolicity is lost are treated using the geometric desingularisation technique known as "blow-up".

1.4 Non-hyperbolic sets and geometric desingularisation

At subsets where normal hyperbolicity is lost, one can "gain" hyperbolicity by a proper change of coordinates; a typical choice is a transformation that "blows-up" degenerate sets to higher dimensional objects, e.g. points are blown-up to hyperspheres, lines are blown-up to

hypercylinders, etc. This technique originates from the field of algebraic geometry, and has been widely used to resolve singularities in non-linear dynamical systems, see for instance [Anosov et al., 1997].

This method was first used in the slow-fast context by Dumortier and Roussarie in [Dumortier et al., 1996], and was later formulated in an *entry-*, *rescaling-*, *exit-*chart form in [Krupa and Szmolyan, 2001a, Krupa and Szmolyan, 2001b, Krupa and Szmolyan, 2001c, Szmolyan and Wechselberger, 2001, Szmolyan and Wechselberger, 2004] and other works, to mention but a few.

As described above, the main idea is that degeneracies at sets $\mathcal{F}_{\mathcal{M}}$ where normal hyperbolicity of a critical manifold $\mathcal{M}$ is lost, recall (1.14) and (1.17), can be resolved by replacing these sets by higher dimensional manifolds. To outline the method, here we will consider the case where the nonhyperbolic set is a point, replaced by a hypersphere.

Consider a vector field

$$\dot{w} = f(w),$$

where $w \in \mathbb{R}^k$ and $f : \mathbb{R}^k \to \mathbb{R}^k$ smooth, and assume that $w = 0$ is a nonhyperbolic point; in particular, for the sake of simplicity, assume that the Jacobian matrix of the linearisation about the origin is a nilpotent matrix. Consider now a transformation

$$\begin{aligned} \Phi : B &\to \mathbb{R}^k, \\ (r, \bar{w}_1, \cdots, \bar{w}_k) &\mapsto (r^{a_1}\bar{w}_1, \cdots, r^{a_k}\bar{w}_k); \end{aligned} \tag{1.20}$$

here, $B = [0, \infty) \times \mathbb{S}^{k-1}$ and $\mathbb{S}^{k-1} = \left\{(\bar{w}_1, \ldots, \bar{w}_k) \in \mathbb{R}^k \mid \sum_{j=1}^k \bar{w}_j^2 = 1\right\}$, and $(a_1, \ldots, a_k) \in \mathbb{N}^k$. The map Φ is a diffeomorphism for $r > 0$, and its inverse *"blows-up"* the origin in $\mathbb{R}^k$ to $\{0\} \times \mathbb{S}^{k-1}$ or, alternatively viewed, replaces it by the real projective space $\mathbb{RP}^{k-1}$ [Anosov et al., 1997]. Denoting by X the vector field defined by $\dot{w} = f(w)$, a vector field $\bar{X}$ is defined on B via $\Phi_* \bar{X} = X$, where Φ_* is the push-forward induced by Φ. The corresponding commutative diagram is illustrated in Figure 1.1 (a).

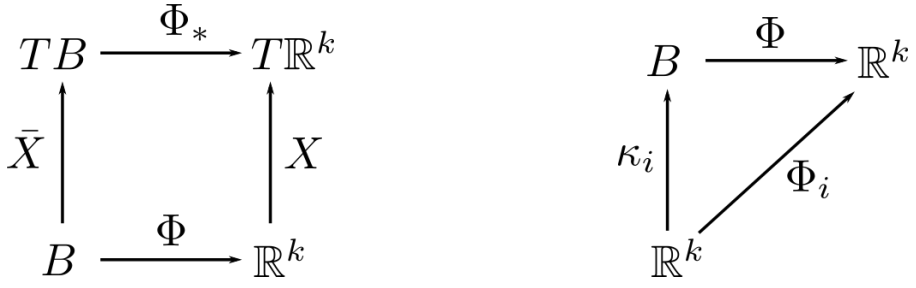

Figure 1.1: Commutative diagrams for the general blow-up method (a) for the induced vector field, (b) for the directional charts κ_i.

Instead of using spherical coordinates to study the dynamics of the vector field $\bar{X}$ on $\mathbb{S}^{k-1}$, it is typically more convenient to use *directional charts*

$$\kappa_i : B \to \mathbb{R}^k, \quad \text{with} \quad i \in I, \quad B = \bigcup_i B_i,$$

and then the map Φ induces vector fields X_i on B_i for all $i \in I$. The *directional blow-ups* Φ_i, $i = 1, \ldots, 2k$, are then obtained by setting $\bar{w}_i = \pm 1$, $i = 1, \ldots, 2k$ in (1.20), and the directional charts κ_i, $i = 1, \ldots, 2k$, are defined such that the diagram in Figure 1.1 (b) commutes. The charts κ_i then cover $\mathbb{S}^k$ by planes perpendicular to the axes, and in every chart κ_i, the blown-up vector field $\bar{X}$ is described by a vector field X_i [Szmolyan and Wechselberger, 2001].

We will now illustrate the above idea for the simple case of the planar fold point from [Krupa and Szmolyan, 2001a]. Consider the two-dimensional slow-fast system

$$x' = -y + x^2 \tag{1.21a}$$
$$y' = -\varepsilon \tag{1.21b}$$

which is obtained by setting $n = 1 = m$, $f(x, y, \varepsilon) = -y + x^2$ and $g(x, y, \varepsilon) = -1$ in (1.1). The critical manifold is given by $\mathcal{M} = \{y = x^2\}$. At the origin, there holds that

$$f(0, 0, 0) = 0, \qquad f_x(0, 0, 0) = 0,$$

therefore $\mathcal{M}$ is not normally hyperbolic there.

One can then augment system (1.21) by including ε as a dynamic variable

$$x' = -y + x^2, \tag{1.22a}$$
$$y' = -\varepsilon, \tag{1.22b}$$
$$\varepsilon' = 0 \tag{1.22c}$$

and consider a transformation $\Phi : B \to \mathbb{R}^3$,

$$x = r\bar{x}, \quad y = r^2\bar{y}, \quad \varepsilon = r^3\bar{\varepsilon}, \tag{1.23}$$

where $B = [0, \infty) \times \mathbb{S}^2$, $\mathbb{S}^2 = \{(\bar{x}, \bar{y}, \bar{\varepsilon}) \in \mathbb{R}^3 \mid \bar{x}^2 + \bar{y}^2 + \bar{\varepsilon}^2 = 1\}$. The map Φ is a diffeomorphism for $r > 0$, and its inverse blows-up the origin in $\mathbb{R}^3$ to a hypershpere as shown in Figure 1.2. Denoting by X the vector field defined by (1.22), a vector field $\bar{X}$ is defined on B via $\Phi_* \bar{X} = X$, where Φ_* is the push-forward induced by Φ.

The directional charts κ_1 and κ_3 are then obtained by setting $\{\bar{y} = 1\}$ and $\{\bar{x} = 1\}$, respectively, and they describe the dynamics in neighbourhood of parts of the equator $\{\bar{\varepsilon} = 0\}$; they are called the *entry* and *exit* chart, respectively. The chart κ_2, obtained by setting $\{\bar{\varepsilon} = 1\}$, describes a neighbourhood of the upper hemisphere, and is called the *rescaling* chart. The corresponding directional blow-up transformation $\Phi_i : \mathbb{R}^3 \to \mathbb{R}^3$ in each chart κ_i is given by

$$\kappa_1 : \qquad x = r_1 x_1, \qquad y = r_1^2, \qquad \varepsilon = r_1^3 \varepsilon_1, \tag{1.24a}$$
$$\kappa_2 : \qquad x = r_1 x_1, \qquad y = r_1^2 y_1, \qquad \varepsilon = r_1^3, \tag{1.24b}$$
$$\kappa_3 : \qquad x = x_1, \qquad y = r_1^2 y_1, \qquad \varepsilon = r_1^3 \varepsilon_1. \tag{1.24c}$$

The transformations (1.24a), (1.24b), and (1.24c) are then inserted in (1.22), and three individual systems are obtained. Once the dynamics in each one of these systems has been resolved, they can be glued together via the changes of coordinates

- $\kappa_{12} : \kappa_1 \to \kappa_2$,

$$x_2 = x_1 \varepsilon_1^{-1/3}, \qquad y_2 = \varepsilon_1^{-2/3}, \qquad r_2 = r_1 \varepsilon_1^{1/3}, \tag{1.25}$$

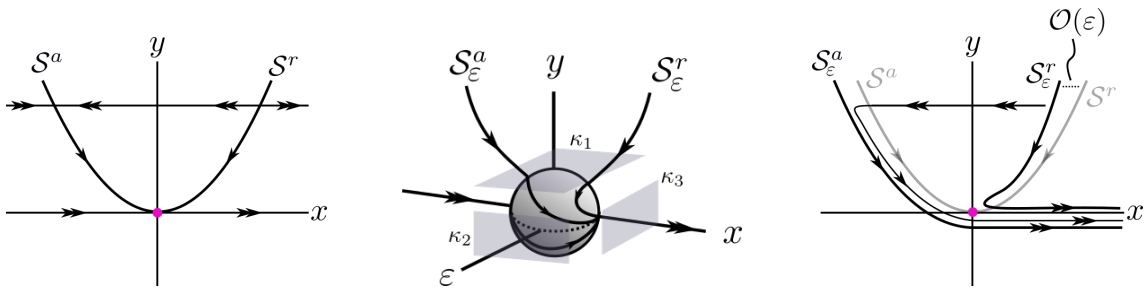

(a) (b) (c)

Figure 1.2: Blow-up analysis of the planar fold point of (1.22). Panel (a) illustrates the geometry of (1.22) at the singular limit $\varepsilon = 0$, where the system admits a critical manifold $\mathcal{M}$ which is normally hyperbolic at $\mathcal{S} = \mathcal{S}^a \cup \mathcal{S}^r$ but not a the origin. Panel (b) illustrates the sphere $\mathbb{S}^2$ introduced by the transformation (1.23) and the relevant directional charts κ_1, κ_2, κ_3 to cover the dynamics. Panel (c) illustrates the dynamics of the "perturbed" system (1.22) with $\varepsilon > 0$ small.

- $\kappa_{23} : \kappa_2 \to \kappa_3$,

$$r_3 = r_2 y_2^{-1/2}, \qquad y_3 = y_2 x_2^{-2}, \qquad \varepsilon_3 = x_2^{-3}, \tag{1.26}$$

which follow easily from (1.24), and then the global picture of the original system (1.22) is obtained, cf. Figure 1.2 and see [Krupa and Szmolyan, 2001a] for details.

Some examples of desingularisation of higher dimensional objects, where, for instance, lines are blown-up to hypercylinders, are included in [Szmolyan and Wechselberger, 2004, Kosiuk and Szmolyan, 2016]. For the rest of this section, we focus on the phenomena that can occur near such sets in three-dimensional slow-fast systems with one fast variable and two slow ones, before addressing systems with three-timescales in Chapter 2.

1.5 Relaxation oscillations in $\mathbb{R}^3$

In this section we discuss two-timescale relaxation oscillations (ROs) in three-dimensional systems in the formulation of [Szmolyan and Wechselberger, 2004]. Relaxation oscillations are a type of nonlinear oscillations that, in two-timescale systems, consist of alternating fast and slow segments, cf. Figure 1.3 panel (b). To this end, we recall system (1.10) with $\delta = 1$ and $\varepsilon > 0$ sufficiently small therein, so that it has one fast variable x and two slow variables (y, z); this yields

$$x' = f(x, y, z) \tag{1.27a}$$
$$y' = \varepsilon g(x, y, z) \tag{1.27b}$$
$$z' = \varepsilon h(x, y, z) \tag{1.27c}$$

In the following, we outline the necessary assumptions on (1.27) so that the system features relaxation oscillations, as described in [Szmolyan and Wechselberger, 2004]

Assumption 1. *The critical manifold $\mathcal{S}$ is S-shaped, i.e.*

$$\mathcal{S} = \mathcal{S}^{a^-} \cup \mathcal{L}^- \cup \mathcal{S}^r \cup \mathcal{L}^+ \cup \mathcal{S}^{a^+}$$

with attracting outer branches

$$\mathcal{S}^{a^\mp}, \mathcal{S}^{a^-} \cup \mathcal{S}^{a^+} := \{(x,y,z) \in \mathcal{S} \mid f_x(x,y,z) < 0\}$$

a repelling branch

$$\mathcal{S}^r := \{(x,y,z) \in \mathcal{S} \mid f_x(x,y,z) > 0\}$$

and fold-curves

$$\mathcal{L}^\mp, \mathcal{L}^- \cup \mathcal{L}^+ := \{(x,y,z) \in \mathcal{S} \mid f_x(x,y,z) = 0,\ f_{xx}(x,y,z) \neq 0\}\,.$$

A fairly simple and typical example of a function on the RHS of (1.27a) that satisfies Assumption 1 is $f(x,y,z) = -y + f_2 x^2 + f_3 x^3$, with $f_2 < 0$, $f_3 > 0$; the fold lines are then given by $\mathcal{L}^- = \{x = 0\}$, $\mathcal{L}^+ = \{x = -2f_2/(3f_3)\}$, and separate $\mathcal{S}^r$ from $\mathcal{S}^{a^-}$ and $\mathcal{S}^{a^+}$ respectively, see Figure 1.3.

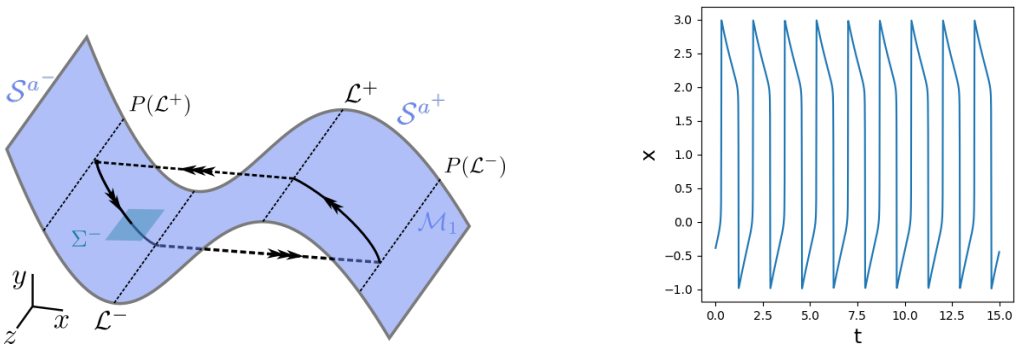

(a) (b)

Figure 1.3: Schematic illustration of the emergence of relaxation oscillation trajectories in (1.27). (a) singular geometry and singular cycle, (b) corresponding time series.

Assumption 2. *The fold-curves $\mathcal{L}^\mp$ are given as graphs $(x^\mp(z), y^\mp(z), z)$, $z \in I^\mp$ for certain intervals $I^\mp$. The points $p \in \mathcal{L}^\mp$ of the fold curves are jump points, i.e.*

$$l(p) := \begin{pmatrix} f_y \\ f_z \end{pmatrix} \cdot \begin{pmatrix} g \\ h \end{pmatrix} \Bigg|_{p \in \mathcal{L}^\mp} \neq 0 \tag{1.28}$$

and the reduced flow near the fold-curves is directed towards the fold-curves.

Equation (1.28) is called the *transversality condition* or the *normal switching condition*, and its interpretation is that the projection of the reduced flow onto the yz-plane is not tangent to $\mathcal{L}^\mp$.

We denote by $P(\mathcal{L}^\mp) \subset \mathcal{S}^{a^\pm}$ the projection along the fast fibres of the fold-curve $\mathcal{L}^\mp$ on the corresponding opposite attracting branch $\mathcal{S}^{a^\pm}$.

Assumption 3. *The reduced flow is transversal to the curve* $P\left(\mathcal{L}^{\mp}|_{I^{\mp}}\right) \subset \mathcal{S}^{a^{\pm}}$.

We now introduce the concept of *singular orbits* or *candidate trajectories*. Such orbits are piecewise smooth curves that consist of slow segments $\Gamma_a^{\mp} \subset \mathcal{S}^{a^{\mp}}$ that are solutions of the reduced flow on $\mathcal{S}^{a^{\mp}}$, recall (1.16), and of fast segments $\Gamma_f^{\mp}$ that connect the above slow segments from $\mathcal{L}^{\mp}$ to $P\left(\mathcal{L}^{\mp}\right)$.

Assumption 4. *There exists a singular periodic orbit* $\Gamma = \Gamma_a^- \cup \Gamma_f^- \cup \Gamma_a^+ \cup \Gamma_f^+$.

Therefore, in order to have a trajectory with slow and fast segments in the perturbed system (1.27) with $\varepsilon > 0$ small, the existence of a singular periodic orbit with such segments needs to be established at the limit $\varepsilon = 0$. The final assumption, which concerns this periodic orbit is that:

Assumption 5. *The singular periodic orbit* Γ *is hyperbolic.*

The hyperbolicity property is with respect to a one-dimensional map $\pi^- : \Sigma^- \to \Sigma^-$ induced by the reduced flow on $\mathcal{S}^{a^{\mp}}$, see Section 2.3 and [Szmolyan and Wechselberger, 2004] for details. In essence, it means that, locally, Γ is either the α- or the ω-set of nearby singular trajectories.

Assumption 1 to Assumption 5 are illustrated in Figure 1.3, and yield the following result.

Theorem 3 ([Szmolyan and Wechselberger, 2004])**.** *Assume that system (1.27) satisfies Assumption 1 to Assumption 5. Then there exists a locally unique, hyperbolic relaxation orbit of system (1.27) close to the singular orbit* Γ *for sufficiently small values of* ε.

The result outlined here concerns two-timescale relaxation oscillations in inherently two-timescale systems of the form (1.27) with $\varepsilon > 0$ sufficiently small, or, equivalently, of (1.10) with $\varepsilon > 0$ sufficiently small and $\delta = 1$. In Chapter 2, using Theorem 3, we will show that such cycles can exist in inherently three-timescale systems of the form of (1.10) with $\varepsilon, \delta > 0$ sufficiently small.

1.6 Folded singularities and canards in $\mathbb{R}^3$

Consider system (1.27) and assume that at the origin there holds that

$$l(0,0,0) = 0,$$

recall the transversality condition (1.28). The origin is then called a *canard point*, see [Szmolyan and Wechselberger, 2001]. System (1.27) can be locally written as

$$\varepsilon \dot{x} = y + x^2 + \mathcal{O}\left(y^2, x, x^3, xyz\right), \tag{1.29a}$$

$$\dot{y} = cx + bz + \mathcal{O}\left(y, (x+z)^2\right), \tag{1.29b}$$

$$\dot{z} = a + \mathcal{O}\left(x + y + z\right); \tag{1.29c}$$

it can be easily seen that, at the singular limit $\varepsilon = 0$, it has a critical manifold $\mathcal{S} = \mathcal{S}^a \cup \mathcal{S}^r$, where $\mathcal{S}^a = \{x < 0\}$, $\mathcal{S}^r = \{x > 0\}$. For $\varepsilon > 0$ sufficiently small, $\mathcal{S}^{a,r}$ perturb to locally invariant slow manifolds $\mathcal{S}_\varepsilon^{a,r}$.

The reduced flow on $\mathcal{S}$ is given by

$$\dot{x} = cx + bz + \mathcal{O}\left((x+z)^2\right), \tag{1.30a}$$
$$\dot{z} = -2ax + \mathcal{O}(xz, x^2), \tag{1.30b}$$

recall (1.16), and it reverses orientation on $\mathcal{S}^r$ and maintains it on $\mathcal{S}^a$.

Lemma 3. *For $c < 0$, the origin is an equilibrium of the desingularised system (1.30a) of the following type*

$$\begin{array}{ccc} ab < 0, & \lambda_1 < 0 < \lambda_2, & \text{saddle}, \\ ab = 0, & \lambda_1 < 0 = \lambda_2, & \text{saddle-node}, \\ 0 < 8ab < c^2, & \lambda_1 < \lambda_2 < 0, & \text{node}, \\ 8ab = c^2, & \lambda_1 = \lambda_2 < 0, & \text{degenerate node}, \\ c^2 < 8ab, & \Re\{\lambda_i\} < 0, & \text{focus}. \end{array} \tag{1.31}$$

Phase portraits of some of the equibria outlined in Lemma 3 are illustrated in Figure 1.4. The orbits Γ_1 illustrated therein are the unique solutions that correspond to the strong stable manifold (or *the* stable manifold, in case of a folded saddle) that passes through the origin in each case. Solutions of the reduced problem passing through a canard point from an attracting critical manifold to a repelling critical manifold are called *singular canards* [Szmolyan and Wechselberger, 2001]. Moreover, the intersections of the slow manifolds $\mathcal{S}_\varepsilon^{a,r}$ are called *maximal canards*. Note that FSN I corresponds to the case where $a \neq 0$, $b = 0$, and FSN II corresponds to the case where $a = 0$, $b \neq 0$, while there exists also the type of FSN III which assumes slightly different structure in (1.29), see [Roberts et al., 2015] for details.

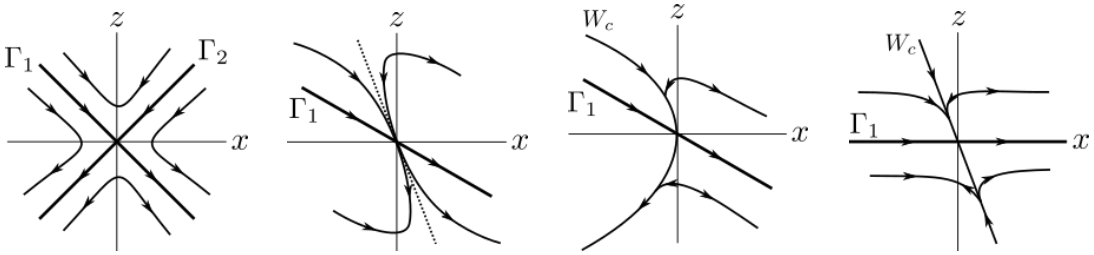

(a) folded saddle (b) folded node (c) FSN I (d) FSN II

Figure 1.4: Phase portraits of (1.30a), in accordance with the classification of Lemma 3.

Of interest in this work will be folded nodes (FN), and folded saddle-nodes of type II (FSN II), due to the existence of maximal canards in the perturbed system $\varepsilon > 0$ sufficiently small. In the case of FN, the singular strong canard Γ_1 always perturbs to a maximal strong canard solution for $\varepsilon > 0$ sufficiently small. Moreover, the singular canard solution corresponding to the weak eigendirection perturbs to a maximal weak canard for $\varepsilon > 0$ sufficiently small, provided that $\mu_2 := \lambda_s/\lambda_w \notin \mathbb{N}$, where λ_s and λ_w are the strong and weak eigenvalues of the canard point, respectively; see [Szmolyan and Wechselberger, 2001].

In the case of FSN II, the singular strong canard Γ_1 always perturbs to a maximal strong canard solution for $\varepsilon > 0$ sufficiently small. Moreover, the singular canard solution corresponding to the weak eigendirection perturbs to a maximal weak canard for $\varepsilon > 0$ sufficiently small, under additional conditions on a, b, c, see [Krupa and Wechselberger, 2010] for details.

The existence of maximal canards is of interest because, when trajectories approach their vicinity, the latter can potentially undergo small-amplitude oscillations (SAOs), before they escape following the fast flow. In the FN case, depending on the values of a, b, c, trajectories are trapped in *sectors of weak canards*, which determine the number of SAOs [Wechselberger, 2005]. In the FSN II case, trajectories undergo bifurcation delay, which can result in a different kind of SAOs [Krupa and Wechselberger, 2010]. The above, combined with appropriate *return mechanisms*, could lead to *mixed-mode oscillations* (MMOs), i.e. trajectories that consist of alternating SAOs and large amplitude oscillations (LAOs); MMOs have been extensively studied in the two timescale setting and some representative works include [Wechselberger, 2005, Brøns et al., 2006, Krupa et al., 2008, Desroches et al., 2012], to mention but a few.

The theory of MMOs in systems with three timescales, which is the main focus of this work, is relatively recent and less well-developed; some examples include [Vo et al., 2013, De Maesschalck et al., 2016, Desroches and Kirk, 2018]. In [Letson et al., 2017], a novel type of folded singularity is introduced via a local analysis of a variation of (1.29), where z is assumed to evolve on a slower timescale; this singularity is called the *canard-delayed-Hopf* singularity (CDH), and features characteristics of both a(n) FN and a(n) FSN II. By extending the local system studied in [Letson et al., 2017] to include global return mechanisms that allow MMOs, in Chapter 2 we study the properties of MMOs in the three-timescale setting, as well as any effect that these additional terms might have locally, extending some results from [Letson et al., 2017]. In Chapter 3 and Chapter 4, we show how the theory that we develop in Chapter 2 can be used to explain documented behaviours of the Koper model from chemical kinetics and the Hodgkin-Huxley equations from mathematical neuroscience, respectively, and in Chapter 5 we show how this theory can be used or extended in order to gain a priori insight on the behaviour of a system modelling the El Niño Southern Oscillation phenomenon.

Chapter 2

Three-timescale systems: an extended prototypical example

2.1 Introduction

The main purpose of this work is to understand the mechanisms that produce different MMO behaviours in three-timescale systems, motivated by systems from applications, like the Koper model from chemical kinetics Chapter 3 and the Hodgkin-Huxley equations from mathematical neuroscience Chapter 4. To this end, a natural first step would be to consider the prototypical three-timescale system introduced in [Krupa et al., 2008]

$$\varepsilon\dot{x} = -y + f_2x^2 + f_3x^3, \tag{2.1a}$$
$$\dot{y} = x - z, \tag{2.1b}$$
$$\dot{z} = \varepsilon\left(\mu + \phi(x, y, z)\right), \tag{2.1c}$$

and investigate whether it can capture the dynamics of these two systems. As became apparent a posteriori, however, system (2.1) is not general enough in order to successfully capture the dynamics of these systems. Therefore, here we introduce an *extended prototypical example*, which, as will become apparent, captures the geometric mechanisms that are responsible for the various different qualitative behaviours and transitions between them in the aforementioned systems from applications.

In particular, we introduce the family of three-dimensional singularly perturbed systems of the form

$$\varepsilon\dot{x} = -y + f_2x^2 + f_3x^3 =: f(x, y, z), \tag{2.2a}$$
$$\dot{y} = \alpha x + \beta y - z =: g(x, y, z), \tag{2.2b}$$
$$\dot{z} = \delta\left(\mu + \phi\left(x, y, z\right)\right) =: \delta h(x, y, z), \tag{2.2c}$$

with f_2, ε, and δ positive and f_3 negative; moreover, $\phi : \mathbb{R}^3 \to \mathbb{R}$ is a smooth function in (x, y, z) that will be specified further in the following. When ε and δ are sufficiently small, Equation (2.2) exhibits dynamics on three distinct timescales; the variables x, y, and z are then called the *fast*, *intermediate*, and *slow variables*, respectively. Correspondingly, Equations (2.2a), (2.2b), and (2.2c) are called the *fast*, *intermediate*, and *slow equations*,

respectively. We remark that the extended prototypical example (2.2) can be viewed as combining the prototypical system (2.1) with the local canonical form

$$x' = y + x^2, \tag{2.3a}$$
$$y' = \varepsilon\left(-\alpha^2 x + \beta y + z\right), \tag{2.3b}$$
$$z' = \varepsilon\delta, \tag{2.3c}$$

introduced in [Letson et al., 2017], which, however, although it features richer local dynamics compared to (2.1) because of the presence of y-terms in (2.3b), it lacks a return mechanism and therefore MMO trajectories are not possible, due to the absence of cubic x-terms in (2.3a).

Our principal aim in this Chapter is a classification of the MMO dynamics in Equation (2.2) in the three-timescale scenario where ε and δ are sufficiently small, on the basis of Fenichel's geometric singular perturbation theory (GSPT) [Fenichel, 1979]. While the underlying local and global mechanisms that can generate SAOs and LAOs, respectively, in singularly perturbed systems of the type in Equation (2.2) are known in the two-timescale context, here we study the combination of those in the context of three-timescales. Our focus is on local and global bifurcations of the resulting MMO trajectories which encode transitions between the corresponding Farey sequences, as illustrated in Figure 1: we construct families of singular cycles for Equation (2.2) in the double singular limit of $\varepsilon = 0 = \delta$; then, we study the persistence of these families for ε and δ sufficiently small, and we show how the MMO dynamics of (2.2) can be classified in dependence of the underlying singular geometries – denoted as "remote", "aligned", or "connected".

One of our main results is the classification of that dynamics for Equation (2.2), as summarised in the bifurcation diagram in Figure 2.1: we identify subregions in the μ-parameter space which correspond to the various Farey sequences illustrated in Figure 1. Moreover, we derive asymptotic approximations for the boundaries between those subregions, which are marked by transitions between the above singular geometries, as well as by bifurcations of the associated fast subsystems; see Section 2.3 for details. Of particular interest here are MMOs that exhibit double epochs of perturbed slow dynamics, as shown in panel (c) of Figure 1; while such MMOs were reported in [Desroches et al., 2012, Curtu and Rubin, 2011] in the context of two-timescale systems, they were found to be highly delicate there [Desroches et al., 2012, Figures 16 and 22], whereas they are relatively robust in the three time-scale context. Our analysis provides a clear geometric explanation for the transition from MMOs with single epochs of SAOs to those with double epochs, as well as for the robustness of the latter. We showcase our results in two examples, the Koper model from chemical kinetics and the Hodgkin-Huxley equations from mathematical neuroscience, in Chapter 3 and Chapter 4, respectively. In particular, the Koper model, Equation (6), has typically been treated as a two-timescale system with one fast and two slow variables, with $\delta = 1$ in (6c); while the corresponding MMO trajectories are induced by a folded node, and are highly regular [Desroches et al., 2012, Guckenheimer and Lizarraga, 2015, Kuehn, 2011], our three-timescale analysis near folded saddle-nodes of type II [Szmolyan and Wechselberger, 2001] in (2.2) uncovers rich MMO dynamics which is not captured by the conventional two-scale approach.

As will become apparent through our analysis, Equation (2.2) exhibits properties of

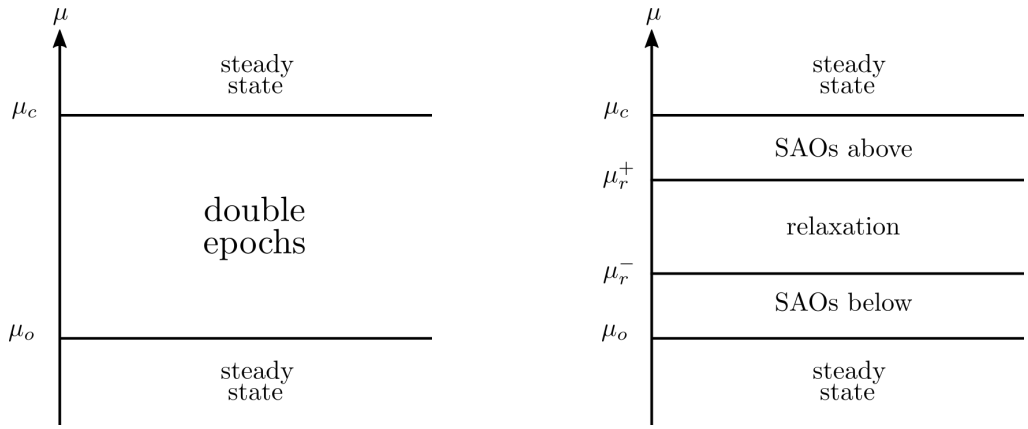

(a) $\frac{\alpha}{\beta} \geq \frac{2f_2^2}{9f_3}$ (b) $\frac{\alpha}{\beta} < \frac{2f_2^2}{9f_3}$

Figure 2.1: Dynamics of Equation (2.2) with f_2, f_3, α, and β fixed and $\varepsilon, \delta > 0$ sufficiently small: the μ-values μ_o, μ_c distinguish between oscillatory dynamics and steady-state behaviour. When $\frac{\alpha}{\beta} \geq \frac{2f_2^2}{9f_3}$, the singular geometry of system (2.2) is such that double epochs of perturbed slow dynamics occur for $\varepsilon, \delta > 0$ sufficiently small, as shown in panel (a). When $\frac{\alpha}{\beta} < \frac{2f_2^2}{9f_3}$, the singular geometry of system (2.2) is such that there exist two values $\mu_r^{\mp}$ which separate MMOs with single epochs of SAOs from relaxation oscillation, in dependence of the properties of $\phi(x, y, z)$ in (2.2c); see panel (b).

both (2.1) and (2.3); however, it captures a plethora of phenomena that are not captured by either of those systems, as discussed in detail in Section 2.3. Specifically, due to the absence of a linear term in y in (2.1b), the intermediate dynamics therein is regular, which implies that the so-called supercritical manifold considered in [Krupa et al., 2008, De Maesschalck et al., 2016] admits no degeneracies; the fact that no cubic x-dependence is present in (2.3a), on the other hand, diminishes the global applicability of results in [Letson et al., 2017] due to the lack of a return mechanism.

The Chapter is organised as follows. In Section 2.2, we describe the geometry of the three-time-scale Equation (2.2) in the double singular limit of $\varepsilon = 0 = \delta$: we define critical and supercritical manifolds; then, we construct families of singular cycles which form the basis for MMO analysis of Equation (2.2). In Section 2.3, we study the singularly perturbed system in (2.2) for ε and δ sufficiently small; we classify the MMO dynamics of (2.2), as illustrated in Figure 1, by establishing a correspondence with the cycles constructed in Section 2.2. We summarise the properties of MMO dynamics in the three-timescale context in Section 2.5. In Section 2.6 we perform a blow-up analysis in the vicinity of the singularity at q^- in accordance with [Letson et al., 2017] and we point out differences in local behaviours between (2.3) and (2.2), due to the presence of cubic terms in (2.2a). In Section 2.7 we analyse the case where the fold point of the supercritical manifold lies on the fold line of the critical manifold, cf. Figure 2.8 panel (b).

2.2 The double singular limit: geometry and singular cycles

In this section, we study the double singular limit of $\varepsilon = 0 = \delta$ in Equation (2.2). To that end, we first describe the singular geometry for $\varepsilon = 0$; then, we consider the resulting flow in the limit of $\delta \to 0$. Finally, we construct singular cycles which will form the basis of MMO trajectories for Equation (2.2) when ε and δ are sufficiently small, as considered in Section 2.3 below.

2.2.1 The critical manifold $\mathcal{M}_1$

For ε sufficiently small and $\delta = \mathcal{O}(1)$ fixed, Equation (2.2) is singularly perturbed with respect to the small parameter ε; in particular, (2.2) describes the dynamics in terms of the *intermediate* time t. Rewriting the governing equations in the fast time $\tau = t/\varepsilon$, we have

$$x' = -y + f_2 x^2 + f_3 x^3, \tag{2.4a}$$
$$y' = \varepsilon\left(\alpha x + \beta y - z\right), \tag{2.4b}$$
$$z' = \varepsilon\delta\left(\mu + \phi\left(x, y, z\right)\right), \tag{2.4c}$$

which is a two-timescale system with one fast variable x and two slow variables y and z. The reduced problem of the above is obtained by setting $\varepsilon = 0$ in (2.2),

$$0 = -y + f_2 x^2 + f_3 x^3, \tag{2.5a}$$
$$\dot{y} = \alpha x + \beta y - z, \tag{2.5b}$$
$$\dot{z} = \delta\left(\mu + \phi\left(x, y, z\right)\right), \tag{2.5c}$$

while the layer problem is found for $\varepsilon = 0$ in (2.4):

$$x' = -y + f_2 x^2 + f_3 x^3, \tag{2.6a}$$
$$y' = 0, \tag{2.6b}$$
$$z' = 0. \tag{2.6c}$$

We will refer to the flow that is induced by the one-dimensional vector field in Equation (2.6) as the *fast flow*; the corresponding trajectories will be denoted as the *fast fibres*. The critical manifold $\mathcal{M}_1$ for (2.2) is a set of equilibria for (2.6), and is given by

$$\mathcal{M}_1 := \left\{(x, y, z) \in \mathbb{R}^3 \;\middle|\; f(x, y, z) = 0\right\} = \left\{(x, y, z) \in \mathbb{R}^3 \;\middle|\; y = F(x)\right\}, \tag{2.7}$$

where we define

$$F(x) = f_2 x^2 + f_3 x^3. \tag{2.8}$$

The manifold $\mathcal{M}_1$ can be written as $\mathcal{M}_1 = \mathcal{S}^a \cup \mathcal{S}^r \cup \mathcal{F}_{\mathcal{M}_1}$, where

$$\mathcal{S}^a = \left\{(x, y, z) \in \mathcal{S} \;\middle|\; \frac{\partial f}{\partial x}(x, y, z) < 0\right\} \quad \text{and} \quad \mathcal{S}^r = \left\{(x, y, z) \in \mathcal{S} \;\middle|\; \frac{\partial f}{\partial x}(x, y, z) > 0\right\}$$

are normally attracting and normally repelling, respectively, whereas $\mathcal{F}_{\mathcal{M}_1}$ is degenerate due to a loss of normal hyperbolicity:

$$\mathcal{F}_{\mathcal{M}_1} := \left\{ (x,y,z) \in \mathcal{M}_1 \;\middle|\; \frac{\partial f}{\partial x}(x,y,z) = 0 \right\} = \left\{ (x,y,z) \in \mathcal{M}_1 \;\middle|\; 2f_2 x + 3f_3 x^2 = 0 \right\}. \quad (2.9)$$

In particular, we may write $\mathcal{F}_{\mathcal{M}_1} = \mathcal{L}^- \cup \mathcal{L}^+$, where

$$\mathcal{L}^- = \left\{ (x,y,z) \in \mathbb{R}^3 \;\middle|\; x = 0 = y \right\} \quad \text{and} \quad \mathcal{L}^+ = \left\{ (x,y,z) \in \mathbb{R}^3 \;\middle|\; x = -\frac{2}{3}\frac{f_2}{f_3},\ y = \frac{4}{27}\frac{f_2^3}{f_3^2} \right\}; \quad (2.10)$$

hence, it follows that $\mathcal{S}^a = \mathcal{S}^{a^-} \cup \mathcal{S}^{a^+}$, with

$$\mathcal{S}^{a^-} = \{ (x,y,z) \in \mathcal{S} \mid x < 0 \} \quad \text{and} \quad \mathcal{S}^{a^+} = \left\{ (x,y,z) \in \mathcal{S} \;\middle|\; x > -\frac{2}{3}\frac{f_2}{f_3} \right\}, \quad (2.11)$$

while

$$\mathcal{S}^r = \left\{ (x,y,z) \in \mathcal{S} \;\middle|\; 0 < x < -\frac{2}{3}\frac{f_2}{f_3} \right\}. \quad (2.12)$$

The set $\mathcal{S}$ therefore consists of a repelling middle sheet S^r and two attracting sheets $S^{a^\mp}$ that meet $\mathcal{S}^r$ along $\mathcal{L}^\pm$, respectively; see Figure 2.2. From the above, it is apparent that $\mathcal{L}^-$ always coincides with the z-axis, whereas variation in f_2 and f_3 translates $\mathcal{L}^+$, therefore "stretching" or "compressing" $\mathcal{M}_1$. (Clearly, variation in α, β and μ has no effect on the geometry of $\mathcal{M}_1$.) Finally, the elements of the sets $\mathcal{Q}^\mp$ defined by

$$\mathcal{Q}^\mp = \left\{ (x,y,z) \in \mathcal{L}^\mp \mid f(x,y,z) = 0 = g(x,y,z) \right\}$$

are called the *folded singularities* of $\mathcal{M}_1$ on $\mathcal{L}^\mp$, respectively [Szmolyan and Wechselberger, 2001]; for (2.2), these sets are the singletons $\mathcal{Q}^- = \{q^-\}$ and $\mathcal{Q}^+ = \{q^+\}$, with

$$x_{q^-} = 0, \quad y_{q^-} = 0, \quad z_{q^-} = 0, \quad (2.13a)$$

$$x_{q^+} = -\frac{2f_2}{3f_3}, \quad y_{q^+} = \frac{4f_2^3}{27f_3^2}, \quad z_{q^+} = \frac{4\beta f_2^3}{27f_3^3} - \frac{2\alpha f_2}{3f_3}.. \quad (2.13b)$$

Finally, we consider the reduced problem on $\mathcal{M}_1$, as given by (2.5), with δ sufficiently small; Equation (2.5) is then singularly perturbed with respect to the small parameter δ, written in the intermediate time t. To classify the folded singularities $q^\mp$ of $\mathcal{M}_1$, we project the flow of (2.5) onto $\mathcal{M}_1$ [Szmolyan and Wechselberger, 2001]: using the algebraic representation of $\mathcal{M}_1$ $f(x,y,z) = 0$, we can apply the chain rule to find

$$-f_x x' = f_y y',$$

where $f_x = (2f_2 x + 3f_3 x^2)$ and $f_y = -1$ from (2.5). We therefore obtain

$$-f_x x' = -\alpha x - \beta F(x) + z, \quad (2.14a)$$

$$z' = \delta\left(\mu + \phi\left(x, F(x), z\right)\right) \quad (2.14b)$$

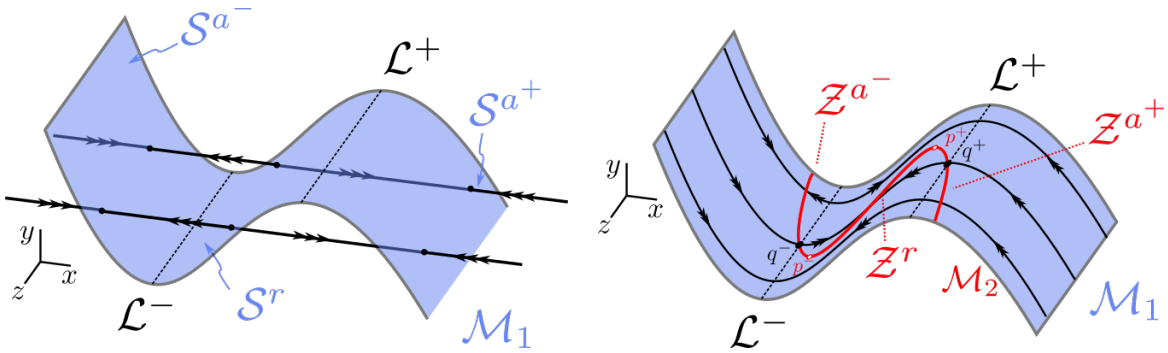

(a) (b)

Figure 2.2: (a) The critical manifold $\mathcal{M}_1$ as the set of equilibria for the fast flow of (2.6); the fast fibres are parallel to the x-direction. (b) The supercritical manifold $\mathcal{M}_2$ as the set of equilibria for the intermediate flow of (2.19); the intermediate fibres are confined to $\mathcal{M}_2$ and evolve on planes with $z = \text{const}$.

or

$$x' = -\alpha x - \beta F(x) + z, \tag{2.15a}$$
$$z' = -\delta f_x \left(\mu + \phi\left(x, F(x), z\right)\right) \tag{2.15b}$$

after a rescaling of time with a factor of f_x, which reverses the direction of the flow on $\mathcal{S}^r$. The folded singularities of Equation (2.2) then correspond to equilibria of (2.15). The eigenvalues of the latter are given by

$$\lambda_{s,w} = \frac{1}{2}\left(-\alpha - \sqrt{\alpha^2 - 8\delta f_2 \mu}\right).$$

Therefore, for $\delta > 0$ sufficiently small, the folded singularities $q^{\mp}$ are *folded nodes* [Szmolyan and Wechselberger, 2001, Letson et al., 2017]. Their strong and weak stable manifolds define "funnel regions" on the corresponding sheets $\mathcal{S}^{a^{\mp}}$, which essentially determine the basins of attraction to $q^{\mp}$ on $\mathcal{S}^{a^{\mp}}$. Here and in the following, we focus on the flow of Equation (2.2) in the vicinity of the fold line $\mathcal{L}^-$; with regard to the strong stable manifold of the folded node q^-, we hence have the following result:

Lemma 4. *Let*

$$\mathcal{G}\left(x_0, x_1; z_0; \mu\right) = \int_{x_0}^{x_1} \frac{F'(\sigma)\left(\mu + \phi\left(\sigma, F(\sigma), z_0\right)\right)}{\alpha\sigma + \beta F(\sigma) - z_0} \mathrm{d}\sigma, \tag{2.16}$$

where F is defined as in (2.8). Then, for δ sufficiently small, the strong stable manifold of the origin in Equation (2.15) can be written as the graph

$$z = \delta \mathcal{G}(0, x; 0, \mu) + \mathcal{O}(\delta^2) \qquad \text{for } x \in I, \tag{2.17}$$

where I is an appropriately defined, fixed interval about $x = 0$.

Proof. Given a trajectory of (2.15) with initial condition (x_0, y_0, z_0) on $\mathcal{S}^{a^\mp}$, i.e., with $y_0 = F(x_0)$, let s denote the displacement in the x-direction of that trajectory under the corresponding flow. Then, in a first approximation, the displacement in the z-direction is given by $\delta\mathcal{G}(x_0, x_0 + s; z_0; \mu)$, where $\mathcal{G}$ is defined as in (2.16); see [Krupa et al., 2008] for details. The result is obtained by setting $x_0 = 0 = z_0$ in the resulting expression, which corresponds to the unique trajectory of (2.15) that passes through the origin. □

An analogous representation can be obtained for the strong stable manifold of the folded node q^+. From the above, we conclude in particular that the funnels of the folded singularities $q^\mp$ are "stretched" as δ decreases. In the limit of $\delta = 0$, $q^\mp$ are *folded saddle-nodes* (FSN); see again Section 1.6 and [Szmolyan and Wechselberger, 2001] for details. In [Letson et al., 2017], this has been identified as a novel FSN singularity and has been distinguished from the other FSN types, because the vanishing parameter δ is independent from ε; this singularity has therefore been called the *canard-delayed-Hopf* singularity (CDH). Locally, the CDH singularity of (2.2) is qualitatively similar to that of (2.3), and we elaborate on the quantitative differences due to the higher order terms in the former, as well as their implications for global phenomena, in Section 2.4 and Section 2.6. For future reference, we note that the associated strong manifolds ("strong canards") correspond to the unique intermediate fibres on $\mathcal{S}^{a^\mp}$ that cross $q^\mp$, respectively, while the corresponding weak manifolds ("weak canards") can be locally approximated by the supercritical manifold $\mathcal{M}_2$ which is introduced in the following subsection [Letson et al., 2017].

2.2.2 The supercritical manifold $\mathcal{M}_2$

We can view the differential-algebraic systems in (2.5) and (2.15) as slow-fast vector fields on $\mathcal{M}_1$. The layer problem corresponding to (2.5) therefore reads

$$0 = -y + f_2x^2 + f_3x^3, \tag{2.18a}$$
$$\dot{y} = \alpha x + \beta y - z, \tag{2.18b}$$
$$\dot{z} = 0 \tag{2.18c}$$

or

$$0 = -y + F(x), \tag{2.19a}$$
$$-f_x x' = -\alpha x - \beta F(x) + z, \tag{2.19b}$$
$$\dot{z} = 0; \tag{2.19c}$$

we will refer to the above as the *intermediate flow*, and to the corresponding trajectories as the *intermediate fibres*; see panel (b) of Figure 2.2.

Rewriting Equation (2.2) in the slow time $s = \delta t$, we have

$$\varepsilon\delta x' = -y + f_2x^2 + f_3x^3, \tag{2.20a}$$
$$\delta y' = (\alpha x + \beta y - z), \tag{2.20b}$$
$$z' = \delta(\mu + \phi(x, y, z)); \tag{2.20c}$$

the reduced system that is obtained from (2.20) is given by

$$0 = -y + F(x), \tag{2.21a}$$
$$0 = \alpha x + \beta F(x) - z, \tag{2.21b}$$
$$z' = \mu + \phi\left(x, F(x), z\right), \tag{2.21c}$$

which we will refer to as the *slow flow* of Equation (2.2). The supercritical manifold $\mathcal{M}_2$ is the set of equilibria for (2.19), and is given by

$$\mathcal{M}_2 := \left\{(x,y,z) \in \mathbb{R}^3 \;\middle|\; f(x,y,z) = 0 = g(x,y,z)\right\} = \left\{(x,y,z) \in \mathcal{M}_1 \;\middle|\; z = G(x)\right\}, \tag{2.22}$$

where we define

$$G(x) = \alpha x + \beta F(x). \tag{2.23}$$

The manifold $\mathcal{M}_2$ can be written as the union $\mathcal{M}_2 = \mathcal{Z} \cup \mathcal{F}_{\mathcal{M}_2}$, where

$$\mathcal{Z} = \left\{(x,y,z) \in \mathcal{M}_2 \;\middle|\; \frac{dg}{dx}\left(x, F(x), G(x)\right) \neq 0\right\} \tag{2.24}$$

is normally hyperbolic, and the set

$$\begin{aligned} \mathcal{F}_{\mathcal{M}_2} :&= \left\{(x,y,z) \in \mathcal{M}_2 \;\middle|\; \frac{dg}{dx}\left(x, F(x), G(x)\right) = 0\right\} \\ &= \left\{(x,y,z) \in \mathcal{M}_2 \;\middle|\; \alpha + 2\beta f_2 x + 3\beta f_3 x^2 = 0\right\} \end{aligned} \tag{2.25}$$

is degenerate. Equation (2.25) implies $\mathcal{F}_{\mathcal{M}_2} = \{p^-, p^+\}$, with

$$p^{\mp} = \left\{(x,y,z) \in \mathcal{M}_2 \;\middle|\; x = x_{p^{\mp}}\right\}, \tag{2.26}$$

where

$$x_{p^{\mp}} = \frac{-\beta f_2 \pm \sqrt{\beta^2 f_2^2 - 3\alpha\beta f_3}}{3\beta f_3}, \quad y_{p^{\mp}} = F\left(x_{p^{\mp}}\right), \quad \text{and} \quad z_{p^{\mp}} = G\left(x_{p^{\mp}}\right). \tag{2.27}$$

The points $p^{\mp}$ are called the fold points of $\mathcal{M}_2$. Equation (2.27) immediately implies

Proposition 1. *The manifold $\mathcal{M}_2$ admits*

1. *exactly two fold points if and only if $\beta^2 f_2^2 - 3\alpha\beta f_3 > 0$;*
2. *exactly one fold point if and only if $\beta^2 f_2^2 - 3\alpha\beta f_3 = 0$; and*
3. *no fold points if and only if $\beta^2 f_2^2 - 3\alpha\beta f_3 < 0$.*

Remark 1. *Under the conditions stated in Proposition 1, the fold points $p^{\mp}$ of $\mathcal{M}_2$ are "inherited" from the fold lines $\mathcal{L}^{\mp}$ of $\mathcal{M}_1$, in the sense that $G(x)$ in (2.22) is a cubic polynomial because $F(x)$ in (2.7) is.*

We note that a necessary (but not sufficient) condition for $\mathcal{M}_2$ to have two fold points is the requirement that $\beta \neq 0$. If $\mathcal{M}_2$ admits two fold points, then the normally hyperbolic portion $\mathcal{Z}$ of $\mathcal{M}_2$ consists of three branches: $\mathcal{Z} = \mathcal{Z}^- \cup \mathcal{Z}^0 \cup \mathcal{Z}^+$, where

$$\begin{gathered}\mathcal{Z}^- = \left\{(x,y,z) \in \mathcal{Z} \mid x < x_p^-\right\}, \quad \mathcal{Z}^+ = \left\{(x,y,z) \in \mathcal{Z} \mid x > x_p^+\right\}, \quad \text{and} \\ \mathcal{Z}^0 = \left\{(x,y,z) \in \mathcal{Z} \mid x_p^- < x < x_p^+\right\}.\end{gathered} \tag{2.28}$$

Proposition 2. *Assume that $\mathcal{M}_2$ admits two fold points, i.e., that $\beta^2 f_2^2 - 3\alpha\beta f_3 > 0$, by Proposition 1. If $\beta < 0$ ($\beta > 0$), then the middle branch $\mathcal{Z}^0$ of $\mathcal{M}_2$ in (2.28) is repelling (attracting) under the flow of Equation (2.19), while the outer branches $\mathcal{Z}^\mp$ of $\mathcal{M}_2$ are attracting (repelling).*

Proof. The statement follows directly from (2.19b), (2.25) and (2.28). □

If $\beta < 0$, we may hence write $\mathcal{Z} = \mathcal{Z}^{a^-} \cup \mathcal{Z}^r \cup \mathcal{Z}^{a^+}$, whereas for $\beta > 0$, we may write $\mathcal{Z} = \mathcal{Z}^{r^-} \cup \mathcal{Z}^a \cup \mathcal{Z}^{r^+}$. We emphasise that Proposition 2 refers to the flow on $\mathcal{M}_1$ before desingularisation, cf. Equations (2.14) and (2.19), whereas the direction of the flow is reversed on $\mathcal{S}^r$ after desingularisation; see (2.15) and Figure 2.2.

Remark 2. *We remark that the above discussion of the stability of $\mathcal{Z}$ in the double singular limit of $\varepsilon = 0 = \delta$ is alternative to the approach outlined in [Cardin and Teixeira, 2017], where x is expressed as a function of y in (2.18b) via the algebraic constraint in (2.18a), as well as to that in [Letson et al., 2017], where only the stability of the partially perturbed counterpart of $\mathcal{Z}$ with $\varepsilon > 0$ small and $\delta = 0$ is investigated; see Section 2.4 for an extension of the latter within the framework of Equation (2.2).*

Remark 3. *By the above, the folded singularities $q^\mp$ of $\mathcal{M}_1$ are located at the intersections between $\mathcal{M}_2$ and $\mathcal{L}^\mp$. In the double singular limit of $\varepsilon = 0 = \delta$, the points $q^\mp$ coincide with the folded singularities of $\mathcal{M}_1$ for $\varepsilon = 0$ and $\delta = \mathcal{O}(1)$, i.e., in the two-timescale limit, which stems from the fact that the fast and intermediate Equations (2.2a) and (2.2b) do not depend on δ in our case.*

2.2.3 Relative geometry

In this subsection, we describe the position of the folded singularities $q^\mp$ of $\mathcal{M}_1$ relative to each other, as well as of the fold points $p^\mp$ of $\mathcal{M}_2$ – assuming that a pair of such points exists – relative to the fold lines $\mathcal{L}^\mp$.

Proposition 3. *Assume that $\mathcal{M}_2$ admits two fold points, i.e., that $\beta^2 f_2^2 - 3\alpha\beta f_3 > 0$, by Proposition 1.*

1. *If $\alpha\beta < 0$, then both fold points of $\mathcal{M}_2$ lie on $\mathcal{S}^r$;*
2. *if $\alpha\beta > 0$, then one fold point of $\mathcal{M}_2$ lies on $\mathcal{S}^{a^-}$, while the other fold point lies on $\mathcal{S}^{a^+}$;*
3. *if $\alpha = 0$, then one fold point of $\mathcal{M}_2$ lies on $\mathcal{L}^-$, while the other fold point lies on $\mathcal{L}^+$.*

Proof. The result follows from a comparison of the values of $x^{\mp}$ in (2.27) with the x-coordinates of $\mathcal{L}^{\mp}$ in the three cases where $\alpha\beta < 0$, $\alpha\beta > 0$, and $\alpha = 0$, respectively. □

The statements of Proposition 2 and Proposition 3 are summarised in Figure 2.3. We remark that the symmetry described in Proposition 3 breaks down when $\mathcal{O}(x^2)$-terms are included in the intermediate Equation (2.2b); see [Desroches and Kirk, 2018] for an example. If $\beta = 0$, then the projection of the critical manifold $\mathcal{M}_2$ onto the (x, z)-plane is a straight line. That case has been studied in [Krupa et al., 2008, De Maesschalck et al., 2014, De Maesschalck et al., 2016]; recall also Equation (2.1).

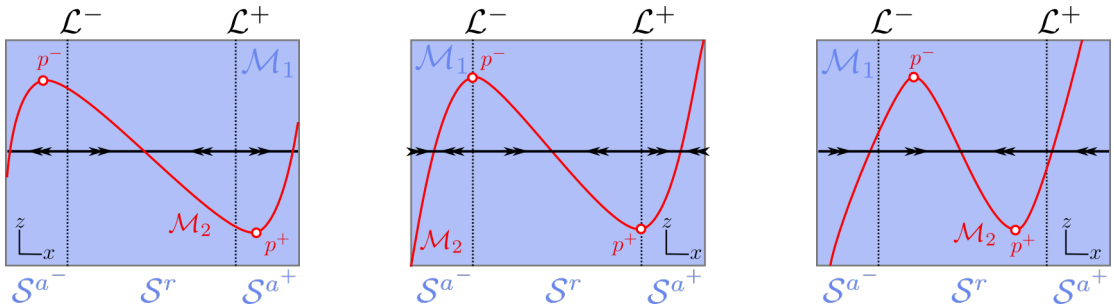

(a) $\beta < 0$, $\alpha < 0$. (b) $\beta < 0$, $\alpha = 0$. (c) $\beta < 0$, $\alpha > 0$.

(d) $\beta > 0$, $\alpha < 0$. (e) $\beta > 0$, $\alpha = 0$. (f) $\beta > 0$, $\alpha > 0$.

Figure 2.3: Projection of the supercritical manifold $\mathcal{M}_2$ and of the fold lines $\mathcal{L}^{\mp}$ of the critical manifold $\mathcal{M}_1$ onto the (x, z)-plane: in dependence on the parameters α and β, the pair of fold points $p^{\mp}$ of $\mathcal{M}_2$ lies either on $\mathcal{S}^r$ (panels (c) and (d)), on $\mathcal{S}^{a^{\mp}}$ (panels (a) and (f)), or on $\mathcal{L}^{\mp}$ (panels (b) and (e)).

We now turn our attention to the location of the folded singularities of $\mathcal{M}_1$ relative to each other and with respect to the fast and intermediate fibres defined previously; recall Figure 2.2. We first define planes that contain the folded singularities and that are perpendicular to the fold lines $\mathcal{L}^-$ and $\mathcal{L}^+$, as follows.

Definition 3. *Denote by $\mathcal{P}^{\mp}$ the planes $\mathcal{P}^{\mp} = \{(x, y, z) \in \mathbb{R}^3 \mid z = z_{q^{\mp}}\}$, where $z_{q^{\mp}}$ are the z-coordinates of the folded singularities $q^{\mp}$ of $\mathcal{M}_1$ on $\mathcal{L}^{\mp}$, respectively. We will refer to $\mathcal{P}^{\mp}$ as* normal planes *in the following.*

Definition 4. *The folded singularities $q^{\mp}$ of $\mathcal{M}_1$ are said to be*

1. *geometrically aligned if $\mathcal{P}^- \equiv \mathcal{P}^+$;*

2. *geometrically connected if they are not aligned and if* $\mathcal{P}^{\mp} \cap \mathcal{Z}^{\pm} \neq \emptyset$*; and*

3. *geometrically remote if they are neither aligned nor connected, i.e., if* $\mathcal{P}^{-} \not\equiv \mathcal{P}^{+}$ *and* $\mathcal{P}^{\mp} \cap \mathcal{Z}^{\pm} = \emptyset$*.*

In dependence of the parameters α, β, f_2, and f_3 in Equation (2.2), we have the following result on the position of q^{-} and q^{+} relative to each other:

Proposition 4.

1. *For* $\alpha\beta < 0$*, the folded singularities* $q^{\mp}$ *of* $\mathcal{M}_1$ *are geometrically aligned if* $\frac{\alpha}{\beta} = \frac{2f_2^2}{9f_3}$*, geometrically connected if* $\frac{\alpha}{\beta} > \frac{2f_2^2}{9f_3}$*, and geometrically remote if* $\frac{\alpha}{\beta} < \frac{2f_2^2}{9f_3}$*.*

2. *For* $\alpha\beta \geq 0$ *with* $\beta \neq 0$*, the folded singularities* $q^{\mp}$ *are geometrically connected.*

3. *For* $\beta = 0$ *with* $\alpha \neq 0$*, the folded singularities* $q^{\mp}$ *are geometrically remote.*

Proof. The statements follow from Equation (2.13), (2.19b), and the properties of $G(x)$ in (2.23); see panels (c) and (d) of Figure 2.3 for cases corresponding to the first statement, and panels (a), (b), (e), and (f) for cases corresponding to the second and third statements. □

In what is to come, we will restrict our attention to the case that is illustrated in panel (c) of Figure 2.3:

Assumption 6. *In the following, we assume that* $\alpha > 0$ *and* $\beta < 0$ *in Equation (2.2).*

Assumption 6 is made for three reasons. First, it is consistent with the Koper model, Equation (6), after transformation to the prototypical Equation (2.2). (In particular, it follows that the scenarios illustrated in panels (b) and (e) of Figure 2.3 cannot be realised in (6).) Second, given $\beta \neq 0$, geometrically remote singularities can only be present when $\alpha\beta < 0$. Third, given Assumption 6, the outer branches of $\mathcal{M}_2$ are attracting, while the middle branch is repelling, which allows for the construction of closed singular periodic orbits ("cycles"), as will become apparent in the following subsection.

2.2.4 Singular cycles

We now consider the reduced flow on $\mathcal{M}_2$. We impose the following assumption on the function $\phi(x, y, z)$ in the slow Equation (2.2c):

Assumption 7. *The function* $\phi(x, y, z)$ *in (2.2c) is such that* $\phi(x_{q^-}, F(x_{q^-}), G(x_{q^-})) = 0$*,* $\phi(x, F(x), G(x)) > 0$ *for* $x < x_{q^-}$*,* $\phi(x_{q^+}, F(x_{q^+}), G(x_{q^+})) \leq 0$*, and* $\phi(x, F(x), G(x)) < 0$ *for* $x > x_{q^+}$*.*

Assumption 7 ensures that the reduced flow on the portion $\mathcal{Z}^{a^{\mp}}$ of $\mathcal{M}_2$ is directed towards the folded singularities $q^{\mp}$ of $\mathcal{M}_1$. We emphasise that the properties of that therefore crucically depend on μ; in particular, we have that for $\mu = 0$, a true global equilibrium of the system coincides with q^{-}; see Section 2.3.

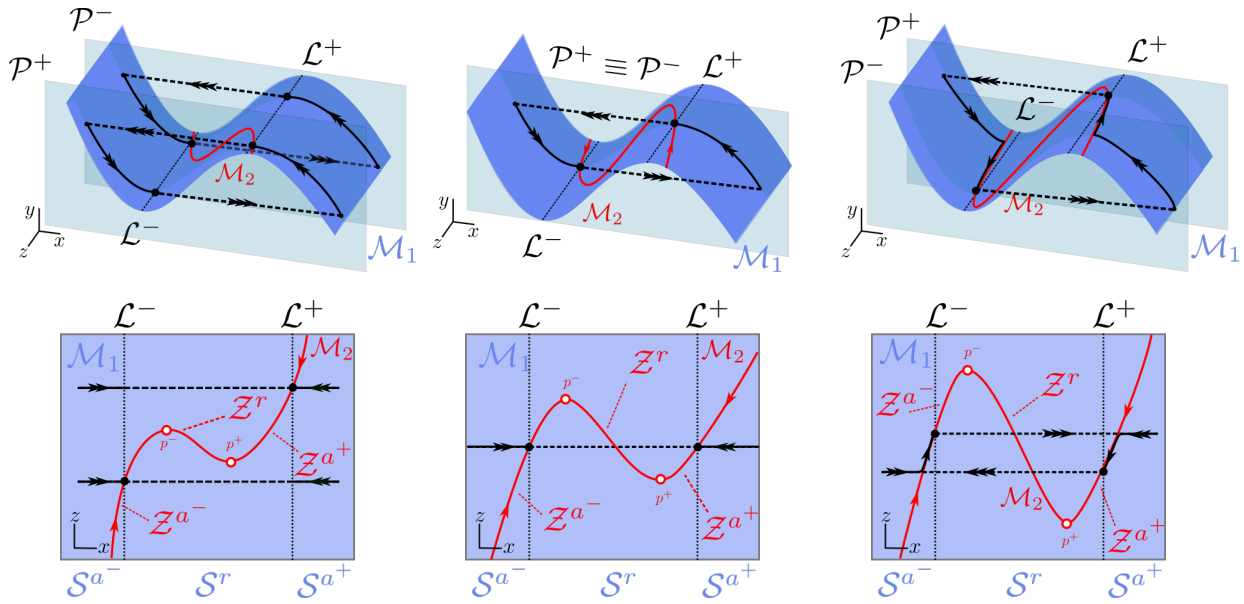

(a) Remote singularities. (b) Aligned singularities. (c) Connected singularities.

Figure 2.4: Relative geometry of the folded singularities $q^{\mp}$ of $\mathcal{M}_1$ according to Definition 4 (top row); bifurcation of the resulting singular cycles, as described in Proposition 5 (bottom row).

Assumption 6 and Assumption 7 together imply the existence of singular cycles in Equation (2.2), the properties of which depend on the relative position of the folded singularities $q^{\mp}$ of $\mathcal{M}_1$, as classified in Proposition 4. (Clearly, the specific choice of $\phi(x, y, z)$ in (2.2c) does not affect that classification.) Here, these cycles are defined as the concatenation of singular orbits for the corresponding limiting systems in (2.6), (2.19), and (2.21), respectively.

Proposition 5. *Assume that Assumption 6 and Assumption 7 hold.*

1. *If the folded singularities $q^{\mp}$ of $\mathcal{M}_1$ are geometrically remote, then there exist a singular cycle evolving on $\mathcal{P}^-$, a singular cycle evolving on $\mathcal{P}^+$, and a family of singular cycles in between; each of the cycles in that family evolves on a plane parallel to $\mathcal{P}^{\mp}$ that lies between $\mathcal{P}^-$ and $\mathcal{P}^+$. These cycles are "two-scale", in the sense that the singular dynamics on them alternates between the fast timescale and the intermediate timescale (on $\mathcal{M}_1 \backslash \mathcal{M}_2$).*

2. *If $q^{\mp}$ are geometrically aligned, then there there exists exactly one singular cycle that evolves on the plane $\mathcal{P} := \mathcal{P}^- \equiv \mathcal{P}^+$. This cycle is "two-scale", in the sense that the singular dynamics on it alternates between the fast timescale and the intermediate timescale (on $\mathcal{M}_1 \backslash \mathcal{M}_2$).*

3. *If $q^{\mp}$ are geometrically connected, then there exists exactly one singular cycle that evolves on a subset of $\mathcal{P}^- \cup \mathcal{Z}^{a-} \cup \mathcal{P}^+ \cup \mathcal{Z}^{a+}$. This cycle is "three-scale", in the sense that the singular dynamics on it alternates between the fast timescale, the intermediate timescale (on $\mathcal{M}_1 \backslash \mathcal{M}_2$), and the slow timescale (on $\mathcal{M}_2$).*

Definition 4 and Proposition 5 are summarised in Figure 2.4, where we recall that the fast, intermediate, and slow dynamics are given by the limiting systems in (2.6), (2.19), and (2.21), respectively.

From the fact that (2.2) and (2.15) are slow-fast systems in the standard form of GSPT, the definition of the "geometric connection" or lack thereof in the sense of Definition 4 combined with Proposition 5 lead to the definition of "orbital connection" or lack thereof as follows:

Definition 5.

1. *The folded singularities $q^{\mp}$ are "orbitally remote" if a singular cycle that passes through q^{-} does not pass through q^{+}; cf. Figure 2.4 (a).*

2. *The folded singularities $q^{\mp}$ are "orbitally connected" if they are contained in the same singular cycle, with the latter containing two slow segments, one on $\mathcal{Z}^{a^-}$ and one on $\mathcal{Z}^{a^+}$; cf. Figure 2.4 (c).*

3. *The folded singularities $q_h^{\mp}$ are "orbitally aligned" if they are neither orbitally remote nor orbitally connected; cf. Figure 2.4 (b).*

We emphasize that $q^{\mp}$ are geometrically connected (resp. aligned or remote) if and only if they are orbitally connected (resp. aligned or remote), and we have the following observation

Remark 4. *Definition 5 is equivalent to the following classification in terms of the x-coordinates $z_{q^{\mp}}$ of the fold points $q^{\mp}$.*

1. *The folded singularities $q_h^{\mp}$ are orbitally remote if $z_{q^+} > 0$; cf. Figure 2.4 (a).*

2. *The folded singularities $q^{\mp}$ are orbitally connected if $z_{q^+} < 0$; cf. Figure 2.4 (c).*

3. *The folded singularities $q_h^{\mp}$ are orbitally aligned if $z_{q^+} = 0$; cf. Figure 2.4 (b).*

The above classification would not hold if either (2.2) or (2.15) were written in the non-standard form of GSPT, where there would not exist linear fast and intermediate directions.

2.3 Global dynamics and MMOs

In this section, we discuss the correspondence between the families of singular cycles constructed in Proposition 5 and qualitative properties of MMO trajectories for ε and δ positive, but sufficiently small, in Equation (2.2). In particular, we give a qualitative characterisation of the resulting mixed-mode dynamics in dependence of system parameters.

In [Cardin and Teixeira, 2017], it was shown that, in the vein of Fenichel's Theorem 1 and Theorem 2, for $\varepsilon, \delta > 0$ sufficiently small, the normally hyperbolic manifolds $\mathcal{S}^{a,r}$ perturb to slow manifolds $\mathcal{S}^{a,r}_{\varepsilon\delta}$, which are diffeomorphic and lie $\mathcal{O}(\varepsilon)$-close (in the Hausdorff distance) to $\mathcal{S}^{a,r}$, as well as that the normally hyperbolic subsets $\mathcal{Z}^{a,r}$ perturb to slow manifolds $\mathcal{Z}^{a,r}_{\varepsilon\delta}$, which are diffeomorphic and lie $\mathcal{O}(\varepsilon+\delta)$-close (in the Hausdorff distance) to $\mathcal{Z}^{a,r}$; these slow manifolds are locally invariant under the flow of (2.2). In particular, $\mathcal{Z}^{a^{\mp}}_{\varepsilon\delta}$ locally approximate the weak canards of the folded singularities $q^{\mp}$, respectively [Letson et al., 2017], recall (2.15).

For ε and δ positive and sufficiently small in (2.2), trajectories can be composed from components that evolve close to fast, intermediate, and slow segments of the corresponding singular cycles, as discussed in Section 2.2. In a first approximation, where the fast and intermediate segments are approximated as straight lines – the latter in the (x, z)-plane – trajectories are attracted to the vicinities of both folded singularities $q^{\mp}$ if these are aligned or connected, and only to one of them if they are remote, as can be seen from Figure 2.4. (In Section 2.2, we showed that the funnels of the folded nodes $q^{\mp}$ for Equation (2.2) stretch with decreasing δ; in the three-timescale limit as δ approaches zero, these funnels can be viewed as having been stretched "infinitely" in one direction.) From the well-established theory of two-timescale singular perturbations, it is known that SAOs arise in the passage past folded singularities under the perturbed flow, recall Section 1.6 and see [Desroches et al., 2012, De Maesschalck et al., 2016, Wechselberger, 2005]; the underlying local two-timescale mechanisms are well understood. We discuss the three-timescale analogues of these mechanisms in Section 2.4 below. In particular, we conclude that SAOs are observed "above" or "below", in the language of Figure 1, depending on which folded singularity of Equation (2.2) trajectories are attracted to; double epochs of SAOs can occur when trajectories are attracted to both folded singularities $q^{\mp}$. The mixed-mode dynamics of Equation (2.2) can hence naturally be classified according to whether the folded singularities $q^{\mp}$ are remote, aligned, or connected; cf. Figure 2.1.

Singular Hopf bifurcations and onset of global dynamics In a first step, we note that, under Assumption 6 and Assumption 7, Equation (2.2) with $\varepsilon, \delta > 0$ small undergoes Hopf bifurcations for two values of the parameter μ in (2.2c), which we denote by $\mu_{SH}^{\mp}$; these bifurcations are referred to as "singular Hopf bifurcations" in the literature [Guckenheimer, 2008, Koper, 1995, Desroches et al., 2012] and separate regions of oscillatory dynamics from steady-state behaviour in Equation (2.2). For $\varepsilon = 0 = \delta$, true equilibria of (2.2) cross the folded singularities $q^{\mp}$ at

$$\mu_{q^-} = -\phi(x_{q^-}, y_{q^-}, z_{q^-}), \qquad \mu_{q^+} = -\phi(x_{q^+}, y_{q^+}, z_{q^+}), \tag{2.29}$$

and the singular Hopf bifurcations of the perturbed system occur at

$$\mu_{SH}^{-} = \mu_{q^-} + \mathcal{O}(\varepsilon, \delta), \qquad \mu_{SH}^{+} = \mu_{q^+} + \mathcal{O}(\varepsilon, \delta); \tag{2.30}$$

in particular, Assumption 7 implies that $0 = \mu_{q^-} < \mu_{q^+}$ in the double singular limit, and therefore $\mu_{SH}^{-} < \mu_{SH}^{+}$. We consider the asymptotics of $\mu_{SH}^{\mp}$ for ε and δ positive and sufficiently small in the following Section 2.4.

We emphasize that, for $\varepsilon, \delta > 0$ small and fixed, for μ-values greater than but close to μ_{SH}^{-} (respectively for μ-values less than but close to μ_{SH}^{+}), system (2.2) features only SAOs in the vicinity of $\mathcal{L}^-$ (resp. $\mathcal{L}^+$), i.e. trajectories converge to small periodic orbits that are product of the two Hopf bifurcations, and the onset (resp. cessation) of MMO-trajectories is marked by values:

$$\mu_o = \mu_{SH}^{-} + \mathcal{O}(\varepsilon, \delta), \qquad \mu_c = \mu_{SH}^{+} + \mathcal{O}(\varepsilon, \delta), \tag{2.31}$$

cf. Figure 2.1 and see [Krupa et al., 2008, Desroches et al., 2012] for details.

2.3.1 Aligned or connected singularities

When the folded singularities of $\mathcal{M}_1$ are connected, "double epochs" of slow dynamics are observed in (2.2) for $\varepsilon, \delta > 0$ sufficiently small and $\mu \in (\mu_o, \mu_c)$; see Figure 2.1 and Figure 2.5.

Theorem 4. *Assume that Assumption 6 and Assumption 7 hold, that the folded singularities of (2.2) are aligned or connected, in the sense of Definition 4, i.e. that* $\frac{\alpha}{\beta} \geq \frac{2f_2^2}{9f_3}$ *in (2.2). Then, there exist* $\varepsilon_0, \delta_0 > 0$ *small such that for every fixed* $(\varepsilon, \delta) \in (0, \varepsilon_0) \times (0, \delta_0)$*, there exist* μ_o *and* μ_c*, given by (2.31), such that system (2.2) features MMOs with double epochs of perturbed slow dynamics for* $\mu \in (\mu_o, \mu_c)$*.*

Proof. Consider the sections

$$\begin{aligned}
\Delta^+ &= \left\{ (x,y,z) \in \mathbb{R}^3 \mid x = \frac{x_{q^+} + x_{q^-}}{2},\ y > \frac{y_{q^+} + y_{q^-}}{2},\ z > \frac{z_{q^+} + z_{q^-}}{2} \right\} \\
\Delta^- &= \left\{ (x,y,z) \in \mathbb{R}^3 \mid x = \frac{x_{q^+} + x_{q^-}}{2},\ y < \frac{y_{q^+} + y_{q^-}}{2},\ z < \frac{z_{q^+} + z_{q^-}}{2} \right\}, \\
\Sigma^- &= \left\{ (x,y,z) \in \mathbb{R}^3 \mid x < x_{q^-},\ y = y_{q^-} + \rho_1,\ \rho_1 > 0 \text{ small} \right\}, \\
\Sigma^+ &= \left\{ (x,y,z) \in \mathbb{R}^3 \mid x > x_{q^-},\ y = y_{q^+} - \rho_2,\ \rho_2 > 0 \text{ small} \right\},
\end{aligned}$$

where the points $p^{\mp} = (x_{p^{\mp}}, y_{p^{\mp}}, z_{p^{\mp}})$ are the fold points of $\mathcal{M}_2$, recall (2.27) and see Figure 2.5. In addition, consider the maps

$$\pi_{out}^- : \Sigma^- \to \Delta^-, \tag{2.32}$$
$$\pi_{in}^+ : \Delta^- \to \Sigma^+, \tag{2.33}$$
$$\pi_{out}^+ : \Sigma^+ \to \Delta^-, \tag{2.34}$$
$$\pi_{in}^- : \Delta^+ \to \Sigma^-, \tag{2.35}$$

that are induced by the flow of (2.2).

The return map $\pi = \pi_{in}^- \circ \pi_{out}^+ \circ \pi_{in}^+ \circ \pi_{out}^- : \Sigma^- \to \Sigma^-$ is well defined for all $\varepsilon, \delta > 0$ sufficiently small. In particular, the transition maps $\pi_{in}^{\mp}$ in the normally hyperbolic regimes are covered by [Cardin and Teixeira, 2017]; that is, trajectories with initial conditions on Δ^- (resp. Δ^+) are attracted exponentially close to $\mathcal{S}_{\varepsilon\delta}^{a^+}$ (resp. $\mathcal{S}_{\varepsilon\delta}^{a^-}$) following the fast flow of the perturbed system, and then they are attracted to $\mathcal{Z}_{\varepsilon\delta}^{a^+}$ (resp. $\mathcal{Z}_{\varepsilon\delta}^{a^-}$) following the intermediate flow of the perturbed system, whereon they follow the slow flow towards q^+ (resp. q^-). The constants $\rho_{1,2}$ are sufficiently small such that trajectories with initial conditions on $\Delta^+|_{z>z_{q^+}}$ (resp. $\Delta^-|_{z<z_{q^-}}$) are attracted exponentially close to $\mathcal{Z}_{\varepsilon\delta}^{a^-}$ (resp. $\mathcal{Z}_{\varepsilon\delta}^{a^+}$) before they cross Σ^- (resp. Σ^+). Moreover, in [Letson et al., 2017] it was shown that trajectories that approach the vicinity of $\mathcal{L}^+$ (resp. $\mathcal{L}^-$) exponentially close to $\mathcal{Z}_{\varepsilon\delta}^{a^+}$ (resp. $\mathcal{Z}_{\varepsilon\delta}^{a^-}$), diverge exponentially from the latter at most at a *buffer point* that is bounded between q^+ and p^+ (resp. q^- and p^-), and that the map π_{out}^+ (resp. π_{out}^-) is well defined.

Therefore, all initial conditions are attracted to either $\mathcal{Z}_{\varepsilon\delta}^{a^-}$ or $\mathcal{Z}_{\varepsilon\delta}^{a^+}$ (possibly after a jump), whereon they follow the slow flow until they jump and reach $\mathcal{Z}_{\varepsilon\delta}^{a^-}$ or $\mathcal{Z}_{\varepsilon\delta}^{a^+}$ on the other side, respectively; this shows the existence of an attractor with double epochs of perturbed slow dynamics. We emphasise that, although not immediately apparent, the above hold also for

the case of aligned singularities. At the singular limit $\varepsilon = 0 = \delta$, the folded singularities $q^{\mp}$ have the same z-coordinates; in the perturbed system (2.2), $\varepsilon, \delta > 0$ small, the buffer points are bounded between $q^{\mp}$ and $p^{\mp}$, respectively, which means that trajectories jump at points near $\mathcal{L}^+$ such that they cross Δ^+ (resp. at points near $\mathcal{L}^-$ such that they cross Δ^-), and are hence attracted to both $\mathcal{Z}_{\varepsilon\delta}^{a^{\mp}}$.

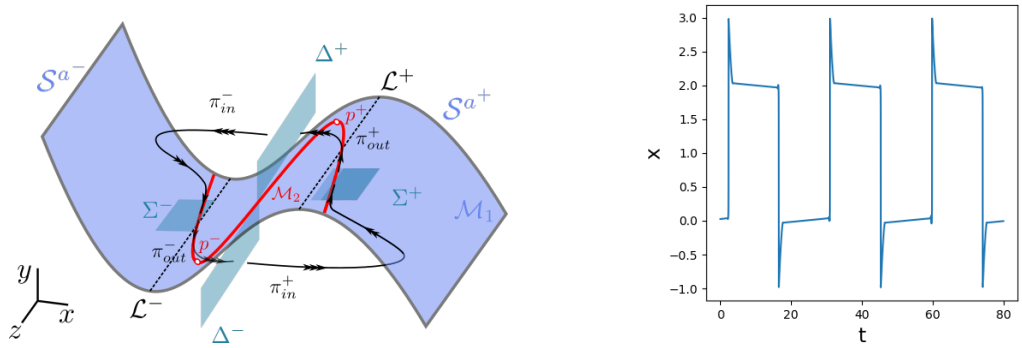

(a) (b)

Figure 2.5: Schematic illustration of the emergence of MMO trajectories with double epochs of perturbed slow dynamics in (2.2), for the case of aligned or connected singularities. (a) singular geometry and transition maps, (b) corresponding time series for the case of the Koper model, see Chapter 3.

□

We remark that Theorem 4 guarantees the existence of an *attractor* in (2.2) with double epochs of perturbed slow dynamics; more specific characterisation of properties like periodicity or chaoticity is dependent on the properties of the function $\phi(x, y, z)$ in (2.2c) and hence requires a case-by-case study. Moreover, we note that the "double epoch" regime can be further divided into cases where SAOs occur "above" and "below"; SAOs are seen "above" with SAO-less slow dynamics below or vice versa; or "three-timescale" relaxation oscillation is found, with the flow alternating between fast, intermediate, and slow SAO-less dynamics. A precise characterisation is dependent on the properties of the function $\phi(x, y, z)$ in (2.2c) and hence also requires a case-by-case study. For instance, for the Koper model from chemical kinetics studied in Chapter 3, we typically observe double-epoch trajectories with only a few small oscillations before the jump (cf. Figure 1 and Figure 3.3), while in the Hodgkin-Huxley equations from mathematical neuroscience studied in Chapter 4, we observe double-epoch trajectories with either prominent SAOs above and mere slow flow below or vice-versa (cf. Figure 4.1 and Figure 4.2).

Moreover, in the proof of Theorem 4 we used the fact that the *buffer points*, i.e. the point at most where trajectories diverge from $\mathcal{Z}_{\varepsilon\delta}^{a^{\mp}}$ exponentially after crossing $\mathcal{L}^{\mp}$ regardless of their entry points, are bounded between $q^{\mp}$ and $p^{\mp}$, respectively. In Section 2.4 we give estimates of these buffer points $\mathcal{O}\left(\sqrt{\varepsilon}, \delta\right)$-close to $\mathcal{L}^{\mp}$, respectively.

2.3.2 Remote singularities

In the case where the folded singularities of $\mathcal{M}_1$ in (2.2) are orbitally remote (recall Definition 4 and Figure 2.4) the perturbed flow (2.2) with $\varepsilon, \delta > 0$ sufficiently small can exhibit MMOs with single epochs of SAOs, or "two-timescale" relaxation oscillation where the flow alternates between the fast and the intermediate dynamics for $\mu \in (\mu_o, \mu_c)$ (recall Figure 2.1 and (2.31)).

To first show the existence of relaxation oscillations in a μ-subregime of (μ_o, μ_c), we combine the approaches of [Krupa et al., 2008] and [Szmolyan and Wechselberger, 2004]. To leading order in ε and δ, the μ-values which separate the corresponding parameter regimes can be determined by requiring that the intermediate flow on $\mathcal{S}^{a^-}$ is "balanced" by that on $\mathcal{S}^{a^+}$; this is done at the singular limit $\varepsilon = 0$ with $\delta > 0$ sufficiently small, so that we only consider the flow on $\mathcal{S}^{a^\mp}$, and the z-displacement during a jump (i.e. away from $\mathcal{S}^{a^\mp}$) is negligible, see [Krupa et al., 2008] for details. We define

$$x_0 := -\frac{f_2}{f_3}, \qquad x_{max} := \frac{-2f_2}{3f_3}, \qquad x^*_{max} := \frac{f_2}{3f_3}, \tag{2.36}$$

where x_0 is the x-coordinate of $P(\mathcal{L}^-)$, x^*_{max} is the x-coordinate of $P(\mathcal{L}^+)$, and x_{max} is the x-coordinate of $\mathcal{L}^+$, cf. Figure 2.6 below; we recall that $P(\mathcal{L}^\mp) \subset \mathcal{S}^\mp$ denotes the projection of $\mathcal{L}^\mp$ onto $\mathcal{S}^\mp$ along the fast fibres (2.6a).

We then define

$$\mathcal{G}_0^- (z, \mu) := \mathcal{G} (x^*_{\max}, 0; z; \mu), \qquad \mathcal{G}_0^+ (z, \mu) := \mathcal{G} (x_0, x_{\max}; z; \mu), \tag{2.37a}$$

$$\mathcal{R}(z, \mu) := \mathcal{G}_0^-(z, \mu) + \mathcal{G}_0^+(z, \mu), \tag{2.37b}$$

where we recall that

$$\mathcal{G} (x_0, x_1; z_0; \mu) = \int_{x_0}^{x_1} \frac{F'(\sigma) (\mu + \phi (\sigma, F(\sigma), z_0))}{\alpha\sigma + \beta F(\sigma) - z_0} \mathrm{d}\sigma,$$

from Lemma 4, which is obtained by eliminating time in the reduced flow on $\mathcal{S}^{a^\mp}$ (2.15) and integrating. In the following we will also denote

$$I := (z_{q^-}, z_{q^+}) \tag{2.38}$$

To leading order in δ and for μ-values appropriately restricted (as will be clarified below), the singular trajectory of a point $(0, 0, z) \in \mathcal{L}^-|_{z\in I}$ returns to $\mathcal{L}^-|_{z\in I}$ at a point $(0, 0, \hat{z})$, where

$$\hat{z} = z + \delta\mathcal{R}(z, \mu) + \mathcal{O}(\delta^2); \tag{2.39}$$

in the following, we will show that this map is well defined, cf. Theorem 5 below.

We will say that the flow on $\mathcal{S}^{a^-}$ is balanced by that on $\mathcal{S}^{a^+}$ *"at"* a point with $z = z^*$ for $\delta > 0$ sufficiently small if there holds that $\hat{z} = z^*$, i.e. if $\mathcal{R}(z^*, \mu) = 0$. To find the μ-values for which the reduced flow on $\mathcal{S}^{a^-}$ is balanced by that on $\mathcal{S}^{a^+}$ at either q^- or q^+, for $\delta > 0$, we first need to show the following.

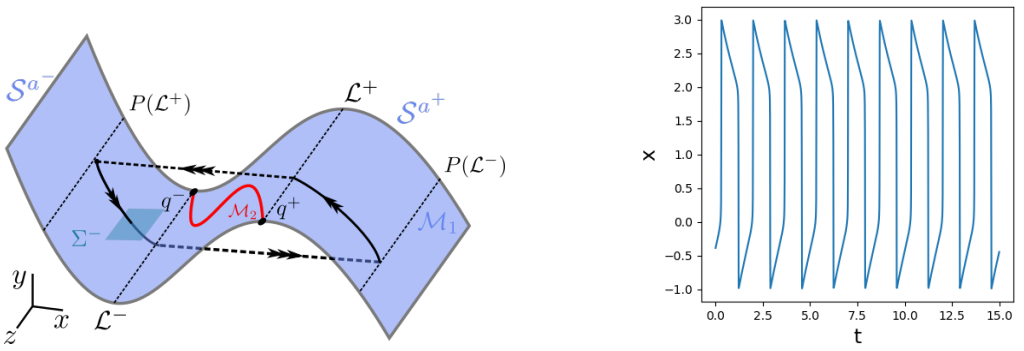

(a) (b)

Figure 2.6: Schematic illustration of the emergence of relaxation oscillation trajectories in (2.2), for the case of remote singularities. (a) singular geometry, (b) corresponding time series for the case of the Koper model, see Chapter 3.

Lemma 5. *If the folded singularities $q^\mp$ of $\mathcal{M}_1$ are remote, i.e., if $\frac{\alpha}{\beta} < \frac{2f_2^2}{9f_3}$, then*

$$\int_{x_0}^{x_{\max}} \frac{F'(\sigma)}{\alpha\sigma + \beta F(\sigma) - z_{q^\mp}} \mathrm{d}\sigma > 0, \qquad \int_{x^*_{\max}}^{0} \frac{F'(\sigma)}{\alpha\sigma + \beta F(\sigma) - z_{q^\mp}} \mathrm{d}\sigma > 0, \tag{2.40}$$

and

$$\mathcal{G}_0^-(z_{q^-}, \mu) > 0, \qquad \mathcal{G}_0^+(z_{q^+}, \mu) < 0. \tag{2.41}$$

Proof. There hold that

1. $F'(x) < 0$ for $x \in (x^*_{max}, 0) \cup (x_0, x_{max})$ (i.e. for points on $\mathcal{S}^a$, recall (2.11)),
2. $\alpha x + \beta F(x) - z < 0$ for $(x, z) \in (x^*_{max}, 0) \times [z_{q^-}, z_{q^+}]$, recall the algebraic constraint for $\mathcal{M}_2$ (2.22) and see Figure 2.4 (a),
3. $\alpha x + \beta F(x) - z > 0$ for $(x, z) \in (x_0, x_{max}) \times [z_{q^-}, z_{q^+}]$, recall (2.22) and see Figure 2.4 (a).
4. $\mu + \phi(\sigma, F(\sigma), z) > 0$ for $(x, z\mu) \in (x^*_{max}, 0) \times [z_{q^-}, z_{q^+}] \times \left[\mu^-_{SH}, \mu^+_{SH}\right]$, recall Assumption 7,
5. $\mu + \phi(\sigma, F(\sigma), z) < 0$ for $(x, z, \mu) \in (x_0, x_{max}) \times [z_{q^-}, z_{q^+}] \times \left[\mu^-_{SH}, \mu^+_{SH}\right]$, recall Assumption 7.

Using the above, the sign-definitiveness of equations (2.40) and (2.41) follows. □

The values μ_b^- and μ_b^+ for which the reduced flow on $\mathcal{S}^{a^-}$ is balanced by that on $\mathcal{S}^{a^+}$ at q^- and q^+ for $\delta > 0$, respectively, to leading order in δ are found by solving $\mathcal{R}(z_{q^-}, \mu) = 0$ and $\mathcal{R}(z_{q^+}, \mu) = 0$, respectively. The relative position of μ_b^- and μ_b^+ on the real line depends on the properties of the function $\phi(x, y, z)$ in (2.2c); we therefore make the following assumption.

Assumption 8. *Denote by $\mu_b^{\mp}$ the μ-values for which*

$$\mathcal{R}(z_{q^-}, \mu_b^-) = 0, \qquad \mathcal{R}(z_{q^+}, \mu_b^+) = 0 \tag{2.42}$$

hold, i.e.,

$$\mu_b^{\mp} := -\frac{\int_{x^*_{\max}}^0 \frac{F'(\sigma)\phi\left(\sigma,F(\sigma),z_{q^{\mp}}\right)}{\alpha\sigma+\beta F(\sigma)-z_{q^{\mp}}}\mathrm{d}\sigma + \int_{x_0}^{x_{\max}} \frac{F'(\sigma)\phi\left(\sigma,F(\sigma),z_{q^{\mp}}\right)}{\alpha\sigma+\beta F(\sigma)-z_{q^{\mp}}}\mathrm{d}\sigma}{\int_{x^*_{\max}}^0 \frac{F'(\sigma)}{\alpha\sigma+\beta F(\sigma)-z_{q^{\mp}}}\mathrm{d}\sigma + \int_{x_0}^{x_{\max}} \frac{F'(\sigma)}{\alpha\sigma+\beta F(\sigma)-z_{q^{\mp}}}\mathrm{d}\sigma}. \tag{2.43}$$

We assume that

$$\mu_{SH}^- < \mu_b^- < \mu_b^+ < \mu_{SH}^-.$$

It is now apparent that from Lemma 5 follows that the denominator in (2.43) is non-zero. Assumption 8 is essentially an assumption on the properties of the function $\phi(x, y, z)$ in (2.2c), which is make because it is consistent with the Koper model, Equation (6), after transformation to the prototypical Equation (2.2). We now make an additional assumption on $\phi(x, y, z)$, which is also consistent with the Koper model.

Assumption 9. *We assume that $\partial_z\phi(x, y, z) \leq 0$ for $z \in [z_{q^-}, z_{q^+}]$.*

We remark that Assumption 9 is sufficient but not necessary in order to show the existence of relaxation oscillators, and we will comment further on this after stating our main result. Before doing so, we introduce a final preliminary technical result.

Lemma 6. *Assume that Assumption 9 holds and that the folded singularities of (2.2) are remote in the sense of Definition 4, i.e. that $\frac{\alpha}{\beta} < \frac{2f_2^2}{9f_3}$ in (2.2). Then, there holds that*

$$\partial_\mu \mathcal{R}(z, \mu) < 0 \tag{2.44}$$

and

$$\partial_z \mathcal{R}(z, \mu) > 0 \tag{2.45}$$

for $z \in [z_{q^-}, z_{q^+}] \times \left[\mu_b^-, \mu_b^+\right]$.

Proof. There holds that

$$\begin{aligned}\frac{\partial}{\partial z}\left[\frac{F'(\sigma)\left(\mu+\phi\left(\sigma,F(\sigma),z\right)\right)}{\alpha\sigma+\beta F(\sigma)-z}\right] =& \frac{F'(\sigma)\partial_z\left[\phi\left(\sigma,F(\sigma),z\right)\right]\left(\alpha\sigma+\beta F(\sigma)-z\right)}{\left(\alpha\sigma+\beta F(\sigma)-z\right)^2} \\ &+ \frac{F'(\sigma)\left(\mu+\phi\left(\sigma,F(\sigma),z\right)\right)}{\left(\alpha\sigma+\beta F(\sigma)-z\right)^2};\end{aligned}$$

moreover,

1. $F'(x) < 0$ for $x \in (x^*_{max}, 0) \cup (x_0, x_{max})$,

2. $\phi_z(x,y,z) < 0$, by Assumption 9,

3. $\alpha x + F(x) - z < 0$ for $(x,z) \in (x^*_{max}, 0) \times [z_{q^-}, z_{q^+}]$, recall (2.22) and Figure 2.4 (a),

4. $\alpha x + F(x) - z > 0$ for $(x,z) \in (x_0, x_{max}) \times [z_{q^-}, z_{q^+}]$, recall (2.22) and Figure 2.4 (a).

5. $\mu + \phi(\sigma, F(\sigma), z) > 0$ for $(x,z,\mu) \in (x^*_{max}, 0) \times [z_{q^-}, z_{q^+}] \times \left[\mu^-_{SH}, \mu^-_{SH}\right]$, recall Assumption 7,

6. $\mu + \phi(\sigma, F(\sigma), z) < 0$ for $(x,z,\mu) \in (x_0, x_{max}) \times [z_{q^-}, z_{q^+}] \times \left[\mu^-_{SH}, \mu^-_{SH}\right]$, recall Assumption 7.

Using the above, the sign-definitiveness in (2.44) follows immediately after changing the order of integration and differentiation therein.

In addition,

$$\frac{\partial}{\partial \mu}\left[\frac{F'(\sigma)\left(\mu + \phi\left(\sigma, F(\sigma), z\right)\right)}{\alpha\sigma + \beta F(\sigma) - z}\right] = \frac{F'(\sigma)}{\alpha\sigma + \beta F(\sigma) - z},$$

and the sign definiteness of (2.45) follows similarly. □

We have introduced the necessary preliminary results in order to show the existence of stable relaxation oscillations in (2.2), and we now state our main result:

Theorem 5. *Assume that Assumption 6 – Assumption 9 hold, and that the folded singularities of (2.2) are remote in the sense of Definition 4, i.e. that* $\frac{\alpha}{\beta} < \frac{2f_2^2}{9f_3}$ *in (2.2). Then, there exist* $\varepsilon_0, \delta_0 > 0$ *small such that, for any fixed* $(\varepsilon, \delta) \in (0, \varepsilon_0) \times (0, \delta_0)$*, there exist*

$$\mu_r^- = \mu_b^- + \mathcal{O}(\delta), \qquad \mu_r^+ = \mu_b^+ + \mathcal{O}(\delta), \tag{2.46}$$

where $\mu_b^\mp$ *are given by (2.43), such that system (2.2) has a stable relaxation oscillation orbit for every* $\mu \in (\mu_r^-, \mu_r^+)$.

Proof. The proof in based on showing that the assumptions of Theorem 3 are satisfied, see [Szmolyan and Wechselberger, 2004, Theorem 4]; these assumptions are summarised in Section 1.5.

- Assumption 1: By construction, $\mathcal{M}_1$ is S-shaped with two attracting sheets $\mathcal{S}^{a^\mp}$ separated by a repelling sheet $\mathcal{S}^r$, recall (2.10), (2.11) and (2.12).

- Assumption 2: The tranversality condition (1.28) is satisfied on $\mathcal{L}^\mp|_{z\in I}$.

- Assumption 3 and Assumption 4: At the singular limit $\varepsilon = 0 = \delta$, one can construct a 1-dimensional map

$$\sigma^- : \qquad P(\mathcal{L}^+)|_{z\in I} \to \mathcal{L}^-, \qquad z \mapsto z, \tag{2.47}$$

  where we recall that $P : \mathcal{L}^\mp \to \mathcal{S}^{a^\pm}$ is the projection along the fast fibres (2.6a) of a point on $\mathcal{L}^\mp$ to a point on $\mathcal{S}^{a^\pm}$. For $\delta > 0$ sufficiently small, the map σ^- perturbs smoothly to

$$\sigma^-_\delta : \qquad P(\mathcal{L}^+)|_{z\in I} \to \mathcal{L}^-, \qquad z \mapsto z + \mathcal{O}(\delta); \tag{2.48}$$

in particular, by eliminating time in (2.15), the map σ_δ^- can be approximated by

$$z \;\mapsto\; z + \delta \mathcal{G}_0^-(z,\mu) + \mathcal{O}(\delta^2). \tag{2.49}$$

Moreover, since

$$\mathcal{G}_0^-(z_{q^-},\mu) > 0 \tag{2.50}$$

for $\mu \in (\mu_{q^-}, \mu_{q^+})$ by Lemma 6, the map $\sigma_\delta^- : P(\mathcal{L}^+)|_{z\in I} \to \mathcal{L}^-|_{z>z_{q^-}}$ is well defined and $\sigma_\delta^-(z) \to \sigma^-(z)$ as $\delta \to 0$ uniformly in z. In particular, (2.50) implies that the point on $P(\mathcal{L}^+)$ with $z = z_{q^-}$ is mapped to a point on $\mathcal{L}^-$ with $z > z_{q^-}$, and by existence and uniqueness of solutions (since the map σ_δ^- is induced by the reduced flow on $\mathcal{S}^{a^-}$), all points on $P(\mathcal{L}^+)$ with $z > z_{q^-}$ are mapped to points on $\mathcal{L}^-$ with $z > z_{q^-}$. Similarly, one can construct an analogous, well defined map $\sigma_\delta^+ : P(\mathcal{L}^-)|_{z\in I} \to \mathcal{L}^+|_{z<z_{q^+}}$, under which points on $P(\mathcal{L}^-)$ with $z \le z_{q^+}$ are mapped to points on $\mathcal{L}^+$ with $z < z_{q^-}$.

The composition of σ_δ^- and σ_δ^+ defines the return map

$$\pi^- := \sigma_\delta^- \circ \sigma_\delta^+ : \qquad \mathcal{L}^-|_I \to \mathcal{L}^-|_I, \qquad z \;\mapsto\; z + \delta \mathcal{R}(z,\mu). \tag{2.51}$$

Since

$$\partial_\mu \mathcal{R}(z,\mu) > 0 \quad \forall\ (z,\mu) \in (z_{q^-}, z_{q^+}) \times (\mu_b^-, \mu_b^+),$$

i.e. since $\mathcal{R}(z,\mu)$ is an increasing function of μ (recall Lemma 6), and since also

$$\mathcal{R}(z_{q^-}, \mu_b^-) = 0, \qquad \mathcal{R}(z_{q^+}, \mu_b^+) = 0$$

by Assumption 8, it correspondingly follows that

$$\mathcal{R}(z_{q^-}, \mu) > 0, \qquad \mathcal{R}(z_{q^+}, \mu) < 0 \qquad \forall\ \mu \in (\mu_b^-, \mu_b^+),$$

and the map $\pi^- : \mathcal{L}^-|_I \to \mathcal{L}^-|_I$ is therefore well defined. By the intermediate value theorem, for any $\mu \in (\mu_b^-, \mu_b^+)$, there exists $z^* \in (z_{q^-}, z_{q^+})$ such that $\mathcal{R}(z^*, \mu) = 0$; therefore, z^* is a fixed point of π^-. Moreover, from (2.44) follows that $\partial_z \mathcal{R}(z,\mu) < 0$ for all $(z,\mu) \in [z_{q^-}, z_{q^+}] \times \left[\mu_b^-, \mu_b^+\right]$; therefore, the fixed point $z^* \in (z_{q^-}, z_{q^+})$ is unique. This implies the existence of a unique singular cycle for any $\delta > 0$ sufficiently small.

- Assumption 5: Consider the section

$$\Sigma^- = \left\{(x,y,z) \in \mathbb{R}^3 \mid x < x_{q^-},\ y = y_{q^-} + \rho_1,\ \rho_1 > 0\right\},$$

see Figure 2.6. The return map $\pi^- : \mathcal{L}^- \to \mathcal{L}^-$ in (2.51) induces a return map $\Pi^- : \Sigma^- \to \Sigma^-$. Correspondingly, fixed points of π^- on $\mathcal{L}^-$ are connected to fixed points of Π^- on Σ^- via trajectories of the reduced flow (2.15) on $\mathcal{S}^{a^-}$, and a fixed point of Π^- is hyperbolic and attracting (resp. repelling) if and only if the corresponding fixed point of π^- is hyperbolic and attracting (resp. repelling).

In the previous part we showed that, for any $\mu \in (\mu_{r^-}, \mu_{r^+})$, there exists a unique fixed point $z^* \in (z_{q^-}, z_{q^+})$ of π^-. Moreover, since $\partial_z\left(z + \delta \mathcal{R}(z,\mu)\right) < 1$ for all $z \in [z_{q^-}, z_{q^+}]$ by (2.44), the fixed point z^* is hyperbolic and attracting, and so is the corresponding fixed point of Π^- on Σ^-. This shows the existence of a hyperbolic and attracting singular periodic orbit.

The above assumptions are established at the singular limit $\varepsilon = 0$, $\delta > 0$ sufficiently small. For $\varepsilon, \delta > 0$ sufficiently small and $z \in I$, under the flow of (2.2) a trajectory with initial condition (x^*_{max}, y_{q^+}, z) on $\mathcal{S}^{a^-}_{\varepsilon,\delta}$ (i.e. at the height of $P(\mathcal{L}^+)$) is mapped to a point on $\mathcal{S}^{a^-}_{\varepsilon,\delta}$ (after a large excursion) as

$$z \mapsto z + \delta\mathcal{R}(z,\mu) + \mathcal{O}(\delta^2, \delta\varepsilon\ln\varepsilon), \tag{2.52}$$

and the above map is smooth in z and μ. To see this, first consider the limit $\varepsilon = 0 = \delta$, where there exists a singular cycle connecting the point (x^*_{max}, y_{q^+}, z) to itself, cf. Figure 2.6; the return map is then the identity. For $\varepsilon = 0$, $\delta > 0$ small, this map perturbs to (2.51). For $\varepsilon, \delta > 0$ small, by [Szmolyan and Wechselberger, 2004, Theorems 3 &4], there is an $\mathcal{O}(\varepsilon\ln\varepsilon)$-contribution, which arises through the perturbation of the $\mathcal{G}^{\mp}_0$ functions and is multiplied by a factor of δ, since at the limit $\delta = 0$ the z-displacement needs to be zero (regardless of ε being positive or not, recall $(2.4)_{\delta=0}$), and this gives (2.52).

Finally, we remark on the asymptotics of $\mu^{\mp}_r$ in (2.46). According to the formulation of [Szmolyan and Wechselberger, 2004, Theorem 3], in the case studied therein the return map (2.52) is written as $z \mapsto G_0(z) + \mathcal{O}(\varepsilon\ln\varepsilon)$, with G_0 independent of ε; this can be viewed as a special case of our return map (2.52) for $\delta = 1$, which, in the same formulation, reads as $z \mapsto G_0(z) + \mathcal{O}(\delta\varepsilon\ln\varepsilon)$, where $G_0 = z + \delta\mathcal{R}(z,\mu) + \mathcal{O}(\delta^2)$. Since the existence and stability of relaxation oscillations depend only on the properties of G_0 at the limit $\varepsilon = 0$ [Szmolyan and Wechselberger, 2004], the asymptotics of $\mu^{\mp}_r$ are as given in (2.46).

□

We reiterate that Assumption 9 is sufficient, but not necessary for the existence of stable relaxation oscillation orbits as described in Theorem 5. That is, it guarantees the existence *and uniqueness* of a singular cycle at the limit $\varepsilon = 0$, $\delta > 0$ small, see third bullet point in the proof of Theorem 5. In general, the function $\phi(x, y, z)$ could be such that more than one singular cycles exist at this limit, and the stability of each one of them would be studied individually; this would result to the existence of more than one relaxation oscillation orbits for $\varepsilon, \delta > 0$ small, and some of these orbits could potentially be stable while others could be unstable. We reiterate that Assumption 9 is satisfied for the case of the Koper model from chemical kinetics that is studied in Chapter 3.

We now state our main result regarding the existence of MMOs with single epochs of perturbed slow dynamics.

Theorem 6. *Assume that Assumption 6 – Assumption 9 hold, and that the folded singularities of (2.2) are remote in the sense of Definition 4, i.e. that* $\frac{\alpha}{\beta} < \frac{2f_2^2}{9f_3}$ *in (2.2). Then, there exist* $\varepsilon_0, \delta_0 > 0$ *small such that, for every fixed* $(\varepsilon, \delta) \in (0, \varepsilon_0) \times (0, \delta_0)$*, there exist* μ_o *and* μ^-_r *given in (2.31) and (2.46), respectively, such that system (2.2) features MMOs with single SAO-epochs for* $\mu \in (\mu_o, \mu^-_r)$*.*

Proof. Consider the section

$$\Sigma^- = \left\{(x, y, z) \in \mathbb{R}^3 \mid x < x_{q^-},\ y = y_{q^-} + \rho_1,\ \rho_1 > 0 \text{ small}\right\}$$

On the basis of Theorem 4 and Theorem 5, the return map $\pi^- : \Sigma^- \to \Sigma^-$ induced by the flow of (2.2) is well defined for all $\varepsilon, \delta > 0$ sufficiently small and $\mu \in (\mu_o, \mu^-_r)$.

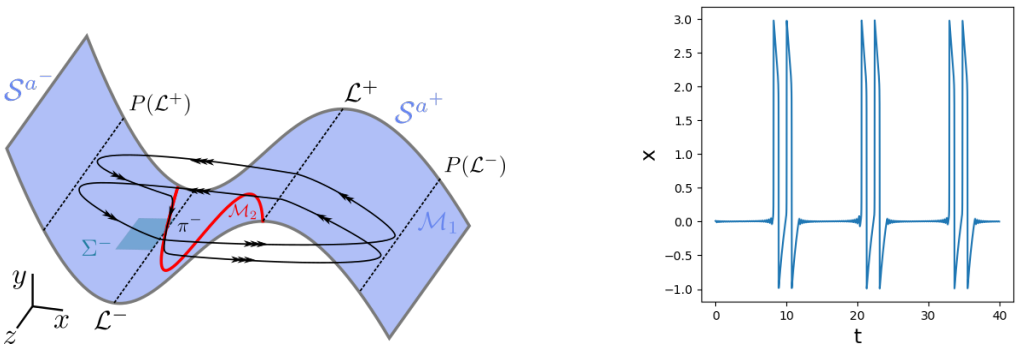

(a) (b)

Figure 2.7: Schematic illustration of the emergence of MMO trajectories with single epochs of perturbed slow dynamics in (2.2), for the case of remote singularities. (a) singular geometry and return map, (b) corresponding time series for the case of the Koper model, see Chapter 3.

Consider now a point (x^*_{max}, y_{q^+}, z) on $\mathcal{S}^{a^-}_{\varepsilon,\delta}$ (i.e. at the height of $P(\mathcal{L}^+)$) , with $z \in (z_{q^-}, z_{q^+})$. The corresponding trajectory returns to $\mathcal{S}^{a^-}_{\varepsilon,\delta}$ (after a large excursion) at a point with $z + \delta\mathcal{R}(z,\mu) + \mathcal{O}(\delta^2, \delta\varepsilon\ln\varepsilon)$, recall the proof of Theorem 5. Moreover, there holds that $\mathcal{R}(z,\mu) < 0$ for all $(z,\mu) \in (z_{q^-}, z_{q^+}) \times (\mu_o, \mu_r^-)$; this follows from (2.44) and (2.45). Therefore, the trajectory is "drifting" towards the negative z-direction, until it reaches a point (x^*_{max}, y_{q^+}, z) on $\mathcal{S}^{a^-}_{\varepsilon,\delta}$ with $z < z_{q^-}$, i.e. until it enters the funnel of q^-. We reiterate that, at a first approximation, the funnel of q^- is the area in $\mathcal{S}^{a^-}$ bounded by $\mathcal{Z}^{a^-}$ and the intermediate fibre of (2.19) that crosses q^-, which is given by $\{z = z_{q^-}\}$.

Points (x^*_{max}, y_{q^+}, z) on $\mathcal{S}^{a^-}_{\varepsilon,\delta}$ with $z < z_{q^-}$ are attracted to the vicinity of q^- and undergo SAOs. According to [Krupa and Wechselberger, 2010, Hayes et al., 2016], the buffer point, i.e the point at most which all trajectories diverge exponentially from $\mathcal{Z}^{a^-}$, lies $o(1)$-close to q^-. Therefore, there exists $\varepsilon_0, \delta_0 > 0$ sufficiently small, for which there holds in particular $\varepsilon_0 < (z_{q^+} - z_{q^-})^2$, $\delta_0 < z_{q^+} - z_{q^-}$, such that, for all $(\varepsilon,\delta) \in (0,\varepsilon_0) \times (0,\delta_0)$, trajectories that diverge exponentially from $\mathcal{Z}^{a^-}_{\varepsilon\delta}$ follow a slow drift towards the negative z-direction, without interacting with $\mathcal{Z}^{a^+}_{\varepsilon\delta}$, until they enter the funnel of q^-. The above implies the existence of MMO trajectories with single epochs of perturbed slow dynamics. □

We remark that the requirement $\varepsilon_0 < (z_{q^+} - z_{q^-})^2$, $\delta_0 < z_{q^+} - z_{q^-}$ is a sufficient condition which guarantees that, regardless of how close the folded singularities are in the z-direction, there exist $\varepsilon, \delta > 0$ small such that MMOs with single epochs of perturbed slow dynamics exist, because the buffer point near $\mathcal{L}^-$ is such that trajectories that diverge exponentially from $\mathcal{Z}^{a^-}$ are not able to reach $\mathcal{Z}^{a^+}$; as will become apparent in the Section 2.4 below, the buffer point lies $\mathcal{O}(\sqrt{\varepsilon}, \delta)$-close to the fold line $\mathcal{L}^-$. If $q^\mp$ are remote but still relatively close in the z-direction, then there could potentially exist ε- and δ-values for which trajectories interact with both $\mathcal{Z}^{a^\mp}$, and hence system (2.2) features MMOs with double epochs of perturbed slow dynamics, or even more exotic patterns, where the two epochs are separated by LAOs; see Chapter 4 for an example of the latter in the context of the multi-timescale

Hodgkin-Huxley equations from mathematical neuroscience. We remark that we have not been able to find such "exotic" behaviour in the context of the Koper model from chemical kinetics, Chapter 3.

Finally, in regard to the number of LAOs between SAO segments, we have the following estimate.

Corollary 1. *Assume that assumptions Assumption 6 – Assumption 9 hold, and that the folded singularities of (2.2) are remote in the sense of Definition 4, i.e. that* $\frac{\alpha}{\beta} < \frac{2f_2^2}{9f_3}$ *in (2.2). Consider* $\varepsilon, \delta > 0$ *sufficiently small and* $\mu \in (\mu_o, \mu_r^-)$*, where* μ_o *and* μ_r^- *are given in (2.31) and (2.46), respectively. Denote by* $p_{\text{out}} = (x_{\text{out}}, y_{\text{out}}, z_{\text{out}})$ *the point at which a trajectory diverges exponentially from* $\mathcal{Z}_{\varepsilon\delta}^{a^-}$*, with* $z_{\text{out}} > 0$*, and denote by* L *the number of large excursions that follow before the trajectory is again attracted exponentially close to* $\mathcal{Z}_{\varepsilon\delta}^{a^-}$*.*

1. *If* $z_{\text{out}} + \delta\mathcal{R}(0,\mu) < 0$*, then* $L = 1$*;*
2. *if* $0 < z_{\text{out}} + \delta\mathcal{R}(0,\mu) < z_{\text{out}}$*, then*

$$L = 1 + \left\lfloor \frac{z_{\text{out}}}{\delta\mathcal{R}(0,\mu)} \right\rfloor, \tag{2.53}$$

where $\lfloor\ \rfloor$ *denotes the floor function.*

Proof. Follows immediately from Theorem 6. □

2.4 Local dynamics and SAOs

In this subsection, we discuss the emergence of SAOs in a vicinity of $\mathcal{L}^{\mp}$ in (2.2) when trajectories are attracted to $\mathcal{Z}^{a^{\mp}}$, respectively; we focus on describing the properties of $\mathcal{Z}^{a^-}$ close to $\mathcal{L}^-$ here, as the description of $\mathcal{Z}^{a^+}$ near $\mathcal{L}^+$ is analogous.

We first consider the partially perturbed fast Equation (2.4) with ε sufficiently small and $\delta = 0$:

$$x' = -y + f_2x^2 + f_3x^3, \tag{2.54a}$$
$$y' = \varepsilon\left(\alpha x + \beta y - z\right), \tag{2.54b}$$
$$z' = 0. \tag{2.54c}$$

By standard GSPT [Fenichel, 1979, Krupa and Szmolyan, 2001a], we can define slow manifolds $\mathcal{S}_{\varepsilon 0}^{a,r}$ for (2.54) as surfaces that are foliated by orbits within $\{z = z_0\}$, with z_0 constant. Since the steady states of (2.54) correspond to portions of the supercritical manifold $\mathcal{M}_2$, it follows that $\mathcal{Z}_{\varepsilon 0}^{a,r} \equiv \mathcal{Z}^{a,r}$, i.e., that the geometry of $\mathcal{Z}_{\varepsilon 0}^{a,r} \equiv \mathcal{Z}^{a,r}$ is, in fact, ε-independent. However, since it will become apparent that the stability properties of $\mathcal{Z}_{\varepsilon 0}^{a,r}$ do depend on ε, we will not suppress the ε-subscript in our notation.

For ε sufficiently small, Equation (2.54) undergoes a Hopf bifurcation at a point $p_{DH}^- = \left(x_{DH}^-, y_{DH}^-, z_{DH}^-\right)$; the periodic orbits that arise in that bifurcation cease to exist at z_{CN}^-, where a connecting trajectory between $\mathcal{S}_{\varepsilon 0}^{a^-}$ and $\mathcal{S}_{\varepsilon 0}^{r}$ is found. In other words, $\mathcal{S}_{\varepsilon 0}^{a^-}$ and $\mathcal{S}_{\varepsilon 0}^{r}$

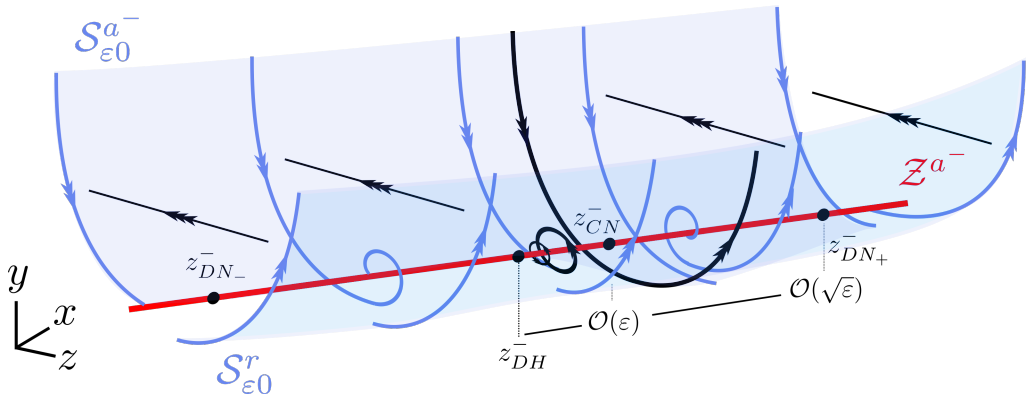

Figure 2.8: Stability of the supercritical manifold $\mathcal{M}_2$ on the various portions of $\mathcal{Z}^{a^-}$, for ε sufficiently small and $\delta = 0$: at $z^-_{DN_\mp}$, the real eigenvalues of the linearisation of Equation (2.54) about $\mathcal{M}_2$ in (2.59) become complex, with a corresponding change from nodal to focal attraction or repulsion, and vice versa; at z^-_{DH}, a Hopf bifurcation occurs which gives rise to small-amplitude periodic orbits. These orbits cease to exist at z^-_{CN}, where a connecting trajectory between $\mathcal{S}^{a^-}_{\varepsilon 0}$ and $\mathcal{S}^{r}_{\varepsilon 0}$ is found. We note that the corresponding z-interval is of width $\mathcal{O}(\varepsilon)$, while the spiralling regime is $\mathcal{O}(\sqrt{\varepsilon})$ wide overall.

intersect transversely within the hyperplane $\mathcal{P}^-_{CN} : \{z = z^-_{CN}\}$ which lies $\mathcal{O}(\varepsilon)$-close to p^-_{DH} in the z-direction. Moreover, two degenerate nodes $p^-_{DN_\mp}$ are located on $\mathcal{M}_2$ around p^-_{DH} at an $\mathcal{O}(\sqrt{\varepsilon})$-distance; see Figure 2.8. The asymptotics (in ε) of these objects is summarised below.

Lemma 7. *A Hopf bifurcation of Equation (2.54) occurs at* $p^-_{DH} : \left(x^-_{DH}, y^-_{DH}, z^-_{DH}\right) \in \mathcal{Z}^{a^-}_{\varepsilon 0}$, *where*

$$x^-_{DH} = -\frac{\beta}{2f_2}\varepsilon + \mathcal{O}(\varepsilon^2), \quad y^-_{DH} = \frac{\beta^2}{4f_2}\varepsilon^2 + \mathcal{O}(\varepsilon^3), \quad \text{and} \quad z^-_{DH} = -\frac{\alpha\beta}{2f_2}\varepsilon + \mathcal{O}(\varepsilon^2). \tag{2.55}$$

Two degenerate nodes $p^-_{DN_\mp}$ *are located at*

$$\begin{aligned} x^-_{DN_\mp} &= \mp\left(\frac{\sqrt{\alpha}}{f_2}\sqrt{\varepsilon} + \frac{\beta}{2f_2}\varepsilon\right) + \mathcal{O}(\varepsilon^{\frac{3}{2}}), \quad y^-_{DN_\mp} = \frac{\alpha}{f_2}\varepsilon + \mathcal{O}(\varepsilon^{\frac{3}{2}}), \quad \text{and} \\ z^-_{DN_\mp} &= \mp\frac{\alpha^{\frac{3}{2}}}{f_2^2}\sqrt{\varepsilon} + \frac{\alpha\beta}{f_2}\left(1 \mp \frac{1}{2}\right)\varepsilon + \mathcal{O}\left(\varepsilon^{\frac{3}{2}}\right), \end{aligned} \tag{2.56}$$

while a canard trajectory is contained in the hyperplane $\mathcal{P}^-_{CN} : \{z = z^-_{CN}\}$, *with*

$$z^-_{CN} = z^-_{DH} + \alpha\beta\frac{5f_2 - 3(1-\alpha f_3)}{4\,(1+f_2)\,f_2}\varepsilon + \mathcal{O}(\varepsilon^2). \tag{2.57}$$

Proof. The hyperplane $\{z = z^-_{CN}\}$, which contains the transverse intersection between $\mathcal{S}^{a^-}_{\varepsilon 0}$ and $\mathcal{S}^{r}_{\varepsilon 0}$, can be obtained by Melnikov-type calculations, see Section 2.6. The remaining estimates follow by considering the Jacobian matrix of the linearisation of (2.54) along $\mathcal{M}_2$,

$$J = \begin{pmatrix} 2f_2x + 3f_3x^2 & -1 \\ \varepsilon\alpha & \varepsilon\beta \end{pmatrix}, \tag{2.58}$$

the eigenvalues of which are

$$\nu_{1,2} = \frac{1}{2}\left[\beta\varepsilon + 2f_2x + 3f_3x^2 \pm \sqrt{\left(\beta\varepsilon + 2f_2x + 3f_3x^2\right)^2 - 4\left(\alpha\varepsilon + 2\beta\varepsilon f_2x + 3\beta\varepsilon f_3x^2\right)}\right]. \tag{2.59}$$

□

Remark 5. *The Hopf bifurcation at p_{DH}^- is "inherited" from the fact that $\mathcal{M}_2$ and $\mathcal{L}^-$ intersect in the folded singularity q^-: for $\varepsilon = 0 = \delta$, the trace of the Jacobian J vanishes at that point.*

It is therefore now apparent how the stability properties of $\mathcal{Z}_{\varepsilon 0}^{a,r}$ depend on ε in spite of the geometry being identical to that of $\mathcal{Z}^{a,r}$, respectively. In addition, we recall that Equation (2.2) with $\varepsilon, \delta > 0$ small undergoes Hopf bifurcations for

$$\mu_{SH}^{\mp} = -\phi(x_{DH}^{\mp}, y_{DH}^{\mp}, z_{DH}^{\mp}) + \mathcal{O}(\delta),$$

where $x_{DH}^{\mp}$, $y_{DH}^{\mp}$, and $z_{DH}^{\mp}$ are estimated in Lemma 7.

The location of z_{CN}^- is given in the singular limit $\delta = 0$; for $0 < \delta \ll 1$, its perturbed counterpart lies $\mathcal{O}(\delta)$-close to the corresponding point in the singular limit. We emphasize that if $z_{q^+} \geq z_{CN}^- + \mathcal{O}(\delta)$, where z_{q^+} is the z-coordinate of the folded singularity q^+ (recall equation (2.13) and see Figure 2.4 (a)), then the system undergoes a complete canard explosion, see Figure 2.9 first row. On the other hand, if $z_q^- \leq z_{CN}^- + \mathcal{O}(\delta)$ (Figure 2.4 (b)), then the system undergoes an "incomplete" canard explosion [De Maesschalck and Wechselberger, 2015]: the layer problem has two equilibria and the equilibrium corresponding to $\mathcal{Z}^r$ is a saddle, therefore at the occurrence of the tangential intersection between $\mathcal{S}^{a^-}$ and $\mathcal{S}^r$ a homoclinic connecion is formed from this saddle to itself; see Figure 2.9 second row. The implications of these two different cases for both the local and the global oscillatory dynamics of the system is part of work in progress.

Motivated by Lemma 7, we introduce the following notation: for $\delta = 0$, we define the intervals

$$\begin{aligned} \mathcal{I}_{\text{nod}}^{\text{in}} &= \left(-\infty, z_{DN_-}^-\right), \quad \mathcal{I}_{\text{spir}}^{\text{in}} = \left(z_{DN_-}^-, z_{DH}^-\right), \\ \mathcal{I}_{\text{can}} &= \left(\min\left\{z_{DH}^-, z_{CN}^-\right\}, \max\left\{z_{DH}^-, z_{CN}^-\right\}\right). \end{aligned} \tag{2.60}$$

Then, it follows that

1. the manifold $\mathcal{S}_{\varepsilon 0}^{a^-}$ connects to $\mathcal{Z}^{a^-}$ for $z < \min\left\{z_{DH}^-, z_{CN}^-\right\}$, while $\mathcal{S}_{\varepsilon 0}^r$ connects to $\mathcal{Z}^{a^-}$ for $z > \max\left\{z_{DH}^-, z_{CN}^-\right\}$;

2. for $f_2 < \frac{3}{5}(1 - \alpha f_3)$ (respectively, $f_2 > \frac{3}{5}(1 - \alpha f_3)$), i.e., for $z_{CN}^- > z_{DH}^-$ (respectively, $z_{CN}^- < z_{DH}^-$), the Hopf bifurcation at p_{DH}^- is supercritical (respectively, subcritical), with the resulting periodic orbits the ω-limit sets (respectively, α-limit sets) of trajectories on $\mathcal{S}_{\varepsilon 0}^{a^-}$ (respectively, $\mathcal{S}_{\varepsilon 0}^r$).

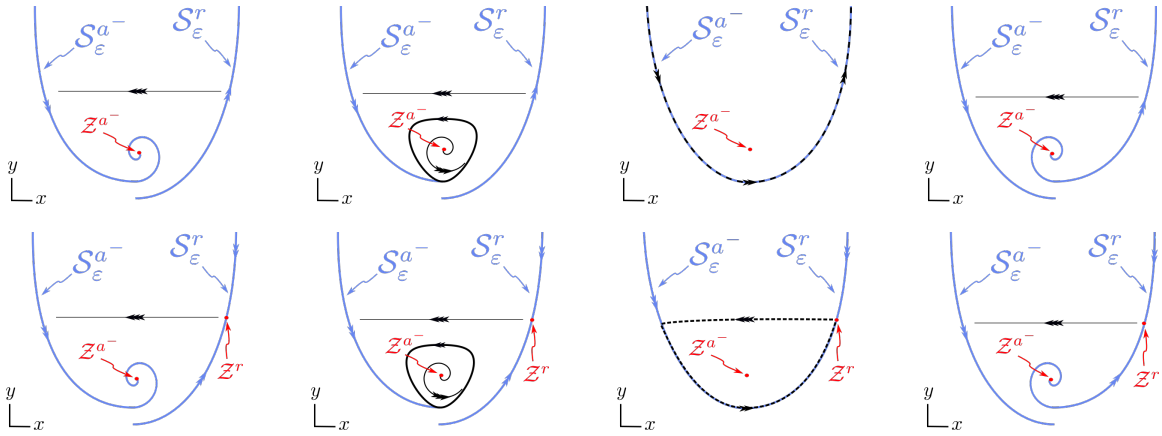

(a) $z < z_{DH}$ (b) $z_{DH} < z < z_{CN}$ (c) $z = z_{CN}$ (d) $z > z_{CN}$

Figure 2.9: The periodic orbits that emanate around $\mathcal{Z}^{a^-}$ at the delayed Hopf bifurcation increase in amplitude until the z-coordinate reaches the critical value z_{CN}, where a tangential connection is formed between $\mathcal{S}^{a^-}$ and $\mathcal{S}^r$. Depending on the location of the fold point p^+, this could lead either to a complete canard explosion (first row) or to an incomplete canard explosion (second row).

The resulting geometry is illustrated in Figure 2.8; we emphasise that analogous objects p_{DH}^+, $\mathcal{P}_{CN}^+$, and $p_{DN_\pm}^+$, which are located symmetrically to the above, exist on $\mathcal{Z}^{a^+}$.

As has already been pointed out in [Letson et al., 2017], the Hopf point p_{DH}^- and the canard point p_{CN}^- on $\mathcal{Z}^{a^-}$ collapse to the origin in the limit of $\varepsilon = 0$; correspondingly, the origin is referred to as the canard-delayed-Hopf (CDH) singularity in the double singular limit of $\varepsilon = 0 = \delta$. As a result, the folded singularity at q^- displays characteristics of both a Hopf point – in that the trace of the Jacobian in (2.58) vanishes – and a canard point – in that $\mathcal{S}^{a^-}$ and $\mathcal{S}^r$ meet along a fold. Moreover, we remark that an "incomplete" canard explosion occurs at z_{CN}^- in Equation (2.3), as the corresponding intermediate problem has two equilibria, with the equilibrium corresponding to $\mathcal{Z}^r$ being a saddle forming a homoclinic connection to itself; see [Letson et al., 2017] for details. On the other hand, Equation (2.2) could feature either complete or incomplete canard explosion, depending on the relative position of q^- and p^+; the implications for the global dynamics of the system are currently being investigated. We elaborate more on the quantitative differences between (2.2) and (2.3) near their corresponding CDH singularity, due to the existence of higher order terms in the former, in Section 2.6.

In the following, we describe the associated two mechanisms: bifurcation delay and sector-type dynamics. We remark that the former is common in two-timescale systems with two fast variables, while the latter typically occurs in two-timescale systems with two slow variables. Therefore, the coexistence of these mechanisms in three-timescale systems is due to the fact that such systems can simultaneously be viewed as having two fast and one slow variables, as well as as one fast and two slow variables. (For four-dimensional two-timescale systems with two fast and two slow variables, that interplay has been documented in [Curtu and Rubin, 2011].)

2.4.1 Bifurcation delay

SAOs due to bifurcation delay are typically encountered in two-timescale systems with two fast and one slow variables. In the context of Equation (2.2), it is realised when trajectories are attracted to $\mathcal{Z}_{\varepsilon\delta}\big|_{z\in\mathcal{I}^{\text{in}}_{\text{nod}}+\mathcal{O}(\delta)}$ or $\mathcal{Z}_{\varepsilon\delta}\big|_{z\in\mathcal{I}^{\text{in}}_{\text{spir}}+\mathcal{O}(\delta)}$, recall (2.60) and Figure 2.8. Following the slow flow on $\mathcal{Z}^{a^-}_{\varepsilon\delta}$, trajectories experience a delay in being repelled away from $\mathcal{Z}^{a^-}_{\varepsilon\delta}$ when crossing the Hopf bifurcation point p^-_{DH}, as the accumulated contraction to $\mathcal{Z}^{a^-}_{\varepsilon\delta}$ needs to be balanced by the total expansion from $\mathcal{Z}^{a^-}_{\varepsilon\delta}$ [Hayes et al., 2016, Krupa and Wechselberger, 2010]. Specifically, given some point $p_{\text{in}} = (x_{\text{in}}, y_{\text{in}}, z_{\text{in}}) \in \mathcal{Z}^{a^-}_{\varepsilon\delta}$, one obtains the x-coordinate of the corresponding point p_{out} from

$$\int_{x_{\text{in}}}^{x_{\text{out}}} \frac{\Re\left\{\nu_{1,2}\left(x\right)\right\}}{\mu+\phi\left(x,F(x),G(x)\right)}\mathrm{d}x = 0; \tag{2.61}$$

here, $\nu_{1,2}$ are the eigenvalues of the linearisation of Equation (2.54) about $\mathcal{Z}^{a^-}_{\varepsilon\delta}$, as defined in (2.59). We remark that, in [Krupa and Wechselberger, 2010, Curtu and Rubin, 2011], the accumulated contraction is balanced by the total expansion across the primary weak canard, which is an orbital connection between the folded singularity q^- and a true equilibrium of the system on $\mathcal{S}^r$; in our case, that orbital connection can be locally approximated by $\mathcal{Z}^{a^-}_{\varepsilon\delta}$ [Letson et al., 2017]. Trajectories that are attracted to $\mathcal{Z}_{\varepsilon\delta}\big|_{\mathcal{I}^{\text{in}}_{\text{spir}}}$ typically exhibit "dense" SAOs with initially decreasing and then increasing amplitude; see panel (e) of Figure 3.3. By contrast, trajectories that are attracted to $\mathcal{Z}_{\varepsilon\delta}\big|_{\mathcal{I}^{\text{in}}_{\text{nod}}}$ are characterised by few SAOs that are followed by a large excursion; cf. Figure 3.3(c).

The case where trajectories enter the spirally attracting regime $\mathcal{I}^{\text{in}}_{\text{spir}}$ is naturally studied in the rescaling chart κ_2 which is introduced as part of the blow-up analysis, see Section 2.6 and [Krupa and Wechselberger, 2010, Hayes et al., 2016, Letson et al., 2017], since that regime is bounded by the degenerate nodes $p^-_{DN_\mp}$ and, thus, of width $\mathcal{O}(\sqrt{\varepsilon})$. In that case, the eigenvalues $\nu_{1,2}$ in (2.59) are complex conjugates, which implies that the corresponding trajectory of (2.2) undergoes damped oscillation towards $\mathcal{Z}^{a^-}_{\varepsilon\delta}$. In this case, we have the following result:

Proposition 6. *Assume that Assumption 6 and Assumption 7 hold, and consider* $(x_{\text{in}}, y_{\text{in}}, z_{\text{in}}) \in \mathcal{Z}^{a^-}_{\varepsilon\delta}|_{\mathcal{I}^{\text{in}}_{\text{spir}}}$. *Then, the exit point* $(x_{\text{out}}, y_{\text{out}}, z_{\text{out}})$ *that is defined by (2.61) satisfies*

$$x_{out} \leq -x_{in} + x_{DH} + \mathcal{O}\left(\varepsilon+\delta\right), \qquad z_{out} \leq -z_{in} + z_{DH} + \mathcal{O}\left(\varepsilon+\delta\right).$$

if $\phi\left(x,F(x),G(x)\right)$ *is non-increasing for* $x \geq x_{in}$, *or*

$$x_{out} \geq -x_{in} + x_{DH} + \mathcal{O}\left(\varepsilon+\delta\right), \qquad z_{out} \geq -z_{in} + z_{DH} + \mathcal{O}\left(\varepsilon+\delta\right)$$

if $\phi\left(x,F(x),G(x)\right)$ *is non-decreasing for* $x \geq x_{in}$

Proof. The integral in (2.61) can be written as

$$\begin{aligned}\int_{x_{in}}^{x_{out}} \frac{\Re\left\{\nu_{1,2}\left(x\right)\right\}}{\mu+\phi\left(x,F(x),G(x)\right)}\mathrm{d}x &= \int_{x_{in}}^{x_{DH}} \frac{\Re\left\{\nu_{1,2}\left(x\right)\right\}}{\mu+\phi\left(x,F(x),G(x)\right)}\mathrm{d}x + \int_{x_{DH}}^{x_{out}} \frac{\Re\left\{\nu_{1,2}\left(x\right)\right\}}{\mu+\phi\left(x,F(x),G(x)\right)}\mathrm{d}x \\ &= -\int_{x_{in}}^{x_{DH}} \frac{\left|\Re\left\{\nu_{1,2}\left(x\right)\right\}\right|}{\mu+\phi\left(x,F(x),G(x)\right)}\mathrm{d}x + \int_{x_{DH}}^{x_{out}} \frac{\Re\left\{\nu_{1,2}\left(x\right)\right\}}{\mu+\phi\left(x,F(x),G(x)\right)}\mathrm{d}x\end{aligned}$$

Recall that to leading order, $\Re\{\nu_{1,2}(x)\}$ is an odd function around x_{DH}. If $\mu+\phi(x,F(x),G(x))$ is non-increasing, then

$$\int_{z_{in}}^{x_{DH}} \frac{|\Re\{\nu_{1,2}(x)\}|}{\mu+\phi(x,F(x),G(x))}\mathrm{d}x \leq \int_{x_{DH}}^{-x_{in}+x_{DH}} \frac{\Re\{\nu_{1,2}(x)\}}{\mu+\phi(x,F(x),G(x))}\mathrm{d}x,$$

therefore $x_{out} \leq -x_{in}+x_{DH}+\mathcal{O}(\varepsilon+\delta)$. The argument for the case where $\mu+\phi(x,F(x),G(x))$ is non-decreasing is similar. □

On the other hand, when trajectories enter the nodally attracting regime $\mathcal{I}^{\mathrm{in}}_{\mathrm{nod}}$, the corresponding entry point is typically $\mathcal{O}(\varepsilon^c)$ away from the folded singularity q^-, with $c<1/2$. One may therefore refer to the unscaled system, Equation (2.2), for the study of that case. The eigenvalues $\nu_{1,2}$ in (2.59) correspond to strong and weak eigendirections: specifically, for $z<z^-_{DN_-}$, the eigenvalue ν_1 represents the weak eigendirection, while the eigenvalue ν_2 corresponds to the strong eigendirection; that correspondence is reversed for $z>z^+_{DN_-}$. Due to the hierarchy of timescales in (2.2), trajectories are first attracted to $\mathcal{S}^{a^-}_{\varepsilon\delta}$ and then to $\mathcal{Z}^{a^-}_{\varepsilon\delta}$. Therefore, for initial conditions $(x,y,z)\in\mathcal{S}^{a^-}_{\varepsilon\delta}$, trajectories are attracted to $\mathcal{Z}^{a^-}_{\varepsilon\delta}$ along the weak eigendirection, while for $(x,y,z)\in\mathcal{S}^{r}_{\varepsilon\delta}$, trajectories are repelled from $\mathcal{Z}^{a^-}_{\varepsilon\delta}$ along the strong eigendirection. It hence seems reasonable to balance the accumulated contraction and expansion using solely ν_1 in (2.61). Since the accumulated contraction on the intermediate timescale has to be balanced by expansion on the fast timescale, we have the following result

Proposition 7 ([Hayes et al., 2016, Krupa and Wechselberger, 2010])**.** *Assume that Assumption 6 and Assumption 7 hold, and consider* $(x_{\mathrm{in}},y_{\mathrm{in}},z_{\mathrm{in}})\in\mathcal{Z}^{a^-}_{\varepsilon\delta}|_{\mathcal{I}^{\mathrm{in}}_{\mathrm{spir}}\cup\mathcal{I}^{\mathrm{in}}_{\mathrm{nod}}}$. *Then, the exit point* $(x_{\mathrm{out}},y_{\mathrm{out}},z_{\mathrm{out}})$ *that is defined by (2.61) satisfies*

$$x_{\mathrm{out}} < x^-_{DN_+}+o(1), \quad y_{\mathrm{out}} < y^-_{DN_+}+o(1), \quad \textit{and} \quad z_{\mathrm{out}} < z^-_{DN_+}+o(1).$$

Remark 6. *The result of Proposition 7 is based on balancing weak attraction to, by strong expansion from* $\mathcal{Z}^{a^-}$*, after trajectories cross the Hopf bifurcation point (2.55). It follows from the analysis in [Hayes et al., 2016] for the passage through such a point in systems with two fast variables and a slow one, as well as from the analysis in [Krupa and Wechselberger, 2010] for the passage through a folded saddle-node of type II, and it applies to all trajectories that enter in* $\mathcal{I}^{\mathrm{in}}_{\mathrm{spir}}\cup\mathcal{I}^{\mathrm{in}}_{\mathrm{nod}}$*, with the exception of an exponentially small interval.*

In [Letson et al., 2017], the weak contraction towards $\mathcal{Z}^{a^-}_{\varepsilon\delta}$ *is balanced by the weak expansion therefrom via*

$$\int_{x_{\mathrm{in}}}^{x^2_{DN}} \Re\{\nu_1\}\,\mathrm{d}x + \int_{x^2_{DN}}^{x_{\mathrm{out}}} \Re\{\nu_2\}\,\mathrm{d}x = 0;$$

this analysis covers all trajectories that enter in $\mathcal{I}^{\mathrm{in}}_{\mathrm{spir}}\cup\mathcal{I}^{\mathrm{in}}_{\mathrm{nod}}$*, including canard solutions, and in this context, the fold point* p^- *was in fact identified as the "buffer point" at which trajectories have to leave* $\mathcal{Z}^{a^-}_{\varepsilon\delta}$*. Here we remark that, according to Proposition 1,* $\mathcal{M}_2$ *can potentially have no fold point, and the analysis of this case in terms of balancing weak contraction by weak expansion is left as question for future investigation.*

Finally, we remark that the existence of an equilibrium point close to p_{DH}^- sets a natural bound on the exit point as follows:

Proposition 8. *Let $0 < \varepsilon, \delta \ll 1$ and assume that Assumption 6 and Assumption 7 hold, as well as that system (2.2) has j equilibrium points on $\mathcal{Z}^{a^-}$, $j \geq 1$, with $x_{eq}^{(j)} > x_{DH}$. Then for the exit point we have:*

$$x_{\text{out}} \leq \min_j \left\{ x_{eq}^{(j)} \right\}, \quad z_{\text{out}} \leq \min_j \left\{ z_{eq}^{(j)} \right\}.$$

Proof. A global equilibrium point with $x > x_{DH}$ has an invariant unstable manifold that is tangent to an unstable linear subspace, with the latter corresponding to the linearization of the fast xy-system around $\mathcal{M}_2$ at the equilibrium point. Trajectories that have been attracted to $\mathcal{M}_2$ at some point $x_{in} < x_{DH}$ can not cross the invariant unstable manifold of the true equilibrium point of the full system, therefore they have to jump at most when they reach its vicinity. □

2.4.2 Sector-type dynamics

Sector-type dynamics is typically encountered in two-timescale systems with one fast variable and two slow variables, and it can be described by exploiting the near-integrable structure of Equation (2.2) in a vicinity of the canard point p_{CN}^-, see [Krupa et al., 2008, De Maesschalck et al., 2016]. Sector-type dynamics is realised when trajectories are attracted to $\mathcal{Z}\big|_{z \in \mathcal{I}_{\text{can}} + \mathcal{O}(\delta)}$, where $\mathcal{I}_{\text{can}}$ is given by (2.60). (We emphasise that, for δ sufficiently small, $\mathcal{S}_{\varepsilon\delta}^{a^-}$ and $\mathcal{S}_{\varepsilon\delta}^{r}$ intersect in a canard trajectory that provides a connection between the two manifolds; recall Section 2.4.) For $\varepsilon, \delta > 0$ sufficiently small and $z_{\text{in}} \in \mathcal{I}_{\text{can}} + \mathcal{O}(\delta)$, trajectories remain "trapped" and undergo SAOs ("loops"), taking $\mathcal{O}(\mu\delta\sqrt{-\varepsilon \ln \varepsilon})$ steps in the z-direction until they reach a point p_{out} at which they can escape following the fast flow of Equation (2.2), as will be shown later. The z-coordinate of that point can hence be approximated by

$$z_{\text{out}} = z_{CN}^- + o(1). \tag{2.62}$$

The number of SAOs that is observed in the corresponding trajectory is due to passage through sectors of rotation [Krupa et al., 2008], the boundaries of which are so-called "secondary" canards. Trajectories that are attracted to this regime typically exhibit few SAOs of near-constant amplitude; see panel (b) of Figure 3.4, where sector-type SAOs are seen in between delay-type segments.

For our analysis, we perform a sequence of coordinate transformations in Equation (2.2): we first translate the delayed Hopf point p_{DH}^- to the origin, writing

$$x = x_{DH}^- + \tilde{x}, \quad y = y_{DH}^- + \tilde{y}, \quad \text{and} \quad z = z_{DH}^- + \tilde{z},$$

which yields

$$x' = -y + f_2 x^2 + f_3 x^3 - \varepsilon\beta \left(x + \frac{3f_3}{2f_2} x^2 \right) + \varepsilon^2 \beta^2 \frac{3f_3}{4f_2^2} x, \tag{2.63a}$$

$$y' = \varepsilon \left(\alpha x + \beta y - z \right), \tag{2.63b}$$

$$z' = \varepsilon\delta \left(\tilde{\mu}(\varepsilon) + \phi(x, y, z) \right); \tag{2.63c}$$

here, we have omitted tildes for convenience of notation. Notice that $\tilde{\mu}(\varepsilon) = \mu + \mathcal{O}(\varepsilon)$, as well as that $\tilde{\mu}(0) = \mu$. Next, we introduce the following rescaling in Equation (2.63):

$$x = \sqrt{\varepsilon}\bar{x}, \quad y = \varepsilon\bar{y}, \quad z = \sqrt{\varepsilon}\bar{z}, \quad \text{and} \quad t = \frac{\bar{t}}{\sqrt{\varepsilon}}, \tag{2.64}$$

which gives

$$\dot{x} = -y + f_2 x^2 + \sqrt{\varepsilon}\left(-\beta x + f_3 x^3\right) - \varepsilon\frac{3\beta f_3}{2f_2}x^2 + \varepsilon^{\frac{3}{2}}\frac{3\beta^2 f_3}{4f_2^2}x, \tag{2.65a}$$

$$\dot{y} = \alpha x - z + \sqrt{\varepsilon}\beta y, \tag{2.65b}$$

$$\dot{z} = \delta\left(\tilde{\mu}(\varepsilon) + \phi(\sqrt{\varepsilon}x, \varepsilon y, \sqrt{\varepsilon}z)\right); \tag{2.65c}$$

here, we have omitted overbars for convenience of notation.

Note that for $z = 0$, Equation (2.65) is a $\sqrt{\varepsilon}$-perturbation of a Hamiltonian system with Hamiltonian function

$$H(x, y) = \alpha e^{-2f_2 y/\alpha}\left(-x^2 + \frac{y}{f_2} + \frac{\alpha}{2f_2^2}\right), \tag{2.66}$$

where α and f_2 are defined as in Equation (2.2); the solutions of that (integrable) system are located on level curves γ_0^h that are given by $H(x, y) = h$. For $H(x, y) = 0$, we find the special solution

$$\gamma_0^0(t) = \left(\frac{\alpha}{2f_2}t, \frac{\alpha^2}{4f_2}t^2 - \frac{\alpha}{2f_2}\right), \tag{2.67}$$

while for $0 < H(x, y) < (2f_2)^{-2}$, solutions form a family of periodic orbits $\gamma_0^{h^+}$. The special solution in (2.67) corresponds to a parabola that separates the closed level curves $\gamma_0^{h^+}$ of H from the open ones, which are denoted by $\gamma_0^{h^-}$; see Figure 2.10, as well as [Krupa et al., 2008].

For $\varepsilon, \delta > 0$ sufficiently small, trajectories that are attracted to this vicinity follow the perturbations $\gamma_\varepsilon^{h^+}$ of the periodic orbits described above. We define by $T^h(z)$ the time that takes for a trajectory with initial condition on the y-axis to return to the y-axis after a small "loop", see Figure 2.10 panel (b). We will therefore define a map that gives the coordinates of the trajectory after a small loop, and we will preferably use the value h of the Hamiltonian of the unperturbed periodic orbit to refer to the xy-coordinates; see [Krupa et al., 2008, Section 2] for more details.

Proposition 9. *(Extension of [Krupa et al., 2008, Proposition 2.2]) Let $\bar{\Pi} : \bar{\Delta}_- \to \bar{\Delta}_-$, and consider $(h, z) \in \bar{\Delta}_-$, where we suppose that $h > 0$, with $h = \mathcal{O}(\varepsilon^M)$ for some $M > 0$ and $\varepsilon > 0$ sufficiently small. Consider $\phi(x, y, z) = -cz + \mathcal{O}((x + y + z)^2)$ for $c \geq 0$ in (2.2), let γ_ε^h be defined as above, and suppose that the trajectory starting at (h, z) undergoes a small oscillation ("loop") before returning to $\bar{\Delta}_-$.*

1. *If $c = 0$, then*

$$\bar{\Pi}(h, z) = \left(h + \sqrt{\varepsilon}d_{\sqrt{\varepsilon}}^h + zd_z^h + \mathcal{O}\left(\left(\sqrt{\varepsilon} + z\right)^2\right), z + \delta\tilde{\mu}(\varepsilon)T^h(z) + \mathcal{O}(\delta^2)\right) \tag{2.68}$$

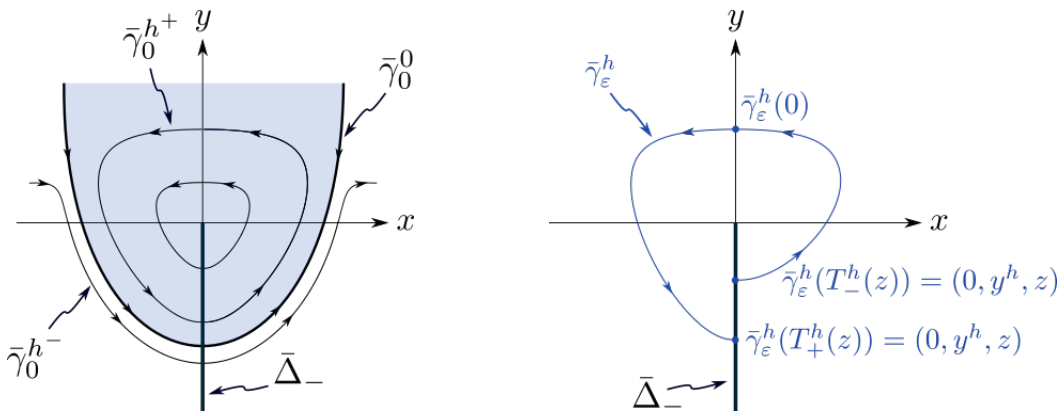

(a) (b)

Figure 2.10: Panel (a) shows the level curves of the planar Hamiltonian system (2.66). Panel (b) contains an illustration of the perturbation of a periodic orbit for system (2.65), projected onto the (x, y)-plane. Each such loop is associated to a shift in the z-direction, as described in Proposition 9.

to leading order in ε and δ, where

$$d^h_{\sqrt{\varepsilon}} = \int_{-T^h}^{T^h} \nabla H(\gamma_0^h(t)) \cdot \left(-\beta x_0^h(t) + f_3 x_0^h(t)^3, 0\right)^T \mathrm{d}t \quad \textit{and}$$

$$d^h_z = \int_{-T^h}^{T^h} \nabla H(\gamma_0^h(t)) \cdot (0, \beta)^T \mathrm{d}t$$

and $T^h(z)$ denotes the time the trajectory takes to undergo a loop.

2. *If $c > 0$, then*

$$\bar{\Pi}(h, z) = \left(h + \sqrt{\varepsilon} d^h_{\sqrt{\varepsilon}} + z d^h_z + \mathcal{O}\left(\left(\sqrt{\varepsilon} + z\right)^2\right), \frac{\tilde{\mu}(\varepsilon)}{c\sqrt{\varepsilon}} + \left(z - \frac{\tilde{\mu}(\varepsilon)}{c\sqrt{\varepsilon}}\right) e^{-c\delta\sqrt{\varepsilon}T^h(z)} + \mathcal{O}(\delta^2)\right) \tag{2.69}$$

to leading order in ε and δ, where $d^h_{\sqrt{\varepsilon}}$ and d^h_z are defined as above.

Proof. The derivation of the h-component of $\bar{\Pi}$ in both (2.68) and (2.69) is similar to that in [Krupa et al., 2008, Proposition 2.2]). For the z-part of (2.68), i.e. for when $\phi(x, y, z) = \mathcal{O}((x + y + z)^2)$, we solve (2.65c). The z-part of (2.69), i.e. for when $\phi(x, y, z) = -cz + \mathcal{O}((x + y + z)^2)$, $c > 0$, follows from solving the linear first order non-homogeneous system:

$$\dot{z} = \delta\tilde{\mu}(\varepsilon) - \delta\sqrt{\varepsilon}cz$$

which is obtained from (2.65c). □

Note that in the above we have $T^h(z) = \mathcal{O}\left(\sqrt{-\ln\varepsilon}\right)$, by [Krupa et al., 2008]. Scaling back to the original variables, recall (2.64), it follows that the step taken in the z-direction after one small loop is $\mathcal{O}(\mu\delta\sqrt{-\varepsilon\ln\varepsilon})$.

Remark 7. *A full extension of [Krupa et al., 2008, Proposition 2.2] would require us to consider the general choice of $\phi(x, y, z) = \mathcal{O}(x, y, z)$ in Equation (2.2), which is, however, analytically complicated, and is still work in progress.*

Let us now relate the integrable structure given by the Hamiltonian in (2.66) to the dynamics of Equation (2.2) with $\varepsilon, \delta > 0$ sufficiently small, as well as to Figure 2.3. For $\varepsilon = 0 = \delta$, (2.2) corresponds to the Hamiltonian system given by (2.66), which has the structure illustrated in Figure 2.10(a) close to the origin. For $\varepsilon > 0$ sufficiently small and $\delta = 0$, we have the "unfolding" of the periodic orbits shown in Figure 2.10(a) to the periodic orbits around $\mathcal{M}_2$ in the $\mathcal{O}(\varepsilon)$-interval, as illustrated in Figure 2.8. Then, for $\varepsilon, \delta > 0$ sufficiently small, the periodic orbits in this $\mathcal{O}(\varepsilon)$-interval break down and we have the perturbed trajectories illustrated in Figure 2.10 panel (b), which give rise to secondary canards that twist around the weak canard (which is approximated by $\mathcal{M}_2$). The dynamics is locally described by Proposition 9.

Plans for future work include a more detailed investigation of the possibility of chaotic MMOs. These could either be realised due to period-doubling bifurcations of the local one-dimensional map (2.69) (or an extension thereof as described in Remark 7), or due to the existence of homoclinic orbits of Shilnikov-type. We remark that Shilnikov-type homoclinic orbits have been found numerically in two-timescale counterparts of (2.2) in [Guckenheimer and Lizarraga, 2015].

2.5 Summary

In summary, the emergence of mixed-mode dynamics in (2.2) can thus be understood as follows. By standard GSPT [Fenichel, 1979], the normally hyperbolic portions $\mathcal{S}^{a^\mp}$ and $\mathcal{Z}^{a^\mp}$ of $\mathcal{M}_1$ and $\mathcal{M}_2$, respectively, perturb to $\mathcal{S}^{a^\mp}_{\varepsilon\delta}$ and $\mathcal{Z}^{a^\mp}_{\varepsilon\delta}$, respectively. Given an initial point $(x, y, z) \in \mathcal{S}^{a^-}_{\varepsilon\delta}$, the corresponding trajectory will follow the intermediate flow on $\mathcal{S}^{a^-}_{\varepsilon\delta}$ until it is either attracted to $\mathcal{Z}^{a^-}_{\varepsilon\delta}$ or until it reaches the vicinity of $\mathcal{L}^-$. If the trajectory is attracted to $\mathcal{Z}^{a^-}_{\varepsilon\delta}$, then it follows the slow flow thereon and can undergo SAOs; if it reaches the vicinity of $\mathcal{L}^-$, then there is no slow dynamics, and the trajectory jumps to the opposite attracting sheet $\mathcal{S}^{a^+}_{\varepsilon\delta}$, resulting in a large excursion. The above sequence then begins anew; see Figure 2.5, Figure 2.6 and Figure 2.7 for schematic illustrations: depending on the relative geometry of the folded singularities $q^\mp$ of $\mathcal{M}_1$, oscillatory trajectories with single, double, or no epochs of slow dynamics can occur, as indicated in Figure 2.1.

We emphasise that the "double epoch" regime in panel (b) of Figure 2.1 does not necessarily imply mixed-mode dynamics with two epochs of SAOs but, rather, with double epochs of *perturbed slow dynamics* of the corresponding singular cycles. That is, MMO trajectories are attracted to the vicinity of both branches $\mathcal{Z}^{a^\mp}_{\varepsilon\delta}$ and hence exhibit slow dynamics; however, whether SAOs will occur depends on which regime of $\mathcal{Z}$ trajectories enter, by (2.60). In particular, if a trajectory is attracted to the spiralling region on both $\mathcal{Z}^{a^-}_{\varepsilon\delta}$ and $\mathcal{Z}^{a^+}_{\varepsilon\delta}$, then two epochs of SAOs are observed. On the other hand, trajectories that are first attracted to the spiralling region on, say, $\mathcal{Z}^{a^-}$, and are then attracted to and repelled from the nodal region on $\mathcal{Z}^{a^+}$, feature SAOs below and mere slow dynamics above. (The corresponding segment of the associated Farey sequence would be 1_s1^0, with $s > 0$.) Similarly, a trajectory that is attracted to and repelled from nodal regions on both $\mathcal{Z}^{a^-}$ and $\mathcal{Z}^{a^+}$ features no SAOs

at all and is hence a relaxation oscillation with fast, intermediate, and slow components; the associated Farey sequence would be $1^0 1_0$. In the transition between remote and connected singularities, exotic MMO trajectories may occur which exhibit segments of two-timescale relaxation oscillation, SAOs above, and SAOs below. (The associated Farey sequence would be $1^s L_k$, with $L, s, k > 0$.) Finally, we postulate that chaotic mixed-mode dynamics may be possible. However, the above characterisation depends substantially on the particular form of the function ϕ in (2.2c); it is hence not feasible to further subdivide that region in Figure 2.1 exclusively on the basis of system parameters in Equation (2.2). Rather, a case-by-case study is required.

Finally, we remark on the role of the ratio between the scale separation parameters ε and δ for the dynamics of Equation (2.2). Locally, in order for the system to exhibit three timescales and for the iterative reduction from the fast via the intermediate to the slow dynamics to be accurate, ε and δ need to be sufficiently small, which is akin to asking "When is ε small enough?" in a two-timescale system. The three-timescale system then features characteristics of both two-fast/one-slow systems and one-fast/two-slow systems. We recall that, by Lemma 7, the width of the various regimes on $\mathcal{Z}$ is either $\mathcal{O}(\varepsilon)$ or $\mathcal{O}(\sqrt{\varepsilon})$. By [Krupa et al., 2008] and Lemma 4, the "step" in the z-direction taken by trajectories after a large excursion and re-injection is $\mathcal{O}(\delta)$; it therefore follows that if $\delta = \mathcal{O}(\varepsilon^c)$ for $0 < c < 1$, then trajectories will typically not undergo sector-type dynamics, since the width of the latter regime is $\mathcal{O}(\varepsilon)$. Hence, delay-type SAOs are expected to dominate in that case. The above are in accordance with a conjecture made in [Vo et al., 2013]; we present numerical evidence for this in Figure 3.4 in Chapter 3.

In the remaining of this chapter, we illustrate a brief blowup analysis in the vicinity of q^-. In Section 2.6 we follow the analysis of [Letson et al., 2017] to give an estimate of canard and buffer points in (2.2) under Assumption 6. In Section 2.7 we analyse the case where $\alpha = 0$, $\beta < 0$ in (2.2), i.e. when $q^\mp \equiv p^\mp$, see Figure 2.8 panel (b).

2.6 Blow-up of folded singularities

Here we perform a blow-up analysis at the point p_{DH}^- where the delayed-Hopf bifurcation occurs. Our main focus is to show that all trajectories that approach this point diverge from $\mathcal{Z}_{\varepsilon\delta}$ in an $\mathcal{O}(\varepsilon)$ neighbourhood of this point. The analysis in this section is based on [Krupa and Szmolyan, 2001a, Krupa and Wechselberger, 2010]; we will follow the approach of [Letson et al., 2017], and we will emphasize the differences with the analysis therein due to cubic terms in (2.2a).

First, using (2.55), we make the following transformation of system (2.2)

$$\begin{aligned} x' &= -y + f_2 x^2 + f_3 x^3 - \varepsilon\beta \left(x + \frac{3f_3}{2f_2} x^2 \right) + \varepsilon^2 \beta^2 \left(\frac{3f_3}{4f_2^2} x \right), \\ y' &= \varepsilon \left(\alpha x + \beta y - z \right), \\ z' &= \varepsilon\delta \left(\tilde{\mu} + \phi(x, y, z) \right), \end{aligned} \tag{2.70a}$$

in which the origin has been translated to the location of the delayed Hopf bifurcation point p_{DH}^- near $\mathcal{L}^-$.

We consider the blow-up transformation $\Phi : B = \mathbb{S}^3 \times \mathbb{R} \to \mathbb{R}^4$ given by

$$x = r\bar{x}, \quad y = r^2\bar{y}, \quad z = r\bar{z}, \quad \varepsilon = r^2\bar{\varepsilon} \tag{2.71}$$

where $r \in [0, \rho]$, $\rho > 0$ and $(\bar{x}, \bar{y}, \bar{z}, \bar{\varepsilon}) \in \mathbb{S}^3$; we remark that the parameter δ is not included in the blow-up transformation. In the following, we study the dynamics in the entry chart κ_1 and in the rescaling chart κ_2, and point out the differences to the canonical form (2.3) studied in [Letson et al., 2017], due to the additional terms in (2.2). The dynamics in the exit chart κ_3 follows from [Szmolyan and Wechselberger, 2004] and we hence omit it here.

2.6.1 The entry chart $\kappa_1 : \{\bar{y} = 1\}$

The blowup $\Phi_1 : \mathbb{R}^4 \to \mathbb{R}^4$ is obtained by setting $\{\bar{y} = 1\}$ in (2.71), i.e.

$$x = r_1 x_1, \quad y = r_1^2, \quad z = r_1 z_1, \quad \varepsilon = r_1^2 \varepsilon_1. \tag{2.72}$$

After transformation of (2.70) using (2.72) and rescaling time by a factor of r_1 we obtain

$$r_1' = \frac{1}{2} r_1 \varepsilon_1 F_1(r_1, x_1, z_1) \tag{2.73a}$$

$$x_1' = -1 + f_2 x_1^2 + f_3 r_1 x_1^3 - \varepsilon_1 x_1 \left(\beta r_1 \left(1 + \frac{3 f_3}{2 f_2} r_1 x_1 \right) + \frac{1}{2} F_1(r_1, x_1, z_1) \right) + \varepsilon_1^2 r_1^3 \frac{3 f_3 \beta^2}{2 f_2^2} x_1 \tag{2.73b}$$

$$z_1' = \varepsilon_1 \delta \left(\tilde{\mu} + \phi(r_1 x_1, r_1^2, r_1 z_1) \right) - \frac{1}{2} z_1 \varepsilon_1 F_1(r_1, x_1, z_1) \tag{2.73c}$$

$$\varepsilon_1' = -\varepsilon_1^2 F_1(r_1, x_1, z_1) \tag{2.73d}$$

where $F_1(r_1, x_1, z_1) = \alpha x_1 + \beta r_1 - z_1$. Notice that (2.73) is a regular perturbation problem in δ.

The hyperplanes $\{\varepsilon_1 = 0\}$ and $\{r_1 = 0\}$ are invariant. In their intersection $\{\varepsilon_1 = 0 = r_1\}$ the dynamics is given by

$$\begin{aligned} x_1' &= -1 + f_2 x_1^2, \\ z_1' &= 0, \end{aligned}$$

and it contains the lines of equilibria

$$\begin{aligned} \ell_{a,1} &= \left\{ (0, -1/\sqrt{f_2}, z_1, 0),\ z_1 \in \mathbb{R} \right\}, \\ \ell_{r,1} &= \left\{ (0, 1/\sqrt{f_2}, z_1, 0),\ z_1 \in \mathbb{R} \right\}, \end{aligned}$$

which have eigenvalues $\lambda_{a,1} = -2/\sqrt{f_2}$ and $\lambda_{r,1} = 2/\sqrt{f_2}$, respectively. The dynamics in the invariant hyperplane $\{r_1 = 0\}$ is given by

$$r_1' = 0 \tag{2.74}$$

$$x_1' = -1 + f_2 x_1^2 - \frac{\varepsilon_1 x_1}{2} F_1(r_1, x_1, z_1) \tag{2.75}$$

$$z_1' = \varepsilon_1 \delta \left(\tilde{\mu} + \phi(r_1 x_1, r_1^2, r_1 z_1) \right) - \frac{1}{2} z_1 \varepsilon_1 F_1(r_1, x_1, z_1) \tag{2.76}$$

and here we recover the lines of equilibria $\ell_{a,1}$ and $\ell_{r,1}$, and there exist two-dimensional centre manifolds $N_{a,1}$, $N_{r,1}$, containing the lines $\ell_{a,1}$ and $\ell_{r,1}$, and whereon (away from $\ell_{a,1}$ and $\ell_{r,1}$) $\varepsilon_1' > 0$ [Szmolyan and Wechselberger, 2004]. In the invariant hyperplane $\{\varepsilon_1 = 0\}$ we obtain normally hyperbolic surfaces $S_{a,1}$ and $S_{a,1}$ which emanate from $\ell_{a,1}$ and $\ell_{r,1}$, respectively, see also [Szmolyan and Wechselberger, 2004, Letson et al., 2017].

The dynamics in chart κ_1 can be summarized as follows.

Proposition 10 ([Szmolyan and Wechselberger, 2004, Letson et al., 2017])**.** *The following assertions hold for system (2.89):*

1. *There exists an attracting three-dimensional centre manifold $M_{a,1}$ at $\ell_{a,1}$ which contains the surface of equilibria $S_{a,1}$ and the centre manifold $N_{a,1}$. Moreover, the manifold $M_{a,1}$ has the graph representation*

$$x_1 = -1/\sqrt{f_2} + \mathcal{O}\left((r_1 + \varepsilon_1 + z_1)^2\right) =: h^-(r_1, z_1, \varepsilon_1) \tag{2.77}$$

for $\varepsilon_1, r_1 > 0$ small. Finally, there exists a stable invariant foliation $\mathcal{F}^s$ with base $M_{a,1}$ and one-dimensional fibres, and for any $c > -2/\sqrt{f_2}$, the contraction along $\mathcal{F}^s$ in a time interval $[0, T]$ is stronger than e^{cT}.

2. *There exists a repelling two-dimensional C^k-center manifold $M_{r,1}$ at $\ell_{r,1}$ which contains the surface of equilibria $S_{r,1}$ and the centre manifold $N_{r,1}$. Moreover, the manifold $M_{r,1}$ has the graph representation*

$$x_1 = 1/\sqrt{f_2} + \mathcal{O}\left((r_1 + \varepsilon_1 + z_1)^2\right) =: h^+(r_1, z_1, \varepsilon_1) \tag{2.78}$$

for $\varepsilon_1, r_1 > 0$ small. Finally, there exists a stable invariant foliation $\mathcal{F}^s$ with base $M_{a,1}$ and one-dimensional fibres, and for any $c < 2/\sqrt{f_2}$, the contraction along $\mathcal{F}^s$ in a time interval $[0, T]$ is stronger than e^{cT}.

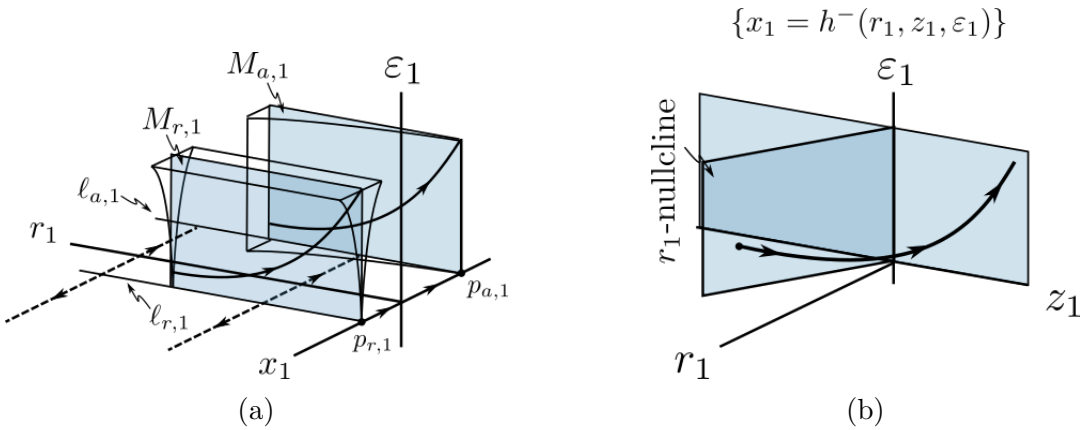

Figure 2.11: (a) Projection of the centre manifolds $M_{a,1}$ and $M_{r,1}$ onto the $(r_1, x_1, \varepsilon_1)$-subspace. (b) Dynamics in $M_{a,1}$, and a trajectory emanating from the r_1-nullcline and approaching the $r_1 = 0$-plane, whereon ε_1 is increasing.

Substituting the representation $x_1 = h^-(r_1, z_1, \varepsilon_1)$ from (2.96) into (2.73) and rescaling time by a factor of ε_1 therein gives the flow in $M_{a,1}$ as

$$\dot{r}_1 = \frac{1}{2} r_1 \left(-\frac{\alpha}{\sqrt{f_2}} + \beta r_1 - z_1 + \mathcal{O}\left((r_1 + \varepsilon_1 + z_1)^2 \right) \right) \tag{2.79a}$$

$$\dot{z}_1 = \delta \left(\tilde{\mu} + \phi \left(-\frac{1}{\sqrt{f_2}}, r_1^2, r_1 z_1 \right) \right) - \frac{1}{2} z_1 \left(-\frac{\alpha}{\sqrt{f_2}} + \beta r_1 - z_1 + \mathcal{O}\left((r_1 + \varepsilon_1 + z_1)^2 \right) \right) \tag{2.79b}$$

$$\dot{\varepsilon}_1 = -\varepsilon_1 \left(-\frac{\alpha}{\sqrt{f_2}} + \beta r_1 - z_1 + \mathcal{O}\left((r_1 + \varepsilon_1 + z_1)^2 \right) \right). \tag{2.79c}$$

The plane $\{r_1 = 0\}$ in (2.79) is invariant, and the dynamics therein is given by

$$z_1' = \delta \left(\tilde{\mu} + \phi \left(-\frac{1}{\sqrt{f_2}}, 0, 0 \right) \right) - \frac{1}{2} z_1 \left(-\frac{\alpha}{\sqrt{f_2}} - z_1 + \mathcal{O}\left((\varepsilon_1 + z_1)^2 \right) \right), \tag{2.80}$$

$$\varepsilon_1' = -\varepsilon_1 \left(-\frac{\alpha}{\sqrt{f_2}} - z_1 + \mathcal{O}\left((\varepsilon_1 + z_1)^2 \right) \right). \tag{2.81}$$

Moreover, the r_1-nullcline in (2.79) is given by $z_1 = \beta r_1 - \frac{\alpha}{\sqrt{f_2}}$, whereon there holds that $z_1' > 0$. It also follows that $r_1' < 0$, $z_1' > 0$ and $\varepsilon_1' > 0$ for $z_1 > \beta r_1 - \frac{\alpha}{\sqrt{f_2}}$. Therefore, all trajectories with $z_1 > \beta r_1 - \frac{\alpha}{\sqrt{f_2}}$ are attracted to the $\{r_1 = 0\}$-plane and increase in the ε_1-direction, transiting to the rescaling chart κ_2, see Figure 2.11.

2.6.2 The rescaling chart $\kappa_2 : \{\bar{y} = 1\}$

The blowup $\Phi_2 : \mathbb{R}^4 \to \mathbb{R}^4$ is obtained by setting $\{\bar{\varepsilon} = 1\}$ in (2.71), i.e.

$$x = r_2 x_2, \quad y = r_2^2 y_2, \quad z = r_2 z_2, \quad \varepsilon = r_2^2, \quad \delta = \delta_2 \tag{2.82}$$

After transformation of (2.70) and rescaling by a factor of r_2 we obtain

$$x_2' = -y_2 + f_2 x_2^2 + r_2 \left(-\beta x_2 + f_3 x_2^3 \right) - r_2^2 \left(\frac{3\beta f_3}{2 f_2} x_2^2 \right) + r_2^3 \left(\frac{3\beta^2 f_3}{4 f_2^2} x_2 \right) \tag{2.83a}$$

$$y_2' = \alpha x_2 + \beta r_2 y_2 - z_2 \tag{2.83b}$$

$$z_2' = \delta_2 \left(\tilde{\mu} + \phi(r_2 x_2, r_2^2 y_2, r_2 z_2) \right) \tag{2.83c}$$

We first remark that system (2.83) is the unfolding of a canard explosion of the x_2, y_2-subsystem in the z_2 direction; this canard explosion has implications for the oscillatory dynamics of the original system (2.2), as described in Section 2.4.

Proposition 11. *For fixed $f_2 > 0$, $f_3 < 0$, $\alpha > 0$, $\beta < 0$, let $0 < \varepsilon \ll 1$, $\delta = 0$ and*

$$z_{cn} = -\frac{\beta \left((5 f_2 - 3) - 3\alpha f_3 \right) \alpha}{4 \left(1 + f_2 \right) f_2} \sqrt{\varepsilon} + \mathcal{O}(\varepsilon), \tag{2.84}$$

Then, the slow manifolds $\mathcal{S}_\varepsilon^{a^-}$ and $\mathcal{S}_\varepsilon^r$ of (2.70) intersect tangentially for z_{cn}.

Proof. For $z_2 = 0$, system {(2.83a)-(2.83b)} is an r_2-perturbation of a Hamiltonian system with Hamiltonian function

$$H\left(x_2, y_2\right) = \alpha e^{-2f_2 y_2/\alpha}\left(-x_2^2 + \frac{y_2}{f_2} + \frac{\alpha}{2f_2^2}\right),$$

which for $H(x_2, y_2) = 0$ has explicit solution

$$\gamma_0^0(t) = \left(\frac{a}{2f_2}t, \frac{a^2}{4f_2}t^2 - \frac{a}{2f_2}\right),$$

recall Section 2.4, Equation (2.67) and Figure 2.10.

The tangential intersection of the slow manifolds is formed for the value of z_2 for which the Melnikov distance function

$$\mathcal{D}_c(r_2, z_2) = d_{r_2} r_2 + d_{z_2} z_2 + \mathcal{O}\left(\left(r_2 + z_2\right)^2\right), \tag{2.85}$$

vanishes, see [Krupa and Szmolyan, 2001a]; in the above, the coefficients are given by

$$d_{r_2} = \int_{-\infty}^{\infty}\left\{\nabla H \cdot \begin{pmatrix} -\beta x_2 + f_3 x^3 \\ \beta y_2 \end{pmatrix}\right\}\Big|_{\gamma_0^0(t)} \mathrm{d}t = \frac{e\left(\beta\left(5f_2 - 3\right) - 3\alpha f_3\right)}{4}\sqrt{\frac{\pi\alpha^3}{2f_2^3}}$$
$$d_{z_2} = \int_{-\infty}^{\infty}\left\{\nabla H \cdot \begin{pmatrix} 0 \\ -1 \end{pmatrix}\right\}\Big|_{\gamma_0^0(t)} \mathrm{d}t = -e\left(1 + f_2\right)\sqrt{\frac{\pi\alpha}{2f_2}}$$

Solving $\mathcal{D}_c(r_2, z_2) = 0$ gives z_{cn}. Scaling back to the variables of system (2.70) gives z_{CN}^- as in (2.57). □

We remark that (2.84) generalises the result in [Letson et al., 2017, Proposition 2 (Supplementary Material)], where the result corresponds to the special case $f_2 = 1$, $f_3 = 0$. Moreover, we notice that the cubic terms in (2.2a) do in fact contribute to the local dynamics, as opposed to what is claimed in the discussion in [Letson et al., 2017, Proposition 1].

2.7 The "double fold" case

Here we study the case where the fold points $p^{\mp}$ lie (simultaneously) on $\mathcal{L}^{\mp}$, i.e. $\alpha = 0$ in (2.2), cf. Figure 2.3 panel (b). We will show that, when trajectories reach this vicinities in the perturbed system (2.2) with $\varepsilon, \delta > 0$, they simply jump to the opposite side. Based on arguments similar to the ones in Theorem 4, it can be shown that the system features three-timescale relaxation oscillations; we remark, however, that this scenario is not realised in any of the systems from applications that we are considering in this work.

Our analysis here will be local in the vicinity of q^-, and the analysis near q^+ is similar. For simplicity, we will consider the case where $f_2 = 1$, $f_3 = 0$, $\beta = -1$ and $\mu + \phi(x, y, z) \equiv 1$, i.e. we will consider

$$x' = -y + x^2, \tag{2.86a}$$
$$y' = \varepsilon\left(-y - z\right), \tag{2.86b}$$
$$z' = \varepsilon\delta. \tag{2.86c}$$

We consider again the blow-up transformation $\Phi : B = \mathbb{S}^3 \times \mathbb{R} \to \mathbb{R}^4$ given by

$$x = r\bar{x}, \quad y = r^2\bar{y}, \quad z = r\bar{z}, \quad \varepsilon = r^2\bar{\varepsilon} \tag{2.87}$$

where $r \in [0, \rho]$, $\rho > 0$ and $(\bar{x}, \bar{y}, \bar{z}, \bar{\varepsilon}) \in \mathbb{S}^3$; we remark that the parameter δ is not included in the blow-up transformation. Agein, we study the dynamics in the entry chart κ_1 and in the rescaling chart κ_2. Like in the general case studied in Section 2.6, the dynamics in the exit chart κ_3 follows from [Szmolyan and Wechselberger, 2004] and we hence omit it here.

2.7.1 The entry chart $\kappa_1 : \{\bar{y} = 1\}$

The blowup $\Phi_1 : \mathbb{R}^4 \to \mathbb{R}^4$ is obtained by setting $\{\bar{y} = 1\}$ in (2.87), i.e.

$$x = r_1 x_1, \quad y = r_2^2, \quad z = r_1 z_1, \quad \varepsilon = r_1^2 \varepsilon_1. \tag{2.88}$$

Substituting the above to (2.86) and rescaling time by a factor of r_1 gives

$$r_1' = -\frac{r_1\varepsilon_1}{2}(z_1 + r_1) \tag{2.89a}$$
$$x_1' = -1 + x_1^2 + \frac{x_1\varepsilon_1}{2}(z_1 + r_1) \tag{2.89b}$$
$$z_1' = \varepsilon_1\left(\delta + \frac{z_1}{2}(z_1 + r_1)\right) \tag{2.89c}$$
$$\varepsilon_1' = \varepsilon_1(z_1 + r_1) \tag{2.89d}$$

System (2.89) is regularly perturbed in δ.

The hyperplanes $\{\varepsilon_1 = 0\}$ and $\{r_1 = 0\}$ are invariant. In their intersection $\{\varepsilon_1 = 0 = r_1\}$ the dynamics is given by

$$x_1' = -1 + x_1^2,$$
$$z_1' = 0,$$

The dynamics in the invariant hyperplane $\{\varepsilon_1 = 0\}$ is given by

$$r_1' = 0, \tag{2.90}$$
$$x_1' = -1 + x_1^2, \tag{2.91}$$
$$z_1' = 0, \tag{2.92}$$

and it contains the lines of equilibria

$$\ell_{a,1} = \{(0, -1, z_1, 0),\ z_1 \in \mathbb{R}\},$$
$$\ell_{r,1} = \{(0, 1, z_1, 0),\ z_1 \in \mathbb{R}\},$$

which have eigenvalues $\lambda_{a,1} = -2$ and $\lambda_{r,1} = 2$, respectively. Moreover, there exist normally hyperbolic surfaces

$$S_{a,1} = \{(r_1, -1, z_1, 0),\ r_1, z_1 \in \mathbb{R}\},$$
$$S_{r,1} = \{(r_1, 1, z_1, 0),\ r_1, z_1 \in \mathbb{R}\},$$

which emanate from $\ell_{a,1}$ and $\ell_{r,1}$, respectively, see also [Szmolyan and Wechselberger, 2004, Letson et al., 2017].

The dynamics in the invariant hyperplane $\{r_1 = 0\}$ is given by

$$r_1' = 0, \tag{2.93}$$

$$x_1' = -1 + x_1^2 + \frac{x_1 \varepsilon_1 z_1}{2}, \tag{2.94}$$

$$z_1' = \varepsilon_1 \left(\delta + \frac{z_1^2}{2} \right), \tag{2.95}$$

and here we recover the lines of equilibria $\ell_{a,1}$ and $\ell_{r,1}$, and there exist two-dimensional centre manifolds $N_{a,1}$, $N_{r,1}$, containing the lines $\ell_{a,1}$ and $\ell_{r,1}$, and whereon (away from $\ell_{a,1}$ and $\ell_{r,1}$) $\varepsilon_1' > 0$ [Szmolyan and Wechselberger, 2004].

The dynamics in chart κ_1 can be summarized as follows.

Proposition 12 ([Szmolyan and Wechselberger, 2004, Letson et al., 2017])**.** *The following assertions hold for system (2.89):*

1. *There exists an attracting three-dimensional centre manifold $M_{a,1}$ at $\ell_{a,1}$ which contains the surface of equilibria $S_{a,1}$ and the centre manifold $N_{a,1}$. Moreover, the manifold $M_{a,1}$ has the graph representation*

$$x_1 = -1 + \mathcal{O}\left((r_1 + \varepsilon_1 + z_1)^2 \right) =: h^-(r_1, z_1, \varepsilon_1) \tag{2.96}$$

   for $\varepsilon_1, r_1 > 0$ small. Finally, there exists a stable invariant foliation $\mathcal{F}^s$ with base $M_{a,1}$ and one-dimensional fibres, and for any $c > -2$, the contraction along $\mathcal{F}^s$ in a time interval $[0, T]$ is stronger than e^{cT}.

2. *There exists a repelling two-dimensional C^k-center manifold $M_{r,1}$ at $\ell_{r,1}$ which contains the surface of equilibria $S_{r,1}$ and the centre manifold $N_{r,1}$. Moreover, the manifold $M_{r,1}$ has the graph representation*

$$x_1 = 1 + \mathcal{O}\left((r_1 + \varepsilon_1 + z_1)^2 \right) =: h^+(r_1, z_1, \varepsilon_1) \tag{2.97}$$

   for $\varepsilon_1, r_1 > 0$ small. Finally, there exists a stable invariant foliation $\mathcal{F}^s$ with base $M_{a,1}$ and one-dimensional fibres, and for any $c < 2$, the contraction along $\mathcal{F}^s$ in a time interval $[0, T]$ is stronger than e^{cT}.

Substituting the representation $x_1 = h^-(r_1, z_1, \varepsilon_1)$ from (2.96) into (2.73) and rescaling time by a factor of ε_1 therein gives the flow in $M_{a,1}$ as

$$r_1' = -\frac{r_1 \varepsilon_1}{2} (z_1 + r_1) \tag{2.98a}$$

$$z_1' = \varepsilon_1 \delta + \frac{z_1 \varepsilon_1}{2} (z_1 + r_1) \tag{2.98b}$$

$$\varepsilon_1' = \varepsilon_1 (z_1 + r_1) \tag{2.98c}$$

The plane $\{r_1 = 0\}$ in (2.98) is invariant, and the dynamics therein is given by

$$z_1' = \varepsilon_1\delta + \frac{z_1^2\varepsilon_1}{2}, \tag{2.99}$$

$$\varepsilon_1' = \varepsilon_1 z_1. \tag{2.100}$$

Moreover, the r_1-nullcline in (2.98) is given by $r_1 = -z_1$, whereon there holds that $z_1' > 0$. It also follows that $r_1' < 0$, $z_1' > 0$ and $\varepsilon_1' > 0$ for $r_1 > -z_1$. Therefore, all trajectories with $r_1 > -z_1$ are attracted to the $\{r_1 = 0\}$-plane and increase in the ε_1-direction, transiting to the rescaling chart κ_2, see Figure 2.11.

2.7.2 The rescaling chart $\kappa_2 : \{\bar{\varepsilon} = 1\}$

The blowup $\Phi_2 : \mathbb{R}^4 \to \mathbb{R}^4$ is obtained by setting $\{\bar{\varepsilon} = 1\}$ in (2.87), i.e.

$$x = r_2 x_2, \quad y = r_2^2 y_2, \quad z = r_2 z_2, \quad \varepsilon = r_2^2. \tag{2.101}$$

Substituting the above to (2.86) and rescaling time by a factor of r_2 gives

$$x_2' = -y_2 + x_2^2 \tag{2.102a}$$

$$y_2' = -y_2 - z_2 \tag{2.102b}$$

$$z_2' = \delta \tag{2.102c}$$

System (2.102) is singularly perturbed with respect to δ, with two fast variables x, y and one slow variable z. Its critical manifold $\mathcal{U}_2$ is given by

$$\mathcal{U}_2 = \left\{(x_2, y_2, z_2) \in \mathbb{R}^2 \mid y_2 = x_2^2,\ y_2 = -z_2\right\}$$

and it has a fold point at the origin. The branch of $\mathcal{U}_2$ with $x_2 < 0$ is attracting,while the branch of $\mathcal{U}_2$ with $x_2 > 0$ is repelling.

Augmenting system (2.102) by including δ as a dynamic variable gives,

$$x_2' = -y_2 + x_2^2, \tag{2.103}$$

$$y_2' = -y_2 - z_2, \tag{2.104}$$

$$z_2' = \delta, \tag{2.105}$$

$$\delta' = 0, \tag{2.106}$$

and it follows that system (2.102) has a centre manifold at the origin given by

$$\mathcal{W}^c = \left\{(x_2.y_2.z_2) \in \mathbb{R}^3 \mid y_2 = -z_2 + \delta + \mathcal{O}\left((x_2 + z_2 + \delta)^2\right)\right\}$$

and the dynamics near the origin is therefore approximated by

$$x_2' = z_2 + x_2^2 + \delta + \mathcal{O}\left((x_2 + z_2 + \delta)^2\right), \tag{2.107}$$

$$z_2' = \delta, \tag{2.108}$$

which corresponds to the case of the fold point studied in [Krupa and Szmolyan, 2001a]. For $\delta > 0$ small, trajectories therefore escape in the positive x_2-direction, cf. Figure 2.12.

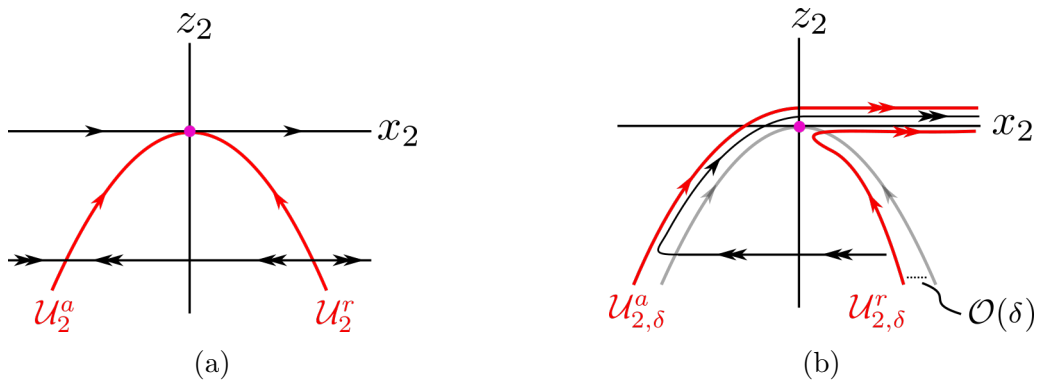

Figure 2.12: (a) Projection of the singular manifold $\mathcal{U}_2$ onto the xz-plane; the branch $\mathcal{U}_2^a$ is attracting and the branch $\mathcal{U}_2^r$ is repelling (b) Dynamics and perturbed branches $\mathcal{U}_{2,\delta}^a$ and $\mathcal{U}_{2,\delta}^r$ for $\delta > 0$ small.

To see this, alternatively, consider $\delta > 0$ small; then, from (2.102c), the z_2-dynamics is given by

$$z_2(t) = \delta t + z_{20},$$

where $z_{20} = z_2(0)$. Substituting the above in (2.102b) and solving the corresponding ODE gives:

$$y_2(t) = \delta(1-t) - z_{20} + (y_{20} + z_{20} - \delta)e^{-t}$$

where $y_{20} = y_2(0)$. It therefore follows that $y_2 \to -\infty$ as $t \to \infty$, and from (2.102a) it also follows that $x_2 \to \infty$ as $t \to \infty$, and therefore trajectories escape in the positive x_2-direction.

Finally, we remark that, considering the more general case of z-dynamics as in (2.2c), which would correspond to $z_2' = \delta\,(\mu + \phi(r_2x_2, r_2^2y_2, r_2y_2))$ in (2.102c), would a canard explosion for system (2.102) with $\varepsilon, \delta > 0$ small when an equilibrium point crossed the vicinity of the fold line as in [Krupa and Szmolyan, 2001a], instead of a singular Hopf bifurcation of the full system (2.2) that is realised for $\alpha > 0$.

Chapter 3

The Koper model from chemical kinetics

As the first realisation of our extended prototypical model, Equation (2.2), we consider the Koper model from chemical kinetics:

$$\epsilon\dot{x} = ky + 3x - x^3 - \lambda, \tag{3.1a}$$
$$\dot{y} = x - 2y + z, \tag{3.1b}$$
$$\dot{z} = \varepsilon\delta\,(y - z)\,, \tag{3.1c}$$

with $k < 0$ and $\lambda \in \mathbb{R}$. The above system is a simplification of theoretical models proposed in [Koper and Gaspard, 1991, Koper and Gaspard, 1992] that describes the spontaneous current oscillations observed during the reduction of indium(III) catalyzed by thiocyanate at a hanging mercury drop electrode; the variable x is related to the electrode potential, and the variables y and z are related to indium concentrations in particular layers of the electrolyte around the drop. In [Koper, 1995], where it was first introduced, it is stated that "Although the model cannot be related to any realistic chemistry, it serves as the simplest possible geometrical interpretation of a bifurcation diagram frequently encountered in nonlinear chemical reactions, known as the cross-shaped phase diagram".

After dividing both sides of (3.1a) by $|k|$ and using the transformation

$$\tilde{x} = x + 1, \qquad \tilde{y} = y + \frac{2+\lambda}{|k|}, \qquad \tilde{z} = -z - 1 + \frac{2(2+\lambda)}{|k|}, \tag{3.2}$$

Equation (3.1) is brought to the form of the extended prototypical example Equation (2.2), with

$$\varepsilon = \frac{\epsilon}{|k|}, \quad f_2 = \frac{3}{|k|}, \quad f_3 = -\frac{1}{|k|}, \tag{3.3a}$$
$$\alpha = 1, \quad \beta = -2, \tag{3.3b}$$
$$\mu = \frac{k+\lambda+2}{k}, \quad \text{and} \quad \phi(x,y,z) = -y - z; \tag{3.3c}$$

henceforth, we will refer to (2.2) with the above choice of parameters as the Koper model; here, $k < 0$ and $\lambda \in \mathbb{R}$ will be our bifurcation parameters.

From Section 2.2, it is apparent that the effect of the parameter k on the dynamics is more substantial than that of λ, since variation in k simultaneously affects the timescale separation (through ε) and the singular geometry (through f_2 and f_3), as well as the slow flow and the global return (through μ). Given $k < 0$ fixed, on the other hand, variation in λ only affects the slow flow and the global return (through μ). It is therefore the parameter k that determines whether the folded singularities in the Koper model are remote or aligned/connected, and whether the model can exhibit single or double epochs of SAOs. For given $k < 0$, the parameter λ can differentiate between steady-state and oscillatory dynamics, as well as between MMOs and relaxation in the case of remote singularities.

Remark 8. *The Koper model can also be written in the symmetric form*

$$\begin{aligned} \epsilon\dot{x} &= y - x^3 + 3x, \\ \dot{y} &= kx - 2\,(y + \lambda) + z, \\ \dot{z} &= \delta(\lambda + y - z), \end{aligned}$$

which is invariant under the transformation $(x, y, z, \lambda, k, t) \to (-x, -y, -z, -\lambda, k, t)$*, see [Desroches et al., 2012] for details.*

In the following, we will restrict to the case where $\lambda > 0$. Moreover, we will investigate the dynamics near $\mathcal{L}^-$ only: by Remark 8, the behaviour near $\mathcal{L}^+$ for $\lambda < 0$ can then be deduced by symmetry; cf. also panels (a) and (b) in Figure 1, where the corresponding time series are seen to be symmetric about the t-axis for k fixed and $\lambda \to -\lambda$.

3.1 Singular geometry

The critical and supercritical manifolds $\mathcal{M}_1$ and $\mathcal{M}_2$, respectively, for the Koper model are given by

$$\begin{aligned} \mathcal{M}_1 &= \left\{ (x, y, z) \in \mathbb{R}^3 \;\middle|\; y = x^2 \frac{3 - x}{|k|} \right\} \quad \text{and} \\ \mathcal{M}_2 &= \left\{ (x, y, z) \in \mathcal{M}_1 \;\middle|\; z = x - 2x^2 \frac{3 - x}{|k|} \right\}; \end{aligned}$$

see Section 2.2. The critical manifold $\mathcal{M}_1$ is normally hyperbolic at

$$\mathcal{S} = \mathcal{S}^{a^{\mp}} \cup \mathcal{S}^r, \tag{3.4}$$

where

$$\mathcal{S}^{a^-} = \left\{ (x, y, z) \in \mathcal{M}_1 \;\middle|\; x < 0 \right\}, \quad \mathcal{S}^{a^+} = \left\{ (x, y, z) \in \mathcal{M}_1 \;\middle|\; x > 2 \right\}, \quad \text{and}$$
$$\mathcal{S}^r = \left\{ (x, y, z) \in \mathcal{M}_1 \;\middle|\; 0 < x < 2 \right\}.$$

The fold lines of $\mathcal{M}_1$ are located at

$$\mathcal{L}^- = \left\{ (x, y, z) \in \mathbb{R}^3 \;\middle|\; x = 0,\ y = 0 \right\} \quad \text{and} \quad \mathcal{L}^+ = \left\{ (x, y, z) \in \mathbb{R}^3 \;\middle|\; x = 2,\ y = \frac{4}{|k|} \right\}; \tag{3.5}$$

the corresponding folded singularities $q^{\mp}$ are found at

$$q^- = (0,0,0) \quad \text{and} \quad q^+ = \left(2,\ \frac{4}{|k|},\ 2-\frac{8}{|k|}\right), \tag{3.6}$$

respectively. For the relative position of the folded singularities $q^{\mp}$, we have the following

Proposition 13. *Let $\varepsilon = 0 = \delta$. Then, the folded singularities of the Koper model are connected for $-4 < k < 0$, aligned for $k = -4$, and remote when $k < -4$.*

Proof. The statement follows from Proposition 4 and (3.3), or by comparison of the z-coordinates of q^- and q^+. □

The supercritical manifold $\mathcal{M}_2$ is normally hyperbolic everywhere except at the fold points $p^{\mp}$, where

$$\begin{aligned} x_p^{\mp} &= 1 \pm \sqrt{1-\tfrac{|k|}{6}}, \quad y_p^{\mp} = \frac{\left(2 \pm \sqrt{1-\frac{|k|}{6}}\right)\left(1 \mp \sqrt{1-\frac{|k|}{6}}\right)^2}{|k|}, \quad \text{and} \\ z_p^{\mp} &= 1 \mp \sqrt{1-\tfrac{|k|}{6}} - 2\frac{\left(2 \pm \sqrt{1-\frac{|k|}{6}}\right)\left(1 \mp \sqrt{1-\frac{|k|}{6}}\right)^2}{|k|}. \end{aligned} \tag{3.7}$$

Based on the above, we have the following

Proposition 14. *If $-6 < k < 0$, then $\mathcal{M}_2$ admits two fold points which are located between the intersections of $\mathcal{M}_2$ with $\mathcal{L}^{\mp}$, i.e., on the repelling sheet of $\mathcal{M}_1$. If $k < -6$, then $\mathcal{M}_2$ admits no fold points.*

We reiterate that, due to $k < 0$, the fold points $p^{\mp}$ in the Koper model cannot cross $\mathcal{L}^{\mp}$, and that the corresponding singular geometry is therefore as depicted in Figure 2.3(c).

Remark 9. *In [Cardin and Teixeira, 2017, Example 4.3], $\mathcal{M}_2$ is characterized as normally hyperbolic everywhere, in spite of its graph being S-shaped. Proposition 14 above shows that $\mathcal{M}_2$ can, in fact, potentially admit two fold points at which normal hyperbolicity is lost.*

3.2 Classification of three-timescale dynamics

Here, we classify the dynamics of the Koper model in the three-timescale context for various choices of the parameters k and λ. In particular, we hence construct the two-parameter bifurcation diagram shown in Figure 3.1. (A two-timescale analogue of Figure 3.1, for one fast and two slow variables in Equation (6), is presented in [Desroches et al., 2012].)

In a first step, we note that the boundary between steady-state behaviour and oscillatory dynamics in the Koper model is marked by curves of (singular) Hopf bifurcations at which the delayed Hopf points $p_{DH}^{\mp}$ coincide with true, global equilibria of Equation (2.2):

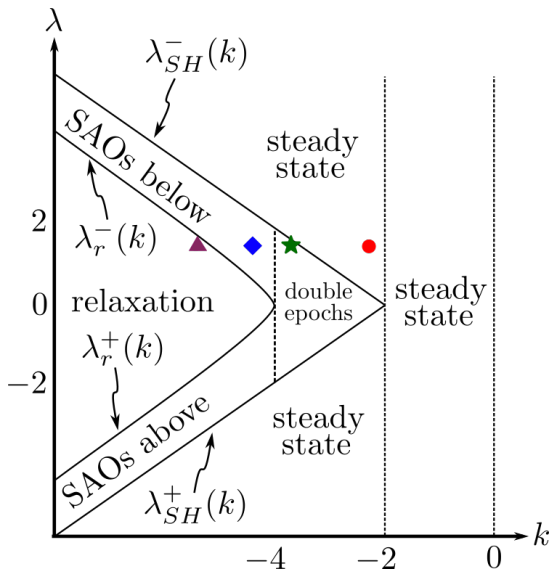

Figure 3.1: Two-parameter bifurcation diagram of the Koper model for $0 < \varepsilon, \delta \ll 1$: oscillatory dynamics is restricted to the triangular region of the (k, λ)-plane that is bounded by $\lambda_{SH}^{\mp}(k)$; MMO dynamics is separated from relaxation oscillation by the curves $\lambda_r^{\mp} = \lambda_r^{\mp}(k)$; to leading order, the mixed-mode regime is subdivided into regions of either single or double epochs of SAOs at $k = -4$.

Proposition 15. *Let $0 < \varepsilon, \delta \ll 1$, and fix $k < 0$. If $k < -2$, then the Koper model undergoes (singular) Hopf bifurcations for $\lambda = \lambda_{SH}^{\mp}(k)$, where*

$$\lambda_{SH}^{-}(k) = -(2+k) + \frac{k^2}{3}\varepsilon + \mathcal{O}(\delta, \varepsilon^2) = -(2+k) + \frac{|k|}{3}\epsilon + \mathcal{O}(\delta, \epsilon^2) \quad \textit{and} \tag{3.8a}$$

$$\lambda_{SH}^{+}(k) = -\lambda_{SH}^{-}(k). \tag{3.8b}$$

Proof. The equilibria of Equation (2.2) are obtained by solving

$$0 = -y + f_2 x^2 + f_3 x^3 = \alpha x + \beta y - z = \mu + \phi(x, y, z). \tag{3.9}$$

Substituting in for x_{DH}^{-}, y_{DH}^{-}, and z_{DH}^{-} from (2.55), using (3.3), and solving for λ, one finds (3.8a). □

It hence follows that oscillatory dynamics is restricted to the triangular area illustrated in Figure 3.1. A further subdivision of that area is obtained by noting that MMO dynamics is separated from relaxation oscillation by two curves $\lambda_r^{-}(k)$ and $\lambda_r^{+}(k) = -\lambda_r^{-}(k)$, which are found by substituting (3.3) into (2.43) and solving for λ. While analytical expressions for $\lambda_r^{\mp}(k)$ can be obtained by direct integration, these are quite involved algebraically, and are hence not included here. We remark that the curves $\lambda_r^{\mp}(k)$ connect tangentially at $k = -4$; cf. Figure 3.1. Numerical experiments show that, for $\varepsilon = \mathcal{O}(10^{-4})$ and $\delta = \mathcal{O}(10^{-2})$, the transition between MMO dynamics and relaxation occurs at $\lambda_r^{\mp}(k) + \mathcal{O}(\delta)$, as is to be expected from Theorem 5.

Finally, the resulting, chevron-shaped region in which MMO dynamics is observed is further divided into subregions in which either single or double epochs of SAOs are found;

to leading order in ε and δ, that division occurs at $k = -4$. Geometrically, the division is due to the fact that the folded singularities $q^{\mp}$ in the Koper model are remote for $k < -4$, while they are connected when $-4 < k < 0$; see Figure 3.3. We emphasize that, in the two-timescale context of $0 < \varepsilon \ll 1$ and $\delta = \mathcal{O}(1)$ in the Koper model, MMOs with double epochs of SAOs occur in a very narrow region of the (k, λ)-plane; that region corresponds to the regime where both folded singularities are of folded-node type and trajectories are attracted to both of them through the associated funnels, by [Desroches et al., 2012]. Here, we have shown that, in the three-timescale context, that parameter regime is "stretched"; hence, trajectories can reach both folded singularities as long as they are attracted to $\mathcal{M}_2$ on both $\mathcal{S}^{a^{\mp}}$, i.e., as long as the folded singularities are aligned or connected.

Remark 10. *Comparing Figure 2.1 and Figure 3.1, we note that panels (a) and (b) of the former are combined in the latter, as two one-parameter diagrams (in μ) are combined into one two-parameter diagram in (k, λ); correspondingly, parallel lines with μ constant in Figure 2.1 are "bent", and hence intersect, in Figure 3.1. (Here, we reiterate that k determines the singular geometry of the Koper model, while λ impacts the resulting flow.)*

3.2.1 The passage from two to three timescales

When $\varepsilon > 0$ is sufficiently small and $\delta = \mathcal{O}(1)$, the folded singularities $q^{\mp}$ of the Koper model are classified as shown in Table 3.1, in accordance with [Szmolyan and Wechselberger, 2001].

Table 3.1: Classification of the folded singularities on q^{+}.

type of singularity $q^{\mp}$	**criterion**
saddle	$\delta\,(k \mp \lambda + 2) > 0$
saddle-node	$\delta\,(k \mp \lambda + 2) = 0$
node	$-k^2/24 < \delta\,(k \mp \lambda + 2) < 0$
degenerate node	$\delta\,(k \mp \lambda + 2) = -k^2/24$
focus	$\delta\,(k \mp \lambda + 2) > -k^2/24$

The classification of Table 3.1, together with the Hopf curves that separate steady states from oscillatory dynamics, are illustrated in Figure 3.2.

From Figure 3.2, it is evident that for $\delta = 1$, the $k\lambda$-regime where MMOs with double SAO epochs are possible, i.e. the regime where both $q^{\mp}$ are of folded node type and the system has no stable equilibrium, is very narrow; this observation was also made in [Desroches et al., 2012]. As δ becomes smaller, this regime stretches, and at $\delta = 1/3$ the bold and dashed curves of the same colour detach. Therefore, as δ decreases and the system transits from the two- to the three-timescale limit, it is not only the funnels of $q^{\mp}$ that stretch, but also $k\lambda$-regime in which SAOs can occur at the vicinity of both $q^{\mp}$, and in this sense MMOs with double SAO-epochs are more robust in the three-timescale context.

3.3 Numerical verification

In this subsection, we verify our classification of the three-timescale dynamics of the Koper model for various representative choices of the parameters k and λ, as indicated in Figure 3.1.

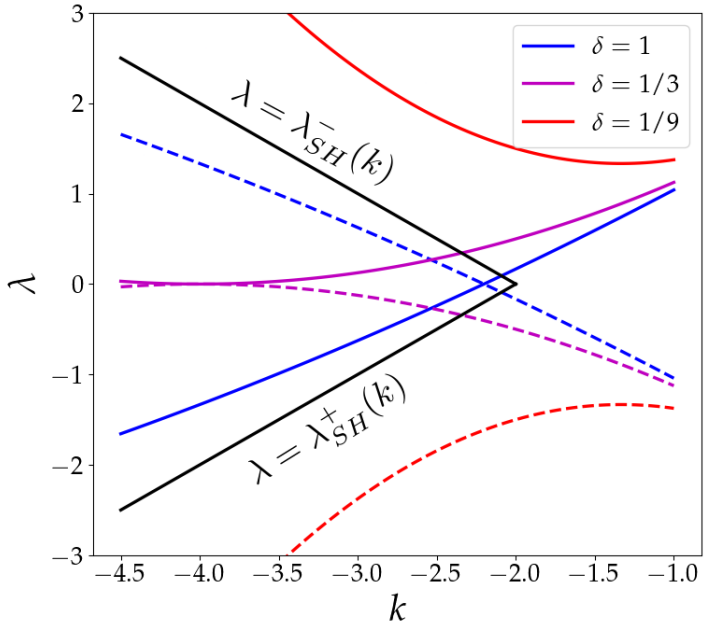

Figure 3.2: The curves corresponding to one of the two folded equilibria being of folded degenerate node type are shown. For each value of δ, which corresponds to a different colour, for $k\lambda$-values in the regime below the bold curve, the folded singularity q^+ on $\mathcal{L}^+$ is of node type. For the same value of δ, and for $k\lambda$-values in the regime above the dashed curve, the folded singularity q^- on $\mathcal{L}^-$ is of folded node type (see also [Desroches et al., 2012] for a similar graph when $\delta = 1$). Non-steady state dynamics is observed in the triangular area defined between the two black curves, which correspond to Hopf bifurcations of the full system, given by (3.8). The narrow diamond-shaped region between the blue and black curves close to $k = -2$ is the region where the Koper model features double epochs of SAOs in the two-timescale setting, $\delta = 1$, as first observed in [Desroches et al., 2012]. By decreasing δ, the parameter regime where both $q^\mp$ are folded nodes stretches, and the curves of the same colour "detach" at $\delta = 1/3$.

We initially fix $\varepsilon = 0.01 = \delta$ and $\lambda = 0.5$, and we vary k. We recall that the Koper model is symmetric in λ, and that it hence suffices to consider positive λ-values; see Remark 8.

For $k = -2.2$ (red circle), the flow of the Koper model converges to a steady state; cf. panel (a) of Figure 3.3. For $k = -3.6$ (green asterisk), we observe MMO dynamics with double epochs of SAOs, since the folded singularities $q^\mp$ are connected in that regime. We note that the dynamics on $\mathcal{Z}^{a^-}$ differs from that on $\mathcal{Z}^{a^+}$ due to the properties of $\phi(x, y, z)$ given in (3.3) in spite of the singular geometry being symmetric; see Figure 3.3,(c). In addition, trajectories "jump" close to the degenerate nodes $z^\mp_{DN_+}$, which is in agreement with Proposition 7. For $k = -4.4$ (blue diamond), the Koper model exhibits MMO dynamics with single epochs of SAOs, as illustrated in panel (e) of Figure 3.3. Finally, for $k = -5.4$ (purple triangle), we observe relaxation oscillation; see Figure 3.3(c).

It was shown in [De Maesschalck et al., 2016] that for $\delta = \mathcal{O}(\varepsilon^2)$, their prototypical

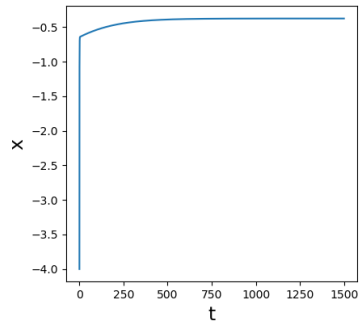

(a) $k = -2.2$, $\lambda = 1.5$.

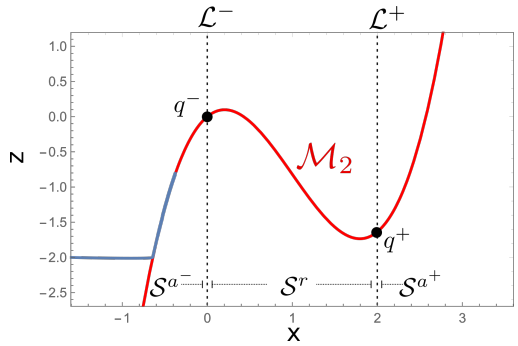

(b) $k = -2.2$, $\lambda = 1.5$.

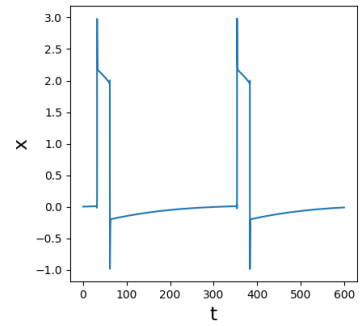

(c) $k = -3.6$, $\lambda = 1.5$.

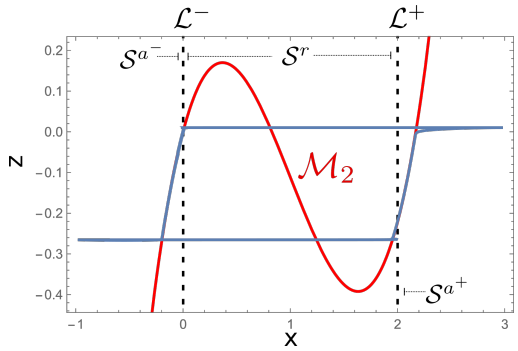

(d) $k = -3.6$, $\lambda = 1.5$.

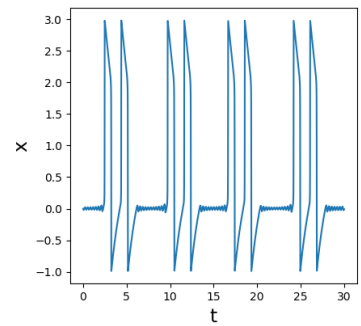

(e) $k = -4.4$, $\lambda = 1.5$.

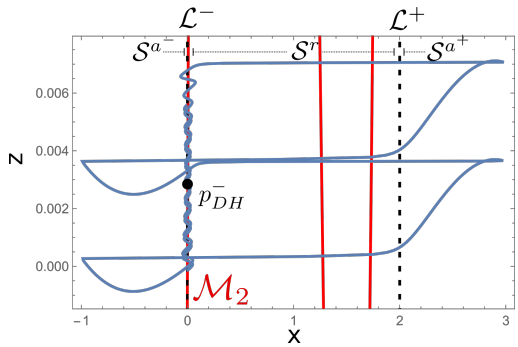

(f) $k = -4.4$, $\lambda = 1.5$.

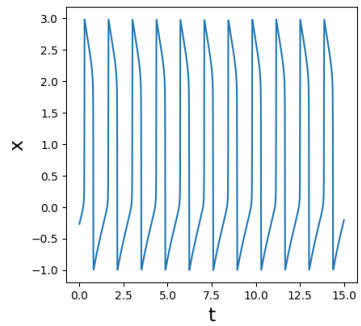

(g) $k = -5.4$, $\lambda = 1.5$.

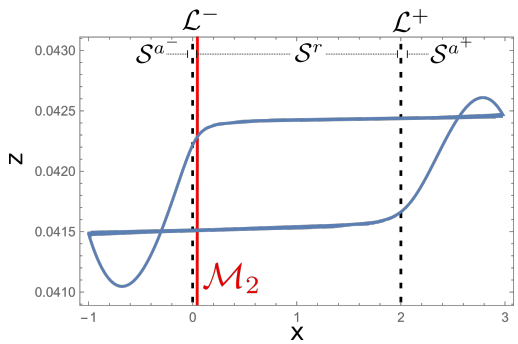

(h) $k = -5.4$, $\lambda = 1.5$.

Figure 3.3: Verification of the bifurcation diagram in Figure 3.1 for representative choices of k, with $\lambda = 1.5$ fixed and $\varepsilon = 0.01 = \delta$: as k decreases, one observes a transition from (a) steady-state behaviour via (c) MMO trajectories with double epochs of SAOs and (e) single epochs of SAOs to (g) relaxation oscillation. The corresponding singular geometry in phase space is shown in panels (b), (d), (f), and (h), respectively.

model, Equation (2.1), can exhibit MMOs which contain SAO segments that are the product of bifurcation delay alternating with sector-type dynamics. In Figure 3.4, we present an example that indicates sector-delayed-Hopf-type dynamics in the Koper model. We remark that the canard point p_{CN}^- coalesces with p_{DH}^- when $k = -4$ and that the interval $\mathcal{I}_{\text{can}}$ hence vanishes, which follows by substitution of (3.3) into (2.57). Since, in addition, $z_{CD} = \mathcal{O}(\sqrt{\varepsilon})$, a crude requirement for the existence of such mixed dynamics is that $\delta = \mathcal{O}(|z_{CN}|^c)$ for $c \geq 1$. Finally, we note that we typically observe more LAO segments between epochs of SAOs for smaller values of δ than for larger ones, by Equation (2.53) of Proposition 1; see again Figure 3.4 and recall the discussion in Section 2.5 regarding the role of the ratio between the timescale separation parameters ε and δ..

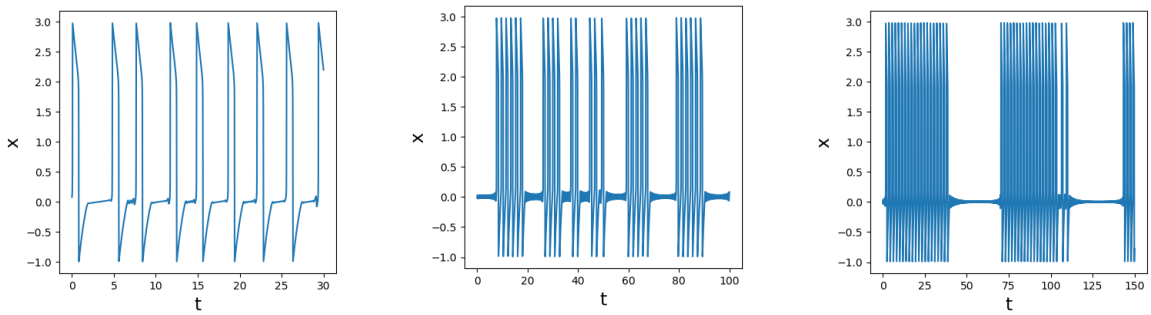

(a) $\delta = 0.1 = \mathcal{O}(\sqrt{\varepsilon})$. (b) $\delta = 0.001 = \mathcal{O}(\varepsilon^{\frac{3}{2}})$. (c) $\delta = 0.0003 = \mathcal{O}(\varepsilon^2)$.

Figure 3.4: Mixed-mode time series in the Koper model for $\varepsilon = 0.01$ fixed and varying δ: as δ decreases, one typically observes more LAOs between SAO segments; additionally, for these particular parameter values, the model seems to exhibit sector-delayed-Hopf-type dynamics [De Maesschalck et al., 2016], as is particularly apparent in panel (b); recall Section 2.5 for a discussion on the ε–δ ratio.

We emphasise that the MMO trajectories described here cannot be viewed, strictly speaking, as perturbations of individual singular cycles, as described in Section 2.2. Rather, we have shown that if the folded singularities of (2.2) are remote, then there exist ε and δ positive and sufficiently small such that the Koper model exhibits MMOs with single epochs of SAOs; correspondingly, we observe double epochs of SAOs if those singularities are aligned or connected. That statement is corroborated by numerical continuation, as illustrated in Figure 3.5, where multiple periodic orbits seem to coexist for k, λ, ε, and δ fixed. (A similar observation was made in the context of the two-timescale Koper model, i.e., for $\delta = 1$ in Equation (6c) [Desroches et al., 2012, Figure 19].) A more detailed study of the properties of these periodic orbits in relation to the MMO dynamics of Equation (2.2) is part of work in progress.

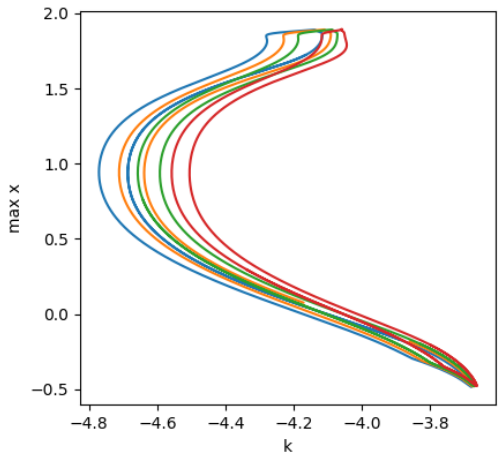

Figure 3.5: Numerical continuation of periodic orbits in the Koper model with the software "auto-07p" for $\lambda = 1.5$ and $\varepsilon = 0.1 = \delta$: one observes coexistence of multiple periodic orbits, as evidenced by the overlap between the corresponding k-intervals.

Chapter 4

The Hodgkin-Huxley equations from mathematical neuroscience

4.1 Introduction

The Hodgkin-Huxley (HH) equations [Hodgkin and Huxley, 1952] comprise a model that describes the generation of action potentials in the squid giant axon. The particular importance of these equations is due to the fact that they constitute one of the most successful mathematical models for the quantitative description of biological phenomena, as the underlying formalism is directly applicable to many types of neurons and other cells [Doi et al., 2001, Izhikevich, 2007].

The three currents that the squid axon carries are the voltage-gated persistent potassium (K^+) current, the voltage-gated transient sodium (Na^+) current, and the Ohmic leak current, which are given by the expressions

$$I_{Na}(V,m,h) = g_{Na}\left(V - E_{Na}\right) m^3 h, \quad I_K(V,n) = g_K\left(V - E_K\right) n^4, \quad I_L(V) = g_L\left(V - E_L\right), \tag{4.1}$$

respectively; here, V denotes the membrane potential, in units of mV, and m and h are the activation and inactivation variables of the Na^+ ion channel, respectively, while n is the activation variable of the K^+ channel. The conductance density g_x and the Nernst potentials E_x ($x = Na, K, L$) are given in units of mS/cm^2 and mV, respectively. The original HH equations [Hodgkin and Huxley, 1952, Doi et al., 2001, Izhikevich, 2007] read

$$C\dot{V} = I - I_{Na} - I_K - I_L, \tag{4.2a}$$

$$\dot{m} = \frac{1}{\tau_m \hat{t}_m\left(V\right)}\left(m_\infty\left(V\right) - m\right), \tag{4.2b}$$

$$\dot{h} = \frac{1}{\tau_h \hat{t}_h\left(V\right)}\left(h_\infty\left(V\right) - h\right), \tag{4.2c}$$

$$\dot{n} = \frac{1}{\tau_n \hat{t}_n\left(V\right)}\left(n_\infty\left(V\right) - n\right), \tag{4.2d}$$

where C denotes the capacitance density, in units of μF/cm^2, and I is the applied current,

in units of μA/cm^2. Moreover,

$$\hat{t}_x(V) = \frac{1}{\alpha_x(V) + \beta_x(V)} \quad \text{and} \quad x_\infty(V) = \frac{\alpha_x(V)}{\alpha_x(V) + \beta_x(V)}, \quad \text{with } x = m, h, n, \tag{4.3a}$$

where the functions $\alpha_x(V)$ and $\beta_x(V)$ are defined as

$$\alpha_m(V) = \frac{(25 - V)/10}{e^{(25-V)/10} - 1}, \quad \alpha_h(v) = \frac{7}{100} e^{-V/20}, \quad \alpha_n(v) = \frac{(10 - V)/100}{e^{(10-V)/10} - 1} \tag{4.4a}$$

$$\beta_m(V) = 4e^{-V/18}, \quad \beta_h(v) = \frac{1}{1 + e^{(30-V)/10}}, \quad \text{and} \quad \beta_n(v) = \frac{1}{4} e^{-V/80} \tag{4.4b}$$

in the original form of Equation (4.2). In [Doi et al., 2001], the parameters I, τ_m, τ_h, and τ_n are considered bifurcation parameters, while the values of the remaining parameters are fixed as

$$C = 1\ \mu\text{F/cm}^2, \quad g_{Na} = 120\ \text{mS/cm}, \quad g_K = 36\ \text{mS/cm}, \quad g_L = 0.3\ \text{mS/cm},$$
$$E_{Na} = 115\ \text{mV}, \quad E_K = -12\ \text{mV}, \quad \text{and} \quad E_L = 10.599\ \text{mV}.$$

When either τ_h or τ_n is large, it is demonstrated in [Doi et al., 2001] that Equation (4.2) evolves on multiple timescales, which gives rise to mixed-mode oscillatory dynamics, as illustrated in Figure 2 therein. However, the geometric mechanisms that are responsible for the transition between qualitatively different mixed-mode oscillations (MMOs) in the framework of geometric singular perturbation theory (GSPT) [Fenichel, 1979] were not addressed in [Doi et al., 2001].

To our knowledge, the first attempt at studying the multi-timescale HH model, Equation (4.2), on the basis of GSPT was made by Rubin and Wechselberger in the references [Rubin and Wechselberger, 2007, Rubin and Wechselberger, 2008]. They applied the scaling

$$v = \frac{V}{k_v}, \quad \tau = \frac{t}{k_t} \quad \bar{I} = \frac{I}{k_v g_{Na}}, \tag{4.5}$$

$$\bar{E}_x = \frac{E_x}{k_v}, \quad \text{and} \quad \bar{g}_x = \frac{g_x}{g_{Na}} \qquad \text{for } \ x = Na, K, L, \tag{4.6}$$

with $k_v = 100$ mV and $k_t = 1$ ms, and considered the following dimensionless version of Equation (4.2),

$$\gamma \dot{v} = \bar{I} - \left(v - \bar{E}_{Na}\right) m^3 h - \bar{g}_K \left(v - \bar{E}_K\right) n^4 - \bar{g}_L \left(v - \bar{E}_L\right), \tag{4.7a}$$

$$\dot{m} = \frac{1}{\tau_m \hat{t}_m(v)} \left(m_\infty(v) - m\right), \tag{4.7b}$$

$$\dot{h} = \frac{1}{\tau_h \hat{t}_h(v)} \left(h_\infty(v) - h\right), \tag{4.7c}$$

$$\dot{n} = \frac{1}{\tau_n \hat{t}_n(v)} \left(n_\infty(v) - n\right), \tag{4.7d}$$

where

$$\gamma = \frac{C}{k_t \cdot g_{Na}} \simeq 0.0083. \tag{4.8}$$

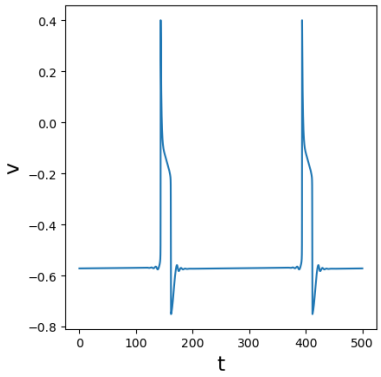

(a) $I = 20.051$

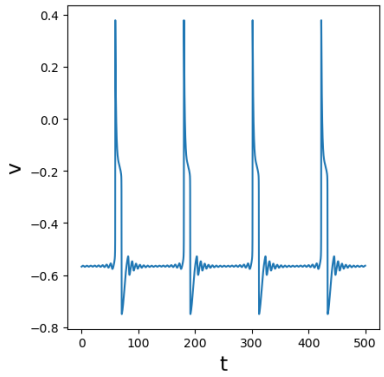

(b) $I = 23.051$

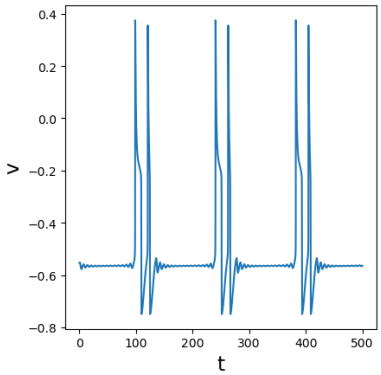

(c) $I = 23.5$

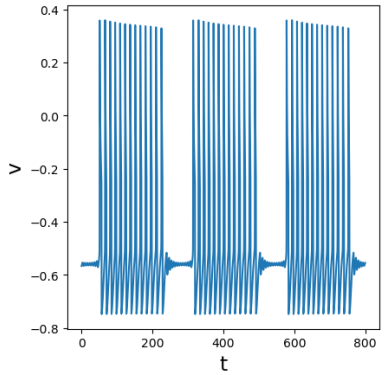

(d) $I = 26.03452346$

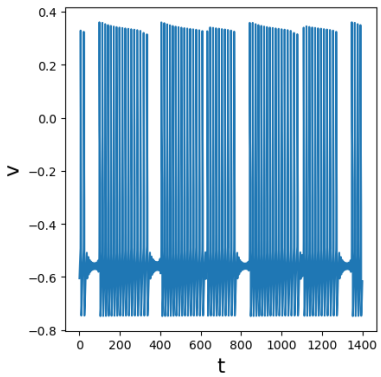

(e) $I = 26.1209956$

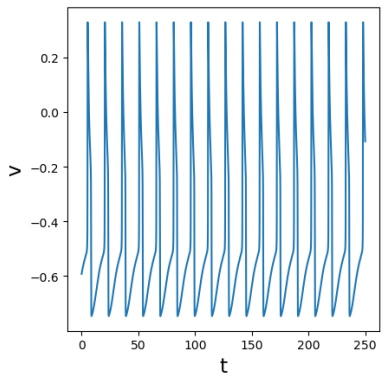

(f) $I = 26.2$

Figure 4.1: Time series of the v-variable in the dimensionless HH model, Equation (4.7), for $\varepsilon = 0.0083$, $\tau_h = 40$, and varying values of $I = k_v g_{Na} \bar{I}$: panels (a) and (b) illustrate MMOs with double SAO epochs; panel (c) gives an example of a transitive, exotic MMO with double epochs of SAOs separated by LAOs; panels (d) and (e) contain MMOs with single SAO epochs. Qualitatively similar time series have been documented in [Doi et al., 2001, Figure 2]; the underlying geometric mechanisms in the phase space that are responsible for the qualitative properties of the associated MMO trajectories are described in Section 4.3.

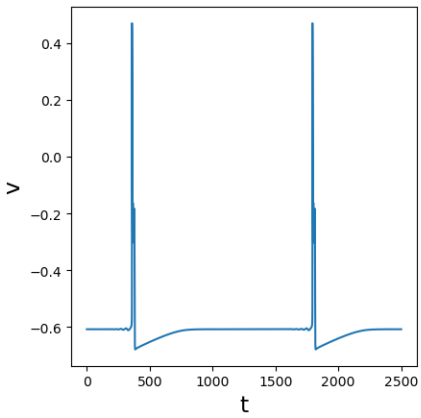

(a) $I = 7$

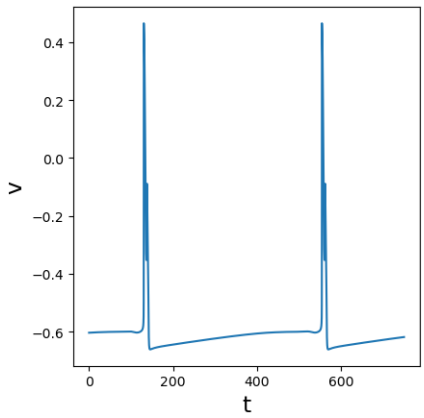

(b) $I = 9$

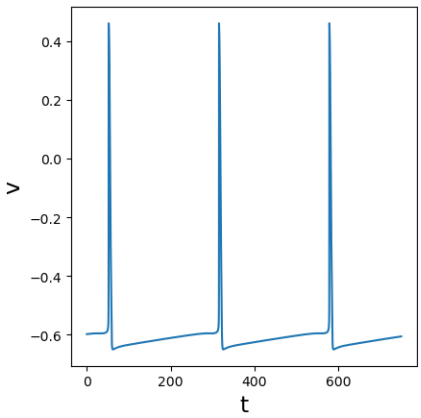

(c) $I = 11$

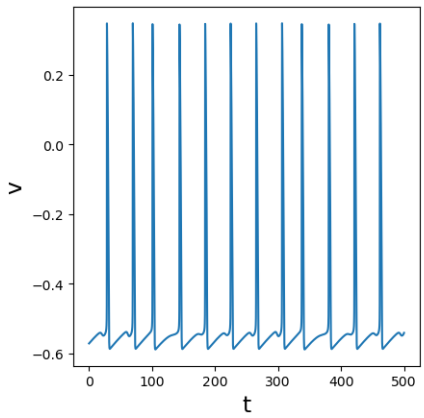

(d) $I = 64.5$

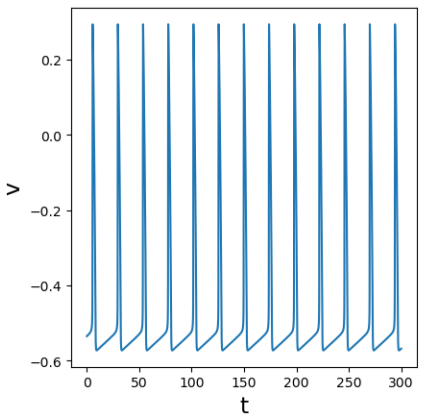

(e) $I = 90$

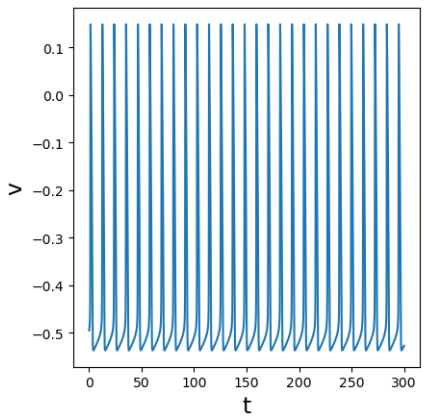

(f) $I = 150$

Figure 4.2: Time series of the v-variable in the dimensionless HH model, Equation (4.7), for $\varepsilon = 0.0083$, $\tau_n = 100$, and varying values of $I = k_v g_{Na} \bar{I}$: panels (a) and (b) illustrate MMOs with double SAO epochs; panels (c) and (d) contain MMOs with single SAO epochs. The underlying geometric mechanisms in the phase space that are responsible for the qualitative properties of the associated MMO trajectories are described in Section 4.4.

Here, the functions $\hat{t}_x(v)$ and $x_\infty(v)$ are defined as in (4.3a), with

$$\alpha_m(v) = \frac{(v+40)/10}{1-e^{-(v+40)/10}}, \quad \alpha_h(v) = \frac{7}{100}e^{-(v+65)/20}, \quad \alpha_n(v) = \frac{(v+55)/100}{1-e^{-(v+55)/10}}$$
$$\beta_m(v) = 4e^{-(v+65)/18}, \quad \beta_h(v) = \frac{1}{1+e^{-(v+35)/10}}, \quad \text{and} \quad \beta_n(v) = \frac{1}{4}e^{-(v+65)/80};$$

in addition, the parameters in (4.7) now read

$$\bar{I} = \frac{I}{k_u g_{Na}}, \quad \bar{g}_K = 0.3, \quad \bar{g}_L = 0.0025,$$
$$\bar{E}_{Na} = 0.5, \quad \bar{E}_K = -0.77, \quad \text{and} \quad \bar{E}_L = -0.544. \tag{4.9}$$

The dimensionless Equation (4.7) captures the different dynamical behaviours of Equation (4.2) when I is varied and the remaining parameters are fixed, as documented in [Doi et al., 2001]: panel (b) in Figure 4.1 shows an MMO with double epochs of small-amplitude oscillations (SAOs); panel (d) illustrates an MMO with single epochs of SAOs, while panel (f) demonstrates (SAO-less) relaxation oscillation. Finally, panel (c) contains an MMO with double epochs of SAOs that includes spikes between the epochs of SAOs "above" and SAOs "below". We note that, due to the non-dimensionalisation in (4.7) by Rubin and Wechselberger [Rubin and Wechselberger, 2007], the corresponding I-values differ from those in [Doi et al., 2001]; moreover, we remark that for ease of comparison and numerical convenience, Figure 4.1 refers to I rather than to its rescaled counterpart $\bar{I}$ in Equation (4.7).

Under the above assumptions, the parameter γ defined in (4.8) can be considered a small perturbation parameter. Moreover, the order of magnitude of the characteristic timescale $[\hat{t}_m(v)]^{-1}$ is larger than those of $[\hat{t}_h(v)]^{-1}$ and $[\hat{t}_n(v)]^{-1}$, as can be seen in Figure 4.3.

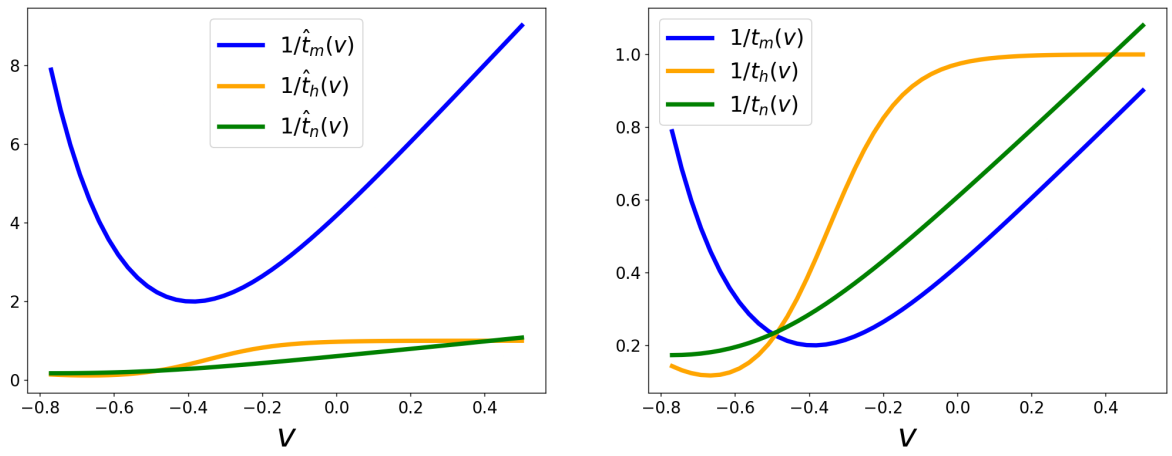

(a) (b)

Figure 4.3: Characteristic timescales (a) $\hat{t}_x(v)^{-1}$ $(x = m, h, n)$, (b) $t_x(v)^{-1}$ $(x = m, h, n)$.

We consider the rescaling

$$T_x = \max_{v \in (E_K, E_{Na})} \frac{1}{\hat{t}_x(v)} \tag{4.10}$$

and define

$$t_x(v) := T_x \hat{t}_x(v). \tag{4.11}$$

Denoting further

$$V(v,m,h,n) := \bar{I} - \left(v - \bar{E}_{Na}\right) m^3 h - \bar{g}_K \left(v - \bar{E}_K\right) n^4 - \bar{g}_L \left(v - \bar{E}_L\right), \tag{4.12}$$

$$M(v,m) := \frac{m_\infty(v) - m}{t_m(v)}, \tag{4.13}$$

$$H(v,h) := \frac{h_\infty(v) - h}{t_h(v)}, \tag{4.14}$$

$$N(v,n) := \frac{n_\infty(v) - n}{t_n(v)}, \quad \text{and} \tag{4.15}$$

$$\delta_x := \frac{T_x}{\tau_x}, \quad x = m,n,h, \tag{4.16}$$

one can write

$$\gamma \dot{v} = V(v,m,h,n) \tag{4.17a}$$

$$\dot{m} = \delta_m M(v,m), \tag{4.17b}$$

$$\dot{h} = \delta_h H(v,h), \tag{4.17c}$$

$$\dot{n} = \delta_n N(v,n). \tag{4.17d}$$

In the following, we will suppress the dependence of Equation (4.17) on the parameter $\bar{I}$, and will only remark on it as required.

From Figure 4.3, it is apparent that $T_m \simeq 10$, while $T_h \simeq T_n \simeq 1$. Based on this observation, in [Rubin and Wechselberger, 2007] it was assumed that $\delta_m^{-1} = T_m^{-1} = \mathcal{O}(\gamma)$, and system (4.17) was thus written as

$$\gamma \dot{v} = V(v,m,h,n), \tag{4.18a}$$

$$\gamma \dot{m} = M(v,m), \tag{4.18b}$$

$$\dot{h} = \delta_h H(v,h), \tag{4.18c}$$

$$\dot{n} = \delta_n N(v,n), \tag{4.18d}$$

where (v,m) are the fast variables and (h,n) are the slow ones. On the basis of centre manifold theory, Rubin and Wechselberger [Rubin and Wechselberger, 2007] then derived the following three-dimensional reduction of (4.18),

$$\gamma \dot{v} = \bar{I} - \left(v - \bar{E}_{Na}\right) m_\infty^3(v) h - \bar{g}_K \left(v - \bar{E}_K\right) n^4 - \bar{g}_L \left(v - \bar{E}_L\right) = V(v, m_\infty, h, n), \tag{4.19a}$$

$$\dot{h} = \delta_h N(v,h), \tag{4.19b}$$

$$\dot{n} = \delta_n N(v,n), \tag{4.19c}$$

where the variable m has been eliminated. However, in their analysis, they considered $0 < \gamma \ll 1$ and $\delta_x = \mathcal{O}(1)$ $(x = m,h,n)$. As a consequence, only MMO trajectories with single epochs of SAOs were documented in previous works [Rubin and Wechselberger, 2007,

Rubin and Wechselberger, 2008], in contrast to [Doi et al., 2001, Figure 2]; cf. panels (d), (e), and (f) of Figure 4.1. As argued in [Desroches et al., 2012], in the two-timescale context – where SAOs arise due to the presence of a folded node singularity [Wechselberger, 2005] – the parameter regimes in which MMOs with double SAO epochs are apparent seem very narrow. By contrast, such MMOs become more prominent in the three-timescale context, which further attests to our claim that the physiologically relevant mixed-mode dynamics of the HH model, Equation (4.7), cannot be fully understood via a standard two-timescale analysis.

In this work, we incorporate the assumption that the variable m is slower than v, but faster than h and n, which is alluded to in [Rubin and Wechselberger, 2007, Remark 1]; that is, we assume $\delta_m^{-1} = \mathcal{O}(\sqrt{\gamma})$ in (4.17). That assumption is realistic, since $\gamma = 0.0083$, $T_m = 10$, and $\tau_m = O(1)$. Crucially, it allows us to apply GSPT to derive a global three-dimensional reduction of Equation (4.7) of the form

$$\varepsilon \dot{v} = U(v, h, n; \gamma, \varepsilon, \delta_h, \delta_n), \quad \dot{h} = \delta_h H(v, h), \quad \dot{n} = \delta_n N(v, n), \tag{4.20}$$

where $\varepsilon = \delta_m^{-1}$ is small; see Theorem 7 in Section 4.2. The geometry of the reduction in (4.20) encodes the mechanisms that are responsible for the transitions between qualitatively different mixed-mode dynamics of the full system, Equation (4.7), as documented in [Doi et al., 2001] and as illustrated in Figure 4.1 and Figure 4.2, in the presence of three distinct timescales.

Remark 11. *The timescale separation at all levels can be controlled by merely varying the parameters τ_x ($x = m, h, n$) in (4.7) or, equivalently, by variation of δ_x in (4.17).*

Specifically, motivated by [Doi et al., 2001], but also by [Rubin and Wechselberger, 2007, Rubin and Wechselberger, 2008], we consider the two different cases where either h or n in Equation (4.20) is assumed to be evolving on the slowest timescale. In other words, we first take $\delta_h > 0$ to be small, with $\delta_n = \mathcal{O}(1)$; then, we consider the case where $\delta_h = \mathcal{O}(1)$, with $\delta_n > 0$ small. We show that these two cases are not fundamentally different in terms of their singular geometry and of the resulting mixed-mode dynamics. In particular, we demonstrate that, when h is taken to be the slowest variable, the geometric mechanism introduced in Chapter 2 can reproduce the various firing patterns observed in (4.7), and the bifurcations between those, with the rescaled applied current $\bar{I}$ the relevant bifurcation parameter. We explain the transition from MMOs with double epochs of SAOs to MMOs with single epochs of SAOs and then to relaxation oscillation, cf. Figure 4.1 and Figure 4.2, and we remark on the "exotic MMOs" that are observed during this transition; cf. Figure 4.1.

The Chapter is organised as follows. In Section 4.2, we present a novel, global geometric reduction of Equation (4.7) after elimination of the variable m. We relate the dynamics of the resulting, reduced three-dimensional slow-fast system, Equation (4.20), to that of Equation (4.17), as well as to the local centre manifold reduction proposed by Rubin and Wechselberger, Equation (4.19). We then consider the scenario where Equation (4.20) exhibits dynamics on three timescales, in which case the full system in (4.2) exhibits dynamics on four timescales. In Section 4.3 and Section 4.4, the variable h and n is taken to be the slow variable, respectively; we demonstrate that the geometric mechanisms proposed in

Chapter 2 can explain bifurcations of MMOs that have been previously documented, but not emphasised in the context of GSPT, in the literature, such as in [Doi et al., 2001]. We conclude the article in Section 4.6 with a summary, and an outlook to future research.

4.2 Global multi-timescale reduction

Equation (4.17) is singularly perturbed with respect to the small parameter γ, written in the "slow formulation". Rescaling time in (4.17) as $\tilde{t} = t/\gamma$, we obtain the "fast formulation"

$$v' = V(v, m, h, n), \tag{4.21a}$$
$$m' = \gamma\delta_m M(v, m), \tag{4.21b}$$
$$h' = \gamma\delta_h H(v, h), \tag{4.21c}$$
$$n' = \gamma\delta_n N(v, n), \tag{4.21d}$$

where the prime denotes differentiation with respect to the new time $\tilde{t}$. Furthermore, in the following we will restrict to the domain $(v, m, h, n) \in \mathcal{D}$, where

$$\mathcal{D} := (\bar{E}_K, \bar{E}_{Na}) \times (0, 1)^3, \tag{4.22}$$

as is also done in [Rubin and Wechselberger, 2007].

Since $\delta_m = \mathcal{O}(\gamma^{-1/2})$, it is apparent that (4.21) features three distinct timescales if $\delta_h, \delta_n = \mathcal{O}(1)$, with v the fast variable, m the slow one, and h and n the super-slow ones. The singular limit of $\gamma = 0$ gives the one-dimensional "layer problem" with respect to the fastest timescale,

$$v' = V(v, m, h, n), \tag{4.23a}$$
$$m' = 0, \tag{4.23b}$$
$$h' = 0, \tag{4.23c}$$
$$n' = 0. \tag{4.23d}$$

Equilibria of (4.23a) define the three-dimensional critical manifold $\mathcal{M}$ as

$$V(v, m, h, n) = 0. \tag{4.24}$$

Since

$$\partial_v V(v, m, h, n) = -m^3 h - \bar{g}_K n^4 - \bar{g}_L < 0 \quad \text{for} \quad (v, m, h, n) \in \mathcal{D}, \tag{4.25}$$

the manifold $\mathcal{M}$ is normally hyperbolic and attracting everywhere in $\mathcal{D}$. Let

$$\mu(v, h, n) := \left[\frac{\bar{I} - \bar{g}_K\left(v - \bar{E}_K\right) n^4 - \bar{g}_L\left(v - \bar{E}_L\right)}{\left(v - \bar{E}_{Na}\right) h}\right]^{\frac{1}{3}}; \tag{4.26}$$

then, by (4.24), $\mathcal{M}$ can be written as a graph of m over (v, h, n), with

$$m = \mu(v, h, n). \tag{4.27}$$

Finally, we emphasise that since $\delta_m^{-1} = 0.1$ and since δ_m is independent of γ, it holds uniformly that $\gamma \ll \delta_m^{-1}$. Therefore, for $\gamma > 0$ sufficiently small, the dynamics of Equation (4.21) can be effectively reduced to a three-dimensional multi-timescale system, which constitutes our first main result in this Chapter.

Theorem 7. *Consider $\gamma > 0$ sufficiently small, and let $\varepsilon = \delta_m^{-1}$. Then, the HH model, Equation (4.21), admits a three-dimensional attracting slow manifold $\mathcal{M}_\gamma$ that is diffeomorphic, and $\mathcal{O}(\gamma)$-close to, $\mathcal{M}$ in the Hausdorff distance. The manifold $\mathcal{M}_\gamma$ can be written as a graph $m = \mu(v,h,n) + \mathcal{O}(\gamma)$ and is locally invariant under the flow of*

$$\begin{aligned}\varepsilon\dot{v} &= \frac{m_\infty(v) - \mu(v,h,n)}{t_m(v)\partial_v\mu(v,h,n)} - \varepsilon\delta_h H(v,h)\frac{\partial_h\mu(v,h,n)}{\partial_v\mu(v,h,n)} - \varepsilon\delta_n N(v,n)\frac{\partial_n\mu(v,h,n)}{\partial_v\mu(v,h,n)} + \mathcal{O}(\gamma) \\ &=: U(v,h,n;\gamma,\varepsilon,\delta_h,\delta_n),\end{aligned} \tag{4.28a}$$

$$\dot{h} = \delta_h H(v,h), \tag{4.28b}$$

$$\dot{n} = \delta_n N(v,n). \tag{4.28c}$$

Proof. The existence of $\mathcal{M}_\gamma$, its diffeomorphic relation to, and distance from, $\mathcal{M}$ follow from Fenichel's First Theorem [Fenichel, 1979], since the critical manifold $\mathcal{M}$ is normally hyperbolic everywhere in $\mathcal{D}$, by (4.24) and (4.25). In particular, $\mathcal{M}_\gamma$ is given as a graph of m over (v,h,n), with

$$m = \mu(v,h,n) + \gamma\mu_1(v,h,n;\gamma). \tag{4.29}$$

The attractivity of $\mathcal{M}_\gamma$ follows from Fenichel's Second Theorem [Fenichel, 1979], since, by (4.25), the critical manifold $\mathcal{M}$ is attracting everywhere. (See also [Hek, 2010] for a concise outline of Fenichel's First and Second Theorems).

Finally, Equation (4.28) for the flow on the slow manifold $\mathcal{M}_\gamma$ is obtained as follows. Equations (4.28b) and (4.28c) follow immediately from (4.21), as the dynamics of h and n is independent of m. To derive (4.28a), we first differentiate (4.29) with respect to $\tilde{t}$. Next, we substitute (4.21b), (4.21c), (4.21d), and (4.26) into the resulting expression and then solve for $\dot{v}$, collecting terms. Dividing the resulting system of equations by δ_m and substituting $\varepsilon = \delta_m^{-1}$ gives the desired result. □

Theorem 7 implies that, for γ positive and sufficiently small, the dynamics of the full, four-dimensional HH model, Equation (4.21), is captured by the three-dimensional reduction in (4.28), where we have eliminated the variable m via the graph representation in (4.29). We remark that (4.28) is a regular perturbation problem in γ in the slow formulation of GSPT with respect to the singular perturbation parameter ε; we will therefore restrict to considering the limit of $\gamma = 0$ in the following:

$$\varepsilon\dot{v} = \frac{m_\infty(v) - \mu(v,h,n)}{t_m(v)\partial_v\mu(v,h,n)} - \varepsilon\delta_h H(v,h)\frac{\partial_h\mu(v,h,n)}{\partial_v\mu(v,h,n)} - \varepsilon\delta_n N(v,n)\frac{\partial_n\mu(v,h,n)}{\partial_v\mu(v,h,n)}, \tag{4.30a}$$

$$\dot{h} = \delta_h H(v,h), \tag{4.30b}$$

$$\dot{n} = \delta_n N(v,n). \tag{4.30c}$$

For $\varepsilon > 0$ sufficiently small, Equation (4.30) is itself a slow-fast system in the standard form of GSPT. Rescaling time in (4.28) as $\tau = t/\varepsilon$ gives the corresponding fast formulation

$$v' = \frac{m_\infty(v) - \mu(v,h,n)}{t_m(v)\partial_v\mu(v,h,n)} - \varepsilon\delta_h H(v,h)\frac{\partial_h\mu(v,h,n)}{\partial_v\mu(v,h,n)} - \varepsilon\delta_n N(v,n)\frac{\partial_n\mu(v,h,n)}{\partial_v\mu(v,h,n)}, \tag{4.31a}$$

$$h' = \varepsilon\delta_h H(v,h), \tag{4.31b}$$

$$n' = \varepsilon\delta_n N(v,n), \tag{4.31c}$$

The layer problem is then obtained by setting $\varepsilon = 0$ in (4.31)

$$v' = \frac{m_\infty(v) - \mu(v,h,n)}{t_m(v)\partial_v\mu(v,h,n)}, \tag{4.32a}$$

$$h' = 0, \tag{4.32b}$$

$$n' = 0. \tag{4.32c}$$

The set of equilibria of the above defines the two-dimensional critical manifold $\mathcal{M}_1$ as

$$m_\infty(v) - \mu(v,h,n) = 0, \tag{4.33}$$

which is equivalent to requiring that

$$V(v, m_\infty(v), h, n) = 0; \tag{4.34}$$

see (4.26) for the definition of $\mu(v,h,n)$ and (4.12) for the definition of $V(v,m,h,n)$.

The manifold $\mathcal{M}_1$ is normally hyperbolic everywhere except on $\mathcal{F}_{\mathcal{M}_1}$, where

$$\partial_v \left[V(v, m_\infty(v), h, n)\right] = 0. \tag{4.35}$$

We note that

$$\partial_h \left[V(v, m_\infty(v), h, n)\right] = -\left(v - \bar{E}_{Na}\right) m_\infty^3(v) > 0 \quad \text{and} \tag{4.36a}$$

$$\partial_n \left[V(v, m_\infty(v), h, n)\right] = -4\bar{g}_K \left(v - \bar{E}_k\right) n^3 < 0 \tag{4.36b}$$

for $v \in (\bar{E}_K, \bar{E}_{Na})$, and we define

$$\nu(v,h) := \left[\frac{\bar{I} - \left(v - \bar{E}_{Na}\right) m_\infty^3(v) h - \bar{g}_L\left(v - \bar{E}_L\right)}{\bar{g}_K\left(v - \bar{E}_K\right)}\right]^{\frac{1}{4}} \tag{4.37}$$

$$\eta(v,n) := \frac{\bar{I} - \bar{g}_K\left(v - \bar{E}_K\right) n^4 - \bar{g}_L\left(v - \bar{E}_L\right)}{\left(v - \bar{E}_{Na}\right) m_\infty^3(v)} \tag{4.38}$$

by solving (4.34) for n and h, respectively. The manifold $\mathcal{M}_1$ can therefore be written globally either as a graph over (v,h), with

$$n = \nu(v,h),$$

or as a graph over (v,n), with

$$h = \eta(v,n).$$

Finally, a parametric expression for $\mathcal{F}_{\mathcal{M}_1}$ can be obtained by using (4.37) and solving the system $\{(4.34),(4.35)\}$. Elementary calculation shows that $\mathcal{F}_{\mathcal{M}_1}$ is a U-shaped curve, which can be viewed as the tangential connection of two fold curves $\mathcal{L}^{\mp}$; see Figure 4.4.

It follows that the manifold $\mathcal{M}_1$ is separated by $\mathcal{F}_{\mathcal{M}_1}$ into a normally attracting portion $\mathcal{S}^a$, where $\partial_v \left[V(v, m_\infty(v), h, n)\right] < 0$, and a normally repelling portion $\mathcal{S}^r$, where $\partial_v \left[V(v, m_\infty(v), h, n)\right] > 0$; cf. again Figure 4.4. We denote the normally hyperbolic submanifold of $\mathcal{M}_1$ by $\mathcal{S} = \mathcal{S}^a \cup \mathcal{S}^r$.

Remark 12. *It is also now apparent that the restriction to* $v \in \left(\bar{E}_K, \bar{E}_{Na}\right)$ *stems from Equations (4.37) and (4.38), since the denominators in those expressions tend to zero when* $v \to \bar{E}_{Na}$ *or* $v \to \bar{E}_K$*, respectively.*

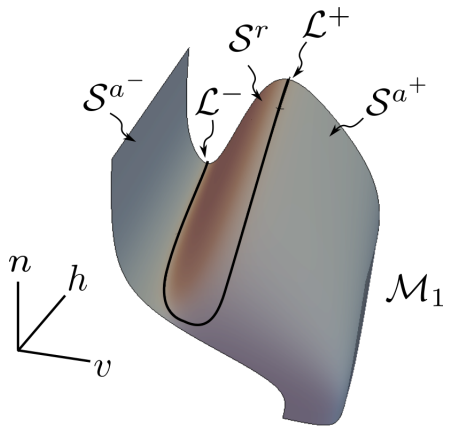

Figure 4.4: The critical manifold $\mathcal{M}_1$ of the three-dimensional reduction, Equation (4.28).

The reduced problem on $\mathcal{M}_1$ is obtained by setting $\varepsilon = 0$ in (4.30)

$$0 = \frac{m_\infty(v) - \mu(v,h,n)}{t_m(v)\partial_v \mu(v,h,n)}, \tag{4.39a}$$

$$\dot{h} = \delta_h H(v,h), \tag{4.39b}$$

$$\dot{n} = \delta_n N(v,n); \tag{4.39c}$$

then, with regard to the reduced flow on $\mathcal{S}$, we have the following result:

Proposition 16. *The reduced flow on* $\mathcal{S}^a$ *is smoothly topologically equivalent to the flow of*

$$\dot{v} = \delta_h \partial_h \left[V(v, m_\infty(v), h, n)\right] H(v,h)|_{n=\nu(v,h)} + \delta_n \partial_n \left[V(v, m_\infty(v), h, n)\right] N(v,n)|_{n=\nu(v,h)}, \tag{4.40a}$$

$$\dot{h} = -\delta_h \partial_v \left[V(v, m_\infty(v), h, n)\right] H(v,h)|_{n=\nu(v,h)} \tag{4.40b}$$

and to that of

$$\dot{v} = \delta_h \partial_h \left[V(v, m_\infty(v), h, n)\right] H(v,h)|_{h=\eta(v,n)} + \delta_n \partial_n \left[V(v, m_\infty(v), h, n)\right] H(v,n)|_{h=\eta(v,n)}, \tag{4.41a}$$

$$\dot{n} = -\delta_n \partial_v \left[V(v, m_\infty(v), h, n)\right] N(v,h)|_{h=\eta(v,n)}. \tag{4.41b}$$

Proof. Differentiating implicitly the algebraic constraint in (4.34) which defines $\mathcal{M}_1$, we obtain

$$-\partial_v \left[V(v, m_\infty(v), h, n)\right] \dot{v} = \partial_h \left[V(v, m_\infty(v), h, n)\right] \dot{h} + \partial_n \left[V(v, m_\infty(v), h, n)\right] \dot{n}. \tag{4.42}$$

Making use of (4.28b) and (4.28c), together with (4.37), on $\mathcal{M}_1$ we obtain

$$\begin{aligned} -\partial_v \left[V(v, m_\infty(v), h, n)\right] \dot{v} = \partial_h \left[V(v, m_\infty(v), h, n)\right] H(v,h)|_{n=\nu(v,h)} \\ + \delta_n \partial_n \left[V(v, m_\infty(v), h, n)\right] N(v,n)|_{n=\nu(v,h)}, \\ \dot{h} = \delta_h H(v,h)|_{n=\nu(v,h)}. \end{aligned}$$

Rescaling time in the above by a factor of $-\left(\partial_v \left[V(v, m_\infty(v), h, n)\right]\right)^{-1}$, which preserves the direction of time on $\mathcal{S}^a$ while reversing it on $\mathcal{S}^r$, we find (4.40), as claimed. Showing the equivalence to (4.41) is similar. □

We remark that, although systems (4.40) and (4.41) are equivalent on $\mathcal{S}^a$, system (4.40) (resp. (4.41)) will be more useful when h is taken to be the slowest variable (resp. when n is taken to be the slowest variable), as this will lead to a two-dimensional slow-fast system in the standard form of GSPT, as will be apparent in Section 4.3 (resp. Section 4.4). If n is taken to be the slow variable in (4.40) (resp. if h is taken to be the slow variable in (4.40)), then the corresponding two-dimensional system is a slow-fast system in the non-standard form of GSPT, recall Section 1.3 and see Section 4.7.

We emphasise that Equation (4.30) and the centre manifold reduction (4.19) that was introduced in [Rubin and Wechselberger, 2007] admit the same critical manifold $\mathcal{M}_1$ as is defined by (4.33) – or, equivalently, by (4.34). In other words, the algebraic constraint in (4.33) corresponds to the v-nullcline in (4.19a), recall (4.12); see [Rubin and Wechselberger, 2007] for details. However, although the factor of $[\partial_v \mu(u,h,n)]^{-1}$ in (4.30a) is positive definite, there are qualitative differences in the dynamics of the two systems due to the terms of order $\mathcal{O}(\varepsilon)$ that occur in (4.30), as is discussed in Section 4.5.

Naturally, and as is the case for (4.19), the slow-fast formulation in Equation (4.30) exhibits dynamics on two timescales when only ε is assumed to be small and $\delta_h, \delta_n = \mathcal{O}(1)$; correspondingly, there is then no separation of scales in the desingularised reduced flow in (4.40). In the following, we therefore consider the two cases where either $\tau_n = \mathcal{O}(1)$ and τ_h is large in (4.7) and, hence, δ_h is small in (4.30); or $\tau_h = \mathcal{O}(1)$ and τ_n is large and, hence, δ_h is small. The system in (4.30) then exhibits dynamics on three distinct timescales, with (4.40) corresponding to the formulation on the "intermediate" timescale. In the following, we will in turn investigate the resulting mixed-mode dynamics in those two cases.

4.3 The h-slow regime

In this section, we consider the regime where the variable h is the slowest variable in (4.21), which is realised for $\delta_h > 0$ sufficiently small and $\delta_n = 1$, that is, when τ_h is large and $\tau_n = \mathcal{O}(1)$ in the original HH model, Equation (4.2). In that case, the reduced system on $\mathcal{M}_1$, Equation (4.40), is a slow-fast system written in the standard form of GSPT which features similar geometric and dynamical properties to the extended prototypical example introduced in Chapter 2.

In particular, we will classify the mixed-mode dynamics of Equation (4.21) with $\gamma, \varepsilon, \delta_h > 0$ small in dependence of the (rescaled) applied current $\bar{I}$, by applying the analysis outlined in Chapter 2 to the three-dimensional reduction (4.28). We will show that, in the parameter regime defined in (4.9), there exist values $0 < \bar{I}_o < \bar{I}_a < \bar{I}_r < \bar{I}_c$ of $\bar{I}$ that distinguish between the various types of oscillatory dynamics in (4.21) for γ, ε, $1/\delta_m$, and δ_h positive and sufficiently small and $\delta_n = \mathcal{O}(1)$. The resulting classification is illustrated in Figure 4.5, with the corresponding mixed-mode oscillatory dynamics as shown in Figure 4.1. While such dynamics was previously documented in [Doi et al., 2001], the underlying geometric mechanisms that generate these various firing patterns, and the transitions between them, were not emphasised in the context of GSPT. Correspondingly, the $\bar{I}$-values for which these transitions occur were not identified.

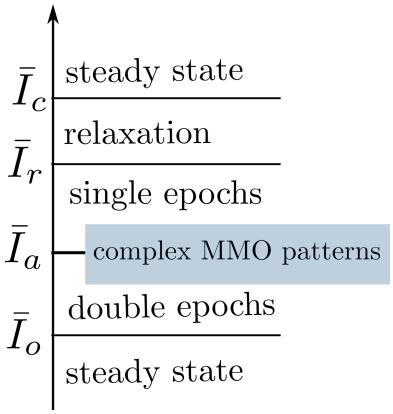

Figure 4.5: Bifurcation of mixed-mode oscillatory dynamics in dependence of the parameter $\bar{I}$ in the h-slow case, for ε and δ_h positive and sufficiently small in Equation (4.28).

As will become apparent through the discussion that follows, the values $\bar{I}_o$ and $\bar{I}_c$ are related to singular Hopf bifurcations of system (4.30), marking the onset and cessation of oscillatory dynamics, respectively. The value $\bar{I}_a$ distinguishes between mixed-mode trajectories with double epochs of SAOs and those with single epochs under the perturbed flow of (4.30), with ε and δ_h sufficiently small; see panels (a,b) and (d,e) of Figure 4.1, respectively. We remark that transitive, complex mixed-mode patterns featuring double epochs of SAOs separated by LAOs are observed during the transition from MMOs with double SAO epochs to those with single epochs, i.e., for $\bar{I}$-values close to $\bar{I}_a$; see Figure 4.1(c). Moreover, there exists an $\bar{I}$-value $\bar{I}_r$ which separates MMOs with single epochs of SAOs from relaxation oscillation, see Figure 4.1 (e) and (f), respectively.

4.3.1 Singular geometry

In the singular limit of $\varepsilon = 0$, with $\delta_h > 0$ sufficiently small and $\delta_n = 1$, the reduced flow in Equation (4.40) reads

$$\dot{v} = \partial_n \left[V(v, m_\infty(v), h, n) \right] N(v, n)|_{n=\nu(v,h)} + \mathcal{O}\left(\delta_h\right), \tag{4.43a}$$

$$\dot{h} = -\delta_h \partial_v \left[V(v, m_\infty(v), h, n) \right] H(v, h)|_{n=\nu(v,h)} \tag{4.43b}$$

in the intermediate formulation, whereas on the slow time-scale $\tau_h = \delta_h t$, we can write

$$\delta_h \dot{v} = \partial_n \left[V(v, m_\infty(v), h, n)\right] N(v, n)|_{n=\nu(v,h)} + \mathcal{O}\left(\delta_h\right), \tag{4.44a}$$

$$\dot{h} = -\partial_v \left[V(v, m_\infty(v), h, n)\right] H(v, h)|_{n=\nu(v,h)}; \tag{4.44b}$$

hence, we obtain a slow-fast system in the standard form of GSPT [Fenichel, 1979].

Setting $\delta_h = 0$ in Equation (4.43) gives the one-dimensional layer problem

$$\dot{v} = \partial_n \left[V(v, m_\infty(v), h, n)\right] N(v, n)|_{n=\nu(v,h)}, \tag{4.45a}$$

$$\dot{h} = 0. \tag{4.45b}$$

Solutions of (4.45) are given by *intermediate fibres* with h constant. Moreover, since by (4.36) holds that $\partial_n \left[V(v, m_\infty(v), h, n)\right] \neq 0$, equilibria of (4.45a) define the supercritical manifold $\mathcal{M}_h$ as the subset of $\mathcal{M}_1$ where

$$n_\infty(v) - \nu(v, h) = 0; \tag{4.46}$$

recall (4.15) and (4.37). The algebraic constraint (4.46) is equivalent to

$$V(v, m_\infty(v), h, n_\infty(v)) = 0, \tag{4.47}$$

see (4.12) for the definition of $V(v, m, h, n)$.

The manifold $\mathcal{M}_h$ is normally hyperbolic on the set $\mathcal{H}$ where

$$\partial_v \left[V(v, m_\infty(v), h, n_\infty(v))\right] \neq 0.$$

Using computer algebra software, calculation shows that the set $\mathcal{F}_{\mathcal{M}_h} = \mathcal{M}_h \backslash \mathcal{H}$ where normal hyperbolicity is lost consists of two points: $\mathcal{F}_{\mathcal{M}_h} = \left\{p_h^-, p_h^+\right\}$, cf. Figure 4.6. These two points separate the normally hyperbolic portion $\mathcal{H}$ of $\mathcal{M}_h$ into two attracting branches $\mathcal{H}^{a^\mp}$, with $\partial_v \left[V(v, m_\infty(v), h, n_\infty(v))\right] < 0$, and a repelling branch $\mathcal{H}^r$, where $\partial_v \left[V(v, m_\infty(v), h, n_\infty(v))\right] > 0$; see Figure 4.9. We emphasize that the fold points $p_h^\mp$ lie on $\mathcal{S}^r$.

In the double singular limit of $\varepsilon = 0 = \delta_h$, the *folded singularities* $Q_h = \left\{q_h^-, q_h^+\right\}$ [Szmolyan and Wechselberger, 2001] of (4.28) are given by

$$q_h^\mp = \mathcal{M}_h \cap \mathcal{L}^\mp; \tag{4.48}$$

see Figure 4.9. In the following, we will denote

$$q_h^\mp = \left(v_{q_h^\mp}, h_{q_h^\mp}, n_{q_h^\mp}\right) \tag{4.49}$$

We emphasise that the properties of all geometric objects defined above – i.e., of $\mathcal{M}_h$, $\mathcal{F}_{\mathcal{M}_h}$, and Q_h – are dependent on the parameter I or, rather, on its rescaled counterpart $\bar{I}$.

Next, setting $\delta_h = 0$ in the slow formulation, Equation (4.44), we obtain the one-dimensional reduced flow on $\mathcal{M}_h$:

$$0 = \partial_n \left[V(v, m_\infty(v), h, n)\right] N(v, n)|_{n=\nu(v,h)}, \tag{4.50a}$$

$$\dot{h} = -\partial_v \left[V(v, m_\infty(v), h, n)\right] H(v, h)|_{n=\nu(v,h)}, \tag{4.50b}$$

Differentiating the algebraic constraint in (4.47) implicitly, via

$$-\partial_v \left[V(v, m_\infty(v), h, n_\infty(v)\right] \dot{v} = \partial_h \left[V(v, m_\infty(v), h, n_\infty(v)\right] \dot{h},$$

and using (4.50b) and (4.38), we find the following expression for the reduced flow on $\mathcal{H}^{a^\mp}$

$$\dot{v} = \frac{\partial_v \left[V(v, m_\infty(v), h, n)\right] \partial_h \left[V(v, m_\infty(v), h, n_\infty(v))\right]}{\partial_v \left[V(v, m_\infty(v), h, n_\infty(v)\right]} H(v,h)\Big|_{h=\eta(v,n), n=n_\infty(v)}. \tag{4.51}$$

Using computer algebra software, calculations show that the reduced flow on $\mathcal{H}^{a^\mp}$ is directed towards $q_h^\mp$, respectively, cf. Figure 4.6 panel (c). The resulting singular geometry is summarised in Figure 4.6. Combining orbit segments from the layer flow of Equation $(4.31a)_{\varepsilon=0}$, the intermediate fibres of (4.45a) on $\mathcal{M}_1$, and the reduced dynamics of (4.51) on $\mathcal{M}_h$, one can construct *singular* or *candidate trajectories*; closed singular trajectories are called *singular cycles*; see Figure 4.7 for an illustration of such a trajectory in the three-dimensional (v, h, n)-space, and Figure 4.6 panel (a) for a projection onto the vh-plane.

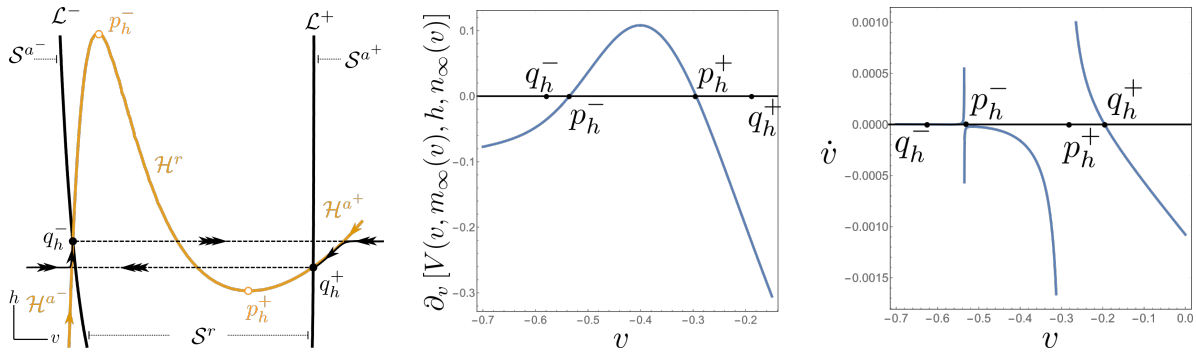

Figure 4.6: In the double singular limit of $\varepsilon = 0 = \delta_h$, the supercritical manifold $\mathcal{H}$ consists of two attracting branches $\mathcal{H}^{a^\mp}$ that are separated by a repelling branch $\mathcal{H}^r$. The folded singularities $q^\mp$ of (4.21) lie on $\mathcal{S}^r$, and the flow on $\mathcal{H}^{a^\mp}$ is directed towards $q_h^\mp$. The above graphs are for $\bar{I} = 20/(k_v g_{Na})$.

We emphasise that, according to the above, system (4.28) with h-slow is in accordance with the implications of Assumption 6 and Assumption 7 that were made for the extended prototypical system (2.2) in Chapter 2 to describe bifurcations of its MMO-trajectories based on the properties of its singular geometry and its singular cycles; namely:

- The critical manifold $\mathcal{M}_1$ is S-shaped (away from the tangential connection of $\mathcal{L}^\mp$), with two attracting sheets $\mathcal{S}^{a^\mp}$ separated by a repelling sheet $\mathcal{S}^r$,
- The supercritical manifold $\mathcal{M}_h$ is S-shaped, with two attracting branches $\mathcal{H}^{a^\mp}$ separated by a repelling branch $\mathcal{S}^r$; moreover, the folds of $\mathcal{M}_h$ lie on the repelling sheet $\mathcal{S}^r$,
- The reduced flow on $\mathcal{H}^{a^\mp}$ is directed towards $q_h^\mp$ respectively.

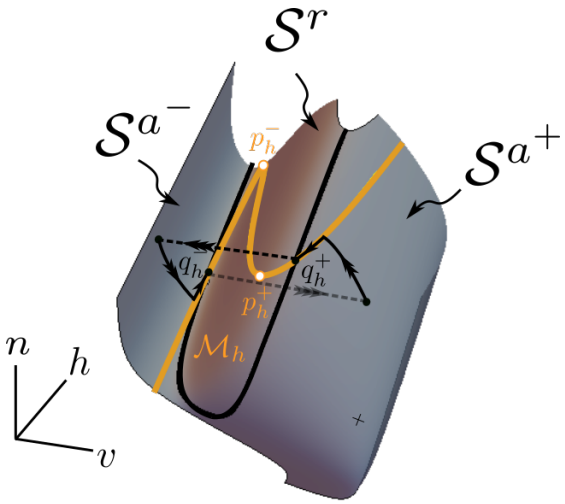

Figure 4.7: A singular cycle, as a concatenation of fast, intermediate and slow segments of $(4.31a)_{\varepsilon=0}$, (4.45a), and (4.51), respectively.

We reiterate that the above assumptions were imposed for the extended prototypical example (2.2) in Chapter 2, of which the Koper model [Koper, 1995] from chemical kinetics is a particular realisation, recall Chapter 3. The HH-equations and the Koper model have been studied extensively in the two-timescale context [Desroches et al., 2012], and here we show that they are fundamentally not very different in the three-timescale context, in terms of MMO-bifurcations in relation to their singular geometry.

4.3.2 Perturbed dynamics and and MMOs

By standard GSPT [Fenichel, 1979] and as shown in Chapter 2, for $\varepsilon, \delta_h > 0$ sufficiently small, there exist invariant manifolds $\mathcal{S}^a_{\varepsilon\delta_h}$ and $\mathcal{S}^r_{\varepsilon\delta_h}$ that are diffeomorphic to their unperturbed, normally hyperbolic counterparts $\mathcal{S}^a$ and $\mathcal{S}^r$, respectively, and that lie $\mathcal{O}(\varepsilon + \delta_h)$-close to them in the Hausdorff distance, for ε and δ_h positive and sufficiently small. The perturbed manifolds $\mathcal{S}^a_{\varepsilon\delta_h}$ and $\mathcal{S}^r_{\varepsilon\delta_h}$ are locally invariant under the flow of (4.31). Moreover, for $\varepsilon, \delta_h > 0$ sufficiently small, there exist invariant manifolds $\mathcal{H}^{a^\mp}_{\varepsilon\delta_h}$ and $\mathcal{H}^r_{\varepsilon\delta_h}$ that are diffeomorphic, and $\mathcal{O}(\delta_h)$-close in the Hausdorff distance, to their unperturbed, normally hyperbolic counterparts $\mathcal{H}^{a^\mp}$ and $\mathcal{H}^r$, respectively. The perturbed branches $\mathcal{H}^{a^\mp}_{\varepsilon\delta_h}$ and $\mathcal{H}^r_{\varepsilon\delta_h}$ are locally invariant under the flow of (4.31).

Given an initial point $(v, h, n) \in \mathcal{S}^a_{\varepsilon\delta_h}$, the corresponding trajectory will follow the intermediate flow thereon until it is either attracted to $\mathcal{H}^a_{\varepsilon\delta_h}$ or until it reaches the vicinity of the fold line $\mathcal{F}_{\mathcal{M}_1}$. If trajectories reach the vicinity of $\mathcal{F}_{\mathcal{M}_1}$ away from the folded singularities $q_h^\mp$, they "jump" to the opposite attracting sheet $\mathcal{S}^a_{\varepsilon\delta_h}$ following the fast flow of (4.23a); see [Wechselberger, 2005, Szmolyan and Wechselberger, 2001]. On the other hand, if trajectories are attracted to appropriate subregions of $\mathcal{H}^a_{\varepsilon\delta_h}$ or to the vicinity of q_h^-, they undergo SAOs; details can be found in Chapter 2. We include a brief discussion of SAO-generating mechanisms, as well as a comparison between (4.19) and (4.28) in that regard, in Section 4.5.

Therefore, orbits for the perturbed flow of Equation (4.28) with ε and δ_h positive and sufficiently small can be constructed by combining perturbations of fast, intermediate and slow segments of singular trajectories, as described above. In Chapter 2, we showed that the qualitative characteristics of the resulting MMO trajectories will depend on the properties of the flow on $\mathcal{S}^a_{\varepsilon\delta_h}$ and $\mathcal{H}^a_{\varepsilon\delta_h}$, as well as on the location of the folded singularities $q_h^{\mp}$ relative to each other.

In the following, we demonstrate how the various $\bar{I}$-values that distinguish between different qualitative behaviours of the system (4.31) with $\varepsilon, \delta_h > 0$ small as shown in Figure 4.5 are obtained.

4.3.3 Onset and cessation of oscillatory dynamics

At the singular limit $\varepsilon = 0 = \delta_h$, using computer algebra software, we find that the reduced flow on $\mathcal{H}$, equation (4.51), has a stable equilibrium point on $\mathcal{S}^r$ for $\bar{I} \in (\bar{I}_1, \bar{I}_2)$, where

$$\bar{I}_1 \simeq \frac{4.8}{k_v g_{Na}}, \qquad \bar{I}_2 \simeq \frac{280}{k_v g_{Na}}, \tag{4.52}$$

cf. Figure 4.8.Moreover, the reduced flow (4.51) has a stable equilibrium point on $\mathcal{H}^{a^-}$ for $\bar{I} < \bar{I}_1$, and on the unique normally hyperbolic branch $\mathcal{H}^a$ for $\bar{I} > \bar{I}_2$, cf Figure 4.8, while the equilibrium point crosses $\mathcal{L}^-$ for $\bar{I} = \bar{I}_1$ and $\bar{I} = \bar{I}_2$

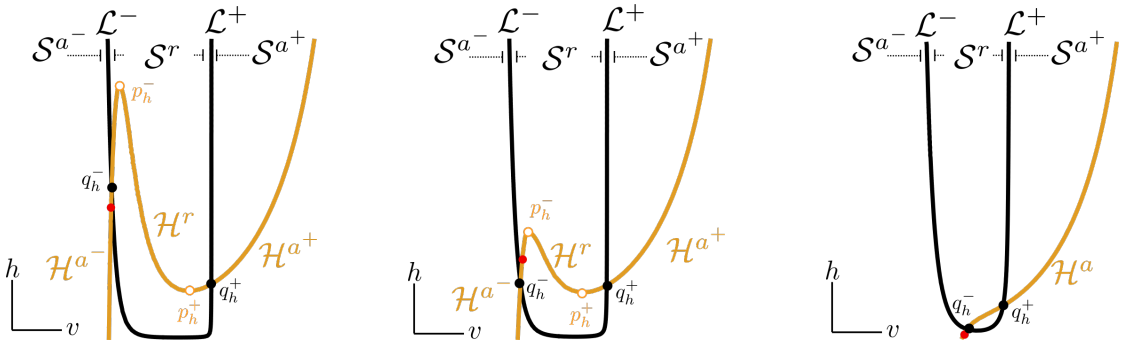

(a) $\bar{I} < \bar{I}_1$ (b) $\bar{I} \in (\bar{I}_1, \bar{I}_2)$ (c) $\bar{I} > \bar{I}_2$

Figure 4.8: A stable equilibrium of the reduced flow (4.68) (red dot) lies in the attracting portion $\mathcal{S}^a$ of $\mathcal{M}_1$ for $\bar{I} < \bar{I}_1$ and $\bar{I} > \bar{I}_2$, panels (a) and (c), respectively, and in the repelling portion $\mathcal{S}^r$ for $\bar{I} \in (\bar{I}_1, \bar{I}_2)$, panel (b). As $\bar{I}$ increases, the distance between $\mathcal{L}^-$ and $\mathcal{L}^+$ becomes more narrow, and the leftmost branch of $\mathcal{H}$ is "moving downwards". For $\bar{I} \gtrsim 120/(k_v g_{Na})$, $\mathcal{M}_h$ consists of one normally hyperbolic, attracting branch $\mathcal{H}^a$.

According to Section 2.3, for $\varepsilon, \delta_h > 0$ sufficiently small, the perturbed system (4.31) undergoes singular Hopf bifurcations for $\bar{I}$-values that are $\mathcal{O}(\varepsilon, \delta_h)$-close to $\bar{I}_1$ and $\bar{I}_2$, and the onset and cessation of global oscillatory dynamics happens $\mathcal{O}(\varepsilon, \delta_h)$-close to these values, respectively, i.e.

$$\bar{I}_o = \bar{I}_1 + \mathcal{O}(\varepsilon, \delta_h), \qquad \bar{I}_c = \bar{I}_2 + \mathcal{O}(\varepsilon, \delta_h),$$

see also [Desroches et al., 2012, Letson et al., 2017, Guckenheimer, 2008, Krupa et al., 2008, Krupa and Wechselberger, 2010] and Chapter 2. By numerical sweeping, we find that for $\gamma = 0.0083$, $\varepsilon = 0.1$, $\delta_h = 0.025$ and for parameter values as in (4.9), the onset of oscillatory dynamics of system (4.21) is at approximately $\bar{I} \simeq 8.1/(k_v g_{Na})$, while the cessation of oscillatory dynamics is at approximately $\bar{I} \simeq 272/(k_v g_{Na})$, which are $\mathcal{O}(\varepsilon, \delta_h)$-close to $\bar{I}_1$ and $\bar{I}_2$, respectivelly.

4.3.4 From double to single SAO-epochs

At the beginning of this section, we introduced the notion of singular cycles, and we showed a particular example in Figure 4.6 and Figure 4.7. However, the configuration of the singular cycle illustrated therein is not the only possible one. Namely, depending on the location of the folded singularities $q_h^{\mp}$ relative to each other, singular cycles can pass through only one or through both of them, as shown in Figure 4.9. We characterise the pair of folded singularities $q_h^{\mp}$ based on whether they are "connected" by singular cycles or not, by slightly rephrasing Definition 5, as follows.

Definition 6.

1. *The folded singularities $q_h^{\mp}$ are "orbitally connected" if they are contained in the same singular cycle, with the latter containing two slow segments, one on $\mathcal{H}^{a^-}$ and one on $\mathcal{H}^{a^+}$, i.e. if $q_h^- > q_h^+$; cf. Figure 4.9 (a).*

2. *The folded singularities $q_h^{\mp}$ are "orbitally remote" if a singular cycle that passes through q_h^- does not pass through q_h^+, i.e. if $q_h^- < q_h^+$; cf. Figure 4.9 (c).*

3. *The folded singularities $q_h^{\mp}$ are "orbitally aligned" if they are neither orbitally remote nor orbitally connected, i.e. if $q_h^- = q_h^+$; cf. Figure 4.9 (b).*

Due to the $\bar{I}$-dependence of of the location of $q_h^{\mp}$, the classification in Definition 6 hence encodes the position of the folded singularities $q_h^{\mp}$ relative to one another in dependence of the rescaled applied current $\bar{I}$. For a given value of $\bar{I}$, the v-coordinates of the folded singularities are obtained by solving the system

$$\eta(v, n_\infty(v)) - \frac{\bar{I} - \bar{g}_L\left(v - \bar{E}_K\right) - \bar{g}_L(v - \bar{E}_L)}{3m'(v)m_\infty^2(v)\left(v - \bar{E}_{Na}\right)\left(v - \bar{E}_K\right) + m_\infty^3(v)\left(2v - \bar{E}_{Na} - \bar{E}_k\right)} = 0, \quad (4.53)$$

where $\eta(v, n_\infty(v))$ corresponds to the graph of $\mathcal{M}_\mathcal{H}$ in the vh-plane, recall (4.38), and the fractional factor corresponds to the graph of $\mathcal{F}_{\mathcal{M}_1}$, recall (4.35). It follows that, in the parameter regime given by (4.9), there exists a unique value $\bar{I}_a$ such that the singularities q_h^- and q_h^+ are orbitally aligned. By numerical computations, this value is approximately

$$\bar{I}_a \simeq \frac{26.5}{k_v g_{Na}}, \quad (4.54)$$

recall (4.9). Correspondingly, $q^{\mp}$ are connected for $\bar{I} < \bar{I}_a$ and remote for $\bar{I} > \bar{I}_a$.

It follows that, for $\bar{I} < \bar{I}_a + \mathcal{O}(\varepsilon, \delta_h)$, the full system (4.21) with $\varepsilon, \delta_h > 0$ sufficiently small features MMOs with double epochs of perturbed slow dynamics, cf. Figure 4.10 & Figure 4.1

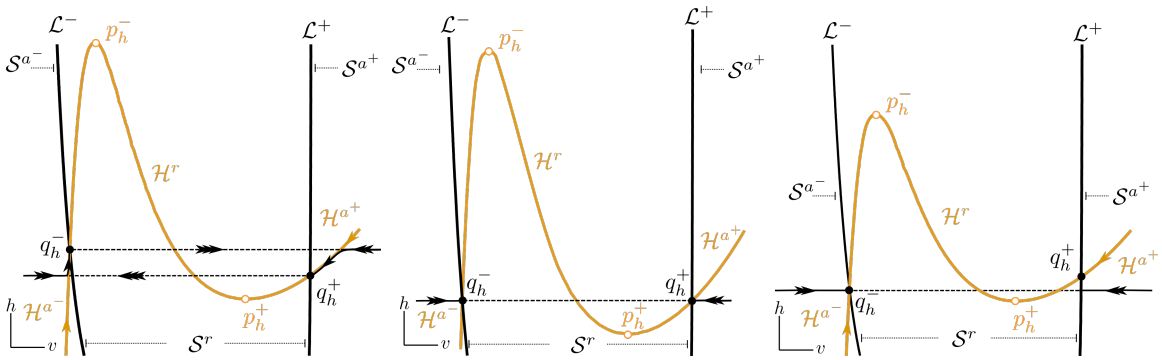

(a) $I < \bar{I}_a$ (b) $\bar{I} = \bar{I}_a$ (c) $\bar{I} > \bar{I}_a$

Figure 4.9: Orbital connection or lack thereof, in accordance with Definition 6. For $\bar{I} < \bar{I}_a$, the folded singularities $q_h^{\mp}$ are orbitally connected, in the sense that, at the limit $\varepsilon = 0 = \delta_h$, there exists a singular cycle that passes through both of them and also has slow segments on both $\mathcal{H}^{a^{\mp}}$, panel (a). For $\bar{I} > \bar{I}_a$, the folded singularities $q_h^{\mp}$ are orbitally remote, in the sense that, at the limit $\varepsilon = 0 = \delta_h$, a singular cycles that passes through one of the folded singularities does not pass through the other, panel (c). For $\bar{I} = \bar{I}_a$, the folded singularities $q_h^{\mp}$ are orbitally aligned, in the sense that, at the limit $\varepsilon = 0 = \delta_h$, there exists a singular cycle that passes through both of them but has no slow segments on both $\mathcal{H}^{a^{\mp}}$, panel (b)

panels (a,b). Correspondingly, for $\bar{I} > \bar{I}_a + \mathcal{O}(\varepsilon, \delta_h)$, the full system (4.17) with $\varepsilon, \delta_h > 0$ sufficiently small features MMOs with at most single epochs of perturbed slow dynamics, cf. Figure 4.10 & Figure 4.1 panels (d,e,f). We elaborate on the transitive behaviour, Figure 4.10 & Figure 4.1 panel (c), as well as on the transition from single epochs of SAOs to relaxation oscillations in the following parts. By numerical sweeping, we find that for $\gamma = 0.0083$, $\varepsilon = 0.1$, $\delta_h = 0.025$ and for parameter values as in (4.9), system (4.21) features MMOs with double SAO-epochs (without LAOs between them) until approximately $\bar{I} \simeq 23.09/(k_v g_{Na})$, which is $\mathcal{O}(\varepsilon, \delta_h)$-close to $\bar{I}_a$.

4.3.5 Transitive, "exotic" MMOs

In Chapter 2 it is clearly stated that MMOs are not, strictly speaking, perturbations of singular cycles; therefore, other (and more complicated) phenomena might occur in dependence on the values of ε and δ_h. In particular, upon variation of $\bar{I}$, during the transition from MMOs with double epochs of SAOs to single-epoch MMOs, i.e. for $\bar{I}$-values close to the value $\bar{I}_a$ for which the folded singularities $q_h^{\mp}$ are orbitally aligned, Equation (4.28) exhibits MMOs of the type illustrated in Figure 4.1 (c). This is due to the fact that for these particular values of I and δ_h, the folded singularities $q_h^{\mp}$ are remote and sufficiently away from each other in the slow h-direction such that:

1. the slow flow on $\mathcal{H}^{a^-}_{\varepsilon\delta_h}$ is such that trajectories that jump away from $\mathcal{H}^{a^-}_{\varepsilon\delta_h}$ are attracted to $\mathcal{H}^{a^+}_{\varepsilon\delta_h}$ after their first jump, whereon they follow the slow flow and SAOs above occur,

2. the slow flow on $\mathcal{H}^{a^+}_{\varepsilon\delta_h}$ is such that trajectories that jump away from $\mathcal{H}^{a^+}_{\varepsilon\delta_h}$, although taken downwards by the slow drift, they reach $\mathcal{L}^-$ after the first excursion instead of

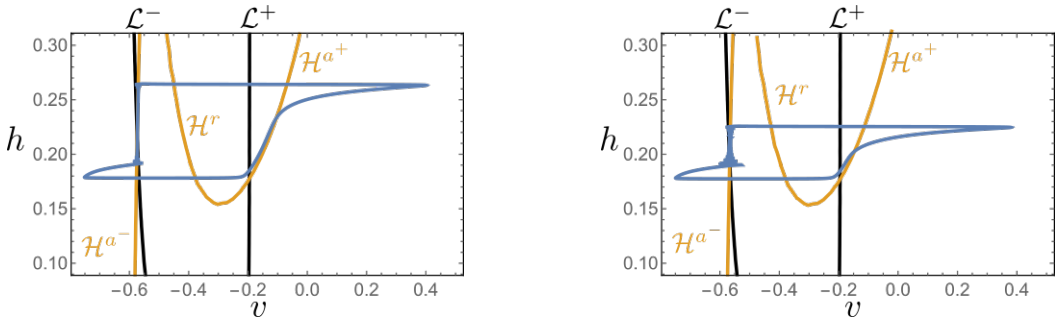

(a) $I = 20.051$

(b) $I = 23.051$

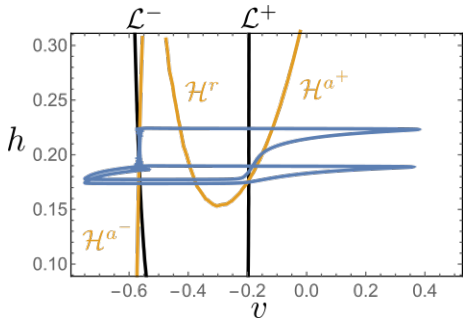

(c) $I = 23.5$

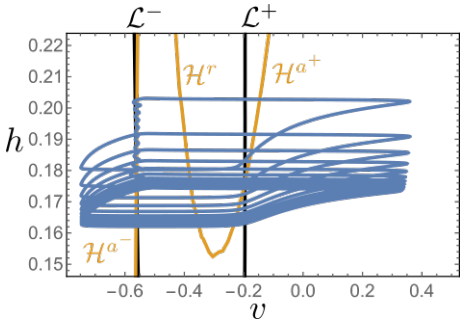

(d) $I = 26.03452346$

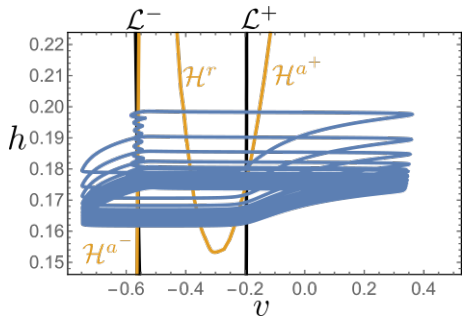

(e) $I = 29.1209956$

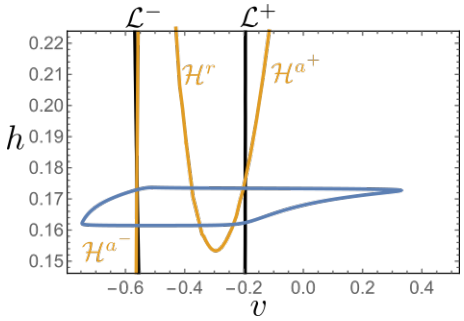

(f) $I = 26.2$

Figure 4.10: Singular geometry of Equation (4.43) which underlies the qualitative properties of the time series, and the associated MMO trajectories, illustrated in Figure 4.1: as $\bar{I}$ is varied, the folded singularities become orbitally remote from orbitally connected. Therefore, system (4.21) with $\varepsilon, \delta_h > 0$ small transits from MMOs with double SAO epochs for $\bar{I} < \bar{I}_a$ (panels (a) and (b)) to MMOs with single SAO epochs for $\bar{I} > \bar{I}_a$ (panels (d) and (e)), via transitive exotic MMO trajectories when $\bar{I}$ is close to $\bar{I}_a$ (panel (c)). Then, for $\bar{I} > \bar{I}_r$, system (4.21) features relaxation oscillations.

being attracted to $\mathcal{H}^{a^-}_{\varepsilon\delta_h}$. Therefore, a number of relaxation-type segments occur before the trajecotry is attracted to $\mathcal{H}^{a^-}_{\varepsilon\delta_h}$ and undergoes SAOs below, see Figure 4.1 and Figure 4.10, panel (c).

We remark that the above is not surprising, as in Chapter 2 it is explicitly stated that for a fixed "remote" geometry of the system, one can find ε and δ_h sufficiently small such that MMOs with single epochs of perturbed slow dynamics occur. In our example here, ε and δ_h are fixed and $\bar{I}$ is varied, which means that the system passes through a geometric configuration that allows for the phenomenon described above to occur.

By numerical sweeping, we find that for $\gamma = 0.0083$, $\varepsilon = 0.1$, $\delta_h = 0.025$ and for parameter values as in (4.9), system (4.21) features such MMOs with double SAO-epochs with LAOs between them until approximately $\bar{I} \simeq 26/(k_v g_{Na})$, which is $\mathcal{O}(\varepsilon, \delta_h)$-close to $\bar{I}_a$.

4.3.6 From MMOs to relaxation

When the folded singularities $q_h^{\mp}$ are orbitally remote, one can compute a critical value $\bar{I}_r$ at which MMOs with single epochs of SAOs turn to relaxation oscillation in the full system (4.28), in accordance with what was described in Section 2.3. In a first approximation, this happens for an $\bar{I}$-value and around an h-coordinate for which the flow on $\mathcal{S}^{a^-}$ is balanced by than on $\mathcal{S}^{a^+}$ [Krupa et al., 2008]. This establishes the existence of a two-timescale singular cycle at the limit $\varepsilon = 0$, $\delta_h > 0$ small, which then by Theorem 3 [Szmolyan and Wechselberger, 2004] implies the existence of a relaxation oscillation in the perturbed system (4.28) for $\varepsilon, \delta_h > 0$ small.

To establish the existence of a relaxation oscillation, we proceed as in Theorem 5; we therefore need to show that Assumption 1 to Assumption 5 hold. Assumption 1, Assumption 2 and Assumption 3 hold on the basis of what has been described so far in this Chapter, and as also shown in [Rubin and Wechselberger, 2007].

To show Assumption 4, we need to establish the existence of a singular periodic orbit Γ_h of system (4.40) with $\varepsilon = 0$, $\delta_h > 0$ small. Eliminating time in (4.40), away from $\mathcal{H}$ the flow on $\mathcal{S}^{a^{\mp}}$ can be approximated by

$$\frac{dh}{dv} = -\delta_h \frac{\partial_v \left[V(v, m_\infty(v), h, n)\right] H(v,h)}{\partial_n \left[V(v, m_\infty(v), h, n)\right] N(v,n)}\bigg|_{n=\nu(v,h)} \tag{4.55}$$

where we have omitted $\mathcal{O}(\delta_h)$-terms in the denominator; recall that $\partial_n \left[V(v, m_\infty(v), h, n)\right] < 0$ by (4.36). Denote

- v_{max}: the value obtained by solving $V\left(v_{max}, m_\infty\left(v_{max}\right), h_{q_h^+}, n_{q_h^+}\right) = 0$; that is, the projection of q_h^- onto $\mathcal{S}^{a^+}$ along the fast fibres $(4.31\text{a})_{\varepsilon=0}$,
- v^*_{max}: the value obtained by solving $V\left(v^*_{max}, m_\infty\left(v^*_{max}\right), h_{q_h^-}, n_{q_h^-}\right) = 0$; that is, the projection of a point on $\mathcal{L}^+$ with $h = h_{q_h^-}$ and $n = n_{q_h^-}$ onto $\mathcal{S}^{a^-}$ along the fast fibres $(4.31\text{a})_{\varepsilon=0}$,

and consider a trajectory on $\mathcal{S}^{a^-}$ with initial condition (v^*_{max}, h^*_{max}), where $h^*_{max} \in (h_{q_h^-}, h_{q_h^+})$ is close to $h_{q_h^-}$. This trajectory reaches a point on $\mathcal{L}^-$ at an h-coordinate approximately given by

$$h = h^*_{max} + \delta_h \mathcal{G}^-_h(h_{q_h^-}, \bar{I}) + \mathcal{O}(\delta_h^2),$$

where we denote

$$\mathcal{G}^-_h(h, \bar{I}) := -\int_{v^*_{max}}^{v_{q_h^-}} \left. \frac{\partial_v \left[V\left(v, m_\infty(v), h, n\right)\right] H\left(v, h\right)}{\partial_n \left[V\left(v, m_\infty(v), h, n\right)\right] N(v, n)} \right|_{n=\nu(v,h)} \mathrm{d}v;$$

see again Section 2.3 and recall (2.37). When this trajectory reaches the vicinity of $\mathcal{L}^-$, it connects to a fast segment that reaches $\mathcal{S}^{a^+}$ at a point (v_{max}, h_{max}). A trajectory with the latter coordinates as initial conditions on $\mathcal{S}^{a^+}$ follows the flow (4.43) thereon and reaches $\mathcal{L}^+$ at an h-coordinate approximately given by

$$h = h_{max} + \delta_h \mathcal{G}^+_h(h_{q_h^-}, \bar{I}) + \mathcal{O}(\delta_h^2),$$

where we denote

$$\mathcal{G}^+_h(h, \bar{I}) := -\int_{v_{max}}^{v_{q_h^+}} \left. \frac{\partial_v \left[V\left(v, m_\infty(v), h, n\right)\right] H\left(v, h\right)}{\partial_n \left[V\left(v, m_\infty(v), h, n\right)\right] N(v, n)} \right|_{n=\nu(v,h)} \mathrm{d}v.$$

Therefore, a trajectory that leaves the vicinity of $\mathcal{L}^-$ at a point with h-coordinate close to h_{q^-} returns to this vicinity after a large excursions to and from $\mathcal{S}^{a^+}$ at a point with $\hat{h}$, where

$$\hat{h} = h + \delta_h \left(\mathcal{G}^-_h(h_{q_h^-}, \bar{I}) + \mathcal{G}^+_h(h_{q_h^-}, \bar{I}) \right) + \mathcal{O}(\delta_h^2). \tag{4.56}$$

A trajectory returns to the same h-coordinate after an excursion if the flow on the two sheets $\mathcal{S}^{a^\mp}$ is balanced, i.e. if

$$\mathcal{G}^-_h(h_{q_h^-}, \bar{I}) + \mathcal{G}^+_h(h_{q_h^-}, \bar{I}) = 0, \tag{4.57}$$

and this trajectory then corresponds to a singular periodic cycle Γ_h. Solving (4.57) for $\bar{I}$, gives the $\bar{I}$-value $\bar{I}_b$ for which, to leading order in δ, the singular periodic orbit Γ_h exists at the limit $\varepsilon = 0$, $\delta > 0$ sufficiently small, with no slow segments on $\mathcal{H}$, see [Krupa et al., 2008, Szmolyan and Wechselberger, 2004] for details. Evaluating the integrals using computer algebra software, this value is obtain approximately

$$\bar{I}_b \simeq \frac{29.2}{k_v g_{Na}}. \tag{4.58}$$

To show hyperbolicity and stability of the singular periodic orbit Γ_h, and hence the existence of a stable relaxation oscillation of the perturbed system $\varepsilon, \delta_h > 0$ small, we need to show that the derivative of the return map (4.56) is less than one. Numerical evaluation shows that

$$\partial_h(\mathcal{G}^-_h(h, \bar{I}) + \mathcal{G}^+_h(h, \bar{I}))|_{h=h_{q_h^-}, \bar{I}=\bar{I}_b} < 0,$$

therefore $\partial_h \left[h + \delta_h \left(\mathcal{G}_h^-(h_{q_h^-}, \bar{I}) + \mathcal{G}_h^+(h_{q_h^-}, \bar{I}) \right) \right] < 1$ and hence Γ_h is stable, and so is the relaxation oscillation of (4.28) for $\varepsilon, \delta_h > 0$ small. Finally, we also calculate that

$$\partial_{\bar{I}}(\mathcal{G}_h^-(h, \bar{I}) + \mathcal{G}_h^+(h, \bar{I}))|_{h=h_{q_h^-}, \bar{I}=\bar{I}_b} < 0;$$

from the implicit function theorem follows that there is an open $\bar{I}$-neighbourhood of $\bar{I}_r$ for which the system exhibits relaxation oscillation.

The asymptotics for the value $\bar{I}_r$ at which system (4.21) with $\varepsilon, \delta_h > 0$ small is expected to transit from MMOs with single SAO-epochs to relaxation are

$$\bar{I}_r = \bar{I}_b + \mathcal{O}(\delta_h, \delta_h \varepsilon \ln \varepsilon), \tag{4.59}$$

recall Theorem 5. By numerical sweeping, we find that for $\gamma = 0.0083$, $\varepsilon = 0.1$, $\delta_h = 0.025$ and for parameter values as in (4.9), system (4.21) features MMOs with single SAO-epochs until approximately $\bar{I} \simeq 26.127/(k_v g_{Na})$, which is in accordance with (4.59).

We remark that in [Doi et al., 2001], chaotic MMOs were documented during the transition from MMOs with single SAO epochs to relaxation; cf. Figure 4.1, panel (e). The study of the mechanisms that are responsible for such behaviour in three-timescale systems of this form is included in plans for future work.

4.4 The n-slow case

In this section, we consider the regime where the variable n is the slowest variable in (4.21), which is realised for $\delta_n > 0$ sufficiently small and $\delta_h = 1$, that is, when τ_n is large and $\tau_h = \mathcal{O}(1)$ in the original HH model, Equation (4.2). In that case, the reduced system on $\mathcal{M}_1$, Equation (4.41), is a slow-fast system written in the standard form of GSPT which features similar geometric and dynamical properties to the extended prototypical example introduced in Chapter 2.

Similarly to the h-slow case, we will classify the mixed-mode dynamics of Equation (4.21) with $\gamma, \varepsilon, \delta_n > 0$ small in dependence of the (rescaled) applied current $\bar{I}$, by applying the analysis outlined in Chapter 2 to the three-dimensional reduction (4.28). We will show that, in the parameter regime defined in (4.9), there exist values $0 < \bar{I}_o' < \bar{I}_a' < \bar{I}_c'$ of $\bar{I}$ that distinguish between the various types of oscillatory dynamics in (4.21) for γ, ε, $1/\delta_m$, and δ_n positive and sufficiently small and $\delta_h = \mathcal{O}(1)$. The resulting classification is illustrated in Figure 4.11, with the corresponding mixed-mode oscillatory dynamics as shown in Figure 4.2.

As will become apparent through the discussion that follows, the values $\bar{I}_o'$ and $\bar{I}_c'$ are related to singular Hopf bifurcations of system (4.30), marking the onset of oscillatory dynamics, respectively. The value $\bar{I}_a'$ distinguishes between mixed-mode trajectories with double epochs of SAOs and those with single epochs under the perturbed flow of (4.30), with ε and δ_n sufficiently small; see panels (a,b) and (d,e) of Figure 4.2, respectively. Moreover, there exists an $\bar{I}$-value $\bar{I}_r'$ which separates MMOs with single epochs of SAOs from relaxation oscillation, see Figure 4.2 (e) and (f), respectively.

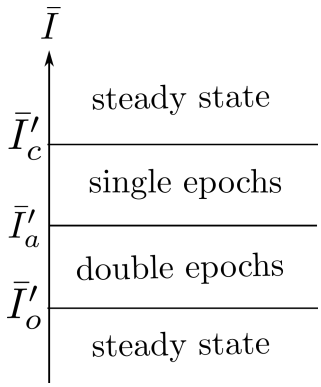

Figure 4.11: Bifurcation of oscillatory dynamics depending on the parameter I in the n-slow case, $\varepsilon, \delta_n > 0$ sufficiently small.

4.4.1 Singular geometry

In the singular limit of $\varepsilon = 0$, with $\delta_n > 0$ sufficiently small and $\delta_h = 1$, the reduced flow in Equation (4.40) reads

$$v' = \partial_h \left[V(v, m_\infty(v), h, n)\right] H(v,h)|_{h=\eta(v,n)} + \mathcal{O}\left(\delta_n\right), \tag{4.60a}$$
$$n' = -\delta_n \partial_v \left[V(v, m_\infty(v), h, n)\right] N(v,n)|_{h=\eta(v,n)}. \tag{4.60b}$$

in the intermediate formulation, whereas on the slow time-scale $\tau_n = \delta_n t$, we can write

$$\delta_n \dot{v} = \partial_h \left[V(v, m_\infty(v), h, n)\right] H(v,h)|_{h=\eta(v,n)} + \mathcal{O}\left(\delta_n\right), \tag{4.61a}$$
$$\dot{n} = -\partial_v \left[V(v, m_\infty(v), h, n)\right] N(v,n)|_{h=\eta(v,n)}. \tag{4.61b}$$

hence, we obtain a slow-fast system in the standard form of GSPT [Fenichel, 1979].

Setting $\delta_n = 0$ in Equation (4.43) gives the one-dimensional layer problem

$$v' = \partial_h \left[V(v, m_\infty(v), h, n)\right] H(v,h)|_{h=\eta(v,n)}, \tag{4.62a}$$
$$n' = 0. \tag{4.62b}$$

Solutions of (4.62) are given by *intermediate fibres* with n constant. Moreover, since by (4.36) holds that $\partial_h \left[V(v, m_\infty(v), h, n)\right] \neq 0$, equilibria of (4.62a) define the supercritical manifold $\mathcal{M}_n$ as the subset of $\mathcal{M}_1$ where

$$h_\infty(v) - \eta(v,h) = 0; \tag{4.63}$$

recall (4.14) and (4.38). The algebraic constraint (4.63) is equivalent to

$$V(v, m_\infty(v), h_\infty(v), n) = 0, \tag{4.64}$$

recall (4.12). Solving (4.64) for n, we can write $n = \nu(v, h_\infty(v))$ on $\mathcal{M}_n$.

The manifold $\mathcal{M}_n$ is normally hyperbolic on the set $\mathcal{N}$ where

$$\partial_v \left[V(v, m_\infty(v), h_\infty(v), n)\right] \neq 0.$$

Calculation shows that the set $\mathcal{F}_{\mathcal{M}_n} = \mathcal{M}_n \backslash \mathcal{N}$ where normal hyperbolicity is lost consists of two points: $\mathcal{F}_{\mathcal{M}_n} = \{p_n^-, p_n^+\}$. These two points separate the normally hyperbolic portion $\mathcal{N}$ of $\mathcal{M}_n$ into a repelling branch $\mathcal{N}^r$, where $\partial_v \left[V(v, m_\infty(v), h_\infty(v), n)\right] > 0$, and two attracting branches $\mathcal{N}^{a^\mp}$, with $\partial_v \left[V(v, m_\infty(v), h_\infty(v), n)\right] < 0$; see Figure 4.15. We emphasize that the fold points $p_n^\mp$ lie on $\mathcal{S}^r$.

In the double singular limit of $\varepsilon = 0 = \delta_n$, the *folded singularities* $Q_n = \{q_n^-, q_n^+\}$ [Szmolyan and Wechselberger, 2001] of (4.28) are given by

$$q_n^\mp = \mathcal{M}_n \cap \mathcal{L}^\mp; \tag{4.65}$$

see Figure 4.15. In the following, we will denote

$$q_n^\mp = \left(v_{q_n^\mp}, h_{q_n^\mp}, n_{q_n^\mp}\right) \tag{4.66}$$

We emphasise that the properties of all geometric objects defined above – i.e., of $\mathcal{M}_n$, $\mathcal{F}_{\mathcal{M}_n}$, and Q_n – are dependent on the parameter I or, rather, on its rescaled counterpart $\bar{I}$.

Next, setting $\delta_n = 0$ in the slow formulation, Equation (4.61), we obtain the one-dimensional reduced flow on $\mathcal{M}_n$:

$$0 = \partial_h \left[V(v, m_\infty(v), h, n)\right] H(v, h)|_{h=\eta(v,n)}, \tag{4.67a}$$

$$\dot{n} = -\partial_v \left[V(v, m_\infty(v), h, n)\right] N(v, n)|_{h=\eta(v,n)}. \tag{4.67b}$$

Differentiating the algebraic constraint in (4.64) implicitly, via

$$-\partial_v \left[V(v, m_\infty(v), h_\infty(v), n\right] \dot{v} = \partial_n \left[V(v, m_\infty(v), h_\infty(v), n\right] \dot{n},$$

and using (4.67b) and (4.37), we find the following expression for the reduced flow on $\mathcal{H}^{a^\mp}$

$$\dot{v} = \frac{\partial_v \left[V(v, m_\infty(v), h, n)\right] \partial_n \left[V(v, m_\infty(v), h_\infty(v), n)\right]}{\partial_v \left[V(v, m_\infty(v), h_\infty(v), n\right]} N(v, h)\Big|_{h=h_\infty(v), n=\nu(v,h)}. \tag{4.68}$$

The reduced flow on $\mathcal{N}^{a^\mp}$ is directed towards $q_n^\mp$, respectively. The resulting singular geometry is summarised in Figure 4.12. Combining orbit segments from the layer flow of Equation $(4.31a)_{\varepsilon=0}$, the intermediate fibres of (4.62a) on $\mathcal{M}_1$, and the reduced dynamics of (4.68) on $\mathcal{M}_n$, one can construct *singular* or *candidate trajectories*; closed singular trajectories are called *singular cycles*; see Figure 4.13 for an illustration of such a trajectory in the three-dimensional (v, h, n)-space, and Figure 4.12 panel (a) for a projection onto the vn-plane.

We emphasise that, according to the above, system (4.28) with h-slow is in accordance with the implications of Assumption 6 and Assumption 7 that were made for the extended prototypical system (2.2) in Chapter 2 to describe bifurcations of its MMO-trajectories based on the properties of its singular geometry and its singular cycles; namely:

- The critical manifold $\mathcal{M}_1$ is S-shaped (away from the tangential connection of $\mathcal{L}^\mp$), with two attracting sheets $\mathcal{S}^{a^\mp}$ separated by a repelling sheet $\mathcal{S}^r$,
- The supercritical manifold $\mathcal{M}_n$ is S-shaped, with two attracting branches $\mathcal{N}^{a^\mp}$ separated by a repelling branch $\mathcal{S}^r$; moreover, the folds of $\mathcal{M}_n$ lie on the repelling sheet $\mathcal{S}^r$,
- The reduced flow on $\mathcal{N}^{a^\mp}$ is directed towards $q_n^\mp$ respectively.

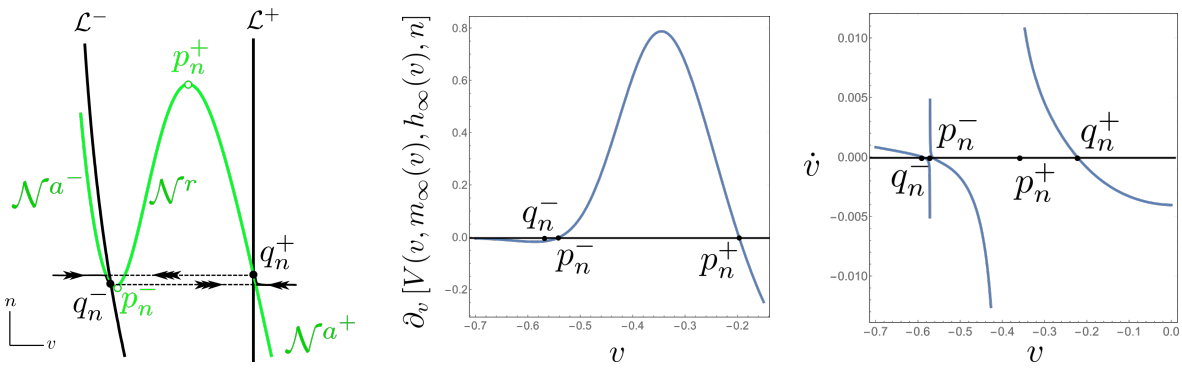

Figure 4.12: In the double singular limit of $\varepsilon = 0 = \delta_n$, the supercritical manifold $\mathcal{N}$ consists of two attracting branches $\mathcal{N}^{a^\mp}$ that are separated by a repelling branch $\mathcal{N}^r$. The folded singularities $q_n^\mp$ of (4.21) lie on $\mathcal{S}^r$, and the flow on $\mathcal{N}^{a^\mp}$ is directed towards $q_n^\mp$.

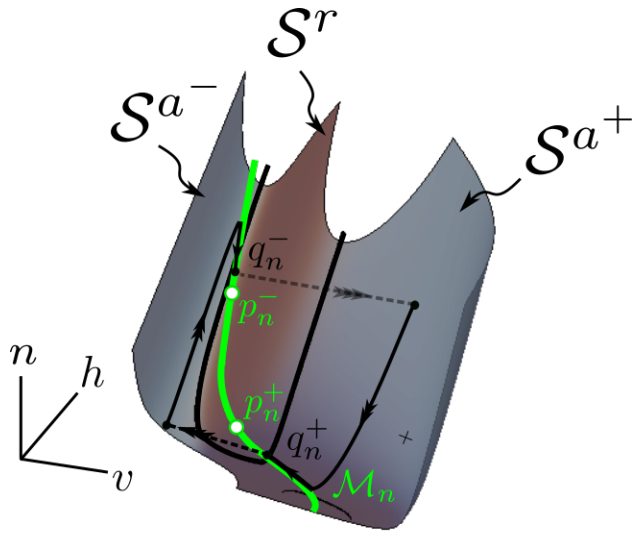

Figure 4.13: A singular cycle, as a concatenation of fast, intermediate and slow segments of $(4.31a)_{\varepsilon=0}$, (4.62a), and (4.68), respectively.

4.4.2 Perturbed dynamics and MMOs

By standard Fenichel Theory [Fenichel, 1979] and as shown in Chapter 2, for $\varepsilon, \delta_n > 0$ sufficiently small, there exist invariant manifolds $\mathcal{S}^{a,r}_{\varepsilon\delta_n}$ that are diffeomorphic and lie $\mathcal{O}(\varepsilon, \delta_n)$-close in the Hausdorff distance to their unperturbed, normally hyperbolic counterparts $\mathcal{S}^{a,r}$. The perturbed sheets $\mathcal{S}^{a,r}_{\varepsilon\delta_n}$ are locally invariant under the flow (4.31).

Moreover, for $\varepsilon, \delta_n > 0$ sufficiently small, there exist invariant manifolds $\mathcal{N}^{a^\mp,r}_{\varepsilon\delta_n}$ that are diffeomorphic and lie $\mathcal{O}(\delta_n)$-close in the Hausdorff distance to their unperturbed, normally hyperbolic counterparts $\mathcal{N}^{a^\mp,r}$. The perturbed branches $\mathcal{N}^{a^\mp,r}_{\varepsilon\delta_n}$ are locally invariant under the flow (4.31).

Given an initial point $(v, h, n) \in \mathcal{S}^a_{\varepsilon\delta_n}$, the corresponding trajectory will follow the intermediate flow thereon until it is either attracted to $\mathcal{N}^{a^\mp}_{\varepsilon\delta_n}$ or until it reaches the vicinity of $\mathcal{F}_{M_1}$.

If trajectories reach the vicinity of the fold curve $\mathcal{F}_{M_1}$ away from the vicinity of the folded singularities $q_n^{\mp}$, they "jump" to the opposite attracting sheet of $\mathcal{S}^a_{\varepsilon\delta_n}$ following the fast flow (4.23a), see [Wechselberger, 2005, Szmolyan and Wechselberger, 2001]. On the other hand, if trajectories are attracted to appropriate subregions of $\mathcal{N}^{a^{\mp}}_{\varepsilon,\delta_n}$ or to the vicinity of $q_n^{\mp}$, they undergo SAOs, see Chapter 2 for details.

Therefore, orbits of the perturbed system (4.28) with $\varepsilon, \delta_n > 0$ sufficiently small can be constructed by combining perturbations of fast, intermediate and slow segments of singular trajectories as described above. Extending the notion of orbital connection of the folded singularities $q^{\mp}$ or lack thereof as described in the previous section, we can show that when the folded singularities $q_n^{\mp}$ are orbitally remote, then for $\varepsilon, \delta_n > 0$ sufficiently small the perturbed system features MMOs with single epochs of perturbed slow dynamics, while if $q_n^{\mp}$ are orbitally connected, the perturbed system features MMOs with double epochs epochs of perturbed slow dynamics, as shown in Figure 4.5, Figure 4.2 and Figure 4.15. The observed qualitative behaviour demonstrated in these figures is in agreement with previous works [Doi et al., 2001].

4.4.3 Onset and cessation of oscillatory dynamics

At the singular limit $\varepsilon = 0 = \delta_n$, using computer algebra software, we find that the reduced flow on $\mathcal{N}$, equation (4.68), has a stable equilibrium point on $\mathcal{S}^r$ for $\bar{I} \in (\bar{I}'_1, \bar{I}'_2)$, where

$$\bar{I}'_1 \simeq \frac{4.8}{k_v g_{Na}}, \qquad \bar{I}'_2 \simeq \frac{281}{k_v g_{Na}}, \tag{4.69}$$

cf. Figure 4.14, and a stable equilibrium point on $\mathcal{N}^{a^-}$ for $\bar{I} < \bar{I}'_1$ and on $\mathcal{N}^a$ $\bar{I} > \bar{I}'_2$, cf. Figure 4.14

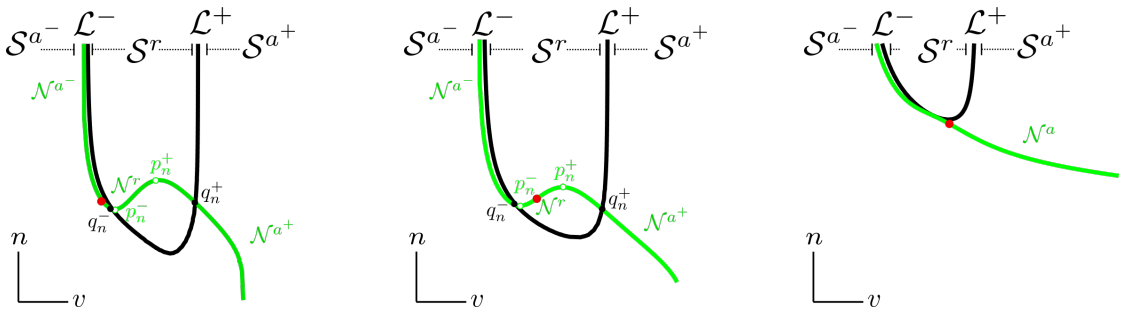

(a) $\bar{I} < \bar{I}'_1$ (b) $\bar{I} \in (\bar{I}'_o, \bar{I}'_c)$ (c) $\bar{I} > \bar{I}'_2$

Figure 4.14: A stable equilibrium of the reduced flow (4.68) lies in the attracting portion $\mathcal{S}^a$ of $\mathcal{M}_1$ for $\bar{I} < \bar{I}'_o$ and $\bar{I} > \bar{I}'_c$, panels (a) and (b), respectively, and in the repelling portion $\mathcal{S}^r$ for $\bar{I} \in (\bar{I}'_o, \bar{I}'_c)$, panel (b). For $\bar{I} \gtrsim 80/(k_v g_{Na})$, $\mathcal{M}_h$ consists of one normally hyperbolic, attracting branch $\mathcal{N}^a$.

According to Section 2.3 and similarly to the h-slow case, for $\varepsilon, \delta_n > 0$ sufficiently small, the perturbed system (4.31) undergoes singular Hopf bifurcations for $\bar{I}$-values that are $\mathcal{O}(\varepsilon, \delta_n)$-close to $\bar{I}'_1$ and $\bar{I}'_2$, and the onset and cessation of oscillatory dynamics happens

$\mathcal{O}(\varepsilon, \delta_n)$-close to the singular Hopf ones, respectively, i.e.

$$\bar{I}'_o = \bar{I}'_1 + \mathcal{O}(\varepsilon, \delta_n), \qquad \bar{I}'_c = \bar{I}'_2 + \mathcal{O}(\varepsilon, \delta_n),$$

see also [Desroches et al., 2012, Letson et al., 2017, Guckenheimer, 2008, Krupa et al., 2008, Krupa and Wechselberger, 2010] and Chapter 2. By numerical sweeping, we find that for $\gamma = 0.0083$, $\varepsilon = 0.1$, $\delta_n = 0.01$ and for parameter values as in (4.9), the onset of oscillatory dynamics of system (4.21) is at approximately $\bar{I} \simeq 6.6/(k_v g_{Na})$, while the cessation of oscillatory dynamics is at approximately $\bar{I} \simeq 268/(k_v g_{Na})$, which are $\mathcal{O}(\varepsilon, \delta_n)$-close to $\bar{I}'_1$ and $\bar{I}'_2$, respectivelly.

4.4.4 From double to single SAO-epochs

We characterise the pair of folded singularities $q_n^{\mp}$ based on whether they are "connected" by singular cycles or not, in accordance with Definition 6, which is equivalent to the following classification in terms of the n-coordinates $n_{q_n^{\mp}}$ of the folded singularities $q_n^{\mp}$.

1. The folded singularities $q_n^{\mp}$ are *orbitally connected* if $n_{q_n^-} > n_{q_n^+}$; cf. Figure 4.15 (a).
2. The folded singularities $q_n^{\mp}$ are *orbitally aligned* if $n_{q_n^-} = n_{q_n^+}$; cf. Figure 4.15 (b).
3. The folded singularities $q_n^{\mp}$ are *orbitally remote* if $n_{q_n^-} < n_{q_n^+}$; cf. Figure 4.15 (c).

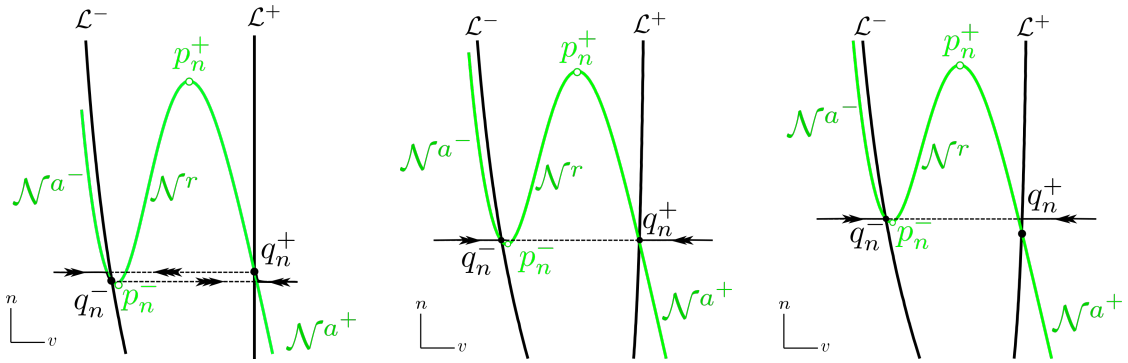

(a) $I < \bar{I}'_a$ (b) $\bar{I} = \bar{I}'_a$ (c) $\bar{I} > \bar{I}'_a$

Figure 4.15: Orbital connection or lack thereof, in accordance with Definition 6. For $\bar{I} < \bar{I}'_a$, the folded singularities $q_n^{\mp}$ are orbitally connected, in the sense that, at the limit $\varepsilon = 0 = \delta_n$, there exists a singular cycle that passes through both of them and also has slow segments on both $\mathcal{N}^{a^{\mp}}$, panel (a). For $\bar{I} > \bar{I}'_a$, the folded singularities $q_n^{\mp}$ are orbitally remote, in the sense that, at the limit $\varepsilon = 0 = \delta_n$, a singular cycles that passes through one of the folded singularities does not pass through the other, panel (c). For $\bar{I} = \bar{I}'_a$, the folded singularities $q_n^{\mp}$ are orbitally aligned, in the sense that, at the limit $\varepsilon = 0 = \delta_n$, there exists a singular cycle that passes through both of them but has no slow segments on both $\mathcal{N}^{a^{\mp}}$, panel (b).

Due to the $\bar{I}$-dependence of of the location of $q_n^{\mp}$, the classification in Definition 6 hence encodes the position of the folded singularities $q_n^{\mp}$ relative to one another in dependence

of the rescaled applied current $\bar{I}$. For a given value of $\bar{I}$, the v-coordinates of the folded singularities are obtained by solving the system

$$h_\infty(v) - \frac{\bar{I} - \bar{g}_L\left(v - \bar{E}_K\right) - \bar{g}_L(v - \bar{E}_L)}{3m'(v)m_\infty^2(v)\left(v - \bar{E}_{Na}\right)\left(v - \bar{E}_K\right) + m_\infty^3(v)\left(2v - \bar{E}_{Na} - \bar{E}_k\right)} = 0,, \tag{4.70}$$

where $h = h_\infty(v)$ corresponds to the graph of $\mathcal{M}_\mathcal{N}$ in the vh-plane, recall (4.37), and the fractional factor corresponds to the graph of $\mathcal{F}_{\mathcal{M}_1}$, recall (4.35). It follows that, in the parameter regime given by (4.9), there exists a unique value $\bar{I}_a$ such that the singularities q_n^- and q_n^+ are orbitally aligned. Using computer algebra software, this value is approximately

$$\bar{I}_a' \simeq \frac{10.1}{k_v g_{Na}}, \tag{4.71}$$

recall (4.9). Correspondingly, $q_n^\mp$ are orbitally connected for $\bar{I} < \bar{I}_a'$ and orbitally remote for $\bar{I} > \bar{I}_a'$. By numerical sweeping, we find that for $\gamma = 0.0083$, $\varepsilon = 0.1$, $\delta_n = 0.01$ and for parameter values as in (4.9), system (4.21) features MMOs with double SAO-epochs until approximately $\bar{I} \simeq 9.4/(k_v g_{Na})$, which is $\mathcal{O}(\varepsilon, \delta_n)$-close to $\bar{I}_a$.

It follows that, for $\bar{I} < \bar{I}_a' + \mathcal{O}(\varepsilon, \delta_n)$, the full system (4.17) with $\varepsilon, \delta_n > 0$ sufficiently small features MMOs with double epochs of perturbed slow dynamics, cf. Figure 4.10 & Figure 4.1 panels (a,b). Correspondingly, for $\bar{I} > \bar{I}_a + \mathcal{O}(\varepsilon, \delta_n)$, the full system (4.17) with $\varepsilon, \delta_n > 0$ sufficiently small features MMOs with at most single epochs of perturbed slow dynamics, cf. Figure 4.10 & Figure 4.1 panels (d,e,f).

In contrast to the h-slow case, we do not find an $\bar{I}$-value for which MMOs with single SAO epochs turn to relaxation oscillations. Consider system (4.60) with $\delta_n > 0$ small. Eliminating time in (4.60), away from $\mathcal{N}$ the flow on $\mathcal{S}^{a^\mp}$ can be approximated by

$$\frac{dn}{dv} = -\delta_n \frac{\partial_v \left[V(v, m_\infty(v), h, n)\right] N(v, n)}{\partial_h \left[V(v, m_\infty(v), h, n)\right] H(v, h)}\bigg|_{h=\eta(v,n)} \tag{4.72}$$

where we have omitted $\mathcal{O}(\delta_n)$-terms in the denominator; recall that $\partial_h \left[V(v, m_\infty(v), h, n)\right] < 0$, by (4.36). Denote

- $\tilde{v}_{max}$: the value obtained by solving $V\left(\tilde{v}_{max}, m_\infty\left(\tilde{v}_{max}\right), h_{q_n^+}, n_{q_n^+}\right) = 0$; that is, the projection of q_n^- onto $\mathcal{S}^{a^+}$ along the fast fibres $(4.31a)_{\varepsilon=0}$,
- $\tilde{v}_{max}^*$: the value obtained by solving $V\left(\tilde{v}_{max}^*, m_\infty\left(\tilde{v}_{max}^*\right), h_{q_n^-}, n_{q_n^-}\right) = 0$; that is, the projection of a point on $\mathcal{L}^+$ with $h = h_{q_n^-}$ and $n = n_{q_n^-}$ onto $\mathcal{S}^{a^-}$ along the fast fibres $(4.31a)_{\varepsilon=0}$,

and consider a trajectory on $\mathcal{S}^{a^-}$ with initial condition (v_{max}^*, n_{max}^*), where $n_{max}^* \in (n_{q_n^-}, n_{q_n^+})$ is close to $n_{q_n^-}$. This trajectory reaches a point on $\mathcal{L}^-$ at an n-coordinate approximately given by

$$n = n_{max}^* + \delta_n \mathcal{G}_n^-(n_{q_n^-}, \bar{I}) + \mathcal{O}(\delta_n^2),$$

where we denote

$$\mathcal{G}_n^-(n, \bar{I}) := -\int_{\tilde{v}_{max}^*}^{\tilde{v}_{q_n^-}} \frac{\partial_v \left[V\left(v, m_\infty(v), h, n\right)\right] N\left(v, n\right)}{\partial_h \left[V\left(v, m_\infty(v), h, n\right)\right] H(v, h)}\bigg|_{h=\eta(v,n)} \mathrm{d}v.$$

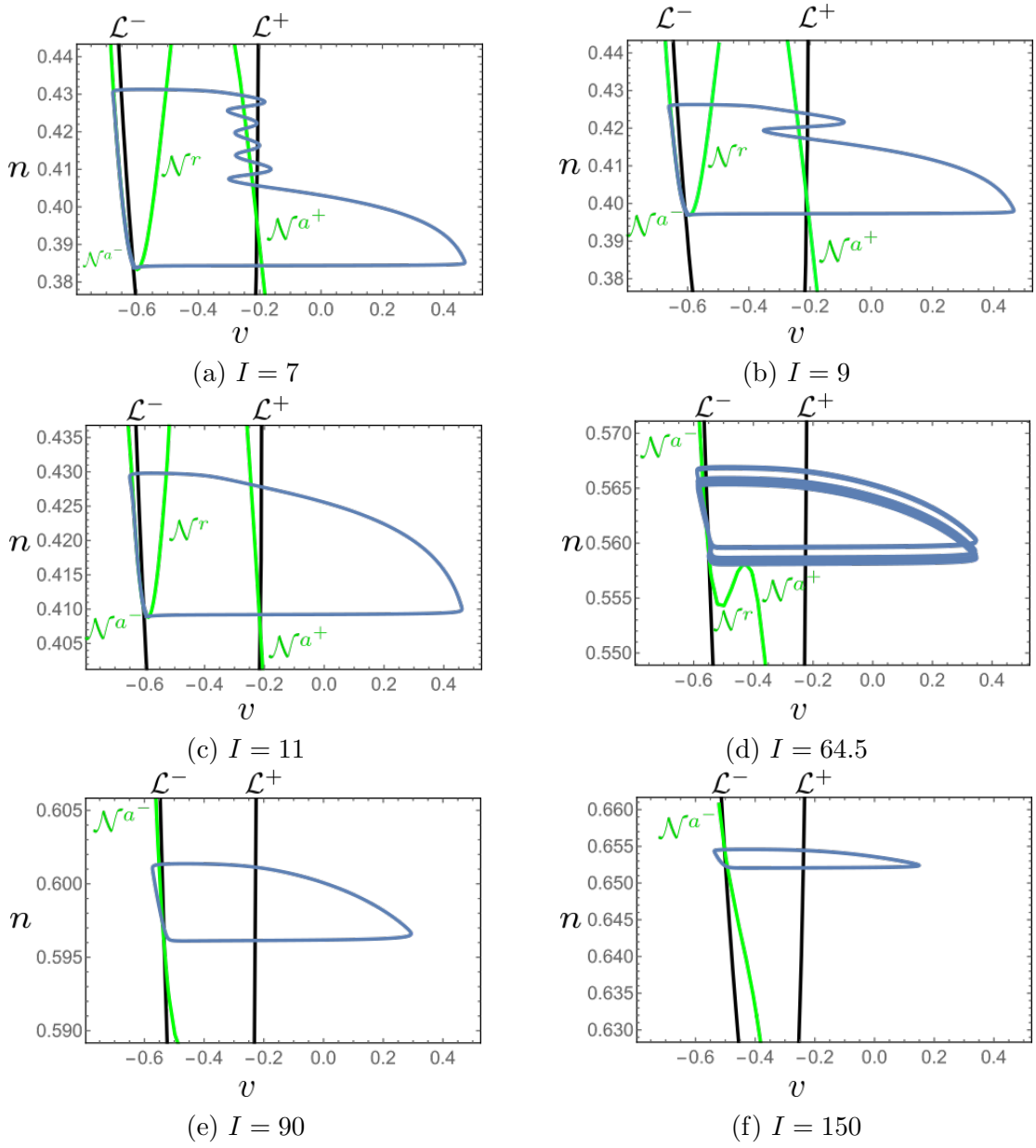

(a) $I = 7$ (b) $I = 9$

(c) $I = 11$ (d) $I = 64.5$

(e) $I = 90$ (f) $I = 150$

Figure 4.16: Singular geometry of Equation (4.60) which underlies the qualitative properties of the time series, and the associated MMO trajectories, illustrated in Figure 4.2: as $\bar{I}$ is varied, the folded singularities become orbitally remote from orbitally connected. Therefore, system (4.17) with $\varepsilon, \delta_n > 0$ small transits from MMOs with double SAO epochs for $\bar{I} < \bar{I}'_a$ (panels (a) and (b)) to MMOs with single SAO epochs for $\bar{I} > \bar{I}'_a$ (panels (d) and (e)).

When this trajectory reaches the vicinity of $\mathcal{L}^-$, it connects to a fast segment that reaches $\mathcal{S}^{a^+}$ at a point (v_{max}, h_{max}). A trajectory with (v_{max}, h_{max}) as initial conditions on $\mathcal{S}^{a^+}$ follows the flow (4.43) thereon and reaches $\mathcal{L}^+$ at an h-coordinate approximately given by

$$n = n_{max} + \delta_n \mathcal{G}_n^+(n_{q_n^-}, \bar{I}) + \mathcal{O}(\delta_n^2),$$

where we denote

$$\mathcal{G}_n^+(n, \bar{I}) := -\int_{\tilde{v}_{max}}^{\tilde{v}_{q_n^+}} \frac{\partial_v \left[V\left(v, m_\infty(v), h, n\right)\right] N\left(v, n\right)}{\partial_h \left[V\left(v, m_\infty(v), h, n\right)\right] H(v, h)}\bigg|_{h=\eta(v,n)} \mathrm{d}v.$$

Therefore, a trajectory that leaves the vicinity of $\mathcal{L}^-$ at a point with n-coordinate close to $n_{q_n^-}$ returns to this vicinity after a large excursions to and from $\mathcal{S}^{a^+}$ at a point with $\hat{n}$, where

$$\hat{n} = n + \delta_n \left(\mathcal{G}_n^-(n_{q_n^-}, \bar{I}) + \mathcal{G}_n^+(n_{q_n^-}, \bar{I})\right) + \mathcal{O}(\delta_n^2) \tag{4.73}$$

Numerical computations show that

$$\mathcal{G}_n^-(n_{q_n^-}, \bar{I}) + \mathcal{G}_n^+(n_{q_n^-}, \bar{I}) > 0$$

for $\bar{I} \in (\bar{I}_1', \bar{I}_2')$; therefore, trajectories are attracted to $\mathcal{N}^{a^+}$ for $\bar{I}$ in this interval and the system features MMOs with single epochs of slow dynamics.

We remark that, for the I-values considered in [Doi et al., 2001], the equilibrium of the system as depicted in Figure 4.16 lies on $\mathcal{N}^r$, and this is why in [Doi et al., 2001] the n-slow is considered to be topologically different than the h-slow one, and it is postulated that chaotic dynamics can be realised only in the latter. Here we show that by considering large enough $\bar{I}$-values, the equilibrium point lies on $\mathcal{N}^a$, and motivated also by the timeseries in Figure 4.2 panel (b), we remark that it would be worth investigating whether chaotic dynamics can be realised in the corresponding $\bar{I}$ regime. The search of such behaviour and the potential study of the corresponding generating mechanisms is included in plans for future work.

4.5 Local dynamics and SAOs

The local, SAO-generating mechanisms are similar to the ones descrived in Section 2.4 for the extended prototypical example (2.2), and we discuss them here in brief.

Consider the fast formulation (4.31), which we reiterate here for convenience:

$$\begin{aligned}
v' &= \frac{m_\infty(v) - \mu(v,h,n)}{t_m(v)\partial_v\mu(v,h,n)} - \varepsilon\delta_h H(v,h)\frac{\partial_h\mu(v,h,n)}{\partial_v\mu(v,h,n)} - \varepsilon\delta_n N(v,n)\frac{\partial_n\mu(v,h,n)}{\partial_v\mu(v,h,n)}, && \text{(4.74a)}\\
&=: U(v,h,n;\varepsilon,\delta_h,\delta_n) \\
h' &= \varepsilon\delta_h H(v,h), && \text{(4.74b)}\\
n' &= \varepsilon\delta_n N(v,n), && \text{(4.74c)}
\end{aligned}$$

and consider the h-slow case, i.e. $\varepsilon, \delta_h > 0$ sufficiently small and $\delta_n = \mathcal{O}(1)$. At the singular limit $\delta_h = 0$ with $\varepsilon > 0$ and $\delta_n = 1$, we obtain the system

$$v' = \frac{m_\infty(v) - \mu(v,h,n)}{t_m(v)\partial_v\mu(v,h,n)} - \varepsilon N(v,n)\frac{\partial_n\mu(v,h,n)}{\partial_v\mu(v,h,n)} = U(v,h,n;\varepsilon,0,1), \tag{4.75a}$$

$$h' = 0 \tag{4.75b}$$

$$n' = \varepsilon N(v,n), \tag{4.75c}$$

whose equilibria are given by $\mathcal{M}_h$. Linearisation of (4.75) about $\mathcal{M}_h$ gives the Jacobian matrix

$$\mathbf{A}_h = \begin{pmatrix} \partial_v U(v,h,n;\varepsilon,0,1) & \partial_n U(v,h,n;\varepsilon,0,1) \\ \varepsilon\partial_v N(v,n) & \varepsilon\partial_n N(v,n) \end{pmatrix}\Bigg|_{\mathcal{M}_h} \tag{4.76}$$

Eigenvalues of $\mathbf{A}_h$ give the regimes where $\mathcal{M}_h$ is attracting/repelling in spiralling or nodal manners under the two-dimensional flow (4.75), recall Section 2.4. In particular, there exists a point on $\mathcal{M}_h$ that system (4.75) undergoes a Hopf bifurcation; whether this Hopf bifurcation is subcritical or supercritical depends on the value of I.

In the fully perturbed system (4.74) with $\varepsilon, \delta_h > 0$ sufficiently small, entrance of trajectories to the spirally-attracting regime implies SAOs of bifurcation delay type, while entrance to the nodally-attracting regime implies absence of SAOs or existence of only a few thereof that occur close to the jump point, cf. respectively the SAOs below and above in Figure 4.1 panels (a) and (b). In both cases, trajectories jump away from $\mathcal{M}_h$ not directly after entering the repelling region but, rather, after the accumulated contraction has been balanced by expansion, and this is calculated via a way-in/way-out function, see [Krupa and Wechselberger, 2010, Letson et al., 2017] and Section 2.4 for details, cf. Figure 4.1 and Figure 4.10. This mechanism is a residual of the 2-fast/1-slow nature of system (4.74). Moreover, a degenerate node where the stability of $\mathcal{M}_h$ turns from spiral to nodal lies $\mathcal{O}(\sqrt{\varepsilon})$-close to the Hopf bifurcation point of(4.75) on $\mathcal{M}_h$.

Finally, the small periodic orbits that emerge at the Hopf bifurcation of (4.75), cease to exist at a transverse intersection between $\mathcal{S}^a_{\varepsilon,\delta_h}$ and $\mathcal{S}^r_{\varepsilon,\delta_h}$ that occurs $\mathcal{O}(\varepsilon)$-close to the Hopf bifurcation-point. These periodic trajectories of the partially perturbed system (4.75) with $\varepsilon, \delta_h > 0$ sufficiently small are associated with *secondary canards* [Wechselberger, 2005] and *sector of rotations* [Krupa et al., 2008]; therefore, if trajectories of the perturbed system are attracted to this vicinity, the system features *canard-induced SAOs*, see [Krupa et al., 2008, De Maesschalck et al., 2016, Desroches et al., 2012] for details. This is a residual of the 1-fast/2-slow nature of the system.

A detailed quantitative analysis of the above is beyond the scope of this work. However, we emphasize that, although the reduction (4.19) proposed by Rubin and Wechselberger in [Rubin and Wechselberger, 2007] and (4.74) have the same critical manifolds $\mathcal{M}_1$ and $\mathcal{M}_h$, there are quantitative difference in terms of the points where the attractivity of $\mathcal{M}_h$ changes, and this is reflected by the fact that the first row in $\mathbf{A}_h$ in (4.77) depends on ε, while it would be independent of ε if one considered the RW-reduction (4.19) instead.

The analysis of the n-slow case is analogous, with a corresponding Jacobian matrix

$$\mathbf{A}_n = \begin{pmatrix} \partial_v U(v,h,n;\varepsilon,1,0) & \partial_h U(v,h,n;\varepsilon,1,0) \\ \varepsilon\partial_v H(v,h) & \varepsilon\partial_h H(v,h) \end{pmatrix}\Bigg|_{\mathcal{M}_n} \tag{4.77}$$

about $\mathcal{M}_n$, and where the function $U(v, h, n; \varepsilon, 1, 0)$ contains $\varepsilon H(v, h)$-terms, instead of $\varepsilon N(v, n)$-ones.

4.6 Summary

In this Chapter, we proposed a novel and global three-dimensional reduction of the four-timescale Hodgkin-Huxley equations (4.2) [Hodgkin and Huxley, 1952, Doi et al., 2001], that is based on a scaled system (4.7) that was proposed in [Rubin and Wechselberger, 2007]; cf. Theorem 7. Here we considered a reduction to a globally normally hyperbolic and attracting slow manifold, instead of a local centre manifold reduction in [Rubin and Wechselberger, 2007, Rubin and Wechselberger, 2008], and we showed that the two reductions feature the same critical manifold $\mathcal{M}_1$. We then showed that, depending on the values of the parameters of the system relative to one-another, our reduction is itself a three-timescale system. We emphasise that this three-timescale structure is also apparent in the RW reduction (4.19) by taking either $\delta_h > 0$ sufficiently small and $\delta_n = \mathcal{O}(1)$, or $\delta_n > 0$ sufficiently small and $\delta_h = \mathcal{O}(1)$, however these cases were not considered in [Rubin and Wechselberger, 2007, Rubin and Wechselberger, 2008].

The timescale separation of the reduced system Equation (4.28) allows for further iterative dimension reduction to invariant manifolds, by studying a series of layer problems and reduced flows. By decomposing the dynamics to segments that evolve on different timescales, we are able to explain qualitative properties of trajectories such as MMOs and transitions between MMOs with different qualitative properties, in accordance with the geometric mechanisms proposed in Chapter 2; we were thus able to classify such behaviours and transitions for the original system (4.21).

In particular, for the cases where h or n is taken to be the slowest variable in the four-dimensional model (4.21), we were able to explain in the framework of multi-timescale GSPT the different qualitative behaviours which are correspondingly illustrated in Figure 4.1 and Figure 4.2, as well as the transitions between them, cf. Figure 4.10 and Figure 4.16, respectively; we reiterate that these behaviours had been previously documented in [Doi et al., 2001]. The local, SAO-generating mechanisms can also be analysed in an approach similar the one introduced in Chapter 2, cf. Section 4.5 and Section 2.4.

Finally, in [Doi et al., 2001] it was numerically demonstrated that system (4.2) features chaotic dynamics in the h-slow case, but the chaos-generating mechanisms were not explained. Moreover, no chaotic trajectories were found for the n-slow case, and it was postulated that this difference is due to the fact that the equilibrium point in the h-slow case lies on $\mathcal{H}^{a^-}$, while in the n-slow case it lies on $\mathcal{N}^r$, cf. Figure 4.8 and Figure 4.14, respectively. Here, we showed that by considering larger values of $\bar{I}$, the equilibrium point in the n-slow case does in fact lie on $\mathcal{N}^r$, cf Figure 4.14 panel (c). Moreover, motivated by the timeseries in Figure 4.2 panel (c), we remark that it would be worth investigating whether chaotic dynamics is possible in this case also, since our analysis shows that, ultimately, these two cases are not topologically different, as claimed in [Doi et al., 2001]. A more systematic analysis of the mechanisms that are responsible for this chaotic behaviour and its potential relation to Shilnikov homoclinic phenomena or to period-doubling bifurcations of small periodic orbits in the three-timescale GSPT framework for both the h-slow and the n-slow cases is part

plans for future work.

4.7 Reduced flow on $\mathcal{M}_1$ in the non-standard form of GSPT

In Section 4.3, we consider the reduced flow (4.40) on $\mathcal{M}_1$ with h being the slow variable, i.e. $\delta_h > 0$ sufficiently small and $\delta_n = \mathcal{O}(1)$. Correspondingly, in Section 4.4 we consider the reduced flow (4.41) on $\mathcal{M}_1$ with n being the slow variable, i.e. $\delta_n > 0$ sufficiently small and $\delta_h = \mathcal{O}(1)$. Both cases corresponded to two dimensional slow-fast systems in the standard form of GSPT.

Equations (4.40) and (4.41) are obtained by eliminating the n- and h- variable in the singular limit of $(4.28)_{\varepsilon=0}$, respectively, and in both Section 4.3 and Section 4.4 this corresponds to eliminating the intermediate variable. Here we outline an alternative approach, namely considering $\delta_n > 0$ sufficiently small and $\delta_h = \mathcal{O}(1)$ in (4.40) and $\delta_h > 0$ sufficiently small and $\delta_n = \mathcal{O}(1)$ in (4.67), which corresponds to eliminating the slow variable when studying the reduced flow on $\mathcal{M}_1$, and which gives two dimensional slow-fast systems in the non-standard form of GSPT [Wechselberger, 2020].

4.7.1 The h-slow case

At the singular limit $\varepsilon = 0$, for $\delta_h > 0$ sufficiently small and $\delta_n = 1$, the reduced flow Equation (4.41) yields

$$v' = \delta_h \partial_h \left[V(v, m_\infty(v), h, n)\right] H(v,h)|_{h=\eta(v,n)} + \partial_n \left[V(v, m_\infty(v), h, n)\right] N(v,n)|_{h=\eta(v,n)} \tag{4.78a}$$

$$n' = -\partial_v \left[V(v, m_\infty(v), h, n)\right] N(v,h)|_{h=\eta(v,n)}, \tag{4.78b}$$

while in the slow formulation $\tau_n = \delta_n t$ we can write

$$\delta_h \dot{v} = \delta_h \partial_h \left[V(v, m_\infty(v), h, n)\right] H(v,h)|_{h=\eta(v,n)} + \partial_n \left[V(v, m_\infty(v), h, n)\right] N(v,n)|_{h=\eta(v,n)} \tag{4.79a}$$

$$\delta_h \dot{h} = -\partial_v \left[V(v, m_\infty(v), h, n)\right] N(v,h)|_{h=\eta(v,n)}. \tag{4.79b}$$

System (4.78) is a slow-fast system in the non-standard form

$$\begin{pmatrix} \dot{v} \\ \dot{n} \end{pmatrix} = B(v,n)N(v,n) + \delta_h P(v,n), \tag{4.80}$$

see [Wechselberger, 2020] and recall Section 1.2, where

$$B(v,n) = \begin{pmatrix} \partial_n \left[V(v, m_\infty(v), h, n)\right] \\ -\partial_v \left[V(v, m_\infty(v), h, n)\right] \end{pmatrix}, \quad P(v,h) = \begin{pmatrix} \partial_h \left[V(v, m_\infty(v), h, n)\right] \\ 0 \end{pmatrix}$$

Setting $\delta_n = 0$ in the intermediate formulation Equation (4.78) gives the two-dimensional layer problem

$$v' = \partial_n \left[V(v, m_\infty(v), h, n)\right] N(v,h)|_{h=\eta(v,n)} \tag{4.81a}$$

$$n' = -\partial_v \left[V(v, m_\infty(v), h, n)\right] N(v,h)|_{h=\eta(v,n)}. \tag{4.81b}$$

Equilibria of (4.81a) define the supercritical manifold $\mathcal{M}_h$ as the subset of $\mathcal{M}_1$ where

$$n_\infty(v) - n = 0 \tag{4.82}$$

recall (4.14).

The Jacobian matrix $\mathbf{J}|_{\mathcal{M}_h}$ of the linearisation of the layer problem (4.81) evaluated along $(v, n) \in \mathcal{M}_h$ is

$$\mathbf{J}|_{\mathcal{M}_n} = \begin{pmatrix} \partial_n \left[V(v, m_\infty(v), h, n)\right] \left(\partial_v N(v, h)\right) & \partial_n \left[V(v, m_\infty(v), h, n)\right] \left(\partial_h N(v, h)\right) \\ -\partial_v \left[V(v, m_\infty(v), h, n)\right] \left(\partial_v N(v, h)\right) & -\partial_v \left[V(v, m_\infty(v), h, n)\right] \left(\partial_n N(v, h)\right) \end{pmatrix}$$

and has one trivial eigenvalue $\lambda_0 = 0$ and one nontrivial eigenvalue given by

$$\lambda_h(v) = \text{tr}\left(\mathbf{J}|_{\mathcal{M}_h}\right)$$

see [Wechselberger, 2020] for details.

The manifold $\mathcal{M}_h$ is normally hyperbolic on the set $\mathcal{H}$ where

$$\lambda_h(v) \neq 0. \tag{4.83}$$

Calculations show that the set $\mathcal{F}_{\mathcal{M}_h} = \mathcal{M}_h \backslash \mathcal{H}$ where normal hyperbolicity is lost consists of two points, $\mathcal{F}_{\mathcal{M}_h} = \left\{p_h^-, p_h^+\right\}$. These two points separate the normally hyperbolic part $\mathcal{H}$ into a repelling branch $\mathcal{H}^r$, where $\lambda(v) > 0$, and to two attracting branches $\mathcal{H}^{a^\mp}$, where $\lambda(v) < 0$, see Figure 4.17. We remark that the fold points $p_h^\mp$, lie on $\mathcal{S}^r$ see Figure 4.17.

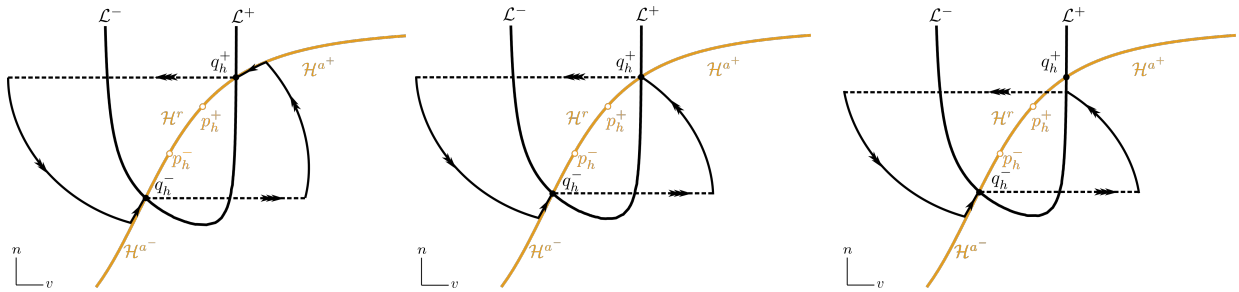

(a) $\bar{I} < \bar{I}_a$ (b) $\bar{I} = \bar{I}_a$ (c) $\bar{I} > \bar{I}_a$

Figure 4.17: Singular geometry featuring singular cycles. For $\bar{I} < \bar{I}_a$ the folded singularities $q_h^\mp$ are orbitally connected, for $\bar{I} = \bar{I}_a \simeq \frac{26.5}{k_v g_{Na}}$ they are orbitally aligned and for $\bar{I} > \bar{I}_a$ they are orbitally remote, c.f. Definition 6.

Non-stationary solutions of the layer problem (4.89) are not characterized by $n = const$ like in the standard form case, cf.Figure 4.9 and Figure 4.17. By eliminating time in (4.78) and since $N(v, h) \neq 0$ away from $\mathcal{M}_h$, we can write

$$\frac{\mathrm{d}v}{\mathrm{d}n} = \frac{\partial_n \left[V(v, m_\infty(v), h, n)\right]}{\partial_v \left[V(v, m_\infty(v), h, n)\right]}$$

on $\mathcal{S} \backslash \mathcal{M}_h$.

Setting $\delta_h = 0 = \varepsilon$ in the slow formulation (4.61) gives the reduced problem

$$0 = \partial_n \left[V(v, m_\infty(v), h, n)\right] N(v,h)|_{h=\eta(v,h)} \tag{4.84a}$$
$$0 = -\partial_v \left[V(v, m_\infty(v), h, n)\right] N(v,h)|_{h=\eta(v,h)}. \tag{4.84b}$$

The slow flow on $\mathcal{M}_h$ is given by

$$\begin{pmatrix} \dot{v} \\ \dot{n} \end{pmatrix} = \left[\frac{\det(B|P)}{\langle \nabla H, B \rangle} \begin{pmatrix} -\partial_n N \\ \partial_v N \end{pmatrix} \right] \Bigg|_{\mathcal{M}_h}, \tag{4.85}$$

see [Jelbart and Wechselberger, 2020], and the reduced flow on $\mathcal{H}^{a^\mp}$ is directed towards $q_h^\mp$, respectively. The resulting singular geometry is summarised in Figure 4.17.

Notice that, by (4.82), the geometry of $\mathcal{H}$ is independent of the parameter $\bar{I}$, and the orbital connection or lack thereof of $q_h^\mp$ is encoded in the layer problem (4.81).

4.7.2 The n-slow case

At the singular limit $\varepsilon = 0$, for $\delta_n > 0$ sufficiently small and $\delta_h = 1$, the reduced flow Equation (4.40) yields

$$v' = \partial_h \left[V(v, m_\infty(v), h, n)\right] H(v,h)|_{n=\nu(v,h)} + \delta_n \partial_n \left[V(v, m_\infty(v), h, n)\right] N(v,n)|_{n=\nu(v,h)} \tag{4.86a}$$
$$h' = -\partial_v \left[V(v, m_\infty(v), h, n)\right] H(v,h)|_{n=\nu(v,h)}, \tag{4.86b}$$

while in the slow formulation $\tau_n = \delta_n t$ we can write

$$\delta_n \dot{v} = \partial_h \left[V(v, m_\infty(v), h, n)\right] H(v,h)|_{n=\nu(v,h)} + \delta_n \partial_n \left[V(v, m_\infty(v), h, n)\right] N(v,n)|_{n=\nu(v,h)} \tag{4.87a}$$
$$\delta_n \dot{h} = -\partial_v \left[V(v, m_\infty(v), h, n)\right] H(v,h)|_{n=\nu(v,h)}. \tag{4.87b}$$

System (4.86) is a slow-fast system in the non-standard form [Wechselberger, 2020]

$$\begin{pmatrix} \dot{v} \\ \dot{h} \end{pmatrix} = B(v,h)H(v,h) + \delta_n P(v,h), \tag{4.88}$$

where

$$B(v,h) = \begin{pmatrix} \partial_h \left[V(v, m_\infty(v), h, n)\right] \\ -\partial_v \left[V(v, m_\infty(v), h, n)\right] \end{pmatrix}, \quad P(v,h) = \begin{pmatrix} \partial_n \left[V(v, m_\infty(v), h, n)\right] \\ 0 \end{pmatrix}$$

Setting $\delta_h = 0$ in the intermediate formulation Equation (4.86) gives the two-dimensional layer problem

$$v' = \partial_h \left[V(v, m_\infty(v), h, n)\right] H(v,h)|_{n=\nu(v,h)} \tag{4.89a}$$
$$h' = -\partial_v \left[V(v, m_\infty(v), h, n)\right] H(v,h)|_{n=\nu(v,h)}. \tag{4.89b}$$

Equilibria of (4.89a) define the supercritical manifold $\mathcal{M}_n$ as the subset of $\mathcal{M}_1$ where

$$h_\infty(v) - h = 0 \tag{4.90}$$

recall (4.14).

The Jacobian matrix $\mathbf{J}|_{\mathcal{M}_n}$ of the linearisation of the layer problem (4.89) evaluated along $(v,h) \in \mathcal{M}_n$ is

$$\mathbf{J}|_{\mathcal{M}_n} = \begin{pmatrix} \partial_h \left[V(v, m_\infty(v), h, n)\right] (\partial_v H(v,h)) & \partial_h \left[V(v, m_\infty(v), h, n)\right] (\partial_h H(v,h)) \\ -\partial_v \left[V(v, m_\infty(v), h, n)\right] (\partial_v H(v,h)) & -\partial_v \left[V(v, m_\infty(v), h, n)\right] (\partial_h H(v,h)) \end{pmatrix}$$

and has one trivial eigenvalue $\lambda_0 = 0$ and one nontrivial eigenvalue given by

$$\lambda_n(v) = \mathrm{tr}\left(\mathbf{J}|_{\mathcal{M}_n}\right)$$

see [Wechselberger, 2020] for details.

The manifold $\mathcal{M}_n$ is normally hyperbolic on the set $\mathcal{N}$ where

$$\lambda_n(v) \neq 0. \tag{4.91}$$

Calculations show that the set $\mathcal{F}_{\mathcal{M}_n} = \mathcal{M}_n \backslash \mathcal{N}$ where normal hyperbolicity is lost consists of two points, $\mathcal{F}_{\mathcal{M}_n} = \{p_n^-, p_n^+\}$. These two points separate the normally hyperbolic part $\mathcal{N}$ into a repelling branch $\mathcal{N}^r$, where $\lambda(v) > 0$, and to two attracting branches $\mathcal{N}^{a^\mp}$, where $\lambda(v) < 0$, see Figure 4.15. We remark that the fold points $p_n^\mp$, lie on $\mathcal{S}^r$ see Figure 4.15.

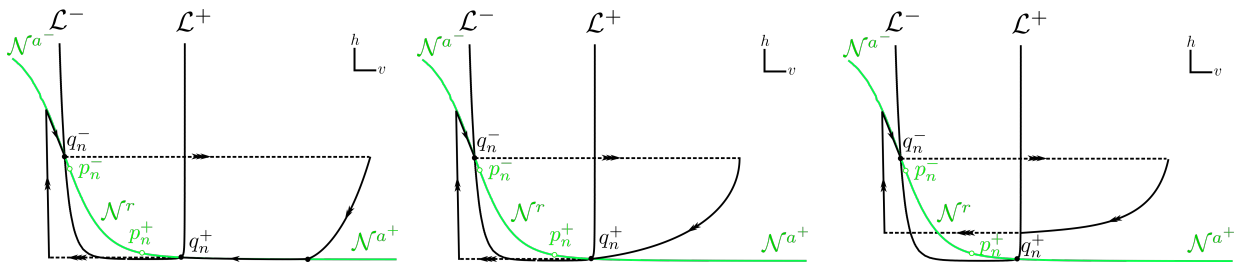

(a) $\bar{I} < \bar{I}'_a$ (b) $\bar{I} = \bar{I}'_a$ (c) $\bar{I} > \bar{I}'_a$

Figure 4.18: Singular geometry featuring singular cycles. For $\bar{I}' < \bar{I}'_a$ the folded singularities $q_n^\mp$ are orbitally connected, for $\bar{I}' = \bar{I}'_a \simeq \frac{10.1}{k_v g_{Na}}$ they are orbitally aligned and for $\bar{I} > \bar{I}'_a$ they are orbitally remote, c.f. Definition 6.

Non-stationary solutions of the layer problem (4.89) are not characterized by $h = const$ like in the standard form case, cf.Figure 4.15 and Figure 4.18. By eliminating time in (4.86) and since $H(v,h) \neq 0$ away from $\mathcal{M}_n$, we can write

$$\frac{\mathrm{d}v}{\mathrm{d}h} = \frac{\partial_n \left[V(v, m_\infty(v), h, n)\right]}{\partial_v \left[V(v, m_\infty(v), h, n)\right]}.$$

on $\mathcal{S} \backslash \mathcal{M}_n$.

Setting $\delta_h = 0 = \varepsilon$ in the slow formulation (4.61) gives the reduced problem

$$0 = \partial_h \left[V(v, m_\infty(v), h, n)\right] H(v,h)|_{n=\nu(v,h)} \tag{4.92a}$$
$$0 = -\partial_v \left[V(v, m_\infty(v), h, n)\right] H(v,h)|_{n=\nu(v,h)}. \tag{4.92b}$$

The slow flow on $\mathcal{M}_n$ is given by

$$\begin{pmatrix} \dot{v} \\ \dot{h} \end{pmatrix} = \left[\frac{\det(B|P)}{\langle \nabla H, B \rangle} \begin{pmatrix} -\partial_h H \\ \partial_v H \end{pmatrix} \right] \Big|_{\mathcal{M}_n}, \tag{4.93}$$

see [Jelbart and Wechselberger, 2020], and the reduced flow on $\mathcal{N}^{a^\mp}$ is directed towards $q_n^\mp$, respectively. The resulting singular geometry is summarised in Figure 4.15.

Notice that, by (4.90), the geometry of $\mathcal{N}$ is independent of the parameter $\bar{I}$, and the orbital connection or lack thereof of $q_n^\mp$ is encoded in the layer problem (4.89).

Chapter 5

The El-Niño Southern Oscillation model from climate science

5.1 Introduction

The El-Niño Southern Oscillation (ENSO) phenomenon is associated with the variation in winds and sea surface temperatures over the Pacific Ocean. It is composed of the El-Niño and La-Niña phases, when, respectively, warm or cold water develops in the central and east-central equatorial Pacific Ocean. Although highly irregular, these patters are oscillatory in nature.

Here we consider the dimensionless system

$$x' = x\left(x + y + c(1 - \tanh\left(x + z\right))\right) + \rho\delta(x^2 - ax), \tag{5.1a}$$

$$y' = -\rho\delta(ay + x^2), \tag{5.1b}$$

$$z' = \delta(k - z - \frac{x}{2}), \tag{5.1c}$$

with $x \leq 0$, $y \in \mathbb{R}$, $z \geq 0$, $c > 1$, $k \in (0, 1)$, $a > 0$, which captures the dynamics of the ENSO phenomenon [Roberts et al., 2016]. The variable x corresponds to the temperature difference between the eastern and western Pacific surface water, y corresponds to the departure of the western Pacific surface ocean temperature from a climatological mean state, i.e. the temperature that the tropical Pacific would attain in the absence of ocean dynamics, and z represents the western Pacific thermocline depth anomaly. The parameters c, k, a are scaled. The parameter c is proportional to the maximum temperature difference between the eastern and western Pacific surface water, the parameter k is related to the discharging (recharging) process for El Niño (La Niña) events, and corresponds to the ratio of some reference depths over the sharpness of the thermocline, and, finally, the parameter a is the constant of Newton's law of cooling applied to the difference of the western Pacific surface ocean temperature from the climatological mean state, see [Roberts et al., 2016, Section 2a.] for more details.

In [Roberts et al., 2016], system (5.1) was studied in the two timescale context, that is, for $\delta > 0$ sufficiently small and $\rho = \mathcal{O}(1)$. Here we study system (5.1) in the three-timescale context, that is, for $\delta, \rho > 0$ sufficiently small. We apply Geometric Singular Perturbation Theory (GSPT) to analyse the behaviour of system (5.1) in dependence of variation of the

parameters $c, k, a > 0$. Our focus is again on the various types of mixed-mode oscillations (MMOs) that the system exhibits, and on explaining the transitions between qualitative different scenarios.

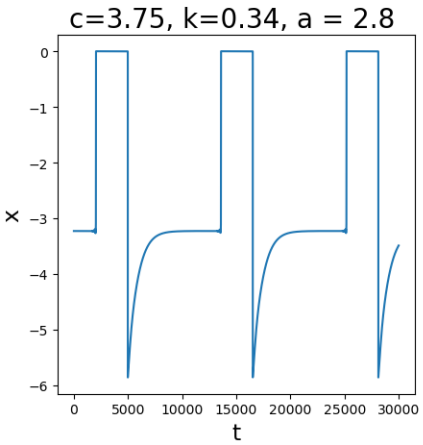

(a) MMO with plateau

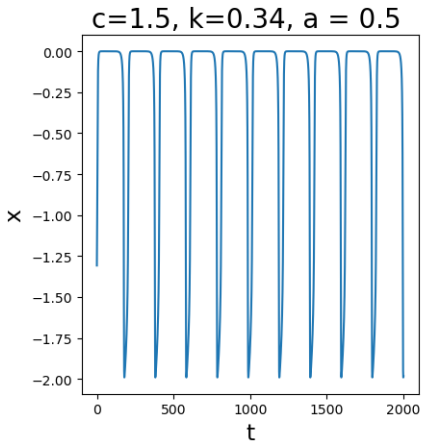

(b) Relaxation oscillation with plateau

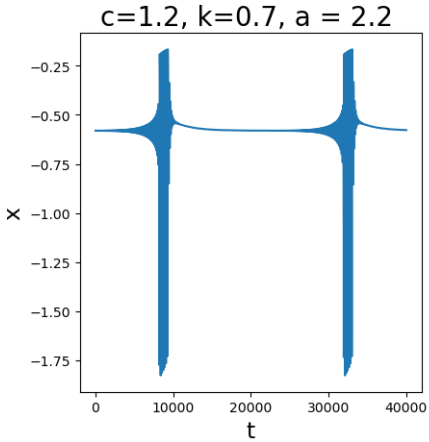

(c) MMO with SAOs above

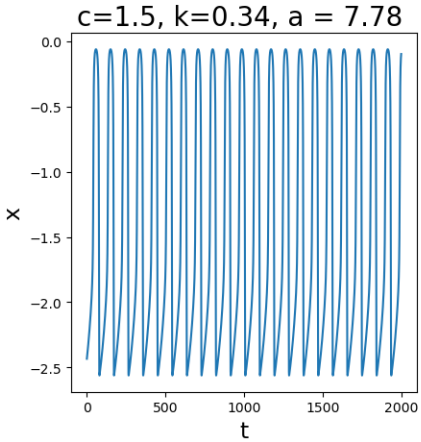

(d) Plateau-less relaxation oscillation

Figure 5.1: Outline of some possible MMO trajectories of Equation (5.1)

.

Our approach in this Chapter goes in the opposite direction than in Chapter 4. That is, in Chapter 4, our aim was to explain the various documented qualitative behaviours from previous works, using the theory developed in Chapter 2. On the other hand, in this Chapter our aim is to gain insight about the possible qualitative behaviours of trajectories of system (5.1) based on its singular geometry in the three-timescale framework, and to uncover new scenarios that had not been previously documented. To this end, we identify the roles of the parameters $c, k, a > 0$ in the behaviour of system (5.1) in the aforementioned three-timescale setting, $\delta, \rho > 0$ sufficiently small. We expose the following hierarchy: first, we show that the parameter c is associated with the geometric properties of two-dimensional invariant manifolds. Following an approach similar to Chapter 2, Chapter 4, we show that the dynamics on these manifolds are described by two dimensional slow-fast systems whether in the stan-

dard or in the non-standard form [Wechselberger, 2020]. For fixed $c > 1$, the parameter k is associated with the geometric properties of one-dimensional immersed invariant submanifolds. The parameter a is not associated with the properties of the geometry of invariant (sub)manifolds, but it is associated with dynamical phenomena such as Hopf bifurcations and the reduced flow on these (sub)manifolds.

Some examples of MMOs of system (5.1) are outlined in Figure 5.1. We emphasize that, from the trajectories illustrated in this figure, only the ones with a plateau above were documented in [Roberts et al., 2016] in the two-timescale context (we present a wider variety of qualitatively different examples in Section 5.3 for the three-timescale case). The distinction between oscillatory trajectories with different qualitative properties is based on extending the notion of relative position of folded singularities of Chapter 2 to the notion of relative position of sets where normal hyperbolicity is lost in general. This distinction is also potentially relevant in the two-timescale context. For the MMOs that do feature a plateau above, we address the bifurcation delay phenomena, which are relevant also in the two-timescale context but which were left as open question in [Roberts et al., 2016] and also in a system with similar geometry [Duncan et al., 2019].

The Chapter is organised as follows. In Section 5.2 we study the singular limit(s) of system (5.1) and we investigate different geometric scenarios in dependence its parameters. In Section 5.3 we relate the various singular geometries to the qualitative behaviours of the perturbed system, Equation (5.1) with $\delta, \rho > 0$ sufficiently small. We summarise our findings in Section 5.4. As an appendix, we include a blow-up analysis of the self-intersection of the critical manifold of (5.1) in Section 5.5.

5.2 Singular limit

5.2.1 The slow manifold $\mathcal{M}_1 = \mathcal{M}_\mathcal{P} \cup \mathcal{M}_\mathcal{S}$

Consider $\delta > 0$ small. System (5.1) is then written in the fast formulation, and the overdot denotes differentiation with respect to the fast time t. In the intermediate formulation, i.e. by a rescaling of time $\tau = \delta t$, system (5.1) is written as

$$\delta \dot{x} = x\left(x + y + c(1 - \tanh(x + z))\right) + \rho\delta(x^2 - ax) \tag{5.2a}$$
$$\dot{y} = -\rho(ay + x^2) \tag{5.2b}$$
$$\dot{z} = k - z - \frac{x}{2} \tag{5.2c}$$

At the singular limit $\delta = 0$, the layer problem is defined from Equation (5.1) as

$$x' = x\left(x + y + c - c\tanh(x + z)\right) =: F(x, y, z) \tag{5.3a}$$
$$y' = 0 \tag{5.3b}$$
$$z' = 0 \tag{5.3c}$$

and the reduced problem is defined by setting $\delta = 0$ in Equation (5.2)

$$0 = x\left(x + y + c(1 - \tanh\left(x + z\right))\right) \tag{5.4a}$$
$$\dot{y} = -\rho(ay + x^2) \tag{5.4b}$$
$$\dot{z} = k - z - \frac{x}{2} \tag{5.4c}$$

Equilibrium solutions of the one-dimensional problem Equation (5.3) define the critical manifold $\mathcal{M}_1 = \mathcal{M}_\mathcal{P} \cup \mathcal{M}_\mathcal{S}$, where

$$\mathcal{M}_\mathcal{P} = \left\{(x, y, z) \in \mathbb{R}^3 \mid x = 0\right\} \tag{5.5}$$
$$\mathcal{M}_\mathcal{S} = \left\{(x, y, z) \in \mathbb{R}^3 \mid x + y + c(1 - \tanh\left(x + z\right)) = 0\right\}. \tag{5.6}$$

By (5.6), $\mathcal{M}_\mathcal{S}$ can be written as a graph of y over x and z as

$$y = -x - c(1 - \tanh\left(x + z\right)) =: h(x, z). \tag{5.7}$$

Remark 13. *The plane $\mathcal{M}_\mathcal{P} = \{x = 0\}$ is invariant for the full system (5.1), and in what is to follow, we will restrict to $x \leq 0$.*

The stability of $\mathcal{M}_1$ is given by linearisation with respect to the fast variable x in (5.3a)

$$F_x = x\left(1 - c\mathrm{sech}^2(x + z)\right) + \left(x + y + c(1 - \tanh\left(x + z\right))\right); \tag{5.8}$$

the normally hyperbolic subset of $\mathcal{M}_\mathcal{S}$ is therefore defined as

$$\mathcal{S} = \left\{(x, y, z) \in \mathcal{M}_\mathcal{S} \mid F_x|_{y=h(x,z)} \neq 0\right\}, \tag{5.9}$$

where, from (5.8) and (5.7),

$$F_x|_{y=h(x,z)} = x\left(1 - c\mathrm{sech}^2(x + z)\right). \tag{5.10}$$

For $x < 0$, the attracting and repelling subsets $\mathcal{S}^a, \mathcal{S}^r \subset \mathcal{S}$ are therefore respectively given by

$$\mathcal{S}^a = \left\{(x, y, z) \in \mathcal{M}_\mathcal{S} \mid \left(1 - c\mathrm{sech}^2(x + z)\right) > 0\right\}, \tag{5.11a}$$
$$\mathcal{S}^r = \left\{(x, y, z) \in \mathcal{M}_\mathcal{S} \mid \left(1 - c\mathrm{sech}^2(x + z)\right) < 0\right\}, \tag{5.11b}$$

notice that we have accounted for the x factor in (5.10) which is not included in (5.11). The manifold $\mathcal{M}_\mathcal{S}$ is not normally hyperbolic at $\mathcal{F}_\mathcal{S} = \mathcal{M}_\mathcal{S} \backslash \mathcal{S}$, where

$$\mathcal{F}_\mathcal{S} = \left\{(x, y, z) \in \mathcal{M}_1 \mid \left(1 - c\mathrm{sech}^2(x + z)\right) = 0\right\} = \mathcal{L}^- \cup \mathcal{L}^+; \tag{5.12}$$

the fold curves $\mathcal{L}^\mp$ separate the normally hyperbolic part as $\mathcal{S} = \mathcal{S}^{a^-} \cup \mathcal{S}^r \cup \mathcal{S}^{a^+}$, and they are given as graphs in the xz-plane by

$$\mathcal{L}^\mp : \; z = -x \mp \mathrm{arcsech}\left\{\frac{1}{\sqrt{c}}\right\}. \tag{5.13}$$

Similarly, by (5.5), $\mathcal{M}_\mathcal{P}$ is given as a graph $x = 0$; the normally hyperbolic subset of $\mathcal{M}_\mathcal{P}$ is therefore defined as

$$\mathcal{P} = \{(x, y, z) \in \mathcal{M}_\mathcal{P} \mid F_x|_{x=0} \neq 0\}, \tag{5.14}$$

where, from (5.8) and $x = 0$,

$$F_x|_{x=0} = y + c(1 - \tanh(z)). \tag{5.15}$$

The attracting and repelling subsets $\mathcal{P}^a$ and $\mathcal{P}^r$ are therefore respectively given by

$$\mathcal{P}^a = \{(x, y, z) \in \mathcal{M}_\mathcal{S} \mid y + c(1 - \tanh(z)) < 0\}. \tag{5.16a}$$
$$\mathcal{P}^r = \{(x, y, z) \in \mathcal{M}_\mathcal{S} \mid y + c(1 - \tanh(z)) > 0\}. \tag{5.16b}$$

The manifold $\mathcal{M}_\mathcal{P}$ is not normally hyperbolic at $\mathcal{F}_\mathcal{P} = \mathcal{M}_\mathcal{S} \backslash \mathcal{P}$,

$$\mathcal{F}_\mathcal{P} = \{(x, y, z) \in \mathcal{M}_1 \mid y + c(1 - \tanh(z)) = 0\}. \tag{5.17}$$

The above geometric objects are illustrated in Figure 5.2. In the following, we study the reduced flows on $\mathcal{M}_\mathcal{S}$ and $\mathcal{M}_\mathcal{P}$ under the assumption that these flows are slow-fast systems themselves, i.e. for $\rho > 0$ sufficiently small.

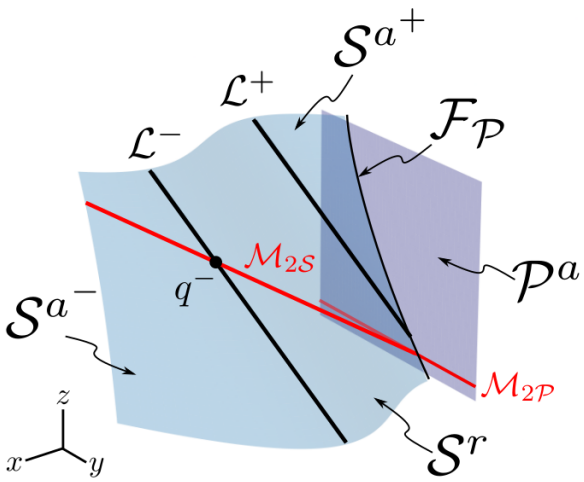

Figure 5.2: Critical and supercritical manifolds of system (5.1).

5.2.2 The reduced flow on $\mathcal{M}_\mathcal{P}$

The reduced flow on $\mathcal{M}_\mathcal{P}$ is given by setting $\delta = 0$ in (5.4)

$$\dot{y} = -\rho a y, \tag{5.18a}$$
$$\dot{z} = k - z; \tag{5.18b}$$

it is linear with explicit solutions

$$y(t) = y_0 e^{-\rho a t}, \quad z(t) = k + (z_0 - k)e^{-t}, \tag{5.19}$$

from which we can parametrise

$$y(z) = y_0 \left(\frac{z-k}{z_0-k} \right)^{\rho a}. \tag{5.20}$$

System (5.18) admits a stable node at $p_n = (0, k)$ with eigenvalues $\lambda_s = -1$, $\lambda_w = -\rho a$; we will refer to the associated eigenspaces as the *strong* and *weak* eigendirections, respectively. We remark that the coordinates (y_*, z_*) of the intersection of the corresponding trajectory with $\mathcal{F}_{\mathcal{P}}$ can be calculated by solving

$$y_0 \left(\frac{z_*-k}{z_0-k} \right)^{\rho a} + c\,(1 - \tanh(z_*)) = 0.$$

Considering $\rho > 0$ sufficiently small, System (5.18) is a slow fast system in the standard form, where y is the slow variable and z is the fast one. In the slow formulation, i.e. by a rescaling time as $s = \rho\tau$, System (5.18) is written as

$$\dot{y} = -ay \tag{5.21a}$$
$$\rho\dot{z} = k - z \tag{5.21b}$$

The layer problem on $\mathcal{M}_{\mathcal{P}}$ is given by setting $\rho = 0$ in (5.21)

$$\dot{y} = 0, \tag{5.22a}$$
$$\dot{z} = k - z, \tag{5.22b}$$

and its solutions, as can also be seen by setting $\rho = 0$ in (5.19), are given by straight fibres with $y = const.$ Equilibria of (5.22) define the supercritical manifold

$$\mathcal{M}_{2\mathcal{P}} = \left\{ (x, y, z) \in \mathbb{R}^3 \mid x = 0, \quad k - z = 0 \right\} \tag{5.23}$$

and the reduced flow on $\mathcal{M}_{2\mathcal{P}}$ is obtained by setting $\rho = 0$ in (5.21)

$$\dot{y} = -ay \tag{5.24a}$$
$$0 = k - z \tag{5.24b}$$

Linearising the fast flow (5.22b) with respect to z follows that $\mathcal{M}_{2\mathcal{P}}$ is normally hyperbolic everywhere.

We make the following observation:

Lemma 8. *The stable node $(0, k)$ of System (5.18) lies on $\mathcal{P}^r$ for all $c, k, a > 0$.*

Proof. From (5.15) we have that $F_x|_{\{x=0,y=0,z=k\}} > 0 \ \forall\ c, k, a > 0$; from (5.16) follows that $(0, 0, k)$ lies on $\mathcal{P}^r$. □

5.2.3 The reduced flow on $\mathcal{M}_{\mathcal{S}}$

Differentiating the graph expression (5.7) of $\mathcal{M}_1$ gives $\dot{y} = h_x\dot{x} + h_z\dot{z}$; inserting this in the reduced flow (5.4) and rearranging gives

$$\begin{aligned}\left(1 - c\text{sech}^2\left(x+z\right)\right)\dot{x} &= c\left(k - z - \frac{x}{2}\right)\text{sech}^2\left(x+z\right) + \rho\left(ah(x,z) + x^2\right)\\ \dot{z} &= k - z - \frac{x}{2}\end{aligned}$$

which is singular along $\mathcal{F}_{\mathcal{S}}$. Rescaling time by a factor of $\left(1 - c\text{sech}^2\left(x+z\right)\right)$ in the above gives

$$\dot{x} = c\left(k - z - \frac{x}{2}\right)\text{sech}^2\left(x+z\right) + \rho\left(ah(x,z) + x^2\right) \tag{5.26a}$$

$$\dot{z} = \left(1 - c\text{sech}^2\left(x+z\right)\right)\left(k - z - \frac{x}{2}\right). \tag{5.26b}$$

System (5.26) is a slow-fast system in the non-standard form [Wechselberger, 2020]

$$\begin{pmatrix}\dot{x}\\ \dot{z}\end{pmatrix} = N(x,z)f(x,z) + \rho G(x,z) \tag{5.27}$$

where

$$N(x,z) = \begin{pmatrix} c\text{sech}^2\left(x+z\right)\\ 1 - c\text{sech}^2\left(x+z\right)\end{pmatrix}, \quad f(x,z) = k - z - \frac{x}{2}, \quad G(x,z) = \begin{pmatrix} ah(x,z) + x^2\\ 0\end{pmatrix} \tag{5.28}$$

The intermediate problem at the double singular limit $\rho = 0 = \delta$ is obtained by setting $\rho = 0$ in (5.26):

$$\dot{x} = c\left(k - z - \frac{x}{2}\right)\text{sech}^2\left(x+z\right) \tag{5.29a}$$

$$\dot{z} = \left(1 - c\text{sech}^2\left(x+z\right)\right)\left(k - z - \frac{x}{2}\right). \tag{5.29b}$$

Non-stationary solutions of (5.29) will be called the *intermediate fibres*. We remark that in the above we have eliminated the slow variable y, as opposed to the analysis of the extended prototypical example in Chapter 2 and to that of the Hodgkin-Huxley equation Chapter 4, where in the corresponding reduced problems on the critical manifolds $\mathcal{M}_1$ we had eliminated the intermediate variable. We remark on the difficulties that arise from this in Section 5.3.

Lemma 9. *For initial conditions $(x_0, z_0) \in \mathcal{S}^a$, the intermediate fibres of (5.29) are given as graphs $z = \zeta(x; x_0, z_0)$, where*

$$\zeta(x; x_0, z_0) = -x + \text{arctanh}\left\{\frac{x - x_0 + c\tanh\left(x_0 + z_0\right)}{c}\right\} \tag{5.30}$$

Proof. By (5.29), for $k - z - \frac{x}{2} \neq 0$ we write

$$\frac{\mathrm{d}z}{\mathrm{d}x} = \frac{1 - c\mathrm{sech}^2(x+z)}{c\mathrm{sech}^2(x+z)} = \frac{1}{c\mathrm{sech}^2(x+z)} - 1 = \frac{\cosh^2(x+z)}{c} - 1. \tag{5.31}$$

Writing $u = x + z$, $\frac{\mathrm{d}u}{\mathrm{d}x} = 1 + \frac{\mathrm{d}z}{\mathrm{d}x}$ gives

$$\frac{\mathrm{d}u}{\mathrm{d}x} = \frac{\cosh^2(u)}{c}.$$

Separating variables, integrating and switching back to the original coordinates gives the result. □

The supercritical manifold $\mathcal{M}_{2\mathcal{S}}$ as the set of equilibria of (5.29) is given by

$$\mathcal{M}_{2\mathcal{S}} = \left\{(x,y,z) \in \mathbb{R}^3 \mid x + y + c\left(1 - \tanh\left(\frac{x}{2} + k\right)\right) = 0, \quad k - z - \frac{x}{2} = 0\right\} \tag{5.32}$$

The Jacobian of the linearisation of the intermediate problem about $\mathcal{M}_{2\mathcal{S}}$ has one trivial eigenvalue $\lambda_0 = 0$ and a nontrivial one given by

$$\begin{aligned}\lambda(x,z) &= \langle \nabla f, N\rangle \\ &= -1 + \frac{c\mathrm{sech}^2(x+z)}{2},\end{aligned}$$

recall (1.9). Therefore, $\mathcal{M}_{2\mathcal{S}}$ consists of the normally hyperbolic part $\mathcal{Z}$:

$$\mathcal{Z} = \{(x,y,z) \in \mathcal{M}_{\mathcal{P}} \mid \lambda(x,z) \neq 0\} \tag{5.33}$$

which is the union $\mathcal{Z} = \mathcal{Z}^a \cup \mathcal{Z}^r$, where

$$\mathcal{Z}^a = \{(x,y,z) \in \mathcal{M}_{\mathcal{P}} \mid \lambda(x,z) < 0\}, \quad \mathcal{Z}^r = \{(x,y,z) \in \mathcal{M}_{\mathcal{P}} \mid \lambda(x,z) > 0\}, \tag{5.34}$$

and the folds $\mathcal{F}_{\mathcal{M}_{2\mathcal{S}}}$ are defined as

$$\mathcal{F}_{\mathcal{M}_{2\mathcal{S}}} = \{(x,y,z) \in \mathcal{M}_{\mathcal{P}} \mid \lambda(x,z) = 0\}. \tag{5.35}$$

Moreover, the folded singularities of $\mathcal{M}_{\mathcal{S}}$ are defined as the set $Q = \mathcal{M}_{2\mathcal{S}} \cap \mathcal{L}^{\mp} = \{q^-, q^+\}$, recall Chapter 2. The coordinates of the folded singularities $q^{\mp} = (x_{q^{\mp}}, y_{q^{\mp}}, z_{q^{\mp}})$ are

$$x_{q^{\mp}} = -2k \mp 2\mathrm{arcsech}\left\{\sqrt{\frac{1}{c}}\right\}, \quad y_{q^{\mp}} = h\left(x_{q^{\mp}}, z_{q^{\mp}}\right), \quad z_{q^{\mp}} = 2k \pm \mathrm{arcsech}\left\{\sqrt{\frac{1}{c}}\right\} \tag{5.36}$$

It is crucial that the above coordinates depend on the parameters c and k, although we will suppress this dependence in the notation in the following.

In the previous Chapters we emphasised that the singular geometry, and especially the sets where normal hyperbolicity at the singular limit is lost, play an important role in the dynamics of the perturbed system in relation to the properties of MMOs. In particular, we showed that the positions of the folded singularities $q^{\mp}$ relative to each other can distinguish

between MMOs with different qualitative properties. We emphasize that for system (5.1), from (5.36) it easily follows that $q^{\mp}$ are always remote. Extending the above notion, we will focus on the position of $q^{\mp}$ relative to $\mathcal{F}_{\mathcal{P}}$; we emphasize that these are both sets where normal hyperbolicity is lost, but in different manners. More accurately, we will focus on the projection of q^{-} onto $\mathcal{M}_{\mathcal{P}}$ relative to $\mathcal{F}_{\mathcal{P}}$, and as we will show later this is important in distinguish between MMOs with different qualitative properties in the perturbed system.

We start with the following observation:

Lemma 10. *If*

$$-k + 2\text{arcsech}\left\{\sqrt{\frac{1}{c}}\right\} < 0, \tag{5.37}$$

then $x_{q^+} < 0$.

Proof. Follows immediately from (5.36). □

The implication of Lemma 10 is that q^+ lies on the left of the $\{x = 0\}$ plane, i.e. on the portion of $\mathcal{L}^+$ adjacent to $\mathcal{S}^{a^+}$ for $x < 0$. Equation (5.37) is satisfied for (c, k) above the dashed curve in Figure 5.5 (b)

Similarly to the previous Chapters, we denote by $P(\cdot)$ the projection of a point on $\mathcal{L}^{\mp}$ onto a portion of the critical manifold along the fast flow, in particular onto the first portion that the fast fibre that emanates from this point intersects with (cf. Figure 5.3 panels (a) and (c)).

Lemma 11. *Denote*

$$A_{q^-}(c, k) := y_{q^-} + c(1 - \tanh(z_{q^-})), \tag{5.38}$$

where y_{q^-} *and* z_{q^-} *are given by (5.36).*

1. *If* $A_{q^-}(c, k) = 0$, *then* $P(q^-) \in \mathcal{F}_{\mathcal{P}}$;
2. *If* $A_{q^-}(c, k) > 0$, *then* $P(q^-) \in \mathcal{S}^{a^+}$;
3. *If* $A_{q^-}(c, k) < 0$, *then* $P(q^-) \in \mathcal{P}^a$.

Proof. The first point follows by requiring that y_{q^-} and z_{q^-}, which are given in (5.36) and depend on c and k, satisfy the algebraic constraint in (5.17). The other two points follow by using the y_{q^-} and z_{q^-} coordinates in (5.16). □

Lemma 11 implies that, if the parameters c and k satisfy $A_{q^-}(c, k) = 0$, then at the singular limit $\delta = 0 = \rho$, the folded singularity q^- is connected to $\mathcal{F}_{\mathcal{P}}$ by a fast fibre of (5.3), and is illustrated in Figure 5.3 (b). More generally, we will denote by $p_* = (x_*, y_*, z_*)$ the point on $\mathcal{L}^-$ that is connected to $\mathcal{F}_{\mathcal{P}}$ by a fast fibre of (5.3), i.e.

$$p_* = \left\{p \in \mathcal{L}^- \mid P(p) \in \mathcal{F}_{\mathcal{P}}\right\}; \tag{5.39}$$

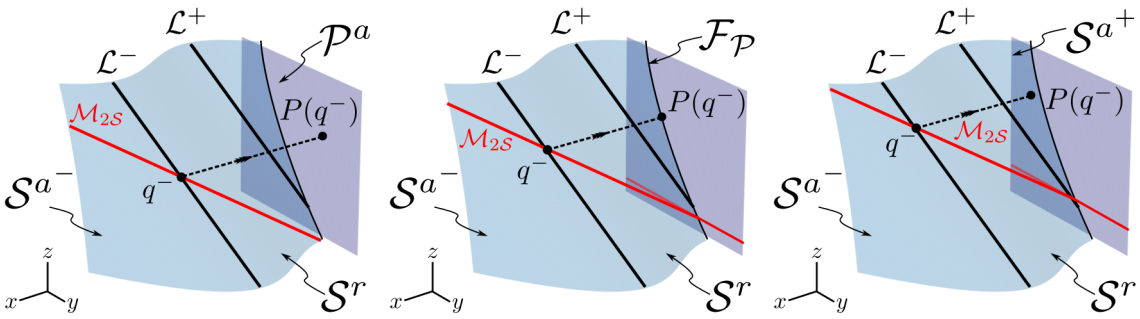

(a) $A_{q^-}(c,k) < 0$ (b) $A_{q^-}(c,k) = 0$ (c) $A_{q^-}(c,k) > 0$

Figure 5.3: Illustration of Lemma 11. If $A_{q^-}(c,k) < 0$, then $P(q^-) \in \mathcal{P}^a$, which implies that there exists a singular cycle with a segment evolving in the plane $\{x = 0\}$ and not in $\mathcal{S}^{a^+}$; in Section 5.3, this (c,k)-parameter regime will be associated with oscillatory trajectories that feature plateau above in the perturbed system $\delta, \rho > 0$. If $A_{q^-}(c,k) > 0$, then $P(q^-) \in \mathcal{S}^{a^+}$, which implies that there exists a singular cycle with a segment evolving in $\mathcal{S}^{a^+}$ and not in the plane $\{x = 0\}$; in Section 5.3, this (c,k)-parameter regime will be associated with the existence of oscillatory trajectories without plateau above in the perturbed system $\delta, \rho > 0$, in dependence also of the parameter a.

by the geometry of the system it follows that p_* is unique for fixed c and k, and that

$$P(\mathcal{L}^-|_{y>y_*}) \subset \mathcal{S}^{a^+}, \qquad P(\mathcal{L}^-|_{y<y_*}) \subset \mathcal{P}^a.$$

Moreover, we will denote by $q^* = (x_{q^*}, y_{q^*}, z_{q^*})$ the point on $\mathcal{L}^-$ that has the same y- and z-coordinates as q^+, (i.e. q^* lies on the same plane that is parallel to the fast fibres as q^+); that is

$$q^* = \left\{(x,y,z) \in \mathcal{L}^- \mid y = y_{q^+},\ z = z_{q^+}\right\}; \tag{5.40}$$

Lemma 12. *Denote*

$$A_{q^*}(c,k) := y_{q^+} - \operatorname{arcsech}\left\{\frac{1}{\sqrt{c}}\right\} - \operatorname{arctanh}\left\{\frac{y_{q^+}}{c} + 1\right\} - c\left(1 - \tanh\left\{\operatorname{arcsech}\left\{\frac{1}{\sqrt{c}}\right\}\right\}\right) \tag{5.41}$$

where y_{q^+} is given by (5.36).

1. *If $A_{q^*}(c,k) = 0$, then $P(q^*) \in \mathcal{F}_{\mathcal{P}}$;*
2. *If $A_{q^*}(c,k) > 0$, then $P(q^*) \in \mathcal{P}^a$;*
3. *If $A_{q^*}(c,k) < 0$, then $P(q^*) \in \mathcal{S}^{a^+}$.*

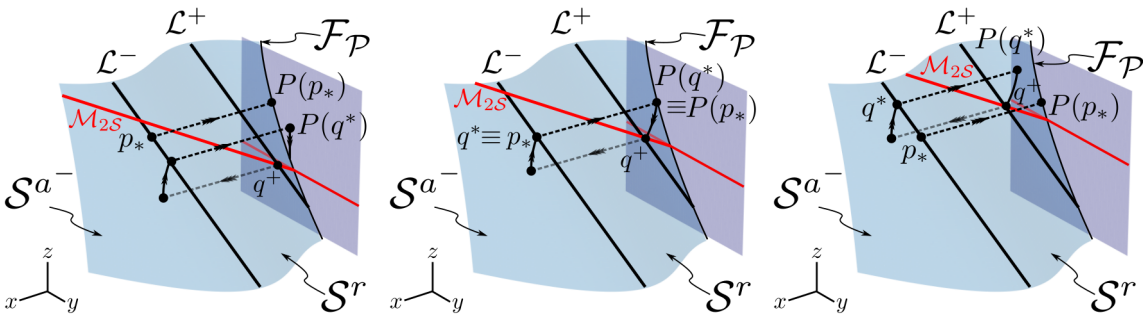

(a) $A_{q^*}(c,k) > 0$ (b) $A_{q^*}(c,k) = 0$ (c) $A_{q^*}(c,k) < 0$

Figure 5.4: Illustration of Lemma 12. (a) If $A_{p^*}(c,k) > 0$, then the location of q^+ is such that there exists no singular cycle with endpoint in $\mathcal{S}^{a^+}$ that passes through q^+ – notice that the singular trajectory that emanates from q^+ does not form a closed orbit. In Section 5.3, it will be illustrated that MMOs with SAOs above are not possible in this (c,k)-regime. (c) If $A_{p^*}(c,k) < 0$, then there exists a singular cycle with endpoint in $\mathcal{S}^{a^+}$ that passes through q^+, panel (c); in Section 5.3, it will be illustrated that MMOs with SAOs above are in fact possible in this (c,k)-regime, in dependence of the parameter a.

Proof. To show the first point, we require that

$$y_q^+ = y_*;$$

recall that $p_* = (x_*, y_*, z_*)$ is defined in (5.39) and $q^* = (x_{q^*}, y_{q^*}, z_{q^*})$ in (5.40). Then,

$$z_* = \operatorname{arctanh}\left\{\frac{y_{q^+}}{c} + 1\right\},$$

by the algebraic constraint in (5.17). Moreover,

$$x_* = \operatorname{arcsech}\left\{\frac{1}{\sqrt{c}}\right\} - z_*,$$

by the algebraic constraint in (5.12). The first point in the statement follows by requiring that

$$y_{q^+} = h(x_*, z_*), \tag{5.42}$$

recall (5.7) and (5.36), and the other two points follow from the properties of the function $A_{q_*}(c,k)$. □

Lemma 12 is illustrated in Figure 5.4. Lemma 11 and Lemma 12 are summarised in the following corollary.

Corollary 2. *Denote*

$$\begin{aligned}
\mathcal{D}_1 &= \{(c,k) \in (1,\infty) \times (0,1) \mid A_{q^-}(c,k) < 0,\ A_{q_*}(c,k) > 0\}, \\
\mathcal{D}_2 &= \{(c,k) \in (1,\infty) \times (0,1) \mid A_{q^-}(c,k) > 0,\ A_{q_*}(c,k) > 0\}, \\
\mathcal{D}_3 &= \{(c,k) \in (1,\infty) \times (0,1) \mid A_{q^-}(c,k) > 0,\ A_{q_*}(c,k) < 0\},
\end{aligned}$$

as shown in Figure 5.5.

1. *If* $(c,k) \in \mathcal{D}_1$, *then* $P(q^-), P(q^*) \in \mathcal{P}^a$;

2. *If* $(c,k) \in \mathcal{D}_2$, *then* $P(q^-) \in \mathcal{S}^{a^+}$, $P(q^*) \in \mathcal{P}^a$;

3. *If* $(c,k) \in \mathcal{D}_3$, *then* $P(q^-), P(q^*) \in \mathcal{S}^{a^+}$.

Corollary 2 implies that, if $(c,k) \in \mathcal{D}_1$, then there exists no singular cycle that passes through q^- and which has segments that evolve on $\mathcal{S}^{a^+}$. Moreover, if $(c,k) \in \mathcal{D}_2$, then there exists a singular cycle that passes through q^- and which has a segment that evolves on $\mathcal{S}^{a^+}$, but there exists no singular cycle that passes through q^+ and which has a segment that evolves on $\mathcal{S}^{a^+}$. Finally, if $(c,k) \in \mathcal{D}_3$, then there exist a singular cycle that passes through q^- which has a segment that evolves on $\mathcal{S}^{a^+}$, and a singular cycle that passes through q^+ which has a segment that evolves on $\mathcal{S}^{a^+}$, see Figure 5.3 and Figure 5.4. We will relate the above parameter regimes to properties of MMOs of (5.1) for $\delta, \rho > 0$ sufficiently small in Section 5.3.

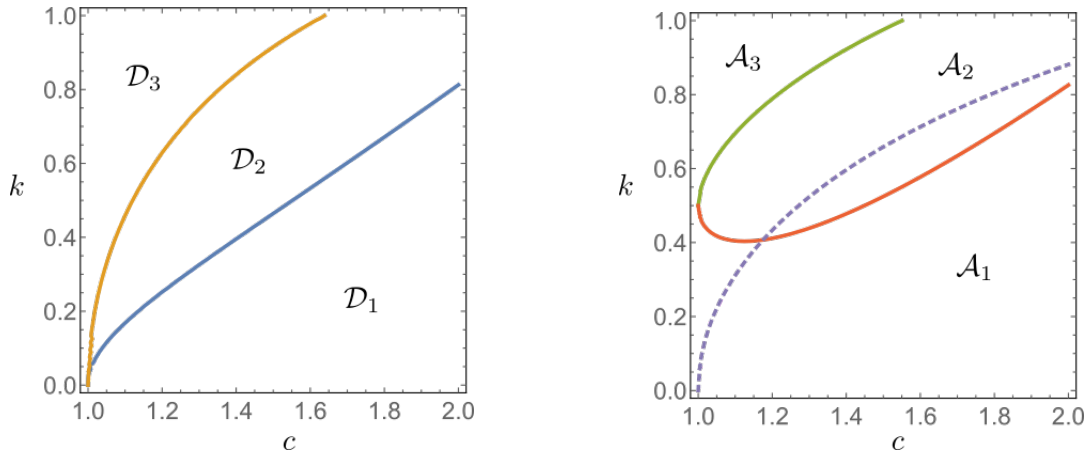

(a) (b)

Figure 5.5: (a) Parameter regimes described in Corollary 2. For $(c.k) \in \mathcal{D}_1$, the projection of the folded singularity q^- lies in $\mathcal{P}^a$; for $(c.k) \in \mathcal{D}_2$, the projection of the folded singularity q^- lies in $\mathcal{S}^{a^-}$, and the projection of a point on $\mathcal{L}^-$ with the same y- coordinate as q^+ lies in $\mathcal{P}^a$; for $(c.k) \in \mathcal{D}_3$, the projection of the folded singularity q^- and of a point on $\mathcal{L}^-$ with the same y- coordinate as q^+ lie in $\mathcal{S}^{a^-}$, cf. Figure 5.3 and Figure 5.4.
(b) parameter regimes described in Corollary 3. For $(c.k) \in \mathcal{A}_1$ (i.e. below the red curve), there exist $a^- = a^-(c,k) > 0$ and $a^+ = a^+(c,k) > 0$, with $a^- > a^+$, such that an equilibrium point p_{eq} of the slow flow, computed by (5.44), lies on $\mathcal{S}^r$ for $a \in (a^+, a^-)$. For $(c,k) \in \mathcal{A}_2$, there exists $a^+ = a^+(c,k) > 0$, such that an equilibrium point of the slow flow, given by (5.44), lies on $\mathcal{S}^r$ for $a > a^+$. For $(c.k) \in \mathcal{A}_3$, there exists no $a > 0$ such that an equilibrium point of the slow flow, given by (5.44), lies on $\mathcal{S}^r$. Note that the dashed purple curve is not meant to divide $\mathcal{A}_1$ and $\mathcal{A}_2$ into further subregions, and that it is related to the location of q^+ in accordance with Lemma 10.

Moreover, the reduced flow on $\mathcal{M}_{2\mathcal{S}}$ is given by

$$\begin{pmatrix} \dot{x} \\ \dot{z} \end{pmatrix} = \left[\frac{\det(N|G)}{\langle \nabla f, N \rangle} \begin{pmatrix} -\partial_z f \\ \partial_x f \end{pmatrix} \right], \tag{5.43}$$

see [Jelbart and Wechselberger, 2020]. Equilibria on $\mathcal{M}_{2\mathcal{S}}$ are found either by calculating the reduced flow (5.43), or by requiring that, in addition to the algebraic constraints in (5.32), the reduced flow thereon vanishes, i.e. $(ay + x^2) = 0$ by Equation (5.1b); this is equivalent to solving

$$ax - x^2 + ac\left(1 - \tanh\left(\frac{x}{2} + k\right)\right) = 0. \tag{5.44}$$

It immediately follows that the equilibrium of the slow flow on $\mathcal{M}_{2\mathcal{S}}$ lies on $\mathcal{S}^{a^-}$ (resp. on on $\mathcal{S}^r$) if $x_{eq} < x_{q^-}$ (resp. $x_{eq} > x_{q^-}$), see for instance Figure 5.3. Solving (5.44) for a we obtain

$$a = \frac{x^2}{x + c\left(1 - \tanh\left(\frac{x}{2} + k\right)\right)}, \tag{5.45}$$

and we denote

$$a^{\mp}(c,k) := \frac{x_{q^{\mp}}^2}{x_{q^{\mp}} + c\left(1 - \tanh\left(\frac{x_{q^{\mp}}}{2} + k\right)\right)}. \tag{5.46}$$

If $a^-(c,k) > 0$ (resp. if $a^+(c,k) > 0$), then for fixed $(c,k) \in (1,\infty) \times (0,1)$, an equilibrium point lies on q^- (resp. on q^+) for $a = a^-(c,k)$ (resp. for $a = a^+(c,k)$). The graphs of $a^{\mp}(c,k) = 0$ on the ck-plane are shown in Figure 5.5, panel (b).

Corollary 3. *Denote*

$$\begin{aligned}
\mathcal{A}_1 &= \left\{(c,k) \in (1,\infty) \times (0,1) \mid a^-(c,k) > 0,\ a^+(c,k) < 0\right\},\\
\mathcal{A}_2 &= \left\{(c,k) \in (1,\infty) \times (0,1) \mid a^-(c,k) < 0,\ a^+(c,k) > 0\right\},\\
\mathcal{A}_3 &= \left\{(c,k) \in (1,\infty) \times (0,1) \mid a^-(c,k) < 0,\ a^+(c,k) < 0\right\},
\end{aligned}$$

as shown in Figure 5.5.

1. *If $(c,k) \in \mathcal{A}_1$, then $\exists\ a^{\mp} = a^{\mp}(c,k)$, given by (5.46), such that*
   - *(a) if $a^+ = a^+(c,k)$, then $p_{eq} \equiv q^+$,*
   - *(b) if $a^- = a^-(c,k)$, then $p_{eq} \equiv q^-$,*
   - *(c) if $a \in (a^+, a^-)$, then $x_{eq} \in (x_{q^-}, x_{q^+})$;*
2. *If $(c,k) \in \mathcal{A}_2$, then $\exists\ a^+ = a^+(c,k)$, given by (5.46), such that*
   - *(a) if $a^+ = a^+(c,k)$, then $p_{eq} \equiv q^+$,*
   - *(b) if $a > a^+$, then $x_{eq} < x_{q^+}$, and $\nexists\ a > 0$ s.t. $p_{eq} \equiv q^-$*
3. *If $(c,k) \in \mathcal{A}_3$, then $\nexists\ a > 0$ s.t. $p_{eq} \in \mathcal{S}^r$.*

To see the above more clearly, consider (c, k) such that $a^-(c, k) = 0$. Then, for $a = a^- = 0$, we have that $x_{eq} = x_{q^-}$. For $(c, k) \in \mathcal{A}_1$, it holds that $a^-(c, k) > 0$, i.e. $x_{eq} = x_{q^-}$ for some $a = a^- > 0$. Symbolic calculations show that, the parameter a in (5.45) is a decreasing function with respect to x for $x \in (x_{q^-}, x_{q^+})$; therefore, for $a < a^-$, we have that $x_{eq} > x_{q^-}$, and the equilibrium point lies on $\mathcal{S}^r$ (see again Figure 5.3). The argument is similar for $a^+(c, k)$ and values $a > a^+$; however, notice that for (c, k)-values below the dashed purple curve in Figure 5.5 (b), it holds that $x_{q^+} > 0$ by Lemma 10, and q^+ lies on the right of the plane $\{x = 0\}$; therefore, as will be apparent in the following, for (c, k)-values below the dashed purple curve in Figure 5.5 (b), a^+ is irrelevant.

We now combine the two panels in Figure 5.5 into one figure, separating the ck-plane into six parameter regimes as shown in Figure 5.6. In Section 5.3 we will relate these parameter regimes to qualitative properties of MMOs of (5.1) for $\delta, \rho > 0$ sufficiently small, in dependence of the parameter a.

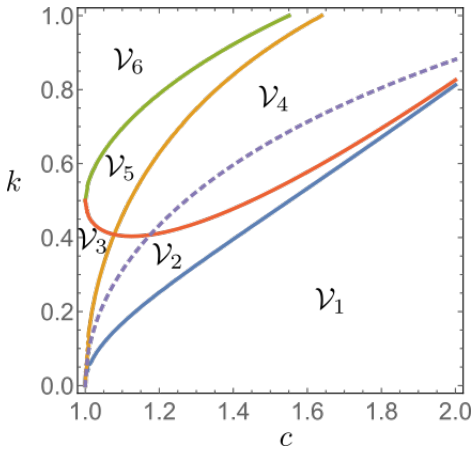

Figure 5.6: Combination of the two panels of Figure 5.5 into one figure, dividing the ck-plane into six parameter regimes that correspond to different qualitative scenarios of MMOs and transitions between them, in dependence of the parameter a. The dashed purple line is not meant to further divide the (c, k)-parameter regimes and does not distinguish between different qualitative behaviours, but is associated with the a-values that separate oscillatory dynamics and steady state.

Remark 14. *Using the implicit function theorem, from (5.1a) and (5.44), one can deduce that for $\delta, \rho > 0$ sufficiently small and $a = \mathcal{O}(1)$, an equilibrium of system (5.1) lies $\mathcal{O}(\delta, \rho)$-close to an equilibrium point on $\mathcal{M}_2$ given by solving (5.44). This is not true, however, for $a \gg 1$, as the time-scale separation in the standard form of GSPT of (5.1) breaks down because of the large $\mathcal{O}(a\rho)$-terms on the RHS. Further investigation of the latter is included in plans for future work.*

5.3 Outline of dynamics

Here we will illustrate various MMO scenarios of system (5.1) with $\delta, \rho > 0$ in dependence of the parameters c, k and a. We start with general remarks on the perturbed dynamics.

5.3.1 Perturbed dynamics and delayed loss of stability

Normally hyperbolic parts

Based on GSPT for normally hyperbolic manifolds [Fenichel, 1979, Cardin and Teixeira, 2017] and in accordance with Chapter 2, it follows that, for $\delta, \rho > 0$ sufficiently small, there exist invariant manifolds $\mathcal{P}^a_{\delta\rho}$, $\mathcal{P}^r_{\delta\rho}$, $\mathcal{S}^{a^\mp}_{\delta\rho}$, $\mathcal{S}^r_{\delta\rho}$. The perturbed manifolds $\mathcal{S}^{a^\mp}_{\delta\rho}$ and $\mathcal{S}^r_{\delta\rho}$ are diffeomorphic, and lie $\mathcal{O}(\delta)$-close in the Hausdorff distance, to their unperturbed, normally hyperbolic counterparts $\mathcal{S}^{a^\mp}$ and $\mathcal{S}^r$, respectively. Since $\mathcal{M}_\mathcal{P}$ is invariant for system (5.1) for all δ, ρ, it holds that $\mathcal{P}^a_{\delta\rho} \equiv \mathcal{P}^a$, $\mathcal{P}^r_{\delta\rho} \equiv \mathcal{P}^r$. These manifolds are locally invariant under the flow of (5.1).

Moreover, for $\delta, \rho > 0$ sufficiently small, there exist invariant manifolds $\mathcal{M}_{2\mathcal{P},\delta\rho}$, $\mathcal{Z}^a_{\delta\rho}$, $\mathcal{Z}^r_{\delta\rho}$ that are diffeomorphic and lie $\mathcal{O}(\delta+\rho)$-close in the Hausdorff distance to their unperturbed counterparts $\mathcal{M}_{2\mathcal{P}}$, $\mathcal{Z}^a$, $\mathcal{Z}^r$, respectively. These manifolds are locally invariant under the flow of (5.1).

Loss of normal hyperbolicity

We start by describing the behaviour of trajectories near the vicinity of $\mathcal{F}_\mathcal{P}$.

Initially, in the perturbed system (5.1) with $\delta, \rho > 0$ sufficiently small, the slow sheet $\mathcal{S}^r_{\delta\rho}$ is "detached" from the plain $\{x = 0\}$. The plain $\{x = 0\}$ is invariant under the flow of (5.1), and trajectories that evolve on $\mathcal{S}^r_{\delta\rho}$ exit a vicinity of $\{x = 0\}$ following fast fibres; this can be shown by introducing an appropriate scaling at the vicinity of $\mathcal{F}_\mathcal{P}$, see Section 5.5 for details, and [Poggiale et al., 2020] for a similar analysis in a two-dimensional Rosenzweig–MacArthur model with similar singular geometry.

For $\delta, \rho > 0$ small, a trajectory of (5.1) that enters an $\mathcal{O}(\delta)$ neighbourhood of $\mathcal{P}^a_{\delta\rho}$ but $\mathcal{O}(\sqrt{\delta})$-away from $\mathcal{F}_\mathcal{P}$, follows the slow flow (5.18) therein. After crossing the vicinity of $\mathcal{F}_\mathcal{P}$ and instead of being "immediately" repelled away from an $\mathcal{O}(\delta)$-neighbourhood of $\mathcal{P}^r_{\delta\rho}$, it follows the slow flow (5.18) therein until the accumulated attraction to $\mathcal{P}^a_{\delta\rho}$ is balanced by repulsion from $\mathcal{P}^r_{\delta\rho}$. This is calculated using the *way-in/way-out* function:

$$\int_{z_{in}}^{z_{out}} \frac{F_x|_{x=0}}{k-z} \mathrm{d}z = 0, \tag{5.47}$$

recall (5.15) and see [De Maesschalck, 2008]; this phenomenon is also known as Pontryagin's delay of stability loss and has also been used in a system with a similar self-intersecting critical manifold in [Sadhu, 2019]. We remark that this approach is also applicable but was not implemented in the analysis of a two-dimensional Rosenzweig–MacArthur model in [Duncan et al., 2019].

Lemma 13. *Let $\delta, \rho > 0$ sufficiently small and consider a point (x_{in}, y_{in}, z_{in}) in an $\mathcal{O}(\delta)$ neighbourhood of $\mathcal{P}^a_{\delta,\rho}$ and outside an $\mathcal{O}(\sqrt{\delta})$ neighbourhood of $\mathcal{F}_\mathcal{P}$. A trajectory under the flow of (5.1) with initial condition (x_{in}, y_{in}, z_{in}) leaves an $\mathcal{O}(\delta)$ neighbourhood of $\mathcal{P}^a_{\delta,\rho}$ at a point $(x_{out}, y_{out}, z_{out})$ for which*

$$W(z_{in}, z_{out}) := \int_{z_{in}}^{z_{out}} \frac{y_{in}\left(\frac{z-k}{z_{in}-k}\right)^{\rho a} + c\,(1-\tanh(z))}{k-z} \mathrm{d}z = 0 \tag{5.48}$$

holds.

Proof. The result is based on [De Maesschalck, 2008] and follows from (5.47) and (5.20). The restriction $\mathcal{O}(\sqrt{\delta})$-away from $\mathcal{F}_{\mathcal{P}}$ is related to the scalings introduced for the local analysis in Section 5.5. □

Unfortunately, the exit point $(x_{out}, y_{out}, z_{out})$ is not given by an explicit expression.

We now turn our attention to the behaviour of the perturbed system (5.1) near $\mathcal{F}_S$ for $\delta, \rho > 0$ sufficiently small. We describe the scenarios near $\mathcal{L}^-$ and the description of $\mathcal{L}^+$ is similar.

When trajectories reach the vicinity of the fold line $\mathcal{L}^-$ away from the vicinity of the folded singularity q^-, they "jump" to the opposite attracting sheet following the fast flow, see [Wechselberger, 2005, Szmolyan and Wechselberger, 2001]. On the other hand, when trajectories are attracted to the vicinity of q^- or to appropriate subregions of $\mathcal{Z}^a_{\delta,\rho}$, they undergo SAOs. Namely, $\mathcal{Z}^a_{\delta,\rho}$ can be decomposed to nodally and spirally attracting regimes. If trajectories are attracted to the latter regime, then they undergo SAOs of bifurcation delay type, while if trajectories are attracted to the former, then they typically undergo no SAOs, see Chapter 2 for details.

Singular Hopf bifurcations

Here we discuss the distinction between steady states and oscillatory dynamics of system (5.1), in dependence of the parameter a, for fixed $(c, k) \in (1, \infty) \times (0, 1)$. We first observe that, near the fold lines $\mathcal{L}^{\mp}$ and away from $\{x = 0\}$, system (5.1) can be transformed to either the extended prototypical example (2.3) or to the canonical form (2.1).

It then follows that, for $(c, k) \in \mathcal{A}_1$, system (5.1) with $\delta, \rho > 0$ sufficiently small undergoes singular Hopf bifurcations for $a = a^-(c, k) + \mathcal{O}(\delta, \rho)$, since for $a = a^-(c, k)$ an equilibrium of the slow flow (5.43) crosses the fold line $\mathcal{L}^-$ at the singular limit $\delta = 0 = \rho$.

Similarly, for $(c, k) \in \mathcal{A}_2$, for which also (5.37) holds, i.e. above the dashed purple curve in Figure 5.5 (b), system (5.1) with $\delta, \rho > 0$ sufficiently small undergoes singular Hopf bifurcations for $a = a^+(c, k) + \mathcal{O}(\delta, \rho)$, since for $a = a^+(c, k)$ an equilibrium of the slow flow (5.43) crosses the fold line $\mathcal{L}^+$ at the singular limit $\delta = 0 = \rho$ in the negative x-orthant.

For $(c, k) \in \mathcal{A}_3$, there exist no $a > 0$ for which an equilibrium of the reduced flow (5.43) crosses a fold line $\mathcal{L}^{\mp}$ at the singular limit $\delta = 0 = \rho$ in the negative x-orthant, therefore system (5.1) converges to a steady state for all $a > 0$.

5.3.2 Oscillatory trajectories

Here we present the main qualitative results of this Chapter and we summarise the oscillatory dynamics of system (5.1) for $\delta, \rho > 0$ sufficiently small. We combine panels (a) and (b) of Figure 5.5 into Figure 5.6, thus separating the ck-plane into further regimes, and we remark on the dynamics of system (5.1) for c, k-values in each one of these regimes.

In all numerical simulations below, we consider $\delta = 0.01 = \rho$.

- $\underline{(c,k) \in \mathcal{V}_1 = \mathcal{D}_1 \cap \mathcal{A}_1}$

Fix $(c,k) \in \mathcal{V}_1$, as shown in Figure 5.6.

By Corollary 2, it holds that $P(q^-), P(q^*) \in \mathcal{P}^a$. Moreover, by (5.46), there exists $a^- = a^-(c,k)$ for which $p_{eq} \equiv q^-$, i.e an equilibrium point given by solving (5.44) coincides with the folded singularity q^-, and for $a < a^-$, it holds that $p_{eq} \in \mathcal{S}^r$. Therefore, for $a \in (0, a^-)$, system (5.1) features singular cycles that have segments which evolve on $\mathcal{P}^a$, and for $\delta, \rho > 0$ sufficiently small, system (5.1) features oscillations with plateau above, for $0 < a < a^- + \mathcal{O}(\delta, \rho)$.

In particular, fixing $(c,k) = (1.4, 0.2)$, we calculate that $a^- \simeq 4.57$. Numerically, we obtain that system (5.1) converges to a steady state for $a \gtrsim 4.5$. Some simulated trajectories for (c,k) fixed in this regime and various values of a, with $\delta = 0.01 = \rho$, are illustrated in Figure 5.7.

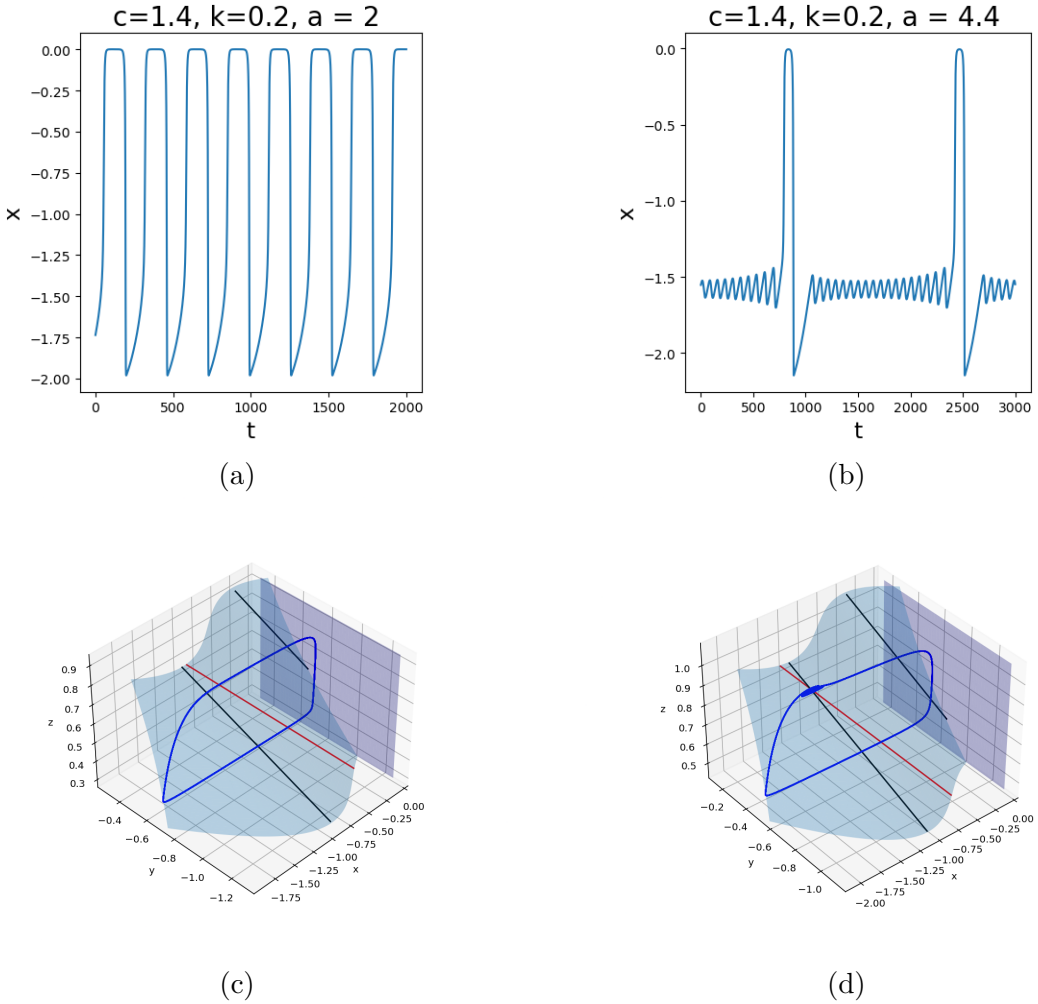

Figure 5.7: For all $(c,k) \in \mathcal{V}_1$, see Figure 5.6, oscillatory trajectories of system (5.1) feature plateau above. For fixed $(c,k) \in \mathcal{V}_1$, there exists unique $a^- = a^-(c,k) > 0$ for which an equilibrium point of (5.1) coincides with q^-. For $0 < a < a^-$, system (5.1) exhibits oscillatory dynamics. Moreover, for a close to a^-, system (5.1) exhibits MMOs with SAOs below.

Finally, we observe that during the transition from oscillatory dynamics to steady state, the system features MMOs with SAOs below, see Figure 5.7. Unfortunately, we are not able to apply the techniques described in Chapter 2, recall Lemma 4 and Theorem 5, where we used the slow drift in order to predict the transition from relaxation oscillations to MMOs with SAOs below in dependence of a, since this slow drift is not available from the reduction in (5.29) and from the elimination of time in (5.31), as z therein is the intermediate and not the slow variable. Further investigation of this is included in plans for future work.

• $\underline{(c,k) \in \mathcal{V}_2 = \mathcal{D}_2 \cap \mathcal{A}_1}$

Fix $(c,k) \in \mathcal{V}_2$, as shown in Figure 5.6.

By Corollary 2, it holds that $P(q^-) \in \mathcal{S}^{a^-}$, $P(q^*) \in \mathcal{P}^a$. In addition, by (5.46), there exists $a^- = a^-(c,k)$ for which $p_{eq} \equiv q^-$, i.e an equilibrium point given by solving (5.44) coincides with the folded singularity q^-, and for $a < a^-$, it holds that $p_{eq} \in \mathcal{S}^r$. Moreover, there exists $a^+ = a^+(c,k)$ for which $p_{eq} \equiv q^+$, i.e an equilibrium point given by solving (5.44) coincides with the folded singularity q^+. However, for (c,k)-values below the dashed purple curve in Figure 5.6, the value a^+ is irrelevant. For (c,k)-values in this regime (i.e. below the dashed purple curve), and for $\delta, \rho > 0$ sufficiently small, system (5.1) features oscillatory dynamics for $0 < a < a^- + \mathcal{O}(\delta, \rho)$.

In particular, fixing $(c,k) = (1.4, 0.4)$, we calculate that $a^- \simeq 25.55$. Numerically, we obtain that system (5.1) converges to a steady state for $a \gtrsim 25.5$. Some simulated trajectories for (c,k) fixed in this regime and various values of a, with $\delta = 0.01 = \rho$, are illustrated in Figure 5.8.

Moreover, we observe that there exists a value a_p that distinguishes between MMOs that feature plateaus from those that do not, i.e.

1. system (5.1) features MMOs with plateaus above for $a \in (0, a_p)$,
2. system (5.1) features MMOs without plateaus for $a \in (a_p, a^-)$.

In a first approximation, we estimate a_p as the a-value for which the equilibrium point $p_{eq} = (x_{eq}, y_{eq}, z_{eq})$, recall (5.44), lies in the plane given by $\{y = y_*\}$, recall (5.39). This is obtained by approximating the unstable manifold $\mathcal{W}(p_{eq})$ of p_{eq} by

$$\mathcal{W}(p_{eq}) = \left\{(x,y,z) \in \mathbb{R}^3 \mid y = y_{eq} + \mathcal{O}(\delta, \rho)\right\}.$$

Then, for $a < a_p$ it holds that $P(\mathcal{L}^- \cap \mathcal{W}(p_{eq})) \in \mathcal{P}^a$, while for $a > a_p$ it holds that $P(\mathcal{L}^- \cap \mathcal{W}(p_{eq})) \in \mathcal{S}^{a^-}$, and oscillatory trajectories do and do not feature plateaus above, respectively, cf. Figure 5.8.

• $\underline{(c,k) \in \mathcal{V}_3 = \mathcal{D}_3 \cap \mathcal{A}_1}$

Fix $(c,k) \in \mathcal{V}_3$, as shown in Figure 5.6.

By Corollary 2, it holds that $P(q^-), P(q^*) \in \mathcal{S}^{a^-}$. In addition, by (5.46), there exist $a^- = a^-(c,k)$ for which $p_{eq} \equiv q^-$, and $a^+ = a^+(c,k) > 0$ for which $p_{eq} \equiv q^+$, and for $a^+ < a < a^-$ it holds that $p_{eq} \in \mathcal{S}^r$. Therefore, for $\delta, \rho > 0$ sufficiently small, system (5.1) features oscillations oscillatory dynamics for $a \in (a^+ + \mathcal{O}(\delta, \rho), a^- + \mathcal{O}(\delta, \rho))$, and oscillatory trajectories with plateau are not possible.

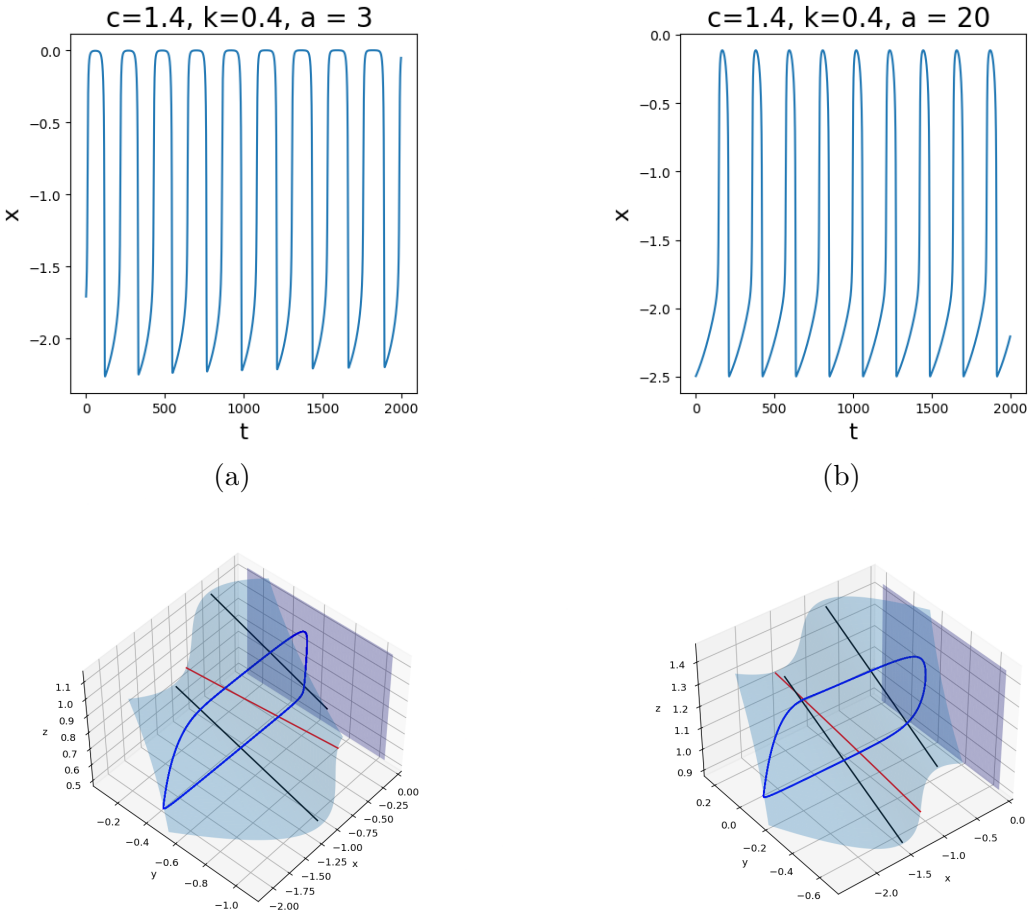

Figure 5.8: For $(c,k) \in \mathcal{V}_2$, see Figure 5.6, oscillatory trajectories of system (5.1) can either feature plateau above or not. For fixed $(c,k) \in \mathcal{V}_2$, there exists unique $a^- = a^-(c,k) > 0$ for which an equilibrium point of (5.1) coincides with q^-. For $0 < a < a^-$, system (5.1) exhibits oscillatory dynamics. Moreover, there exists a_p such that for $a < a_p$, system (5.1) exhibits MMOs with plateaus above, while for $a > a_p$, system (5.1) exhibits MMOs without plateaus above.

In particular, fixing $(c,k) = (1.06, 0.4)$, we calculate that $a^+ \simeq 0.2$ and $a^- \simeq 61.02$. Numerically, we obtain that system (5.1) converges to a steady state for $a \lesssim 0.5$ and for $a \gtrsim 40$. (This seeming discrepancy for large a-values is related to Remark 14.) Some simulated trajectories for (c,k) fixed in this regime and various values of a, with $\delta = 0.01 = \rho$, are illustrated in Figure 5.9.

- $(c,k) \in \mathcal{V}_4 = \mathcal{D}_2 \cap \mathcal{A}_2$

Fix $(c,k) \in \mathcal{V}_4$, as shown in Figure 5.6.

By Corollary 2, it holds that $P(q^-) \in \mathcal{S}^{a^-}$, $P(q^*) \in \mathcal{P}^a$. In addition, by (5.46), there

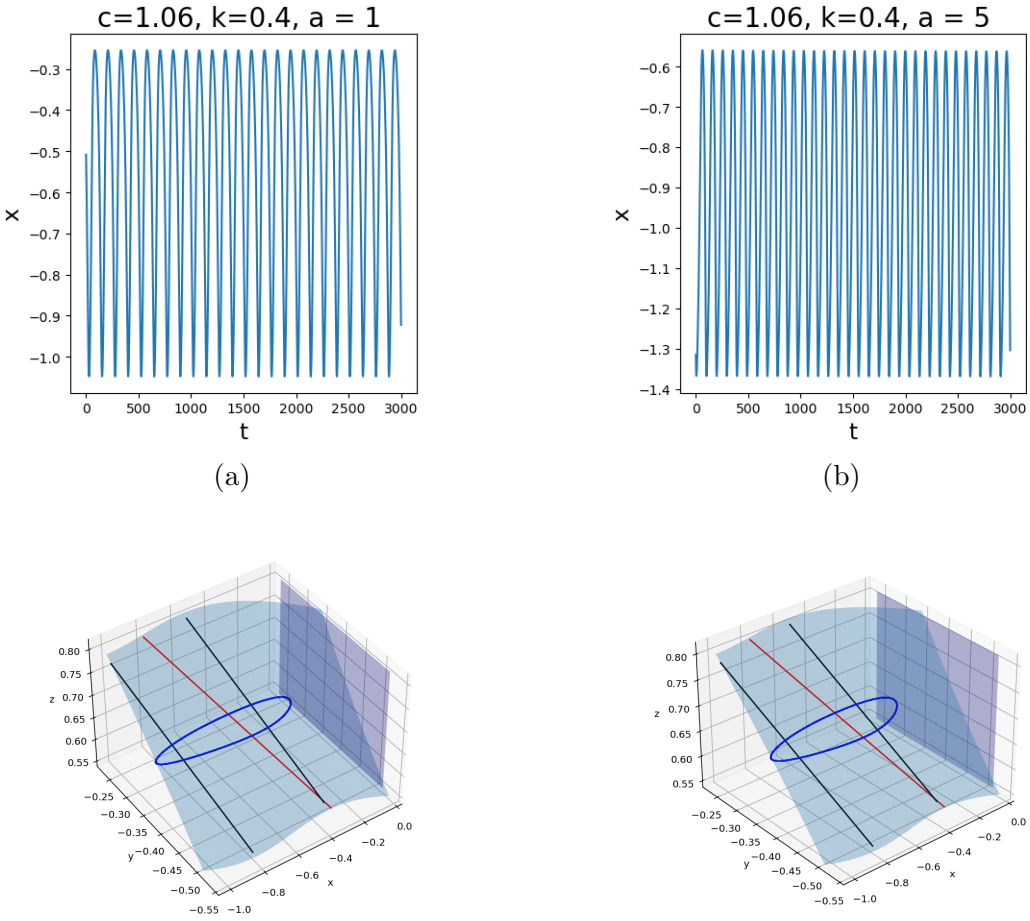

Figure 5.9: For $(c,k) \in \mathcal{V}_3$, see Figure 5.6, oscillatory trajectories of system (5.1) can not feature plateau above. For fixed $(c,k) \in \mathcal{V}_3$, there exist unique $a^- = a^-(c,k) > 0$ and $a^+ = a^+(c,k) > 0$ for which an equilibrium point of (5.1) coincides with q^- and q^+, respectively. For $a^+ < a < a^-$, system (5.1) exhibits oscillatory dynamics.

exist $a^+ = a^+(c,k) > 0$ for which $p_{eq} \equiv q^+$, and for $a > a^+$ it holds that $p_{eq} \in \mathcal{S}^r$ – we emphasize that there exist *no* $a^- = a^-(c,k) > 0$ for which $p_{eq} \equiv q^-$. Therefore, for $\delta, \rho > 0$ sufficiently small, system (5.1) features oscillatory dynamics without plateau for $a \in (a^+ + \mathcal{O}(\delta,\rho), a^- + \mathcal{O}(\delta,\rho))$.

In particular, fixing $(c,k) = (1.4, 0.7)$, we calculate that $a^+ \simeq 0.1$. Numerically, we obtain that system (5.1) converges to a steady state for $a \lesssim 0.1$. Some simulated trajectories for (c,k) fixed in this regime and various values of a, with $\delta = 0.01 = \rho$, are illustrated in Figure 5.10.

We remark that, similarly to the previous case, the above analysis is valid only for $a = \mathcal{O}(1)$; i.e., for $a \gg 1$, the terms multiplied by a in (5.1) become large, therefore the three-timescale separation where x is fast, y is intermediate and z is slow as described here is no longer valid, in accordance with Remark 14. The study of this case is included in plans

for future work.

Moreover, similarly to the case where $(c,k) \in \mathcal{V}_2$, we observe that there exists a value $a_p = a_p(c,k)$ that distinguishes between MMOs that feature plateaus from those that do not, i.e.

1. system (5.1) features MMOs with plateaus above for $a \in (0, a_p)$,
2. system (5.1) features MMOs without plateaus for $a > a_p$ and $a = \mathcal{O}(1)$.

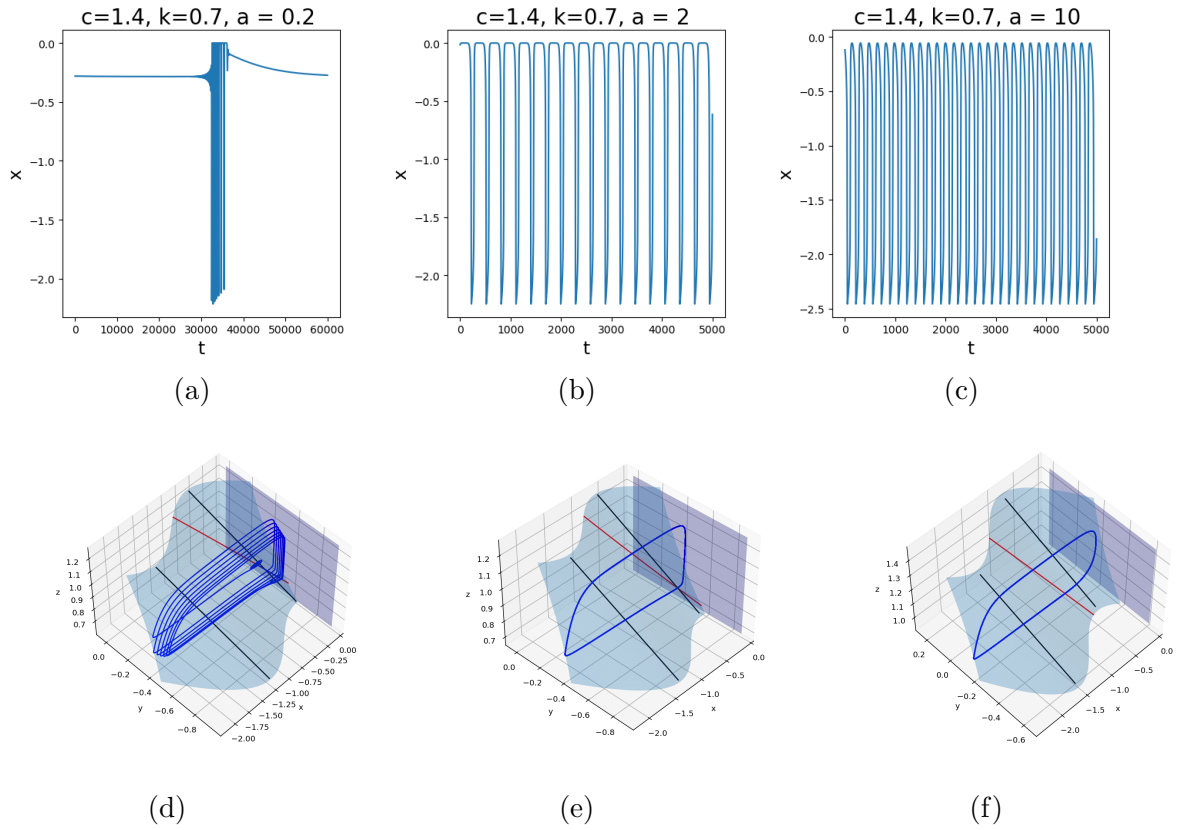

Figure 5.10: For $(c,k) \in \mathcal{V}_4$, see Figure 5.6, oscillatory trajectories of system (5.1) can either feature plateau above or not. For fixed $(c,k) \in \mathcal{V}_3$, there exist unique and $a^+ = a^+(c,k) > 0$ for which an equilibrium point of (5.1) coincides with q^+. For $a > a^+$, system (5.1) exhibits oscillatory dynamics. Moreover, there exists a_p such that for $a < a_p$, system (5.1) exhibits oscillatory trajectories with plateaus above, while for $a > a_p$, system (5.1) exhibits oscillatory trajectories without plateaus above. Finally, for a-values close to a^+, system (5.1) exhibits MMOs with SAOs above. Notice that the LAOs of the latter consist of segments with plateau, due to corresponding intermediate segments on $\mathcal{P}^a$, and compare with Figure 5.11.

- $(c,k) \in \mathcal{V}_5 = \mathcal{D}_3 \cap \mathcal{A}_2$

Fix $(c,k) \in \mathcal{V}_5$, as shown in Figure 5.6.

By Corollary 2, it holds that $P(q^-), P(q^*) \in \mathcal{S}^{a^-}$. In addition, by (5.46), there exist $a^+ = a^+(c,k) > 0$ for which $p_{eq} \equiv q^+$, and for $a > a^+$ it holds that $p_{eq} \in \mathcal{S}^r$ – we emphasize that exist *no* $a^- = a^-(c,k) > 0$ for which $p_{eq} \equiv q^-$. Therefore, for $\delta, \rho > 0$ sufficiently small, system (5.1) features oscillatory dynamics for $a > a^+$ and $a = \mathcal{O}(1)$.

In particular, fixing $(c,k) = (1.2, 0.7)$, we calculate that $a^+ \simeq 1.6$. Numerically, we obtain that system (5.1) converges to a steady state for $a \lesssim 2.2$. Some simulated trajectories for (c,k) fixed in this regime and various values of a, with $\delta = 0.01 = \rho$, are illustrated in Figure 5.11.

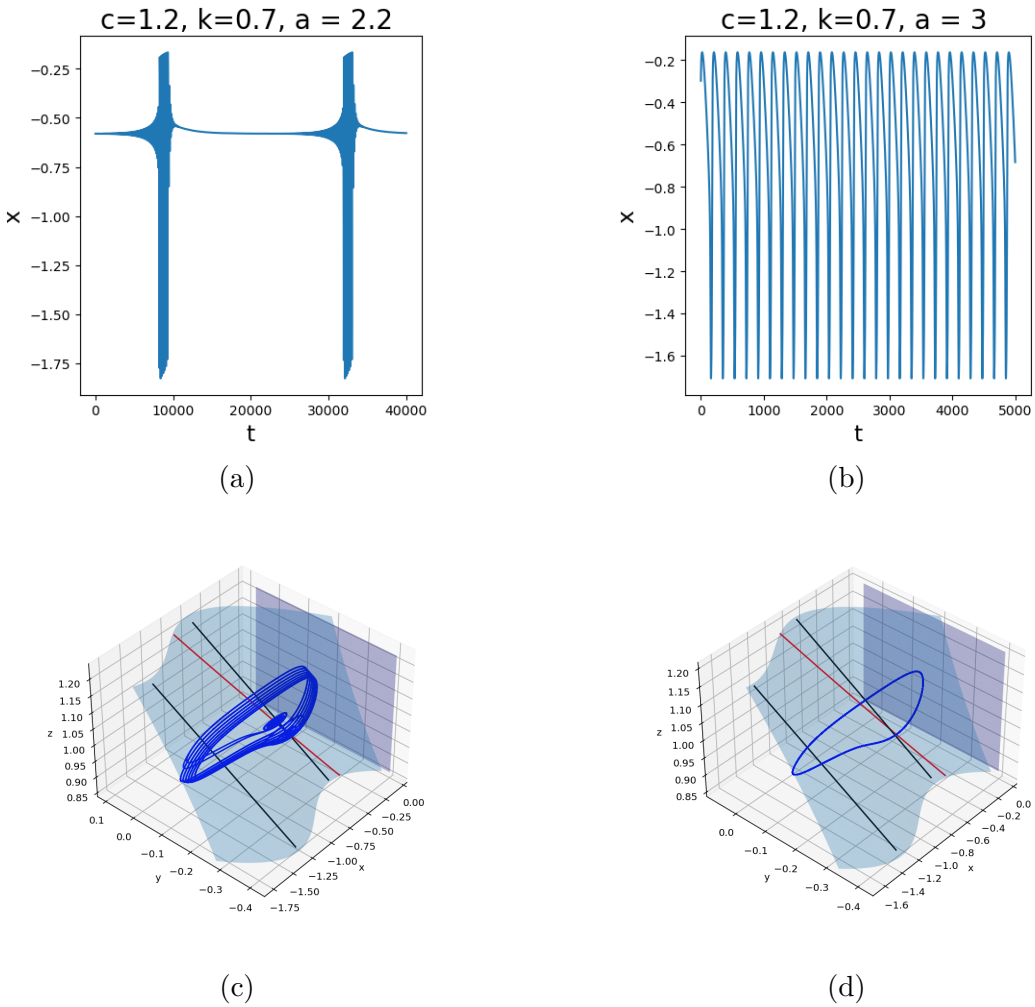

Figure 5.11: For $(c,k) \in \mathcal{V}_5$, see Figure 5.6, oscillatory trajectories of system (5.1) can not feature plateau above. For fixed $(c,k) \in \mathcal{V}_5$, there exists unique $a^+ = a^+(c,k) > 0$ for which an equilibrium point of (5.1) coincides with q^+. For $a > a^+$, system (5.1) exhibits oscillatory dynamics. Finally, for a-values close to a^+, system (5.1) exhibits MMOs with SAOs above. Notice that the LAOs of the latter consist of "typical" relaxation oscillation segments, due to corresponding intermediate segments on $\mathcal{S}^{a^-}$, and compare with Figure 5.10.

We remark that, similarly to the previous cases, the above analysis is valid only for $a = \mathcal{O}(1)$; i.e., for $a \gg 1$, the terms multiplied by a in (5.1) become large, therefore the

three-timescale separation where x is fast, y is intermediate and z is slow as described here is no longer valid, in accordance with Remark 14. The study of this case is included in plans for future work.

- $\underline{(c,k) \in \mathcal{V}_6 = \mathcal{D}_3 \cap \mathcal{A}_3}$

Fix $(c,k) \in \mathcal{V}_5$, as shown in Figure 5.6. For this case, there exist no $a > 0$ for which system (5.1) features oscillatory dynamics, since such a-values exist only for $(c,k) \in \mathcal{A}_1 \cup \mathcal{A}_2$.

5.4 Summary

In this Chapter, we extended the analysis in [Roberts et al., 2016] to the three-timescale context of Equation (5.1), i.e. for $\delta, \rho > 0$ sufficiently small. We explored the properties of oscillatory trajectories in dependence of the parameters c, k, a of Equation (5.1), and we associated them with the geometric properties of the system at the singular limit $\delta = 0 = \rho$.

In Section 5.2 we studied the geometric properties of the critical and supercritical manifolds of (5.1) at the singular limit $\delta = 0 = \rho$, and we illustrated various scenarios in terms of the locations of sets where normal hyperbolicity is lost relative to each other. We showed that the parameter c is associated with the geometric properties of the two-dimensional critical manifold $\mathcal{M}_1$ of (5.1) at the singular limit $\delta = 0$. For fixed $c > 1$, at the double singular limit $\delta = 0 = \rho$, the parameter $k \in (0,1)$ determines the geometric properties of the supercritical manifold $\mathcal{M}_2$. Finally, the value a does not affect the singular geometry of the system, but for a fixed geometry, it can distinguish between steady state and oscillatory dynamics, as well as between different qualitative properties of oscillations, via the reduced flow on the invariant manifolds of the system.

In Section 5.3, we showed various qualitative behaviours of oscillatory dynamics of (5.1) in dependence of its geometry, for $\delta, \rho > 0$ sufficiently small. By considering these various geometric configurations, we were thus able to find new qualitative behaviours that had not been documented in previous works. In particular, in reference to Figure 5.6, we showed that:

1. If $(c,k) \in \mathcal{V}_1$, only oscillations with plateau above are possible, cf. Figure 5.7;
2. If $(c,k) \in \mathcal{V}_2$, oscillations with or without plateau are possible, in dependence of the parameter a, cf. Figure 5.8;
3. If $(c,k) \in \mathcal{V}_3$, only oscillations without plateau are possible, cf. Figure 5.9;
4. If $(c,k) \in \mathcal{V}_4$, oscillations with or without plateau are possible, in dependence of the parameter a; moreover, MMOs with plateau above can also potentially feature segments of SAOs above, cf. Figure 5.10;
5. If $(c,k) \in \mathcal{V}_5$, only oscillations without plateau are possible, which, in dependence of the parameter a, can also potentially feature SAOs above. cf. Figure 5.11;

Finally, in Section 5.5 below, we briefly address the dynamics in the vicinity of the self-intersection of the critical manifold $\mathcal{M}_1$ for $\delta, \rho > 0$ small.

5.5 Blow-up analysis of $\mathcal{F}_P$

Here we study the vicinity of $\mathcal{F}_\mathcal{P}$ of system (5.1) with $\delta, \rho > 0$ sufficiently small, recall (5.17), with particular interest in the perturbed sheets $\mathcal{S}^{a^+}_{\delta\rho}$ and $\mathcal{S}^r_{\delta\rho}$; recall that $\mathcal{P} = \{x = 0\}$ is invariant under the full flow (5.1). The fold lines $\mathcal{L}^\mp$ intersect with $\mathcal{P}$ at

$$z^\mp_* = \mp \text{arcsech}\left\{\sqrt{\frac{1}{c}}\right\}, \tag{5.49}$$

recall (5.13); we then have that

$$\mathcal{F}_\mathcal{P} = \begin{cases} \mathcal{S}^{a^+} \cap \mathcal{P} & \text{for } z > z^+_*, \\ \mathcal{S}^r \cap \mathcal{P} & \text{for } z < z^+_*. \end{cases} \tag{5.50}$$

We start by considering the partially perturbed system Equation (5.1) with $\delta > 0$ sufficiently small and $\rho = 0$. Solutions are then characterised by $y = y_0$, and we can therefore write

$$x' = x\left(x + y_0 + c(1 - \tanh(x + z))\right) \tag{5.51a}$$
$$z' = \delta(k - z - \frac{x}{2}) \tag{5.51b}$$
$$y' = 0 \tag{5.51c}$$

We choose k and y_0 such that there exists z_0 so that $p_0 = (0, y_0, z_0) \in \mathcal{F}_\mathcal{P}$, and $B_\delta(p_0) \cap \mathcal{M}_2 = \emptyset$; by (5.15) we have $y_0 + c(1 - \tanh(z_0)) = 0$. Since we restrict ourselves away from $\mathcal{M}_2$, the results outlined below hold to leading order for $\rho > 0$ sufficiently small.

We translate the origin to the point p_0 by the change of coordinates $\tilde{z} = z - z_0$. This gives

$$x' = x\left(x + y_0 + c(1 - \tanh(x + z + z_0))\right), \tag{5.52a}$$
$$z' = \delta(k - z - z_0 - \frac{x}{2}), \tag{5.52b}$$
$$y' = 0, \tag{5.52c}$$

where we have dropped the tilde for convenience. We Taylor expand $\tanh(x + z + z_0)$ on the RHS of (5.52a) to obtain

$$x' = x\left(x - \tilde{c}x - \tilde{c}z\right), \tag{5.53a}$$
$$z' = \delta(k - z - z_0 - \frac{x}{2}), \tag{5.53b}$$
$$y' = 0, \tag{5.53c}$$

where, for convenience, we have denoted.

$$\tilde{c} := c(1 - \tanh^2(z_0)).$$

In regard to the above parameter, we make the following observation, which is important for the blow-up analysis to follow.

Lemma 14.

$$c(1-\tanh^2(z_0)) \lesseqgtr 1 \quad \text{for} \quad z_0 \gtreqless z_*^+.$$

Proof. Simple calculations show that $c(1-\tanh^2(z_*^+)) = 1$, where we recall that $z_*^+ = \operatorname{arcsech}\left\{\sqrt{\frac{1}{c}}\right\}$, recall (5.49); moreover, $\tilde{c}(z_0) = c(1-\tanh^2(z_0))$ is a decreasing function of z_0. □

The above implies that $\tilde{c} < 1$ for points in $\mathcal{S}^{a^+} \cap \mathcal{P}$, and $\tilde{c} > 1$ for points in $\mathcal{S}^r \cap \mathcal{P}$. Moreover, we are interested in the region where

$$k - z_0 < 0, \tag{5.54}$$

as this implies that the curve $\mathcal{F}_\mathcal{P}$ is above $\mathcal{M}_{2P}$ in the $\{x=0\}$ plane. If this were not the case, then trajectories would first reach $\mathcal{M}_{2P}$ and then would reach $\mathcal{F}_\mathcal{P} \cap \mathcal{M}_{2P}$, which is not the case that we are considering here.

We now consider the following blow-up transformation $\Phi : \mathbb{S}^2 \times \mathbb{R} \to \mathbb{R}^3$,

$$x = r\bar{x}, \qquad z = r\bar{z}, \qquad \delta = r^2\bar{\delta}. \tag{5.55}$$

which we will apply to the origin of the two dimensional system

$$x' = x\left(x - \tilde{c}x - \tilde{c}z\right), \tag{5.56a}$$

$$z' = \delta(k - z - z_0 - \frac{x}{2}), \tag{5.56b}$$

where we assume that $y = y_0$, recall (5.53). We will show that the dynamics for $\delta, \rho > 0$ sufficiently is as demonstrated in Figure 5.12. The weights in (5.55) are similar to the analysis of a transcritical singularities in [Krupa and Szmolyan, 2001b]; notice, however, that although system (5.56) features a transcritical bifurcation, the z-axis therein is invariant, and therefore the analysis of this case is slightly different to the one in [Krupa and Szmolyan, 2001b].

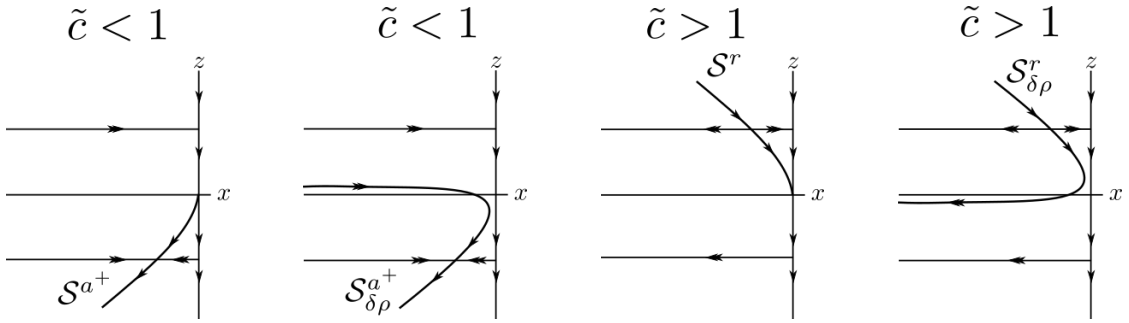

(a) $\delta = 0 = \rho$ (b) $\delta, \rho > 0$ (c) $\delta = 0 = \rho$ (d) $\delta, \rho > 0$

Figure 5.12: Self-intersection of $\mathcal{M}_1$ projected onto the xz-plane. For $\delta, \rho > 0$, $\mathcal{S}^{a^+}$ and $\mathcal{S}^r$ detach from the $\{x=0\}$ plane and connect with the fast flow.

We remark that system (5.56) features similar geometry to slow-fast Rosenzweig–MacArthur models studied in [Duncan et al., 2019, Poggiale et al., 2020], as well as to a two-timescale ecosystem model studied in [Sadhu, 2019]. A geometric desingularisation of the self intersection of a critical manifold of Rosenzweig–MacArthur model is included in [Poggiale et al., 2020]; here, we present an augmented analysis, in dependence also of the parameter $\tilde{c}$ in (5.56).

5.5.1 The entry chart $\kappa_1 : \{\bar{z} = 1\}$

The blow-up $\Phi_1 : \mathbb{R}^3 \to \mathbb{R}^3$ in the entry chart $\kappa_1 : \{\bar{z} = 1\}$ is given by

$$x = r_1 x_1, \qquad z = r_1, \qquad \delta = r_1^2 \delta_1. \tag{5.57}$$

Substituting (5.57) into (5.56) and rescaling time by a factor of r_1 gives

$$r_1' = r_1 \delta_1 \left(k - z_0 - r_1 - \frac{r_1 x_1}{2} \right) \tag{5.58a}$$

$$x_1' = x_1 \left(x_1 - \tilde{c} x_1 - \tilde{c} \right) - x_1 \delta_1 \left(k - z_0 - r_1 - \frac{r_1 x_1}{2} \right) \tag{5.58b}$$

$$\delta_1' = -2\delta_1 \left(k - z_0 - r_1 - \frac{r_1 x_1}{2} \right) \tag{5.58c}$$

The planes $\{\delta_1 = 0\}$ and $\{r_1 = 0\}$ are invariant. Their intersection is the invariant negative x_1-axis, whereon the dynamics is given by

$$x_1' = x_1 \left(x_1 - \tilde{c} x_1 - \tilde{c} \right), \quad x_1 < 0. \tag{5.59}$$

The dynamics in the invariant plane $\{\delta_1 = 0\}$ is given by

$$r_1' = 0, \tag{5.60a}$$

$$x_1' = x_1 \left(x_1 - \tilde{c} x_1 - \tilde{c} \right), \tag{5.60b}$$

while the dynamics in the invariant plane $\{r_1 = 0\}$ is given by

$$x_1' = x_1 \left(x_1 - \tilde{c} x_1 - \tilde{c} \right) - x_1 \delta_1 \left(k - z_0 \right), \tag{5.61a}$$

$$\delta_1' = -2\delta_1 \left(k - z_0 \right). \tag{5.61b}$$

We distinguish between the two cases where either $\tilde{c} \leq 1$ or $\tilde{c} > 1$ as follows:

1. $\tilde{c} \leq 1$: In this case, there exists a hyperbolic and attracting equilibrium for the flow (5.59), $p_{a,1} = (0, 0, 0)$, with corresponding eigenvalue $\lambda_a = -\tilde{c}$.

   In the plane $\{\delta_1 = 0\}$, system (5.60) has an attracting line $\ell_{a,1}$, which emanates from $p_{a,1}$.

   In the plane $\{r_1 = 0\}$, there exists a one-dimensional centre manifold $N_{a,1}$ at $p_{a,1}$, along which δ_1 increases for $\delta_1 > 0$ (recall that $k - z_0 < 0$ from (5.54)).

2. $\tilde{c} > 1$: In this case, there exist two hyperbolic equilibria for the flow (5.59), $p_{a,1} = (0, 0, 0)$ and $p_{r,1} = (\tilde{c}/(1 - \tilde{c}), 0, 0)$, which are respectively attracting and repelling, with corresponding eigenvalues $\lambda_{a,1} = -\tilde{c}$ and $\lambda_{r,1} = \tilde{c}$.

In the plane $\{\delta_1 = 0\}$, system (5.60) has attracting and repelling lines $\ell_{a,1}$ and $\ell_{r,1}$, respectively, which emanate from $p_{a,1}$ and $p_{r,1}$, respectively.

In the plane $\{r_1 = 0\}$, there exist one dimensional centre manifolds $N_{a,1}$ and $N_{r,1}$ at $p_{a,1}$ and $p_{r,1}$, respectively, along which δ_1 increases for $\delta_1 > 0$ (recall that $k - z_0 < 0$ from (5.54)).

The implications of the above are summarised in the following proposition.

Proposition 17 ([Krupa and Szmolyan, 2001a])**.** *The following assertions hold for system (5.58):*

1. *For $\tilde{c} > 0$, there exists an attracting two-dimensional C^k-center manifold $M_{a,1}$ at $p_{a,1}$ which contains the line of equilibria $\ell_{a,1}$ and the centre manifold $N_{a,1}$. The manifold $M_{a,1}$ corresponds to the invariant subspace $\{x_1 = 0\}$. Moreover, there exists a stable invariant foliation $\mathcal{F}^s$ with base $M_{a,1}$ and one-dimensional fibres, and for any $K > -\tilde{c}$, the contraction along $\mathcal{F}^s$ in a time interval $[0, T]$ is stronger than e^{KT}.*

2. *If $\tilde{c} > 1$, there additionally exists a repelling two-dimensional C^k-center manifold $M_{r,1}$ at $p_{r,1}$ which contains the line of equilibria $\ell_{r,1}$ and the centre manifold $N_{r,1}$. For $r_1, \delta_1 > 0$ small, the manifold $M_{a,1}$ is given as a graph $x_1 = h_{r,1}(r_1, \delta_1)$, The branch of $N_{r,1}$ in $r_1 = 0$, $\delta_1 > 0$ is not unique. Moreover, there exists an unstable invariant foliation $\mathcal{F}^u$ with base $M_{r,1}$ and one-dimensional fibres. For any $K < \tilde{c}$, the expansion along $\mathcal{F}^u$ in a time interval $[0, T]$ is stronger than e^{KT}.*

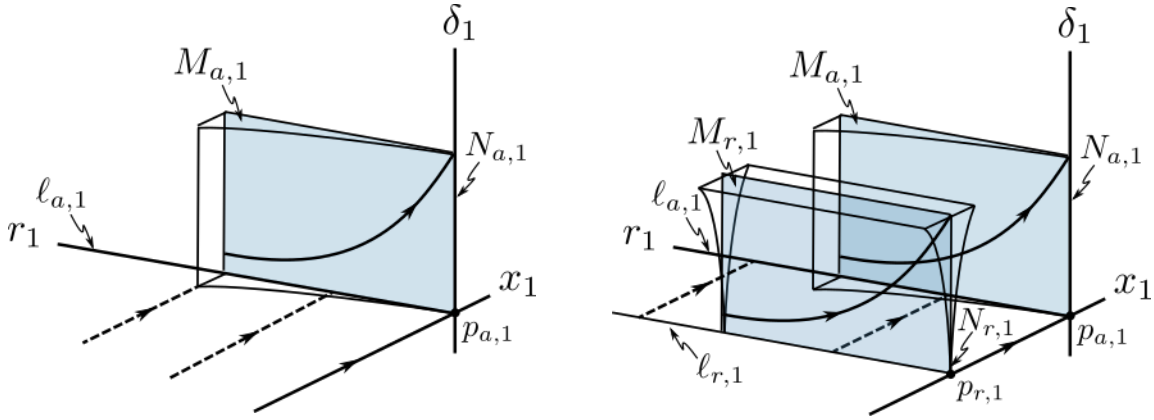

(a) $\tilde{c} \leq 1$: blow up of $\mathcal{S}^{a^+} \cap \mathcal{P}$ (b) $\tilde{c} > 1$: blow up of $\mathcal{S}^r \cap \mathcal{P}$

Figure 5.13: Dynamics in the entry chart κ_1.

We reiterate and emphasize that when $\tilde{c} \leq 1$, we are essentially blowing up a point on $\mathcal{S}^{a^+} \cap \mathcal{P}$, and when $\tilde{c} > 1$, we are essentially blowing up a point on $\mathcal{S}^r \cap \mathcal{P}$, cf. Figure 5.13 and Figure 5.2. Because of the angles of intersection between these manifolds and $\mathcal{P}$, we are only able to trace $\mathcal{S}^r$ in this chart for $\tilde{c} > 1$. Notice, that in this chart there also exists a repelling centre manifold in the x_1-positive orthant for $\tilde{c} \leq 1$, which we disregard, since we are only interested in dynamics restricted to $x_1 \leq 0$.

5.5.2 The rescaling chart $\kappa_2 : \left\{\bar{\delta} = 1\right\}$

The blow-up $\Phi_2 : \mathbb{R}^3 \to \mathbb{R}^3$ in the rescaling chart $\kappa_2 : \left\{\bar{\delta} = 1\right\}$ is given by

$$x = r_2 x_2, \qquad z = r z_2, \qquad \delta = r_2^2. \tag{5.62}$$

Substituting (5.62) into (5.56) and rescaling time by a factor of r_2 gives

$$x_2' = x_2 \left(x_2 - \tilde{c} x_2 - \tilde{c} z_2\right), \tag{5.63a}$$
$$z_2' = k - z_0 - r_2 z_2 - \frac{r_2 x_2}{2}; \tag{5.63b}$$

setting $r_2 = 0$ in the above gives

$$x_2' = x_2 \left(x_2 - \tilde{c} x_2 - \tilde{c} z_2\right), \tag{5.64a}$$
$$z_2' = k - z_0. \tag{5.64b}$$

The x_2-axis in (5.64) is invariant. Moreover, the x_2-nullclines are given by $z_2 = x_2 \left(1 - \tilde{c}\right)/\tilde{c}$. Above the x_2-nullcline, there holds that that $x_2' > 0$, and below the x_2-nullcline, there holds that $x_2' < 0$. Moreover, from (5.64b), it holds that $z_2' < 0$ everywhere, since $k - z_0 < 0$ from (5.54). The dynamics in this chart is summarised in Figure 5.14.

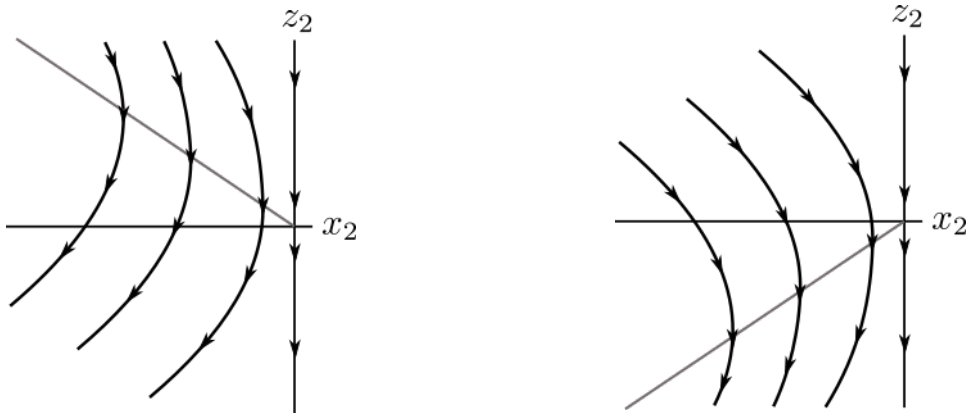

(a) $\tilde{c} > 1$: blow up of $\mathcal{S}^r \cap \mathcal{P}$ (b) $\tilde{c} < 1$: blow up of $\mathcal{S}^{a^+} \cap \mathcal{P}$

Figure 5.14: Dynamics in the rescaling chart κ_2.

Trajectories evolving on the invariant z_1-axis in chart κ_1 transit to trajectories evolving on the invariant z_2-axis in chart κ_2, and trajectories with $x_1 < 0$ in chart κ_1 transit to trajectories with $x_2 < 0$ in chart κ_2 as depicted in Figure 5.14; this idea we will be made more precise in the Summary subsection below.

5.5.3 The exit chart $\kappa_3 : \{\bar{z} = -1\}$

The directional blow-up $\Phi_3 : \mathbb{R}^3 \to \mathbb{R}^3$ in the exit chart $\kappa_3 : \{\bar{z} = -1\}$ is given by

$$x = r_3 x_3, \qquad z = -r_3, \qquad \delta = r_3^2 \delta_3. \tag{5.65}$$

Substituting (5.65) into (5.56) and rescaling time by a factor of r_3 gives

$$r_3' = -r_3\delta_3\left(k - z_0 - r_3 - \frac{r_3 x_3}{2}\right) \tag{5.66a}$$

$$x_3' = x_3\left(x_3 - \tilde{c}x_3 + \tilde{c}\right) - x_3\delta_3\left(k - z_0 - r_3 - \frac{r_3 x_3}{2}\right) \tag{5.66b}$$

$$\delta_3' = 2\delta_3\left(k - z_0 + r_3 - \frac{r_3 x_3}{2}\right) \tag{5.66c}$$

The planes $\{\delta_3 = 0\}$ and $\{r_3 = 0\}$ are invariant. Their intersection is the invariant negative x_3-axis, whereon the dynamics is given by

$$x_3' = x_3\left(x_3 - \tilde{c}x_3 + \tilde{c}\right), \quad x_3 < 0. \tag{5.67}$$

The dynamics in the invariant plane $\{\delta_3 = 0\}$ is given by

$$r_3' = 0, \tag{5.68a}$$

$$x_3' = x_3\left(x_3 - \tilde{c}x_3 + \tilde{c}\right) \tag{5.68b}$$

while the dynamics in the invariant plane $\{r_3 = 0\}$ is given by

$$x_3' = x_3\left(x_3 - \tilde{c}x_3 + \tilde{c}\right) - x_3\delta_3\left(k - z_0\right), \tag{5.69a}$$

$$\delta_3' = 2\delta_3\left(k - z_0\right). \tag{5.69b}$$

We again distinguish between the two cases where either $\tilde{c} \leq 1$ or $\tilde{c} > 1$ as follows:

1. $\tilde{c} > 1$: In this case, there exists one hyperbolic and repelling equilibrium for the flow (5.67), $p_{r,3} = (0, 0, 0)$, with corresponding eigenvalue $\lambda_{r,3} = \tilde{c}$.

   On the plane $\{\delta_3 = 0\}$, system (5.68) has a repelling line $\ell_{a,3}$, which emanates from $p_{r,3}$.

   On the plane $\{\delta_3 = 0\}$, there exists a one-dimensional centre manifold $N_{r,3}$ at $p_{a,3}$, along which δ_3 decreases for $\delta_3 > 0$ (recall that $k - z_0 < 0$ from (5.54)).

2. $\tilde{c} \leq 1$: In this case, there exist two hyperbolic equilibria for the flow (5.67), $p_{r,3} = (0, 0, 0)$ and $p_{a,3} = (-\tilde{c}/(1 - \tilde{c}), 0, 0)$, which are respectively repelling and attracting, with corresponding eigenvalues $\lambda_{r,3} = \tilde{c}$ and $\lambda_{a,3} = -\tilde{c}$.

   In the plane $\{\delta_3 = 0\}$, system (5.68) has attracting and repelling lines $\ell_{r,3}$ and $\ell_{a,3}$, respectively, which emanate from $p_{r,3}$ and $p_{a,3}$, respectively.

   In the plane $\{\delta_3 = 0\}$, there exist one dimensional centre manifolds $N_{r,3}$ and $N_{a,3}$ at $p_{r,3}$ and $p_{a,3}$, respectively, along which δ_3 decreases for $\delta_3 > 0$ (recall that $k - z_0 < 0$ from (5.54)).

The implications of the above are summarised in the following proposition.

Proposition 18 ([Krupa and Szmolyan, 2001a])**.** *The following assertions hold for system (5.66):*

1. *For $\tilde{c} \leq 1$, there exists a repelling two-dimensional C^k-center manifold $M_{r,3}$ at $p_{r,3}$ which contains the line of equilibria $\ell_{r,3}$ and the centre manifold $N_{r,3}$. The manifold $M_{r,3}$ corresponds to the invariant subspace $\{x_1 = 0\}$. Moreover, there exists a stable invariant foliation $\mathcal{F}^u$ with base $M_{r,3}$ and one-dimensional fibres, and for any $K < \tilde{c}$, the expansion along $\mathcal{F}^u$ in a time interval $[0, T]$ is stronger than e^{KT}.*

2. *If $\tilde{c} > 1$, there additionally exists an attracting two-dimensional C^k-center manifold $M_{a,3}$ at $p_{a,3}$ which contains the line of equilibria $\ell_{a,3}$ and the centre manifold $N_{a,3}$. For $r_3, \delta_3 > 0$ small, the manifold $M_{a,3}$ is given as a graph $x_3 = h_{a,3}(r_3, \delta_3)$. Moreover, there exists an unstable invariant foliation $\mathcal{F}^s$ with base $M_{a,3}$ and one-dimensional fibres. For any $K > -\tilde{c}$, the attraction along $\mathcal{F}^s$ in a time interval $[0, T]$ is stronger than e^{KT}.*

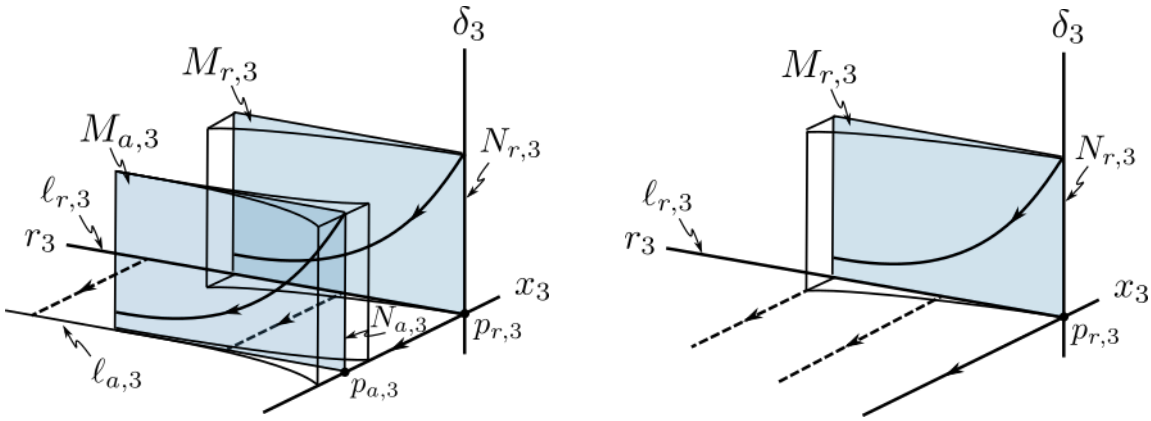

(a) $\tilde{c} \leq 1$: blow up of $\mathcal{S}^{a^+} \cap \mathcal{P}$ (b) $\tilde{c} > 1$: blow up of $\mathcal{S}^r \cap \mathcal{P}$

Figure 5.15: Dynamics in the exit chart κ_3.

We reiterate and emphasize that when $\tilde{c} \leq 1$, we are essentially blowing up a point on $\mathcal{S}^{a^+} \cap \mathcal{P}$, and when $\tilde{c} > 1$, we are essentially blowing up a point on $\mathcal{S}^r \cap \mathcal{P}$, cf. Figure 5.13 and Figure 5.2. Because of the angles of intersection between these manifolds and $\mathcal{P}$, we are only able to trace $\mathcal{S}^r$ in this chart for $\tilde{c} \leq 1$. Notice, that in this chart there also exists a repelling centre manifold in the x_1-positive orthant for $\tilde{c} > 1$, which we disregard, since we are only interested in dynamics restricted to $x_1 \leq 0$.

5.5.4 Summary

The changes of coordinates between the charts $\kappa_{ij} : \kappa_i \to \kappa_j$ are given by

- $\kappa_{12} : \kappa_1 \to \kappa_2$;

$$x_2 = \delta_1^{-1/2} x_1 \qquad z_2 = \delta_1^{-1/2} \qquad r_2 = r_1 \delta_1^{1/2} \tag{5.70}$$

- $\kappa_{23} : \kappa_2 \to \kappa_3$;

$$x_3 = x_2 z_2^{-1} \qquad r_3 = r_2 z_2 \qquad \delta_3 = z_2^{-2}. \tag{5.71}$$

It is therefore apparent that trajectories that lie in the plane $\{x_1 = 0\}$ in chart κ_1 transit to trajectories that lie on the axis $\{x_2 = 0\}$ in chart κ_2, and subsequently to trajectories that lie in the plane $\{x_3 = 0\}$ in chart κ_3 as expected, since $\{x = 0\}$ is invariant for the full system. Trajectories with $x_1 < 0$ in chart κ_1 that are attracted to the plane $\{x_1 = 0\}$ therein transit to trajectories with $x_3 < 0$ in chart κ_3, and follow the fast fibres if $\tilde{c} > 1$, or are attracted to $\mathcal{S}^{a^+}$ if $\tilde{c} \leq 1$.

We emphasize that the analysis here covers an $\mathcal{O}(\sqrt{\delta})$-neighbourhood of $\mathcal{F}_\mathcal{P}$. For trajectories that enter an $\mathcal{O}(\delta)$ neighbourhood of $\mathcal{P}$ at points $\mathcal{O}(\sqrt{\delta})$ away from $\mathcal{F}_\mathcal{P}$, the accumulated contraction needs to be balanced by expansion using the way-in/way-out function (5.47) before exiting an $\mathcal{O}(\delta)$ neighbourhood of $\mathcal{P}$, as described in [De Maesschalck, 2008].

Finally, since in none of the scenarios outlined in Section 5.3 trajectories approached a neighbourhood of $\mathcal{F}_\mathcal{P} \cap \mathcal{M}_2$, a detailed blow-up analysis of the latter is left as part of future work.

Chapter 6

Conclusions

The main focus of this work was the dynamics of three-timescale systems of ODEs. In Chapter 1, we presented a brief introduction to the standard and the non-standard forms of geometric singular perturbation theory. We described the notion of invariant slow and superslow manifolds of three-dimensional slow-fast systems as the backbone of their dynamics. We additionally showed that, even in case where a three-dimensional system is written in the standard form of GSPT, i.e. each variable admits its own timescale, the reduced flow on its two-dimensional slow manifold can potentially correspond to a slow-fast system in the non-standard form of GSPT.

In Chapter 2, we introduced an extended prototypical example, that features an S-shaped supercritical manifold embedded in an S-shaped critical manifold in a fairly symmetric manner. This topological setting is featured by many systems in applications and encodes crucial information about mixed-mode oscillations (MMOs) with different qualitative properties and transitions between them. We introduced the notion of orbital connection of the folded singularities of the system or lack thereof, and we associated the former to mixed-mode oscillations (MMOs) with double epochs of perturbed slow dynamics and the latter to MMOs with single epochs of perturbed slow dynamics and relaxation oscillations.

In Chapter 3, we demonstrated that the Koper model from chemical kinetics represents a particular realisation of our extended prototypical example for a specific choice of parameters; therefore, the results from Chapter 2 are directly transferable to this system. Although the Koper model has been extensively studied in the two-timescale context, to our knowledge, its MMO-dynamics had not yet been studied in the three-timescale context. Here we investigated the passage from two to three timescales, and we showed that MMOs with double epochs of perturbed slow dynamics are more robust than in the two-timescale context.

In Chapter 4 we studied the four-dimensional, four-timescale Hodgkin-Huxley equations from mathematical neuroscience in the standard form of GSPT. We introduced a novel and global three-dimensional reduction using GSPT, by reducing the flow to an invariant, three-dimensional, normally hyperbolic slow manifold. Then, we showed that, when either the variable h or the variable n is taken to be the slowest variable in the resulting three-dimensional, three-timescale flow, the system exhibits geometric characteristics and bifurcations of MMOs similar to the extended prototypical example that we introduced in Chapter 2. Moreover, we briefly exposed the viewpoint where the reduced flow on the slow manifold of the three-dimensional system can be treated as a slow-fast system written in the non-standard form of GSPT, where the notion of orbital connection of folded singularities of lack thereof can

be extended in this setting.

In Chapter 5 we studied a three-dimensional, three-timescale system that describes the El-Niño Southern Oscillation phenomenon. The critical manifold of this system is the union of an S-shaped manifold and a plane which intersect transversally. We extended the notion of relative positions of folded singularities to the notion of relative positions of sets where normal hyperbolicity is lost, and we related this to the various MMO-scenarios that can occur, which had not been documented in previous works. Moreover, we studied the vicinity of the intersection between the two critical manifolds in more detail, and we gave estimates about bifurcation delay phenomena, which were left as open questions in previous works.

In conclusion, in this work, we were mostly interested in the global dynamics of three-timescale systems, in relation to qualitative properties of mixed mode oscillations. A posteriori, it was evident that three-timescale systems simultaneously feature characteristics of two-fast/one-slow and one-slow/two-fast systems. Therefore, the local analysis in regions were normal hyperbolicity is lost can be carried out by combining and/or extending techniques from these two cases. The underlying geometric mechanisms of the extended prototypical example of Chapter 2, mainly the notion of orbital connection or lack thereof of folded singularities, proved useful in classifying the behaviour of systems with similar topological properties, like the Koper model of Chapter 3 and the Hodgkin-Huxley equations of Chapter 4. Moreover, by extending these notion, and in general putting emphasis on the configuration of the singular geometry, we were able to uncover qualitative behaviours that had not been documented before for the ENSO model of Chapter 5.

Questions that emerged in the process, such as the potential occurrence of period doubling bifurcations, local and global implications of complete and incomplete canard explosions, and the possibility of Shilnikov-type homoclinic orbits, are included in plans for future work. Moreover, plans for future work also include the study of torus canards [Burke et al., 2012] in three-timescale systems [Baspinar et al., 2021], and investigating whether any techniques and notions described in this work can be transferred in that context, investigating for instance whether the existence of a supercritical manifold provides further insight into the problem, or makes phenomena that are delicate in the two-timescale setting more robust in the three-timescale one.

Bibliography

[Anosov et al., 1997] Anosov, D. V., Aranson, S. K., Arnold, V. I., Bronshtein, I., Il'yashenko, Y. S., and Grines, V. (1997). *Ordinary differential equations and smooth dynamical systems*. Springer-Verlag.

[Baspinar et al., 2021] Baspinar, E., Avitabile, D., and Desroches, M. (2021). Canonical models for torus canards in elliptic bursters. *Chaos: An Interdisciplinary Journal of Nonlinear Science*, 31(6):063129.

[Brøns et al., 2006] Brøns, M., Krupa, M., and Wechselberger, M. (2006). Mixed mode oscillations due to the generalized canard phenomenon. *Fields Institute Communications*, 49:39–63.

[Brunet and Derrida, 1997] Brunet, E. and Derrida, B. (1997). Shift in the velocity of a front due to a cutoff. *Phys. Rev. E*, 56:2597–2604.

[Burke et al., 2012] Burke, J., Desroches, M., Barry, A. M., Kaper, T. J., and Kramer, M. A. (2012). A showcase of torus canards in neuronal bursters. *The Journal of Mathematical Neuroscience*, 2(1):1–30.

[Cardin and Teixeira, 2017] Cardin, P. T. and Teixeira, M. A. (2017). Fenichel theory for multiple time scale singular perturbation problems. *SIAM Journal on Applied Dynamical Systems*, 16(3):1425–1452.

[Cornwell, 2017] Cornwell, P. (2017). Opening the maslov box for traveling waves in skew-gradient systems. *arXiv preprint arXiv:1709.01908*.

[Cornwell and Jones, 2017] Cornwell, P. and Jones, C. K. (2017). A stability index for traveling waves in activator-inhibitor systems. *arXiv preprint arXiv:1703.07773*.

[Cornwell and Jones, 2018] Cornwell, P. and Jones, C. K. (2018). On the existence and stability of fast traveling waves in a doubly diffusive fitzhugh–nagumo system. *SIAM Journal on Applied Dynamical Systems*, 17(1):754–787.

[Curtu and Rubin, 2011] Curtu, R. and Rubin, J. (2011). Interaction of canard and singular Hopf mechanisms in a neural model. *SIAM Journal on Applied Dynamical Systems*, 10(4):1443–1479.

[Davis et al., 2017] Davis, P., van Heijster, P., and Marangell, R. (2017). Absolute instabilities of travelling wave solutions in a keller–segel model. *Nonlinearity*, 30(11):4029.

[De Maesschalck, 2008] De Maesschalck, P. (2008). Smoothness of transition maps in singular perturbation problems with one fast variable. *Journal of Differential Equations*, 244(6):1448–1466.

[De Maesschalck et al., 2014] De Maesschalck, P., Kutafina, E., and Popović, N. (2014). Three time-scales in an extended Bonhoeffer–van der Pol oscillator. *Journal of Dynamics and Differential Equations*, 26(4):955–987.

[De Maesschalck et al., 2016] De Maesschalck, P., Kutafina, E., and Popović, N. (2016). Sector-delayed-Hopf-type mixed-mode oscillations in a prototypical three-time-scale model. *Applied Mathematics and Computation*, 273:337–352.

[De Maesschalck and Wechselberger, 2015] De Maesschalck, P. and Wechselberger, M. (2015). Neural excitability and singular bifurcations. *The Journal of Mathematical Neuroscience (JMN)*, 5(1):16.

[Desroches et al., 2012] Desroches, M., Guckenheimer, J., Krauskopf, B., Kuehn, C., Osinga, H. M., and Wechselberger, M. (2012). Mixed-mode oscillations with multiple time scales. *SIAM Review*, 54(2):211–288.

[Desroches and Kirk, 2018] Desroches, M. and Kirk, V. (2018). Spike-adding in a canonical three-time-scale model: superslow explosion and folded-saddle canards. *SIAM Journal on Applied Dynamical Systems*, 17(3):1989–2017.

[Doi et al., 2001] Doi, S., Nabetani, S., and Kumagai, S. (2001). Complex nonlinear dynamics of the Hodgkin–Huxley equations induced by time scale changes. *Biological Cybernetics*, 85(1):51–64.

[Dumortier et al., 2007] Dumortier, F., Popović, N., and Kaper, T. J. (2007). The critical wave speed for the fisher–kolmogorov–petrowskii–piscounov equation with cut-off. *Nonlinearity*, 20(4):855.

[Dumortier and Roussarie, 2001] Dumortier, F. and Roussarie, R. (2001). Multiple canard cycles in generalized Liénard equations. *Journal of Differential Equations*, 174(1):1–29.

[Dumortier et al., 1996] Dumortier, F., Roussarie, R., Roussarie, R., and Society, A. M. (1996). *Canard Cycles and Center Manifolds*. American Mathematical Society: Memoirs of the American Mathematical Society. American Mathematical Society.

[Duncan et al., 2019] Duncan, J. P., Aubele-Futch, T., and McGrath, M. (2019). A fast-slow dynamical system model of addiction: Predicting relapse frequency. *SIAM Journal on Applied Dynamical Systems*, 18(2):881–903.

[Fenichel, 1979] Fenichel, N. (1979). Geometric singular perturbation theory for ordinary differential equations. *Journal of Differential Equations*, 31(1):53–98.

[Guckenheimer, 2008] Guckenheimer, J. (2008). Singular hopf bifurcation in systems with two slow variables. *SIAM Journal on Applied Dynamical Systems*, 7(4):1355–1377.

[Guckenheimer and Lizarraga, 2015] Guckenheimer, J. and Lizarraga, I. (2015). Shilnikov homoclinic bifurcation of mixed-mode oscillations. *SIAM Journal on Applied Dynamical Systems*, 14(2):764–786.

[Hayes et al., 2016] Hayes, M. G., Kaper, T. J., Szmolyan, P., and Wechselberger, M. (2016). Geometric desingularization of degenerate singularities in the presence of fast rotation: A new proof of known results for slow passage through hopf bifurcations. *Indagationes Mathematicae*, 27(5):1184–1203.

[Hek, 2010] Hek, G. (2010). Geometric singular perturbation theory in biological practice. *Journal of mathematical biology*, 60(3):347–386.

[Hodgkin and Huxley, 1952] Hodgkin, A. L. and Huxley, A. F. (1952). A quantitative description of membrane current and its application to conduction and excitation in nerve. *The Journal of Physiology*, 117(4):500–544.

[Izhikevich, 2007] Izhikevich, E. M. (2007). *Dynamical systems in neuroscience*. MIT press.

[Jalics et al., 2010] Jalics, J., Krupa, M., and Rotstein, H. G. (2010). Mixed-mode oscillations in a three time-scale system of odes motivated by a neuronal model. *Dynamical Systems*, 25(4):445–482.

[Jelbart and Wechselberger, 2020] Jelbart, S. and Wechselberger, M. (2020). Two-stroke relaxation oscillators. *Nonlinearity*, 33(5):2364.

[Kaklamanos and Kristiansen, 2019] Kaklamanos, P. and Kristiansen, K. U. (2019). Regularization and geometry of piecewise smooth systems with intersecting discontinuity sets. *SIAM Journal on Applied Dynamical Systems*, 18(3):1225–1264.

[Kapitula and Promislow, 2013] Kapitula, T. and Promislow, K. (2013). *Spectral and dynamical stability of nonlinear waves*, volume 457. Springer.

[Keener and Sneyd, 1998] Keener, J. P. and Sneyd, J. (1998). *Mathematical physiology*, volume 1. Springer.

[Koper, 1995] Koper, M. T. (1995). Bifurcations of mixed-mode oscillations in a three-variable autonomous Van der Pol-Duffing model with a cross-shaped phase diagram. *Physica D: Nonlinear Phenomena*, 80(1-2):72–94.

[Koper and Gaspard, 1991] Koper, M. T. and Gaspard, P. (1991). Mixed-mode and chaotic oscillations in a simple model of an electrochemical oscillator. *The Journal of Physical Chemistry*, 95(13):4945–4947.

[Koper and Gaspard, 1992] Koper, M. T. and Gaspard, P. (1992). The modeling of mixed-mode and chaotic oscillations in electrochemical systems. *The Journal of chemical physics*, 96(10):7797–7813.

[Kosiuk and Szmolyan, 2016] Kosiuk, I. and Szmolyan, P. (2016). Geometric analysis of the goldbeter minimal model for the embryonic cell cycle. *Journal of mathematical biology*, 72(5):1337–1368.

[Krupa et al., 2008] Krupa, M., Popović, N., and Kopell, N. (2008). Mixed-mode oscillations in three time-scale systems: a prototypical example. *SIAM Journal on Applied Dynamical Systems*, 7(2):361–420.

[Krupa and Szmolyan, 2001a] Krupa, M. and Szmolyan, P. (2001a). Extending geometric singular perturbation theory to nonhyperbolic points—fold and canard points in two dimensions. *SIAM Journal on Mathematical Analysis*, 33(2):286–314.

[Krupa and Szmolyan, 2001b] Krupa, M. and Szmolyan, P. (2001b). Extending slow manifolds near transcritical and pitchfork singularities. *Nonlinearity*, 14(6):1473.

[Krupa and Szmolyan, 2001c] Krupa, M. and Szmolyan, P. (2001c). Relaxation oscillation and canard explosion. *Journal of Differential Equations*, 174(2):312–368.

[Krupa and Wechselberger, 2010] Krupa, M. and Wechselberger, M. (2010). Local analysis near a folded saddle-node singularity. *Journal of Differential Equations*, 248(12):2841–2888.

[Kuehn, 2011] Kuehn, C. (2011). On decomposing mixed-mode oscillations and their return maps. *Chaos: An Interdisciplinary Journal of Nonlinear Science*, 21(3):033107.

[Kuehn, 2015] Kuehn, C. (2015). *Multiple time scale dynamics*, volume 191. Springer.

[Letson et al., 2017] Letson, B., Rubin, J. E., and Vo, T. (2017). Analysis of interacting local oscillation mechanisms in three-timescale systems. *SIAM Journal on Applied Mathematics*, 77(3):1020–1046.

[Leyva and Plaza, 2020] Leyva, J. F. and Plaza, R. G. (2020). Spectral stability of traveling fronts for reaction diffusion-degenerate fisher-kpp equations. *Journal of Dynamics and Differential Equations*, 32(3):1311–1342.

[Li et al., 2020] Li, Y., van Heijster, P., Marangell, R., and Simpson, M. J. (2020). Travelling wave solutions in a negative nonlinear diffusion–reaction model. *Journal of Mathematical Biology*, 81(6):1495–1522.

[Nan, 2014] Nan, P. (2014). *Dynamical Systems Analysis of Biophysical Models with Multiple Timescales*. PhD thesis, ResearchSpace@ Auckland.

[Nan et al., 2015] Nan, P., Wang, Y., Kirk, V., and Rubin, J. E. (2015). Understanding and distinguishing three-time-scale oscillations: Case study in a coupled morris–lecar system. *SIAM Journal on Applied Dynamical Systems*, 14(3):1518–1557.

[Poggiale et al., 2020] Poggiale, J.-C., Aldebert, C., Girardot, B., and Kooi, B. W. (2020). Analysis of a predator–prey model with specific time scales: a geometrical approach proving the occurrence of canard solutions. *Journal of mathematical biology*, 80(1):39–60.

[Roberts et al., 2016] Roberts, A., Guckenheimer, J., Widiasih, E., Timmermann, A., and Jones, C. K. (2016). Mixed-mode oscillations of el nino–southern oscillation. *Journal of the Atmospheric Sciences*, 73(4):1755–1766.

[Roberts et al., 2015] Roberts, K.-L., Rubin, J. E., and Wechselberger, M. (2015). Averaging, folded singularities, and torus canards: Explaining transitions between bursting and spiking in a coupled neuron model. *SIAM Journal on Applied Dynamical Systems*, 14(4):1808–1844.

[Rubin and Wechselberger, 2007] Rubin, J. and Wechselberger, M. (2007). Giant squid-hidden canard: the 3D geometry of the Hodgkin–Huxley model. *Biological Cybernetics*, 97(1):5–32.

[Rubin and Wechselberger, 2008] Rubin, J. and Wechselberger, M. (2008). The selection of mixed-mode oscillations in a hodgkin-huxley model with multiple timescales. *Chaos: An Interdisciplinary Journal of Nonlinear Science*, 18(1):015105.

[Sadhu, 2019] Sadhu, S. (2019). Complex oscillatory patterns near singular hopf bifurcation in a two time-scale ecosystem. *arXiv preprint arXiv:1901.02974*.

[Sandstede, 2002] Sandstede, B. (2002). Stability of travelling waves. In *Handbook of dynamical systems*, volume 2, pages 983–1055. Elsevier.

[Szmolyan and Wechselberger, 2001] Szmolyan, P. and Wechselberger, M. (2001). Canards in $\mathbb{R}^3$. *Journal of Differential Equations*, 177(2):419–453.

[Szmolyan and Wechselberger, 2004] Szmolyan, P. and Wechselberger, M. (2004). Relaxation oscillations in r3. *Journal of Differential Equations*, 200(1):69–104.

[Vo et al., 2013] Vo, T., Bertram, R., and Wechselberger, M. (2013). Multiple geometric viewpoints of mixed mode dynamics associated with pseudo-plateau bursting. *SIAM Journal on Applied Dynamical Systems*, 12(2):789–830.

[Wechselberger, 2005] Wechselberger, M. (2005). Existence and bifurcation of canards in $\mathbb{R}^3$ in the case of a folded node. *SIAM Journal on Applied Dynamical Systems*, 4(1):101–139.

[Wechselberger, 2020] Wechselberger, M. (2020). *Geometric Singular Perturbation Theory Beyond the Standard Form*. Frontiers in Applied Dynamical Systems: Reviews and Tutorials. Springer International Publishing.

[Wiggins, 2003] Wiggins, S. (2003). *Introduction to Applied Nonlinear Dynamical Systems and Chaos*. Texts in Applied Mathematics. Springer New York.